Peroxidized docosahexaenoic acid causes RPE dysfunction: Implications for retinal ageing and AMD

Thesis submitted to Cardiff University for the degree of Doctor of Philosophy

Linda Margaretha Bakker

School of Optometry and Vision Sciences

Cardiff University

September 2008

UMI Number: U585123

UMI U585123

ProQuest LLC
789 East Eisenhower Parkway
P.O. Box 1346
Ann Arbor, MI 48106-1346

DECLARATION

This work has not previously been accepted in substance for any degree and is not concurrently submitted in candidature for any degree.

Signed .... (candidate) Date ..17/11/2008..

STATEMENT 1

This thesis is being submitted in partial fulfillment of the requirements for the degree of ......Ph.D................(insert MCh, MD, MPhil, PhD etc, as appropriate)

Signed .... (candidate) Date ..17/11/2008.

STATEMENT 2

This thesis is the result of my own independent work/investigation, except where otherwise stated.
Other sources are acknowledged by explicit references.

Signed .... (candidate) Date ...17/11/2008

STATEMENT 3

I hereby give consent for my thesis, if accepted, to be available for photocopying and for inter-library loan, and for the title and summary to be made available to outside organisations.

Signed .... (candidate) Date ...17/11/2008....

"Wow"

Aihua Ma
September 2005

Acknowledgements

Abstract

The aim of this study was to gain important insights into the effects of peroxidized docosahexaenoic acid (pDHA) on the retinal pigment epithelium (RPE), and whether its effects can cause RPE cell dysfunction in a way similar to that observed in retinal ageing and the pathogenesis of age-related macular degeneration (AMD).

Initially, the time-course of *in vitro* peroxidation of DHA was monitored, culminating in formation of products able to absorb light above 400 nm. Cultured RPE cells were then exposed to this pDHA, which was shown to be toxic, both in dark and light-exposed conditions. Various cell viability assays were carried out indicating RPE cell death after exposure to pDHA is likely to occur by apoptosis. The effects of pDHA were reduced in the presence of various agents – α-tocopherol, glutathione, *N*-acetylcysteine, and phosphatidylethanolamine (PE).

Measurements of singlet oxygen, transient and superoxide production were carried out to determine the photosensitizing properties of pDHA. The ability of PE to reduce the production of these species was investigated but it was shown to have no effect on their yield, although singlet oxygen lifetime was reduced.

Finally, lysosomal enzyme activity, lysosomal integrity and accumulation of fluorescent and undegraded material were monitored after exposure to pDHA, demonstrating that pDHA was able to disrupt the ability of the RPE to fully degrade phagocytosed material.

In summary, pDHA is able to affect RPE cell viability directly when exposed extracellularly, and can also affect essential normal functions of the RPE intracellularly. In conjunction with published findings that pDHA is present in the retina – both within and around the RPE – the data presented here support the theory that pDHA can play an important role in causing RPE dysfunction, resulting in a loss of the protective role these cells play for photoreceptors, as occurs in retinal ageing and AMD.

Contents

Abbreviations

4-HHE	4-hydroxy-2(E)-hexenal
4-HNE	4-hydroxynonenal
A2E	2-[2,6-dimethyl-8-(2,6,6-trimethyl-1-cyclohexen-1-yl)-1E,3E,5E,7E-octotetraenyl]-1-(2-hydroxylethyl)-4-[4-methyl-6-(2,6,6-trimethyl-1-cyclohexen-1-yl)-1E,3E,5E-hexatrienyl]-pyridinium
AA	arachidonic acid
AMD	age-related macular degeneration
ANOVA	analysis of variance
AREDS	Age-Related Eye Disease Study
AT	α-tocopherol
ATCC	American Type Culture Collection
ATR	all-*trans*-retinal
BCA	bicinchoninic acid
BSA	bovine serum albumin
CAREDS	Carotenoids in Age-Related Eye Disease Study
Ccl-2	monocyte chemoattractant protein-1
Ccr-2	C-C chemokine receptor-2
CEP	carboxyethylpyrrole
CFH	complement factor H
CTAB	cetyltrimethylammonium bromide
DHA	docosahexaenoic acid (unperoxidized unless stated otherwise)
dk	dark
DMEM:F12	Dulbecco's modified Eagle's medium and Ham's F12 medium
DMSO	dimethylsulphoxide
DNA	Deoxyribonucleic acid
D-PBS	Dulbecco's phosphate buffered saline
EDTA	ethylenediaminetetraacetic acid
FCS	fetal calf serum
FITC	fluorescein isothiocyanate
FSC	forward scatter (for flow cytometry)
GSH	glutathione

GST	glutathione S-transferase
HBSS	Hank's balanced salt solution
HPLC	high performance liquid chromatography
LC-PUFA	long-chain polyunsaturated fatty acid
lt	light
MPT	mitochondrial permeability transition
MTT	3-(4,5-dimethylthiazol-2-yl)-2,5-diphenyl tetrazolium bromide
MV	microvilli
NAC	*N*-acetylcysteine
Nd:YAG	neodymium-doped yttrium-aluminium-garnet
NK	neuroketal
NP	neuroprostane
NPD1	neuroprotectin D1
OPO	optical parametric oscillator
OS	outer segment
OxCytC	oxidized cytochrome C
PBS	phosphate buffered saline
pDHA	peroxidized docosahexaenoic acid
PC	phosphatidylcholine
PDT	photodynamic therapy
PE	phosphatidylethanolamine
PEDF	pigment epithelium-derived growth factor
PI	propidium iodide
PLA_2	phospholipase A_2
POPC	1-palmitoyl-2-oleoyl-sn-glycero-3-phosphocholine
POPE	1-palmitoyl-2-oleoyl-sn-glycero-3-phosphoethanolamine
POS	photoreceptor outer segment
PS	phosphatidylserine
PUFA	polyunsaturated fatty acid
RB	rose bengal
RedCytC	reduced cytochrome C
RNA	ribonucleic acid
RPE	retinal pigment epithelium
SD	standard deviation

SEM	standard error of the mean
SOD	superoxide dismutase
SSC	side scatter (for flow cytometry)
TEM	transmission electron microscopy
TG	triglyceride
TUNEL	terminal dUTP nick-end labelling
UV	ultraviolet
VEGF	vascular endothelial growth factor
ZX	zeaxanthin

Chapter 1:
Introduction

1.1 General introduction

Cells of the neural retina and the retinal pigment epithelium (RPE) interact closely. Photoreceptor cells depend on RPE cells for provision of nutrients, synthesis of interphotoreceptor matrix, recycling of retinoids and for certain aspects of photoreceptor renewal. Healthy function of the RPE is therefore vital, and dysfunction could lead to a downstream alteration of normal photoreceptor cell function, leading to visual impairment. One disease state in which this occurs is age-related macular degeneration (AMD). This naturally occurring age-dependent condition is thought to involve accumulation of intracellular lipofuscin granules in the RPE, which may induce (photo-)oxidative damage, which can in turn cause RPE dysfunction. The exact mechanism of formation of lipofuscin is not yet fully understood but appears to involve a loss of the ability of the RPE cells to properly degrade phagocytosed outer segment discs, possibly due to alterations in lysosome physiology, lysosomal enzymes, or other physiological properties of RPE cells. Membranes of photoreceptors are enriched with docosahexaenoic acid (DHA), a long-chain polyunsaturated fatty acid (LC-PUFA). It is thought that DHA may be easily peroxidized in the retina due to a variety of factors. This thesis aims to investigate the role that this process may play in age-related changes in the RPE, and in the onset of RPE dysfunction and AMD.

This introduction will provide a background to the normal structure and function of the RPE, with particular focus on its support role for photoreceptor cells, and discuss age-related changes that commonly occur. Additionally, the importance of DHA to the retina will be discussed, including an introduction to the consequences of peroxidation of this LC-PUFA.

1.2 Structure and function of the RPE

The RPE is a monolayer which separates the neural retina from the underlying choroidal circulation (see Figure 1.1). RPE cells have two distinct membrane regions, separated by tight junctions – the apical surface, with its distinctive microvilli which are in intimate contact with photoreceptor outer segments, and the basal region which lies adjacent to Bruch's membrane. Bruch's membrane is an acellular layer consisting

2

of five distinct connective tissue layers. It lies between the RPE and the fenestrated choriocapillaris and functions as a highly porous and permeable membrane which allows free diffusion of nutrients, water and waste material (Marshall *et al.*, 1998).

RPE cells are columnar in the foveal region where photoreceptor cells are more dense, with a diameter of approximately 12 µm, but more flattened in the periphery of the retina, with a 60 µm diameter, where photoreceptor cells are less dense, resulting in an estimated ratio of ~25-45 photoreceptors per RPE cell (Marmor, 1998; Lamb and Simon, 2004).

Vitreous

Inner limiting membrane
Nerve fibre layer
Ganglion cell layer

Inner plexiform layer

Inner nuclear layer

Outer plexiform layer

Outer nuclear layer
Outer limiting membrane
Outer segment

Retinal pigment epithelium
Bruch's membrane
Choriocapillaris
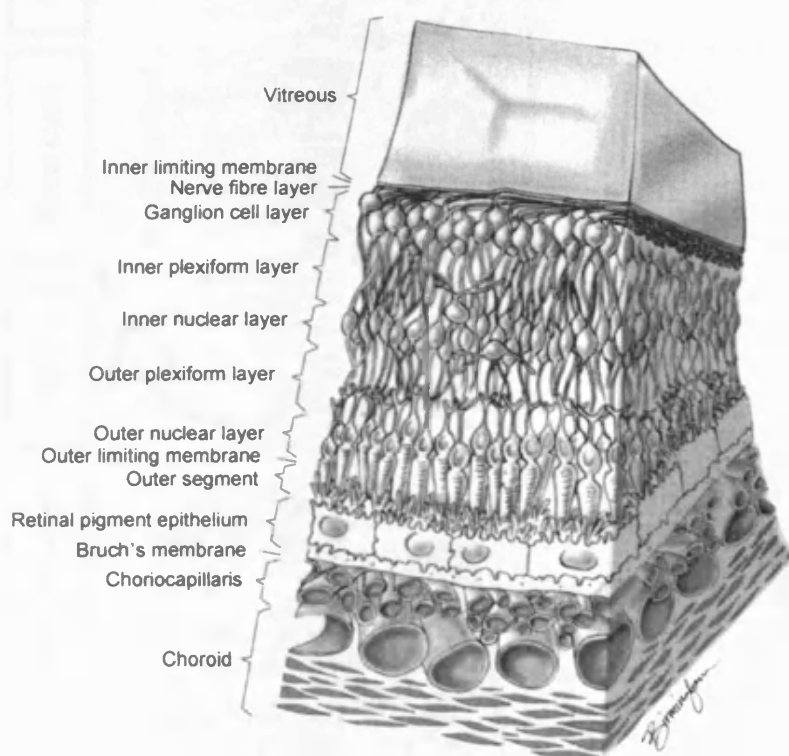
Choroid

Figure 1.1 *The layers of the retina and choroid (from Pulido, 2002)*

The RPE plays an important role in protecting the retina and provides a multi-faceted support role for photoreceptor cells. This support role starts early in the development of the retina, with the RPE actively involved in promoting correct orientation and differentiation of photoreceptors (German *et al.*, 2008). The interaction and support continue in the fully developed retina and are essential for proper functioning of the retina. The main functions of the RPE are summarized in Figure 1.2, and discussed in greater detail below.
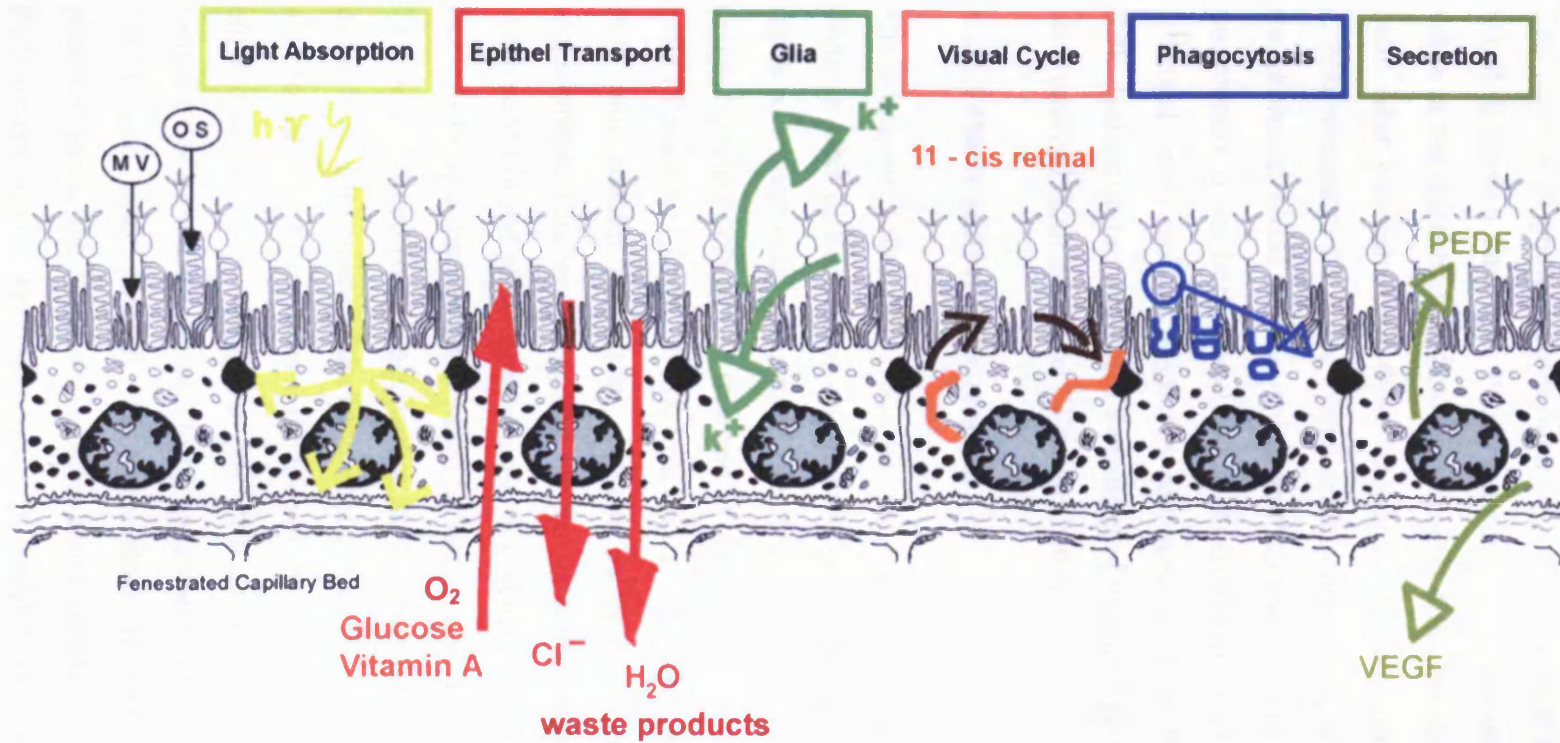
Figure 1.2 *Summary of RPE functions; MV = microvilli; OS = outer segments; epithel = epithelium; PEDF = pigment epithelium-derived growth factor; VEGF = vascular epithelium growth factor (modified from Strauss, 2005).*

1.2.1 Photoreceptor outer segment renewal and phagocytosis by RPE

The renewal of photoreceptor outer segments (POS) is a multi-step process in which the RPE plays a vital role. Photoreceptor discs are synthesized at the inner segment, while at the distal end of the outer segment discs are shed and phagocytosed by RPE cells. After internalization, these discs are degraded, with certain components returned to photoreceptors for re-incorporation into new discs, and waste products removed to the choroidal blood supply. Although the exact reasons for this process are not fully understood, it has been postulated to function effectively as a surrogate antioxidant – oxidized lipids etc. are physically removed from the POS, then (except in cases of RPE dysfunction or excessive formation of oxidized products) they become degraded and removed from the retina (Winkler, 2008).

1.2.1.1 Outer segment disc renewal

Photoreceptor cells, like other neuronal cells, do not generally undergo further division after differentiation and maturation, thus, damaged or dead cells can not be replaced by new cells. They have, therefore, developed a mechanism by which certain cellular components can be renewed in order to maintain healthy and fully functional cells (Young and Droz, 1968). Specifically, the discs which form the rod and cone POS and contain the visual pigment molecules undergo constant renewal and replacement. This was described by Young (1967) who demonstrated that proteins synthesized in rod photoreceptor inner segments are incorporated into the base of the POS, forming a discrete band which is then seen to move along the length of the POS. This well defined band suggests that the proteins form part of the disc structure seen in the POS. Movement of the band implies that the POS discs are constantly renewed, with formation of new discs at the base of the POS, followed by displacement of these older discs along the length of the POS as further discs are formed. The rate of formation of new discs appears to be temperature dependent in some species (Young, 1967), and also possibly light-dependent (Besharse *et al.*, 1977). In cone photoreceptors, the situation is rather more complex as the disc membranes in the POS are continuous with one another, in contrast with the discrete discs present in rod POS. Yet, it has been shown that cones do in fact shed their tips (Hogan *et al.*, 1974).

During development of the photoreceptor cells, disc synthesis results in lengthening of the POS. In mature photoreceptors, however, the formation of new discs is normally balanced with removal of discs at the distal tip of the POS in order to maintain a constant length.

1.2.1.2 Phagocytosis of POS discs

The process of distal tip disc removal has been shown to involve the RPE, by demonstrating the presence of phagosomes in the RPE containing segments of POS discs (Young and Bok, 1969). In contrast to the gradual and continuous process of insertion of new discs at the base of POS, removal of discs seems to occur intermittently, with larger groups of multiple discs detached simultaneously. POS removal and phagocytosis appear to be light sensitive, with the peak rate of phagocytosis of rods occurring at the onset of light after periods of dark, and/or dependent on a circadian clock mechanism (Hollyfield *et al.*, 1976; Besharse *et al.*, 1977; Besharse and Defoe, 1998). The shedding pattern for cones also occurs in a cyclical pattern, but it seems somewhat more complex, with variation in timing between species (summarized in Bok, 1985).

Using electron microscopy it has been demonstrated that the RPE may actually play an active role in the detachment process, rather than a purely passive action of "mopping up" detached discs. As shown in Figure 1.3, RPE cells form actin-containing pseudopodia – processes which are broader and more closely in contact with the POS than the apical microvilli that are also present. These processes have been shown to ensheath and intrude into the rod POS and are thought to aid in the detachment process, then continue to phagocytose the discs (Matsumoto *et al.*, 1987). It has been shown that RPE membrane molecules are also vital for this process. For example, $\alpha v \beta 5$ integrin appears essential for recognition and initial binding of POS (Finnemann *et al.*, 1997). Additionally, the scavenger receptor CD36 appears to play a role in enhancing rates of phagocytosis by interacting with oxidized lipids, thus enhancing phagocytosis in pro-oxidant conditions – possibly also explaining the upregulation of phagocytosis upon light exposure (Finnemann and Silverstein, 2001; Sun *et al.*, 2006).

Phagosomes containing the detached discs, which rapidly start to undergo chemical and physical changes, appear to become localized to the basal region of the RPE cells, closer to the underlying blood supply into which waste products can be delivered after complete degradation of the discs (Young and Bok, 1969).
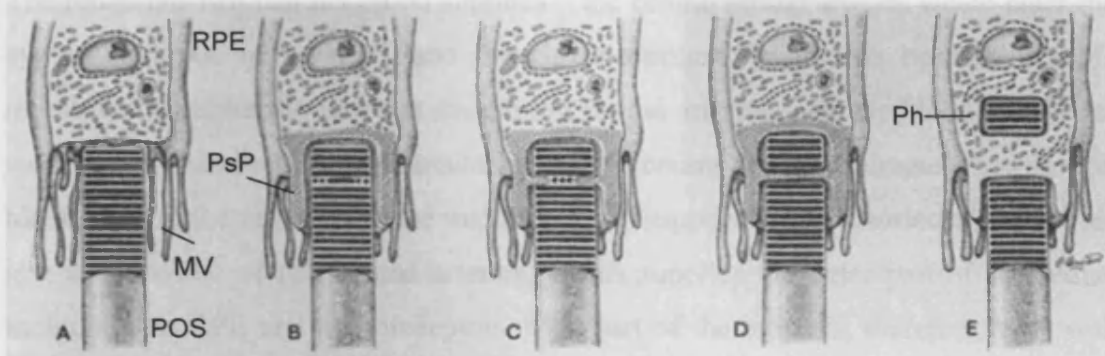
Figure 1.3 *Phagocytosis of POS discs by RPE cells showing (A) RPE cell with microvilli (MV) in close contact with adjacent rod POS; (B) formation of pseudopodia (PsP) and initiation of disc detachment; (C) intrusion of pseudopodia into POS; (D) complete detachment of disc segment while surrounded by pseudopodia; (E) internalization of discs forming phagosome (Ph), and withdrawal of pseudopodia (adapted from Matsumoto et al., 1987).*

1.2.1.3 Lysosomal degradation of phagocytosed tips

RPE lysosomes contain many enzymes: cathepsins, α-mannosidase, N-acetyl-β-D-glucosaminidase, acid lipase, acid phosphatase, α-fucosidase, α-galactosidase, α-glucosidase, β-galactosidase, β-glucosidase, β-glucuronidase, and phospholipases A_1 and A_2 (summarised in Kennedy *et al.*, 1995). These enzymes appear to be specialized for POS membrane degradation, and are, in fact, more potent than liver lysosomal enzymes at degrading these targets. Normal activity of many these enzymes requires a low lysosomal pH of approximately 4.5, which is maintained by a lysosome ATP-driven proton pump (Schutt and Holz, 2001; Bergmann *et al.*, 2004). Distribution of these enzymes varies in different regions of the retina, implying that the functions of the lysosomal system differ throughout the retina, perhaps due to variation in photoreceptor density, or rates of shedding of discs (Cabral *et al.*, 1990). Following degradation of POS by these enzymes, certain products such as DHA (discussed in

Section 1.4.2.2) may be recycled to the photoreceptors, while waste products are released into the choriocapillaris (Schutt and Holz, 2001).

1.2.2 Barrier and protective roles of the RPE

The retina has two distinct blood supplies – the central retinal arteries which enter the eye at the optic nerve head, and the choriocapillaris which lies beneath Bruch's membrane. Despite the fact that the central retinal arteries form the blood supply for most of the neural retina, this circulation only accounts for approximately 5% of total blood-flow to the retina, with the majority being supplied by the choriocapillaris. This is a net-like bed of fenestrated arteries, which supplies the outer part of the retina, including the RPE and photoreceptors. This part of the retina is, therefore, very well oxygenated, which has important consequences in relation to photo-oxidative damage.

The presence of tight junctions between RPE cells results in formation of a physical barrier severely restricting diffusion of molecules directly between blood and the retina *via* an extracellular route. This, along with the endothelial cell layer of the inner retinal blood circulation, forms the blood-retina barrier (Cunha-Vaz, 2004). Selective localization of specific receptors and channels to the apical or basal surfaces of RPE cells does, however, allow transport across the barrier *via* an intracellular route (Forrester *et al.*, 2002). This allows a flow of nutrients into the retina to supply adjacent photoreceptors, and removal of waste products and water from the retina back into the blood supply. Removal of fluids from the interphotoreceptor region, along with the presence of the interphotoreceptor matrix, which is produced by the RPE, helps to maintain adhesion of the neural retina to the RPE layer. Ion channels in the RPE also allow retention of essential ion concentrations to maintain electro-excitability of photoreceptor cells (Wimmers *et al.*, 2007).

In addition to controlling the flow of material between the choroid and the retina, the RPE can itself release growth factors, in particular vascular endothelial growth factor (VEGF) and pigment epithelium derived growth factor (PEDF). These are both important in controlling angiogenesis, and it appears there is a fine balance between these two factors to counteract pro-angiogenic VEGF with anti-angiogenic PEDF (Bhutto *et al.*, 2006). Indeed, in retinas with neovascular AMD, PEDF levels are

shown to decrease, and VEGF is upregulated compared with non-AMD retinas (Lopez *et al.*, 1996; Bhutto *et al.*, 2006).

1.2.3 Melanosomes and melanin

RPE cells contain melanosomes – pigment granules containing melanin. Their putative protective role has been studied, but has revealed conflicting results. They are thought to have several beneficial functions. Firstly, they absorb light, which reduces scatter within the eye, improving vision and reducing light damage. Secondly, they may also act in an antioxidant and free radical scavenging capacity, although the presence of high levels of other antioxidants in the RPE suggests that this function of melanin may not be significant (Boulton, 1998). Although supplementation of cultured cells with melanin appears to protect cells from light damage (Seagle *et al.*, 2006), other studies have shown no protective effect in cultured cells fed with melanosomes (Zareba *et al.*, 2006), and that *in vitro* light-activation of melanosomes may cause lipid peroxidation and production of reactive oxygen species, with increased photoreactivity with age (Dontsov *et al.*, 1999; Rozanowska *et al.*, 2002a).

1.2.4 Renewal of the visual pigment chromophore, 11-cis-retinal

The RPE plays a vital role in the renewal of the photoreceptor visual pigment chromophore 11-*cis*-retinal (summarized in Figure 1.4). Upon excitation of photoreceptors by light, 11-*cis*-retinal, which forms part of the rhodopsin molecule, is converted to all-*trans*-retinal, then enzymatically reduced to all-*trans*-retinol, which is released from the photoreceptor cell. This is then taken up into RPE cells and converted to 11-*cis*-retinol, then 11-*cis*-retinal by a number of enzymes. 11-*cis*-retinal is then transported back to the photoreceptors where it is reinserted into existing discs throughout the POS to regenerate visual pigments and inserted into newly formed discs in the inner segment (Chader *et al.*, 1998). The exact mechanism of transport of the compounds between the photoreceptors and RPE, *via* the extracellular space, is not yet fully understood but appears to involve an interphotoreceptor retinoid binding protein (Liou *et al.*, 1982). High DHA concentrations can directly induce the release of retinoids from this protein, thus providing a mechanism for targeting recycled retinoids to photoreceptors, where DHA concentrations are very high (Chen *et al.*,

1993; Chen *et al.*, 1996). Movement within the RPE may be regulated by a specific cellular retinol binding protein and other retinoid binding proteins. These binding proteins may be important not only for "carrying" the retinoids along the correct pathways, but also for protecting them from oxidative or enzyme attack (Besharse and Defoe, 1998).
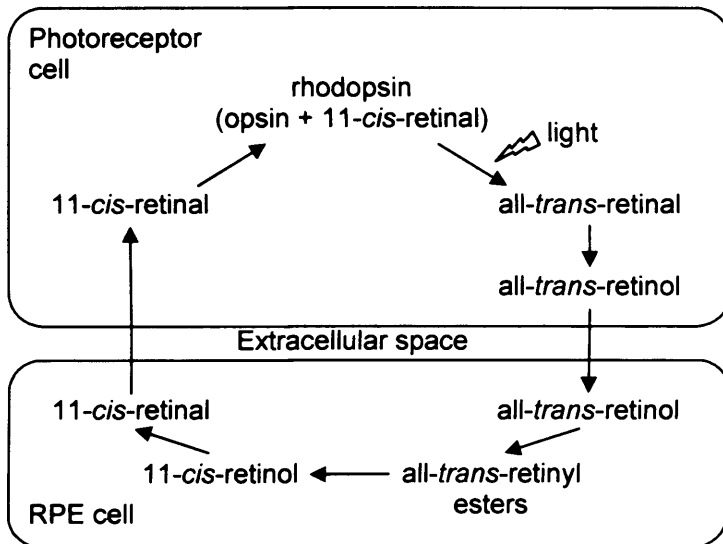
Figure 1.4 *Schematic diagram of retinoid isomerization in photoreceptors and RPE cells (adapted from Chader et al., 1998)*

1.2.5 Antioxidants

The RPE contains several common antioxidant enzymes – superoxide dismutase (SOD), catalase, glutathione peroxidase - and other antioxidants and free radical scavengers - vitamins A and E, and ascorbate (Forrester *et al.*, 2002). In fact, RPE cells appear to show an adaptive response to oxidative stress, resulting in upregulation of antioxidants and increased nuclear DNA protection (Jarrett and Boulton, 2005). Other "detoxification" enzymes, which act through mechanisms other than free radical scavenging, may also be important, such as glutathione-S-transferase, aldose reductase and aldehyde dehydrogenase (Esterbauer *et al.*, 1991; Choudhary *et al.*, 2003). These enzymes have been shown to be active in detoxification of lipid-derived aldehydes in cultured RPE cells (Choudhary *et al.*, 2005).

Another group of molecules which are particularly important in the retina are carotenoids. These are a large family of plant pigments, two of which – lutein and zeaxanthin – are found in the macular region of the retina and give the macula its yellow colour (Whitehead *et al.*, 2006). Levels of these pigments have been shown to increase in the majority of subjects whose diets are supplemented (Curran-Celentano *et al.*, 2001; Trieschmann *et al.*, 2007). Carotenoids are hydrophobic molecules and thus restricted to cell membranes. They display two potential modes of protection in the retina: firstly, they are able to absorb light and thus improve visual acuity and protect other cellular components from photo-damage, and secondly, they act in an antioxidant capacity and are able to quench singlet oxygen and scavenge free radicals (Britton, 1995; Liebler and McClure, 1996; Edge *et al.*, 1997; El-Agamey *et al.*, 2004).

1.3 Age-related macular degeneration

As described above, the RPE has several distinct roles which are vital for supporting photoreceptor cells. It follows that maintenance of RPE cellular homeostasis is essential for the proper functioning of photoreceptor cells and, therefore, of the visual sensory system as a whole. It has been shown, however, that with age, RPE cells undergo changes which may result in RPE dysfunction, possibly leading to development of AMD. These changes are discussed in greater detail below.

It is estimated that approximately 50% of blindness in developed countries is attributable to AMD in the aged population (Owen *et al.*, 2003; Resnikoff *et al.*, 2004), and that it affects approximately 200,000 people over the age of 75 in the UK, with prevalence increasing with age (Owen *et al.*, 2003; Evans *et al.*, 2004).

1.3.1 Age-related changes in the RPE and Bruch's membrane

The retina undergoes many age-related changes, some of which are in part due to the unique environment of the retina, with high blood flow and therefore also high O_2 levels and extensive light exposure in many parts of the retina, in addition to high levels of polyunsaturated fatty acids. Important changes in the RPE involve alterations in pigmentation, with decreased melanosome levels and increased lipofuscin due to

incomplete degradation of phagocytosed POS discs and also changes in optical characteristics of these granules (Feeney-Burns *et al.*, 1984; Boulton *et al.*, 1990; Docchio *et al.*, 1991; Schutt and Holz, 2001; Boulton *et al.*, 2004). With age there is also an increase in formation of pigment complexes such as melanolipofuscin (Feeney-Burns *et al.*, 1984).

The structure of Bruch's membrane, which is normally a highly permeable membrane, also changes and becomes denser and thicker, with some calcification and degeneration of collagen and elastin, potentially resulting in splitting of the membrane (Schutt and Holz, 2001). Accumulation of metabolic products also occurs, resulting in impaired fluid flow through the membrane. These products are likely to be of RPE/POS origin and notably, include lipids which show increased levels of peroxidation with age, and may result in reduction of flow of water and water-soluble molecules through the now lipophilic Bruch's membrane (Spaide *et al.*, 1999). This accumulation may also lead to an immune response. Furthermore, capillaries of the choriocapillaris become smaller and further apart and they are reduced in number (Abdelsalam *et al.*, 1999; Spaide *et al.*, 1999; Schutt and Holz, 2001).

The formation of the main types of AMD-related deposits – lipofuscin (in the RPE) and drusen (on Bruch's membrane) – is discussed in greater detail below.

1.3.2 Lipofuscin

1.3.2.1 Lipofuscin composition and distribution

Retinal lipofuscin forms in the RPE as membrane-bound granules, derived predominantly from lysosomes that are unable to completely degrade phagocytosed POS tips. They have traditionally been thought to consist of a mixture of lipids and proteins (Kennedy *et al.*, 1995; Roth *et al.*, 2004), however, recent studies show minimal levels of proteins but confirm the presence of oxidized lipid-protein adducts (Gu *et al.*, 2003a; Ng *et al.*, 2008).

Lipofuscin granules tend to be localized in the basal half of RPE cells and are more commonly found in macular cells than non-macular cells (Kennedy *et al.*, 1995).

Their topographical distribution also matches that of drusen deposits in Bruch's membrane, suggesting that there may be a link between their formation (Roth *et al.*, 2004). Several distinct fluorophores have been identified in retinal lipofuscin, with the majority of work focused on A2E (2-[2,6-dimethyl-8-(2,6,6-trimethyl-1-cyclohexen-1-yl)-1*E*,3*E*,5*E*,7*E*-octotetraenyl]-1-(2-hydroxylethyl)-4-[4-methyl-6-(2,6,6-trimethyl-1-cyclohexen-1-yl)-1*E*,3*E*,5*E*-hexatrienyl]-pyridinium), which is derived from the interaction of all-*trans*-retinal with phosphatidylethanolamine (Lamb and Simon, 2004). This molecule and its isomers are at least partially responsible for the yellow/gold fluorescence of lipofuscin (Sparrow *et al.*, 1999; Ben-Shabat *et al.*, 2002; Fishkin *et al.*, 2005).

1.3.2.2 Lipofuscin formation

Formation of lipofuscin is predominantly attributed to lysosomal dysfunction. Possible causes include oxidative damage to POS components, particularly lipids, which would be enhanced by the pro-oxidant conditions including high O_2 levels and high fluxes of light, and by the decreased function of antioxidants and free radical scavengers. Decrease in melanin content may also contribute because of the resultant increase in light scatter and decrease in free radical scavenging. Direct decrease of lysosomal enzyme activity may also be induced by other mechanisms – for example, genetic aberrations, or direct effects of peroxidized molecules (Kennedy *et al.*, 1995; Roth *et al.*, 2004). Other findings show that oxidized lipid-protein complexes may affect enzyme activation and lysosomal maturity indirectly through inhibition of different signalling molecules, or they may form products which are resistant to lysosomal digestion (Hoppe *et al.*, 2004a,b). Lipofuscin itself is also able to interfere with lysosomal activity by causing loss of lysosomal integrity and inhibition of lysosomal enzyme activity, thus perpetuating its own formation (Wihlmark *et al.*, 1997; Wassell *et al.*, 1999; Davies *et al.*, 2001; Shamsi and Boulton, 2001).

A2E, which is acquired through POS phagocytosis, has also been shown to reduce lysosomal function. It has been shown, however, that this is not due to direct inhibition of enzymes, but rather due to inhibition of the proton pumps which normally maintain the low pH required by most lysosomal enzymes to function properly (Bermann *et al.*, 2001; Finnemann *et al.*, 2002; Bergmann *et al.*, 2004). This

appears to happen in a concentration-dependent manner, indicative of its detergent-like mechanism of action (Sparrow *et al.*, 1999)

1.3.2.3 Lipofuscin toxicity

Lipofuscin has several detrimental effects on RPE cells – it can inhibit the phagocytic process by causing lysosomal dysfunction, as described above, and it can cause changes in cellular architecture, but importantly, it can act as a photosensitizer – excitation by light can cause lipofuscin, or a component thereof, to produce damaging reactive oxygen species (Ambati *et al.*, 2003a). This has been shown *in vitro* to cause RPE cell death, with particular sensitivity to blue light (Wihlmark *et al.*, 1997; Davies *et al.*, 2001). Light exposure of lipofuscin granules results in O_2 uptake, in an age- and wavelength- dependent manner – increasing with age and at shorter wavelengths, with blue light being the most efficient within the range of light likely to reach the adult retina (Rozanowska *et al.*, 1995; Pawlak *et al.*, 2002; Rozanowska *et al.*, 2002a). In conjunction with O_2 uptake, lipofuscin granules are able to produce several reactive oxygen species: highly reactive singlet oxygen, superoxide, hydrogen peroxide, and lipid peroxides (Boulton *et al.*, 1993; Rozanowska *et al.*, 1995; Rozanowska *et al.*, 1998). Lipofuscin granules can also induce peroxidation of PUFA in dark conditions (Dontsov *et al.*, 1999)

The lipofuscin component, A2E, has been shown to induce photo-damage in RPE cells after artificially loading cells with this molecule (Schutt *et al.*, 2000; Sparrow *et al.*, 2000; Sparrow and Cai, 2001). However, other studies investigating lipofuscin phototoxicity have demonstrated that in lipofuscin-fed cells where photo-damage was observed, A2E concentrations were too low to account for the observed toxicity (Davies *et al.*, 2001). Furthermore, the action spectrum for A2E induced O_2 uptake is different to lipofuscin (Pawlak *et al.*, 2002), and although irradiation of A2E causes formation of singlet oxygen and superoxide, levels are not as high as would be required if A2E were the main cause of lipofuscin-induced oxygen species production (Pawlak *et al.*, 2003). Thus, based on A2E content in lipofuscin and comparison of their photochemical properties, it is clear that the contribution of A2E to lipofuscin photoreactivity is minor (Rozanowska and Sarna, 2005). Therefore, the exact

component(s) of lipofuscin that gives it its photosensitizing properties remains unidentified.

1.3.3 Drusen and other Bruch's membrane deposits

Drusen are lipid-rich deposits which occur between the RPE basement membrane and the collagenous layer of Bruch's membrane. Two main types are identified clinically – hard and soft. Hard drusen are generally small, occur from an early age in a large proportion of the general population, and are not usually regarded as clinically important (Klein *et al.*, 2002a). However, their presence in large numbers may precede formation of soft drusen and their disappearance may precede atrophy of overlying RPE and neural retina (Abdelsalam *et al.*, 1999; Hageman *et al.*, 2001; Klein *et al.*, 2002a). Soft drusen have less well defined margins and are usually larger and, when large and confluent, tend to be considered as precursors to choroidal neovascularization (Abdelsalam *et al.*, 1999; Hageman *et al.*, 2001).

Drusen are composed of a variety of proteins, which differ between drusen from "healthy" and AMD-affected eyes. Lipids are also found, including adducts between proteins and peroxidation products of DHA, such as carboxyethylpyrroles (CEP). These adducts are more abundant in AMD samples compared with normal samples (Crabb *et al.*, 2002).

Other deposits include basal laminar and basal linear deposits. Basal laminar deposits form between the RPE and Bruch's membrane. There are several types including amorphous, and fibrillar deposits which contain high levels of collagen (Hageman *et al.*, 2001; Sarks *et al.*, 2007). It has been shown that these deposits may increase during oxidant stress (Marin-Castano *et al.*, 2006). Basement linear deposits form externally to the RPE basement membrane, within Bruch's membrane. They consist of membranous debris and may fuse to form soft drusen (Sarks *et al.*, 2007). The presence of continuous basal linear and basal laminar deposits in combination is a marker of early AMD, although neither of these deposits, at early stages, are clinically observable (Sarks *et al.*, 2007).

RPE material trapped within Bruch's membrane is also able to initiate an immune response. This may result in removal of the waste products, but these deposits also act as seeding sites for drusen growth, with the final drusen deposits shown to contain various proteins related to inflammation, and complement products (Roth *et al.*, 2004).

Other lipids are also found within Bruch's membrane. These appear to be lipids of cellular origin and include LC-PUFA such as DHA. Levels of peroxidized lipids increase with age and lipids show broad fluorescence emission spectra, indicative of cross-linking with proteins, which would help retain these lipids in the membrane (Spaide *et al.*, 1999)

1.3.4 The role of the immune response in AMD

As described above, in addition to the presence of proteins and lipids derived from POS, drusen deposits may contain inflammatory markers such as components of the complement cascade. It seems that components of RPE lipofuscin, including certain oxidation products of A2E, are able to elicit an immune response (Zhou *et al.*, 2006). It has also been shown that antibodies against CEP are higher in AMD, suggesting the occurrence of an autoimmune mechanism (Gu *et al.*, 2003a). Additionally, several gene knockout experiments have been carried out to investigate the functions of certain genes related to the immune system and identify its role in AMD onset.

In a complement factor H (CFH) knockout, mice developed severe alterations in retinal structure and function (Coffey *et al.*, 2007). CFH is normally expressed and released by RPE cells, and functions as a suppressant of the alternative complement pathway (Hageman *et al.*, 2005). In the knockout mouse, severe disorganization of the retina was observed, and complement component 3 was found in the retina, indicating an immune response (Coffey *et al.*, 2007). Strikingly, although there was an increase in fluorescent material, as observed in AMD, there was a decrease in electron dense material below the RPE layer, and also thinning of Bruch's membrane. These two changes are the opposite of those expected in AMD, and imply that lack of CFH may result in either increased removal of accumulated material (and thus thinning of

Bruch's membrane) due to the increased immune response, or that CFH is required for the initial accumulation of the material (Coffey *et al.*, 2007).

Knockout experiments have also been carried out in mice to induce deficiencies in monocyte chemoattractant protein-1 (Ccl-2) and its receptor, C-C chemokine receptor-2 (Ccr-2) (Ambati *et al.*, 2003b). In wildtype mice, Ccl-2 synthesis by RPE and choroid epithelial cells is induced by the presence of C5a and IgG, and results in attraction of macrophages and infiltration into the choroid, leading to removal of C5a/IgG. In the knockouts, young mice showed normal retinal function. However, older mice displayed AMD-like characteristics – Bruch's membrane thickening, formation of drusen and lipofuscin, neovascularization and general retinal dysfunction and degeneration. It is suggested that this is caused by a deficiency of the chemoattractant system, thus resulting in accumulation of C5a/IgG, and subsequent development of the phenotype observed (Ambati *et al.*, 2003b).

Studies of genetic variations which lead to increased susceptibility to AMD have highlighted other components of the immune system which potentially play a role in the onset of AMD. These are discussed in greater detail in Section 1.3.6.2 below.

1.3.5 Causes of visual impairment in AMD

AMD is generally subdivided into two types – "wet" neovascular AMD, which affects approximately 10% of AMD sufferers but causes 75% of AMD-related serious vision loss, and "dry" AMD, characterized by atrophy of the RPE and outer neural retina and which affects 90% of AMD sufferers but only causes approximately 25% of cases of AMD-related serious vision loss (Abdelsalam *et al.*, 1999).

1.3.5.1 Neovascularization and wet AMD

Choroidal neovascularization is the growth of new blood vessels from the choroid, through Bruch's membrane and into the retina.

Angiogenesis at the level of Bruch's membrane and the RPE is normally prevented by a precise balance of different pro- and anti-angiogenic growth factors, such as PEDF and VEGF. When diffusion of water and molecules through Bruch's membrane is

reduced due to, for example, presence of hydrophobic, lipid-rich drusen or other matter, this balance of factors may be affected and angiogenesis may begin (Schutt and Holz, 2001; Roth *et al.*, 2004).

The lipid-rich composition of drusen and other Bruch's membrane deposits may also contribute to neovascularization. CEP adducts, which increase in Bruch's membrane with age, have been shown to stimulate angiogenesis (Ebrahem *et al.*, 2006), while *in vivo* studies in rabbits have shown that linoleic acid hydroperoxides (introduced by subretinal injection) are able to stimulate choroidal neovascularization, possibly by inducing angiogenic cytokine expression in RPE cells (Tamai *et al.*, 2002). Additionally, exposure of RPE cells to reactive oxygen species, as would occur on photo-activation of lipofuscin and lipids, leads to an increase in VEGF expression, thus promoting angiogenic pathways (Kuroki *et al.*, 1996).

It may also be necessary for Bruch's membrane to be partially damaged to allow angiogenesis to occur, but as described above, this commonly occurs with age. New blood vessels pass through Bruch's membrane then pass horizontally, either between Bruch's membrane and the RPE, or further into the neural retina. Loss of vision may then occur as a result of haemorrhage, scarring, exudation and/or retinal detachment (Schutt and Holz, 2001; Roth *et al.*, 2004; Ebrahem *et al.*, 2006).

1.3.5.2 Geographic atrophy and dry AMD

Geographic atrophy is often preceded by accumulation of lipofuscin in the RPE, a process which is described in greater detail in Section 1.3.2, along with its deleterious effects. Accumulation of lipofuscin, which can be observed clinically by fundus autofluorescence imaging, may lead to RPE dysfunction due to its phototoxic properties, described above. This occurs predominantly in the perifoveal area, correlating with regions of highest rod density. Due to the important support role of the RPE, dysfunction in this cell layer results in loss of photoreceptor cells which directly affects the ability of the retina to process light signals. Cell death also occurs in the choriocapillaris (Schutt and Holz, 2001; Roth *et al.*, 2004).

1.3.6 Risk factors for AMD

The aetiology of AMD is not yet fully understood, but is likely to occur as a result of interplay between a variety of risk factors.

Age is considered to be the most important risk factor for AMD, with prevalence of AMD increasing significantly with age (Klein, 1999; McCarty *et al.*, 2001; AREDS Research Group, 2005). Additionally, several genetic and modifiable environmental risk factors have been studied.

1.3.6.1 Environmental risk factors

Cigarette-smoking is known to be an important modifiable risk factor for AMD. Four major studies – the Beaver Dam Eye Study, the Age-Related Eye Disease Study (AREDS), the US Twin Study of AMD and the Blue Mountains study – have all shown increased risk of AMD amongst smokers (Klein *et al.*, 2002b; AREDS Research Group, 2005; Seddon *et al.*, 2006; Tan *et al.*, 2007). Dietary factors such as raised high density lipoprotein levels also increased the risk of AMD – in some cases on its own, but also by further increasing the risk caused by smoking (Klein *et al.*, 2002a; AREDS Research Group, 2005; Seddon *et al.*, 2006). Intake of omega-3 fatty acids or fish reduced the risk of AMD; however this did also depend on omega-6 fatty acid intake, with a lower ratio of omega-6 to omega-3 shown to provide the greatest benefit (Chua *et al.*, 2006; Seddon *et al.*, 2006).

Several studies have suggested that an important risk factor for AMD, which links with evidence of photosensitized damage occurring in the retina, is sunlight. The Beaver Dam Eye Study in particular has focussed on the effects of light, and has demonstrated in medium and long-term studies that prolonged exposure to high levels of sunlight increases the risk of AMD and that the use of sunglasses in certain groups can confer protection (Cruickshanks *et al.*, 1993; Tomany *et al.*, 2004). In particular, protection from blue light warrants further investigation (Hawse, 2006). It is important to note, however, that other studies have shown no significant effect of light exposure (The Eye Disease Case-Control Study Group, 1992; McCarty *et al.*, 2001). Several studies have indicated there may also be a link between cataract surgery and

increased incidence of AMD, or further progression of early AMD, but results between these studies also seem inconsistent (reviewed in Bockelbrink *et al.*, 2008).

1.3.6.2 Genetic risk factors

As with the environmental risk factors, genetic risk factors do not directly cause AMD, but are regarded as susceptibility factors, where certain genetic variations increase the risk of developing AMD.

At chromosome 10q26 there is a region of high numbers of single nucleotide polymorphisms. One in particular, rs10490824, which is located within the LOC387715 gene, has a strong association with AMD susceptibility. This gene encodes a protein which is localized in the outer mitochondrial membrane, and is expressed at moderate levels in the retina (Kanda *et al.*, 2007). Although the function of this protein is not fully understood, it has been suggested that the observed A69S substitution may alter sensitivity to oxidative damage due to altered mitochondrial function, and that this may explain the statistical interaction between this gene variation and history of smoking in the risk of developing AMD (Haines *et al.*, 2007; Schaumberg *et al.*, 2007).

Another gene which has been linked with AMD is that of CFH, on chromosome 1q32, which shows several variants in humans. As described above, CFH normally suppresses the alternative complement pathway (Hageman *et al.*, 2005), and deficiencies in mice can cause severe retinal abnormalities (Coffey *et al.*, 2007). In humans, one particular variant allele, Y402H, is expressed in nearly 60% of the white population in the USA. Risk of AMD with this variant increases 2-fold for heterozygotes, and 5-fold for homozygotes (Schaumberg *et al.*, 2007).

The combination of these two AMD-related genetic factors increases susceptibility to AMD 50-fold in those homozygous for both changes. In total, ~65% of AMD cases appear to be attributable to variations in these genes (Schaumberg *et al.*, 2007). Additionally, the risks induced by both of the AMD susceptibility factors above are further increased by environmental factors, with smoking and obesity shown to cause significant further increases (Schaumberg *et al.*, 2007).

In addition to CFH being a susceptibility factor for AMD, variations in other complement components appear to show protective properties: in complement component 2/complement factor B (C2/CFB) on chromosome 6, and complement component 3 (C3) on chromosome 19 (Haines *et al.*, 2007). Additionally, associations have been shown between ABCR mutations and AMD. ABCR, a member or the ATP binding cassette transporter family of proteins, is a photoreceptor-specific protein which has known mutations which cause Stargardt disease, an early onset form of macular degeneration with similar characteristics to AMD (Allikmets *et al.*, 1997).

1.3.7 Current therapeutic strategies

The main focus of treatment to date has been to prevent and reduce the choroidal neovascularization observed in "wet" AMD. This has taken two main pathways – ablation of formed vessels by photocoagulation or photodynamic therapy, and prevention of formation through blocking the actions of VEGF.

Photocoagulation for treating neovascularization involves the use of a high power laser to effectively burn the neovascular complexes (Berger and Fine, 1999). This has been shown in a major trial to reduce further severe vision loss compared with untreated patients (Macular Photocoagulation Study Group, 1982). However, due to the high laser power required, damage to retinal cells may occur leading to loss of central vision after treatment of subfoveal lesions, particularly after treatment of larger lesions. Therefore, other treatments have been sought (Macular Photocoagulation Study Group, 1994; Berger and Fine, 1999).

Photodynamic therapy (PDT) involves the use of Verteporfin, a photosensitizer which is given intravenously and is then activated when the retina is exposed to a 689 nm laser source. Long-term studies have shown reduced vision loss in patients who have undergone PDT versus controls (TAP Study Group, 1999; Bresler and TAP Study Group, 2001).

Alternatively, the VEGF-mediated pro-angiogenic signalling cascade is targeted (Lopez *et al.*, 1996; Ng and Adamis, 2005). Several drugs have been found to be beneficial *via* this route in AMD after intravitreal injection. Macugen (or pegaptanib)

21

is an aptamer – a modified RNA oligonucleotide – which has the ability to bind specifically to VEGF165 – the isoform of VEGF found in the retina, thus allowing it to act specifically on AMD-related neovascularization (Ruckman *et al.*, 1998; Ng and Adamis, 2005).

Alternative therapies involve the use of antibodies or antibody fragments, which bind to VEGF, thus disabling it. Examples include Avastin (or Bevacizumab) which has been shown to have a positive effect in AMD, although it is licensed for treatment of colorectal cancer (Bashshur *et al.*, 2006). A related antibody, Lucentis (or Ranibizumab), is a chemically modified version of Avastin with a higher affinity for VEGF and is specifically licensed for treatment of AMD. It has been shown to reduce levels of macular fluid in patients with neovascular AMD and even improve visual acuity, rather than just limit further vision loss, providing an advantage over Macugen and PDT (Bashshur *et al.*, 2006; Brown *et al.*, 2006; Rosenfeld *et al.*, 2006; Fung *et al.*, 2007).

Studies have also shown beneficial effects of combinations of PDT and VEGF inhibition (Heier *et al.*, 2006), also with the addition of anti-inflammatory drugs (Augustin *et al.*, 2007). These combinations enhance results of individual drugs and often require fewer treatment cycles, and therefore potentially have a lower cost and lower risk of negative side-effects.

The treatments described here are only relevant to neovascularization which occurs in "wet" AMD. No treatment or cure for "dry" AMD or geographic atrophy has yet been found. There is some potential in the field of cell transplants, although this has only reached the stage of initial experiments in animal models. RPE cell transplants have been carried out and successfully recovered phenotypes of rodents with dysfunctional RPE, such as for example the Royal College of Surgeons rat (Lavail *et al.*, 1992; Jiang and Hamasaki, 1994) and the RPE65$^{(-/-)}$ mouse (Gouras *et al.*, 2002). Additionally, iris pigment epithelial cells have been used to regenerate RPE cells, as a potential route for autologous transplantation (Abe *et al.*, 2007).

In light of the fact that there is limited opportunity to cure or treat AMD, the effects of antioxidants as preventative agents have been investigated. Several longitudinal

studies of antioxidant protection against AMD have been carried out. These suggest beneficial effects of certain combinations of antioxidants. For example, the Age-Related Eye Disease Study (AREDS) showed that combined high dose vitamins C and E and β-carotene, in conjunction with zinc, reduced the probability of developing advanced AMD. However, this was only observed in a subgroup of participants with the highest risk of progression to advanced AMD (i.e. extensive intermediate drusen, large drusen, or non-central geographic atrophy in one or both eyes, or advanced AMD or vision loss due to non-advanced AMD in a single eye). Subjects with earlier or later stages of AMD did not appear to benefit (AREDS Research Group, 2001; Bartlett and Eperjesi, 2003). The Carotenoids in Age-Related Eye Disease Study (CAREDS) has also shown possible protective effects against AMD in certain age groups of women with diets supplemented with lutein and zeaxanthin (Moeller *et al.*, 2006). It is important to note in studies using carotenoids, however, that β-carotene has been shown to have a detrimental effect in smokers, increasing the risk of lung cancer and cardiovascular disease (Omenn *et al.*, 1996). A further study (AREDS2) is currently being undertaken to investigate the effects of dietary supplementation with lutein, zeaxanthin and omega-3 LC-PUFAs on development of AMD, and whether β-carotene and zinc – used in the original AREDS study – are in fact necessary (Huang *et al.*, 2008)

1.4 Docosahexaenoic acid

1.4.1 DHA structure, synthesis and distribution

DHA is a long chain polyunsaturated omega-3 fatty acid (22:6n-3; Figure 1.5) found in abundance in animal tissues, with particularly high levels in the brain and retina (Tinoco, 1983). It is required for development and normal function of tissue, particularly of the nervous system and retina, but it is not synthesized *de novo* in humans or other animals due to the inability to synthesize the n-3 structure (Yamanaka *et al.*, 1980; Tinoco, 1983). DHA must, therefore, be taken up directly from the diet (e.g. from oily fish) or it may be synthesized from the plant-derived dietary precursor α-linolenic acid (18:3n-3), by the actions of elongase and desaturase

enzymes in the liver (Tinoco, 1983; Scott and Bazan, 1989; Nakamura and Nara, 2003; Das, 2006).

Dietary DHA or DHA converted from α-linolenic acid is released from the liver into blood lipoproteins and transported to the brain and retina where it is selectively taken up and incorporated into cell membranes (Scott and Bazan, 1989; Wang *et al.*, 1992; Bazan *et al.*, 1993). In rod outer segments, LC-PUFA make up approximately 50% of total membrane fatty acids. Approximately 80% of these are accounted for by DHA, which is the dominant fatty acid in both phosphatidylserine and phosphatidylethanolamine (Fliesler and Anderson, 1983; Wang and Anderson, 1992). The presence of multiple double bonds in DHA makes it extremely susceptible to peroxidation – especially in the pro-oxidant conditions found in the retina. This process is discussed in greater detail below.
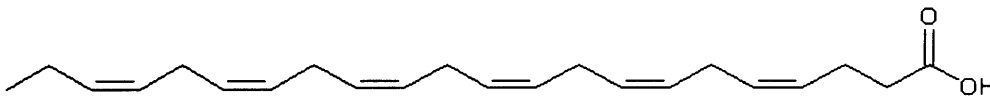
Figure 1.5 *Chemical structure of DHA (22:6n-3) demonstrating the 22 carbons, 6 cis double bonds and n-3 conformation.*
(From: http://www.neuroinformation.org/about_this_site.htm)

1.4.2 DHA insertion into POS membranes

The RPE plays two important roles relating to DHA levels in the rod POS – it allows transport of new DHA (from diet or the liver) from the choriocapillaris to the photoreceptors to be incorporated into newly formed discs, and it recycles DHA from phagocytosed POS and returns it to photoreceptor cells (Wang and Anderson, 1992; Bazan *et al.*, 1993). Uptake of new DHA into POS functions predominantly to establish the high disc concentrations of DHA during development of the POS. In the mature retina most POS DHA is obtained from the RPE mediated recycling process, but some of this DHA may be lost by β-oxidation or peroxidation, necessitating further uptake of new DHA from the diet (Wang and Anderson, 1992). This loss of DHA, however, occurs very slowly in normal circumstances so prolonged dietary

deprivation of n-3 fatty acids would be needed to significantly reduce retinal DHA content (Mukherjee *et al.*, 2004).

1.4.2.1 DHA uptake from blood

DHA levels in the RPE are higher than circulating blood levels but much lower than in POS. This is due to a mechanism which allows the RPE to selectively take up DHA from plasma lipoproteins from the choriocapillaris. It may then accumulate transiently in RPE oil droplets, and/or be released into the interphotoreceptor matrix before being taken up by photoreceptor cells. (Wang and Anderson, 1992; Bazan *et al.*, 1993; Gordon and Bazan, 1993). The mechanism of uptake is not currently known but appears to occur *via* a lipid uptake mechanism which is specific for carbon chain length and level of unsaturation, as other fatty acids are not taken up at the same rate. Because this uptake is so selective, it may involve a specific carrier protein, rather than passive diffusion of DHA through the lipid bilayer (Wang and Anderson, 1992; Wang *et al.*, 1992).

1.4.2.2 RPE mediated recycling of DHA

Similar to the experiments described above which tracked movement of proteins from insertion into the POS up to phagocytosis by RPE cells, DHA movement has been visualized using [^{3}H]DHA (Gordon and Bazan, 1990; Gordon *et al.*, 1992; Gordon and Bazan, 1993). In these experiments, DHA is shown to be taken up by rod photoreceptors and initially localized in the inner segments. Some is transported to synaptic terminals, and a small amount spreads diffusely throughout the POS. The majority, however, accumulates at the base of the outer segments where it is incorporated into newly formed POS discs and can be seen to migrate along the length of the POS. It is then taken up by the RPE as the POS tips are phagocytosed (Gordon and Bazan, 1990).

Studies in the frog have shown that DHA is released from phagocytosed POS membranes. Some DHA is then incorporated into phospholipids but the majority is rapidly esterified into newly synthesized triglycerides (TG). Because of the large amount of DHA released in POS phagocytosis, this results in an increase in cellular lipids and formation of oil droplets, containing predominantly TG, which act as a fatty

acid reservoir. This storage process also protects DHA from oxidation and release into the choriocapillaris (Chen and Anderson, 1993b,a). *In vitro* studies using rat RPE cells have shown synthesis of DHA-TG after phagocytosis (Rodriguez de Turco *et al.*, 1999). However, there appeared to be no increase in accumulation of DHA-TG in *in vivo* studies (Baker *et al.*, 1986), leading to speculation that although cells are capable of producing TG, in the normal situation, DHA is preferentially exported from RPE cells, either to the liver or to be returned to photoreceptor outer segments (Baker *et al.*, 1986; Rodriguez de Turco *et al.*, 1999). Incorporation of DHA into TG differs from the processing of arachidonic acid (AA). This LC-PUFA is also taken up by RPE cells but is incorporated into TG at a slower rate, and by fatty acid exchange rather than synthesis of new TG. This difference could explain how DHA is preferentially taken up and enriched in the photoreceptor POS, while other PUFA are not (Chen and Anderson, 1993b).

1.4.3 Normal role of native DHA

DHA has several important functions in the retina. It appears to be essential for development of photoreceptor cells – addition of DHA to immature photoreceptor cells in culture leads to enrichment of DHA in phospholipids, and enhanced differentiation of these cells. This was shown by increased opsin expression and advancement of formation of apical processes, which later form the outer segments (Rotstein *et al.*, 1998). DHA-enriched phospholipids and rhodopsin are both formed in the endoplasmic reticulum in the inner segment of photoreceptors and are co-transported to the POS for formation of new discs (Rodriguez de Turco *et al.*, 1997).

DHA also appears to be essential for normal function of rhodopsin in the visual response, as DHA deficiency causes a decrease in rhodopsin activation, and also a decrease in downstream protein interactions in the rhodopsin G-protein mediated cascade that normally occur to produce photoreceptor cell hyperpolarization and the visual signal (Niu *et al.*, 2004). DHA appears to interact directly with rhodopsin, altering local membrane properties and, in doing so, enhancing activation kinetics of rhodopsin. In contrast, cholesterol and saturated fatty acids appear to have the opposite effect due to their effects on membrane properties (Litman *et al.*, 2001; reviewed in Stillwell and Wassall, 2003; Grossfield *et al.*, 2006). In dietary deficiency

of DHA and other n-3 fatty acids, these are eventually replaced by n-6 docosapentaenoic acid which is less flexible and has been thought to affect the function of integral membrane proteins, and their movement within the membrane (Eldho *et al.*, 2003). DHA is also able to protect photoreceptor cells from oxidative stress-induced apoptosis, seemingly *via* a different mechanism, by acting as a trophic factor and causing upregulation of Bcl-2 to inhibit apoptosis *via* the mitochondrial pathway (Rotstein *et al.*, 2003).

In addition to these direct effects of DHA, cells may also be protected indirectly by a DHA-derived mediator, 10,17S-docosatriene (neuroprotectin D1; NPD1). NPD1 is produced in the RPE by a lipoxygenase-type enzyme from DHA previously released from the membrane by phospholipase A_2 (PLA_2), and appears to be able to modulate signalling pathways responsible for cell survival, thereby reducing oxidative-stress-induced apoptosis (Mukherjee *et al.*, 2004). In fact, NPD1 has been shown to protect cells from A2E-induced damage, and it is also involved in the signalling pathway of PEDF, which upregulates its synthesis and release from RPE cells (Mukherjee *et al.*, 2007a).

In vivo studies of dietary intake or supplementation with DHA have also shown beneficial effects. Stereoacuity appears to be improved in infants when maternal pre-natal diet was high in oily fish and DHA, and in those infants who were breastfed, apparently due to increased DHA intake compared with non-breastfed infants (Williams *et al.*, 2001). Benefits have also been shown in neurological function of breastfed or dietary DHA-supplemented infants compared with non-supplemented formula fed infants (Salem *et al.*, 2001).

Several animal studies on DHA deficiency have been carried out but it has been found that a significant decline in neural DHA requires more than one generation of dietary deprivation, with a reduction of 50-80% required for impairment of neural function (Salem *et al.*, 2001).

Studies have also indicated broader roles for n-3 LC-PUFA, in protecting against colorectal cancer mortality in males, possibly through alterations of prostaglandin signalling pathways (Caygill and Hill, 1995). Overall, however, studies on the

preventative effects of n-3 fatty acids against cancer and in protection against cardiovascular disease show conflicting results (Hooper *et al.*, 2006).

1.4.4 DHA peroxidation

Lipid peroxidation is known to occur in situations of oxidative stress. In the past, many studies have been carried out on peroxidized metabolites of AA as this fatty acid is found in abundance in many tissues. It has been found that measurement of AA metabolites can give an accurate measurement of levels of oxidative stress, and that some of these metabolites actually have a distinct biological effect and can act as mediators of oxidative injury (Morrow and Roberts, 1997). The similarities between the structure of AA and DHA – they are both long chain polyunsaturated fatty acids – and the more specific localization of DHA in neural and retinal tissue, suggests that DHA metabolites could be used to specifically measure oxidative stress in these tissues, and that they may also have downstream pathological effects on the tissue (Reich *et al.*, 2000; Musiek *et al.*, 2004).

LC-PUFA, such as DHA, are particularly susceptible to peroxidation due to the multiple carbon-carbon double bonds. The process of lipid peroxidation is detailed in Figure 1.6. Singlet oxygen reacts with the double bonds in PUFA, resulting in lipid hydroperoxide formation (Foote and Clennan, 1995). For initiation of the peroxidation cascade, these hydroperoxides must first be decomposed by metal ions, to produce alkoxyl radicals. Alternatively, free radicals can cause hydrogen abstraction from lipid molecules, forming carbon-centred radicals. The bond energy of hydrogen to the lipid carbon atom is weaker in the presence of double bonds, particularly in the case of double bonds on both sides of the carbon (i.e. bis-allylic hydrogen), as is the case in DHA with its 6 double bonds, making it highly oxidizable compared with more saturated fatty acids (Wagner *et al.*, 1994). The rapid reaction of oxygen with the lipid radical allows propagation of the cascade as the newly formed peroxyl radical reacts readily with further unoxidized lipids, and thus the cycle continues until a termination step is provided (Buettner, 1993; Walling, 1995).

Termination involves either production of non-radical products through coupling with other radicals, or through hydrogen abstraction from another compound by the lipid

radical to give a non-radical lipid species and a new radical of the other compound which is less reactive (Porter et al., 1995; Yin and Porter, 2005).
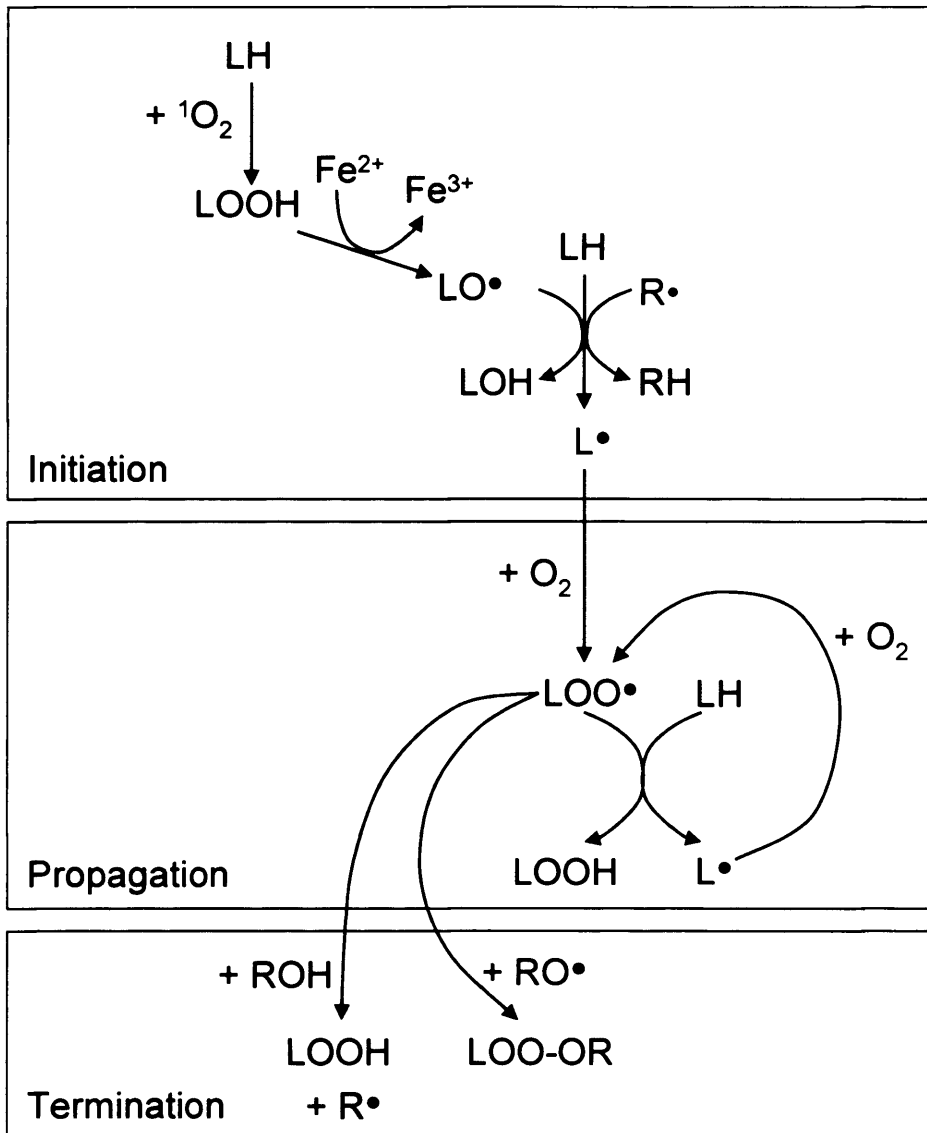
Figure 1.6 *Simplified diagram of the stages of lipid peroxidation: initiation by singlet oxygen or free radicals, propagation, and termination. L = lipid; R = other molecule; L•/R• = lipid/other radical; $^1O_2$ = singlet oxygen; H = weakly bonded hydrogen atom; LOOH lipid hydroperoxide; LO•/RO• = alkoxyl radical; LOO• = lipid peroxyl radical.*

In addition to the cyclic propagation of lipid peroxidation described above, oxidized PUFA may undergo further structural and chemical changes. Initially, after hydrogen abstraction and oxygen addition to the carbon-centred lipid radical, rapid double-bond rearrangement leads to conjugated diene formation (Porter et al., 1995). Possible further reactions of the lipid radicals include cyclization, reduction, further oxidation

and scission (Porter *et al.*, 1995; Bernoud-Hubac and Roberts, 2002; Yin and Porter, 2005). Different peroxidation products which may be produced from DHA include neuroprostanes (NPs) with different ring conformations (A_4 and J_4), (Fam *et al.*, 2002), and highly reactive neuroketals (γ-ketoaldehydes) by rearrangement of intermediates of the NP pathway (Bernoud-Hubac *et al.*, 2001). Additionally, a number of truncated phospholipids are produced by free radical-induced cleavage of DHA phospholipids (Gu *et al.*, 2003b). Due to the number of sites where hydrogen abstraction and downstream reactions can occur on DHA, the non-specific nature of autoxidation results in formation of a large, complex mixture of products and isomers thereof, as indicated in Figure 1.7 (Porter *et al.*, 1995; Walling, 1995; Yin *et al.*, 2005).
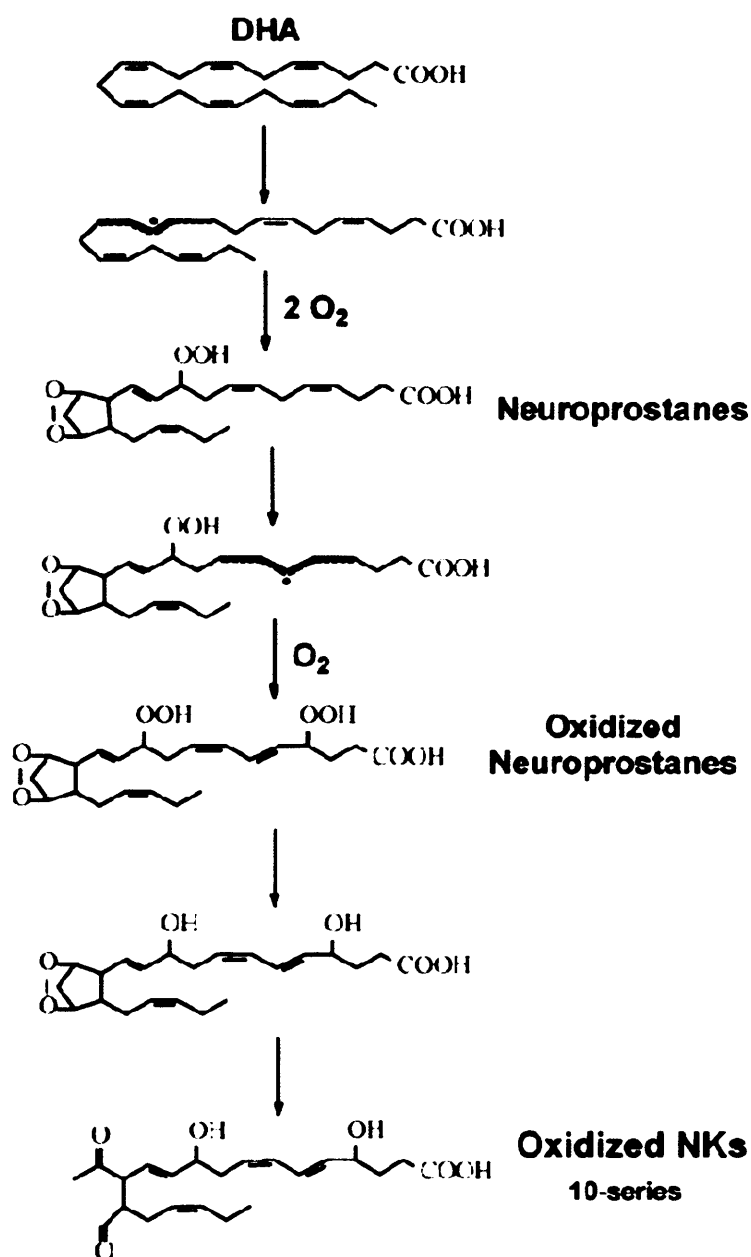
Figure 1.7 *Simplified scheme of the chain of peroxidation products of DHA, indicating the families of products which may be formed after initial radical formation, followed by multiple additions of molecular oxygen, with an end-point of neuroketal (NK; a γ-ketoaldehyde derived from DHA) formation (Bernoud-Hubac and Roberts, 2002). Many more products are possible depending on the precise location of the initial radical formation and subsequent oxygen addition.*

1.4.5 Biological effects of non-enzymatic lipid peroxidation

1.4.5.1 Effects of lipid peroxidation in general

Various studies have been carried out in the past to study the direct effects of different lipid peroxidation products on RPE cells. These have included exposure of cells to the polyunsaturated fatty acid linoleic acid and its hydroperoxides, with hydroperoxides shown to be toxic, causing damage to lysosomes, and leading to formation of undegradable intracellular granules (Akeo 1996). Exogenous lipid hydroperoxides are also able to cause peroxidation of mitochondrial membranes *in vitro* (Terrasa *et al.*, 2003). Sub-retinal injection of linoleic acid hydroperoxides can result in neovascularization as described above, but at higher concentrations they are also directly toxic to RPE and photoreceptor cells (Tamai *et al.*, 2002).

Lipid peroxidation products may also have an indirect effect on cell viability by causing increased lipofuscin accumulation. This is thought to occur due to interactions with other molecules including proteins – in particular, through Schiff's base interactions – which may result in undegradable material. Lipid aldehydes may also act as second messengers, to transmit oxidative damage (reviewed in Esterbauer *et al.*, 1991). In summary, there are many possible ways in which lipid peroxidation products may cause damage or interfere with normal cell function.

1.4.5.2 Specific effects of peroxidized DHA

As native (unperoxidized) DHA has many beneficial and essential functions, an immediate effect of peroxidation would be loss of these functions. Additionally, products of non-enzymatic peroxidation of DHA have several specific detrimental effects.

Products of DHA peroxidation have been shown to mediate photo-induced oxygen uptake, and singlet oxygen and hydroxyl radical generation *in vitro* (Rozanowska *et al.*, 2002b).

Neuroprostanes, like isoprostanes, are formed while DHA is esterified in phospholipids. They can then be released by PLA_2 (Reich *et al.*, 2000). While still

32

attached to the phospholipids, neuroprostanes may have an important effect on membrane fluidity and function (Fam *et al.*, 2002), which could alter the function of membrane proteins such as rhodopsin which, as discussed above, are reliant on interaction with DHA. It has been found that A_4/J_4 neuroprostanes readily conjugate to glutathione, which would rapidly inhibit the negative effects of these reactive compounds, but when they are present in high concentrations, it could result in depletion of cellular glutathione and perhaps other antioxidants (Fam *et al.*, 2002).

Neuroketals have been shown to rapidly form lysine adducts in a pathway similar to that of isoketals (the peroxidized AA equivalent metabolite), with initial reversible formation of Schiff's base adducts, followed by irreversible formation of pyrroles, then lactam or hydroxylactam products (Bernoud-Hubac *et al.*, 2001). This may result in similar downstream effects to that of isoketal-protein adducts which have been shown to inhibit normal membrane protein function (Brame *et al.*, 2004), and inhibit proteasome function, which could explain the formation of lipofuscin (Davies *et al.*, 2002). Reactive aldehyde products such as 4-hydroxy-2(*E*)-hexenal (4-HHE) are also known to interact with proteins and also amine groups on phosphatidylethanolamine (Bacot *et al.*, 2003; Bacot *et al.*, 2007). Additionally, CEP-protein adducts are found in drusen, and apparently have a pro-angiogenic effect (Ebrahem *et al.*, 2006). These adducts with proteins could form products which are resistant to lysosomal degradation, which has important implications for the POS phagocytosis process. They may also be involved in oxidative damage in the retina which is rich in DHA and its degradation products (Crabb *et al.*, 2002; Gu *et al.*, 2003a; Kawai *et al.*, 2006).

1.5 Summary

This introduction has summarised the importance of the RPE in helping to maintain normal function of retinal photoreceptors and, therefore, the visual response. It is easy to understand, therefore, how dysfunction of the RPE which occurs in age-related macular degeneration could lead to loss of photoreceptor function and downstream loss of vision.

The full mechanisms of this pathway, such as the specifics of lipofuscin formation and molecules which cause its toxicity, are not yet fully understood. A greater understanding is therefore vital to better understand the disease process and potentially develop therapeutic or preferably preventative measures to reduce the prevalence of AMD.

DHA has many beneficial and essential functions in the retina, particularly in the photoreceptor outer segments. Loss of these functions by peroxidation of DHA could in itself result in important detrimental effects. However, DHA is present in high concentrations and recycled fairly quickly through the POS disc-shedding process, such that this may only form a minor pathway of cell dysfunction. More important, perhaps, are the various peroxidized DHA metabolites which appear to have similar deleterious effects to some AA metabolites in other tissues, and may, therefore, cause direct damage to both photoreceptor and RPE cells.

1.6 Aims of this project

The overall aim of this project is to gain insights into the effects of DHA peroxidation products on RPE cell function and lipofuscin formation, and of its possible role in age-related RPE dysfunction. To achieve this, the study is divided into several specific objectives:

- determine the susceptibility of DHA to oxidation under physiologically relevant conditions, in preparation for experiments with cultured cells,

- investigate the effects of peroxidized DHA (pDHA) on RPE cell function and viability, and identify the pathway of cell death involved (i.e. apoptosis vs. necrosis)

- investigate whether selected antioxidants and detoxifying agents can protect RPE cells from pDHA toxicity

- examine the mechanisms by which PE protects from pDHA (photo)toxicity by monitoring reactive oxygen species production in its presence

- study the effects of pDHA on lysosomal integrity and enzyme activity

- determine the effect of pDHA on levels of accumulation of fluorescent material and lipofuscin-like granules

It is hoped that these investigations will help to develop a greater understanding of the initial processes which may be involved in the development of age-related macular degeneration and related blindness.

Chapter 2:
Materials and methods

2.1 DHA peroxidation

All experiments in this thesis which involved the use of DHA used this fatty acid as a component of phospholipids in the form of 1,2-didocosahexaenoyl-*sn*-glycero-3-phosphocholine, not as the free fatty acid form. For simplicity, it is referred to as DHA throughout.

2.1.1 Liposome preparation

A lipid film of DHA, as 1,2-didocosahexaenoyl-*sn*-glycero-3-phosphocholine (Avanti Polar lipids, Alabaster, AL, USA; cat # 850400C; supplied in chloroform), was formed using a rotary vacuum evaporator (Büchi, Flawil, Switzerland). The sample flask was maintained at 37 °C and rotated under argon (Pureshield, BOC, UK), and the pressure was gradually decreased to 40 mbar as the solvent evaporated. To ensure the lipid film was dry and solvent-free, waste chloroform was removed from the system, and the pressure was again reduced to 40 mbar then left for 90 minutes (dark, under argon, room temperature, no rotation). To form liposomes, phosphate buffered saline (PBS) was added gradually to the flask containing the lipid film, and the film was rehydrated using a combination of rotation, vortexing and warming to 37 °C. The final DHA concentration was 50 mM. Samples that were to be kept unperoxidized were saturated with argon for at least 30 minutes to remove air/oxygen then stored under argon at -80 °C. To ensure formation of uniformly-sized liposomes, freshly prepared liposomes were put through 5 freeze/thaw cycles (frozen in liquid nitrogen then thawed in a 37 °C water bath).

Prior to use in experiments with cultured cells, liposomes were extruded using a Liposofast 100J extruder (Glen Creston, UK) with two 200 nm filters, powered by compressed argon, to ensure sterility.

2.1.2 DHA peroxidation

DHA films or liposomes to be peroxidized were left on a heating block at 37 °C, in the dark, with containers opened weekly to allow replenishment of oxygen. To ensure that peroxidation occurred as evenly as possible within each liposome

batch, equal aliquots were put into identical tubes. The lipid film was kept in a dry environment on the inner surface of a spherical rotary evaporator flask. After peroxidation, the lipid film was made into liposomes and analysed and used as for the other liposomes. Progress of peroxidation was monitored by extracting lipids from the liposome suspension then measuring decay of native lipid and formation of oxidation products using absorption and fluorescence spectroscopy, with or without initial high performance liquid chromatography (HPLC) separation (Kim and LaBella, 1987). These processes are described in greater detail below.

In total, 3 sets of lipids were allowed to peroxidize: two sets were peroxidized as liposomes, and one was peroxidized as a lipid film and subsequently made into liposomes. The first batch of liposomes and the film were allowed to peroxidize simultaneously for a total of 175 days. The second batch of liposomes was peroxidized for 18 days.

The first batch of liposomes (peroxidized for 175 days) was used for monitoring the time-course of lipid peroxidation by absorption spectroscopy, and formation of fluorescent products. Lipids peroxidized as a dry film were used to produce liposomes and were subsequently used for all the DHA phototoxicity experiments in Chapter 4 and lysosomal enzyme activity assays in Chapter 7. Finally, the second batch of liposomes (peroxidized for 18 days) was used for experiments with antioxidants (all experiments in Chapters 5 and 6), and other phagocytosis and lysosomal function experiments (all experiments in Chapter 7 except for enzyme activity assays).

Concentrations of pDHA stated in methods and results sections below indicate starting DHA concentration. i.e. "2 mM pDHA" indicates 2 mM of DHA which has been allowed to peroxidize.

2.1.3 Monitoring of peroxidation

2.1.3.1 Extraction of lipids

Lipids were extracted from liposomes using a modified Folch's procedure (Folch *et al.*, 1957; Rozanowska *et al.*, 2004): 0.5 ml liposome suspension in PBS (50 mM DHA) was added to 0.8 ml chloroform/methanol (2:1 v/v; both Fisher Scientific, UK) and vortexed briefly, then centrifuged. This resulted in formation of an upper polar phase enriched with methanol/PBS, and a lower chloroform-enriched phase, as shown in Figure 2.1. The two phases were removed and analysed separately. Although these phases are likely to be slightly contaminated with components of the other phase (i.e. small amounts of chloroform in the upper phase and methanol and water in the lower phase), they are referred to from this point as the "methanol/PBS" and "chloroform" phases, to indicate the predominant solvents present.
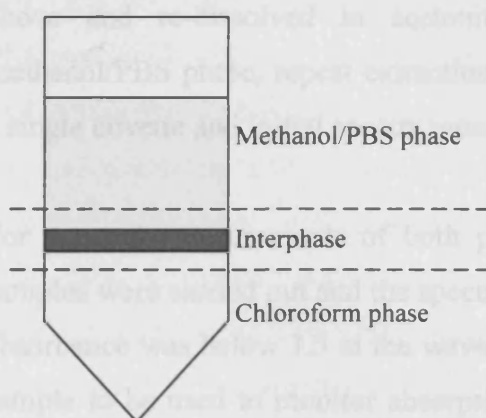
Figure 2.1 *Diagrammatic representation of the layers formed in chloroform/ methanol extraction of highly peroxidized pDHA liposomes.*

2.1.3.2 UV-visible absorption spectroscopy

For sample components solubilized in the chloroform phase, 2 ml of chloroform were added to 450 µl of extracted sample and absorption spectra measured in a quartz cuvette with a 1 cm path length for wavelengths from 200 to 700 nm (U-2800 UV-VIS Spectrophotometer (Hitachi) with Hitachi UV Solutions software). Chloroform was then evaporated off by passing argon gas over the sample while

heating to 37 °C on a heating block in the dark. The dried lipid film was then dissolved in 2 ml acetonitrile (Aldrich, UK) + 100 µl methanol, and spectra measured. Methanol/PBS phase samples (500 µl) were initially diluted in 2 ml methanol + 250 µl PBS for measurement of spectra.

When removing extracted samples as described above, a small amount of each phase was left in the tube to prevent contamination from the other phase during removal. To maximize the total amount of sample extracted, repeat extractions were carried out for certain experiments (as stated in results below): the appropriate volume removed from each phase was replaced with "clean" methanol/PBS or chloroform phases obtained by mock extraction of PBS using the same method described for liposomes above (i.e. using PBS instead of liposome suspension). Samples were vortexed and centrifuged again, further samples removed, then the process was repeated. For spectral measurements after repeat extraction of the chloroform phase, the samples were dried under argon as above and re-dissolved in acetonitrile + methanol (20:1, v/v). For the methanol/PBS phase, repeat extraction samples (500 µl each) were combined in a single cuvette and initial spectra measured without further addition of solvent.

For spectral measurements of both phases, multiple 1 in 10 dilutions of the samples were carried out and the spectra re-measured to ensure the upper limit of absorbance was below 1.5 at the wavelengths of interest. This allowed the same sample to be used to monitor absorption at >400 nm (in the more concentrated samples), and to monitor the upper limit of the remaining unperoxidized DHA and formation of markers of peroxidation in more dilute samples.

Baseline measurements were carried out by the spectrophotometer across the same spectrum for each of the relevant solvents to allow automatic background subtraction. The solvents used consisted of: fresh solvents (either chloroform or 20:1 acetonitrile/methanol as appropriate) for samples extracted in the chloroform phase, and an aliquot of the methanol/PBS phase from "mock" PBS extraction for spectral measurements of the extracted methanol/PBS phase.

2.1.3.3 Fluorescence spectroscopy

Fluorescence emission spectra were measured using a F4500 Fluorescence Spectrophotometer (Hitachi) with Hitachi FL Solutions software. Samples were excited at wavelengths selected from peaks in the absorption spectra (i.e. 230 and 270 nm) and also the wavelength commonly used to measure fluorescence properties of oxidized lipids and lipofuscin (360 nm) (Gutteridge et al., 1982; Kim and LaBella, 1987). Emission intensity was monitored over a spectrum of wavelengths starting above the excitation wavelength. For all measurements, samples were used at a suitable dilution where absorbance was ≤0.1 (1 cm pathlength) at the excitation wavelength. Solvent backgrounds were measured separately. Spectra were not corrected for variations in photomultiplier sensitivity over the spectral range in the spectrophotometer.

2.1.3.4 High performance liquid chromatography

For analysis using HPLC, DHA fatty acids were hydrolyzed from the phospholipid headgroup (DeMar et al., 1996). After repeat chloroform/methanol extractions and drying under argon, samples were saponified by re-suspending in 2 ml of argon-saturated potassium hydroxide in ethanol, and heating at 100 °C for 30 minutes. After cooling to room temperature, 1 ml of argon-saturated dH_2O and 100 µl of concentrated hydrochloric acid were added. The free fatty acids were extracted twice with 3 ml of argon-saturated hexane and dried under argon. Samples were then solubilized in 3:1 methanol/acetonitrile (v/v), filtered using Vectaspin micro filters (0.45 µm, polypropylene; Whatman, UK), then analysed by reverse phase HPLC using a Waters 2695 Separations Module with Millennium[32] software (Waters, UK). Separation was carried out isocratically using an Ace 5 C8 column (150 x 4.6 mm, 5 µm particle size; Hichrom Limited, UK), with mobile phase consisting of acetonitrile/HPLC-grade water/HCl (90/10/0.05%, v/v/v) at a flow rate of 1 ml.min^{-1}. The elution profile was monitored using a Waters 996 Photodiode Array Detector (Waters). Prior to running samples, the column was equilibrated with mobile phase solvent until absorption of the eluent at 210 nm stabilized, then 10 µl of sample was injected, and elution monitored for 10 minutes at 190-600 nm.

2.1.4 Preparation of lipid samples containing antioxidants

To produce liposomes containing pDHA and lipophilic antioxidants, previously peroxidized pDHA liposomes were extracted by the modified Folch's method described above. After addition of selected antioxidants (described below), the lipid-antioxidant mixtures were dried using a rotary evaporator. Liposomes were then produced by hydration with Dulbecco's PBS (D-PBS; GIBCO), and saturated with argon for 20 minutes and put through 5x freeze/thaw cycles prior to use. Samples were stored at -80 °C under argon.

2.1.4.1 Zeaxanthin and α-tocopherol

Zeaxanthin (a generous gift from DSM Nutritional Products (Switzerland)), was solubilized in ethanol and absorbance at 454 nm measured to calculate the concentration using the molar absorption coefficient of $1.52 \times 10^5 \, M^{-1}.cm^{-1}$ (Wrona *et al.*, 2004). α-Tocopherol (Sigma) was weighed and solubilized in chloroform. Antioxidants in their respective solvents were then added to the extracted pDHA.

Alternatively, zeaxanthin was added to liposomes immediately prior to cell exposure by making a stock solution in dimethyl sulfoxide (DMSO; Sigma), and adding this directly to pDHA liposome solutions. In these experiments, all wells contained 0.2% (v/v) DMSO either as a solvent for zeaxanthin or as a carrier control.

2.1.4.2 Phosphatidylethanolamine

Phosphatidylethanolamine (PE) as 1-palmitoyl-2-oleoyl-*sn*-glycero-3-phospho-ethanolamine (POPE; Avanti Polar lipids, USA; cat # 850757c; supplied in chloroform), was added directly to extracted pDHA lipids. 1-Palmitoyl-2-oleoyl-*sn*-glycero-3-phosphocholine (POPC; Avanti Polar lipids, USA; cat # 850457c) was used as a control in these experiments, with liposomes formed as for POPE.

2.1.4.3 Glutathione, glutathione *S*-transferase and *N*-acetylcysteine

Solutions of glutathione (GSH; Sigma), glutathione *S*-transferase (GST; equine liver; Sigma) and *N*-acetylcysteine (NAC; Sigma) were prepared in D-PBS and added to pDHA liposomes immediately prior to cell exposure, either individually or in combination.

2.2 Cell culture

The ARPE-19 cell line (American Type Culture Collection (ATCC), through LGC Promochem, UK), a human RPE cell line, was used to test the effects of pDHA and rose bengal.

2.2.1 Standard cell culture

Cells were grown in a 1:1 mixture of Dulbecco's modified Eagle's medium and Ham's F12 medium (DMEM:F12; GIBCO, UK). This medium was supplemented with antibiotics (100 μg.ml^{-1} streptomycin, 100 μg.ml^{-1} kanamycin and 60 μg.ml^{-1} penicillin; Sigma, UK), Fungizone (1.25 μg.ml^{-1} Amphotericin B; GIBCO), and 10% v/v heat-inactivated fetal calf serum (FCS; Bio-West, UK) until the cells reached confluence (after approximately two days). FCS was then reduced to 2% until cells were required for experiments. Cells were maintained at 37 °C in a humidified incubator containing 5% CO_2 and 95% air, and medium was changed every 3 days. Cell populations were initially built up in 75 cm^2 flasks, then split into 25 cm^2 flasks, or 12- or 24- well plates as required for experiments.

To subculture cells, culture medium was aspirated and cells were rinsed with sterile PBS. Cells were detached by adding 0.25% (w/v) trypsin + 0.02% EDTA (both Sigma) in PBS and incubating at 37 °C for 2 minutes. Trypsin was then deactivated by adding growth medium with 10% FCS, and cells were transferred to new flasks or multi-well plates (at an approximate surface area ratio of 1:3).

2.2.2 Long-term storage

For storage, cells were trypsinized as described above. After addition of medium with 10% FCS, cells were transferred to 15 ml centrifuge tubes and centrifuged at $700 \times g$ for 5 minutes. The supernatant was removed and cells were re-suspended in FCS with 10% v/v dimethylsulphoxide (DMSO; Sigma). Cells were then put in cryovials and frozen, initially in an isopropanol cryostorage box at -80 °C before being transferred to liquid nitrogen storage.

2.2.3 Confirmation of cell identity

An antibody against cytokeratin 18, a protein expressed by RPE cells both *in vivo* and *in vitro* (McKechnie *et al.*, 1988; Hunt and Davis, 1990) was used to positively identify cells used here as RPE cells, rather than any of the non-epithelial neuronal cell types present in the retina, which would not express this marker.

Cells were grown on sterile glass coverslips in 24-well plates until nearly confluent. Medium was aspirated and the cells were washed with PBS. The cells were fixed by immersion in 70% ethanol for 5 minutes, followed by PBS washes, then permeabilized with 0.1% Triton X-100 (v/v in PBS; Sigma) for 10 minutes and washed again with PBS. Cells were then incubated simultaneously with anti-cytokeratin 18 antibody (FITC conjugated; Sigma F4772) at a 1:100 dilution in PBS, and Hoechst 33342 (bisBenzamide; Sigma), which stains AT-rich regions of double-stranded DNA and should therefore label nuclei of all cells (3 μg.ml^{-1} final concentration in the antibody solution). Incubation was carried out for 2 hours in the dark. After washing with PBS, coverslips were mounted on slides in Hydromount (National Diagnostics) and slides were stored (4 °C, dark) until required. Cells were visualized using appropriate filters (Hoechst: 340-380 nm excitation, 450-490 nm emission; cytokeratin-FITC: 450-490 nm excitation, >515 nm emission) on a Leica DMRA2 upright microscope, and images obtained using a Leica DC500 CCD camera and Leica QFluoro software (Leica, UK).

2.3 Exposure of cells to (p)DHA or rose bengal, and light

Rose Bengal stock solution was made in D-PBS, and diluted further to concentrations between 0.05 and 1 μM as required. (p)DHA liposomes, previously prepared as a stock solution of 50 mM in PBS, were further diluted to required concentrations (see individual chapters) in D-PBS. ARPE-19 cells grown in either multi-well plates or 25 cm^2 flasks were rinsed twice with PBS, then (p)DHA liposomes or rose bengal were added.

Light exposure was carried out with a Sol lamp (Hönle UV Ltd, Birmingham; see Figure 2.2 for description of setup). Heat and UV filters (Lee Heat Shield and #226 Lee U.V. respectively; Lee Filters, UK) were placed above the lamp in all experiments. Additionally, a green filter was used for rose bengal experiments (#090 "dark yellow green" filter; Lee Filters, UK). Irradiance spectra of the light to which cells were exposed are shown in Figure 2.3.
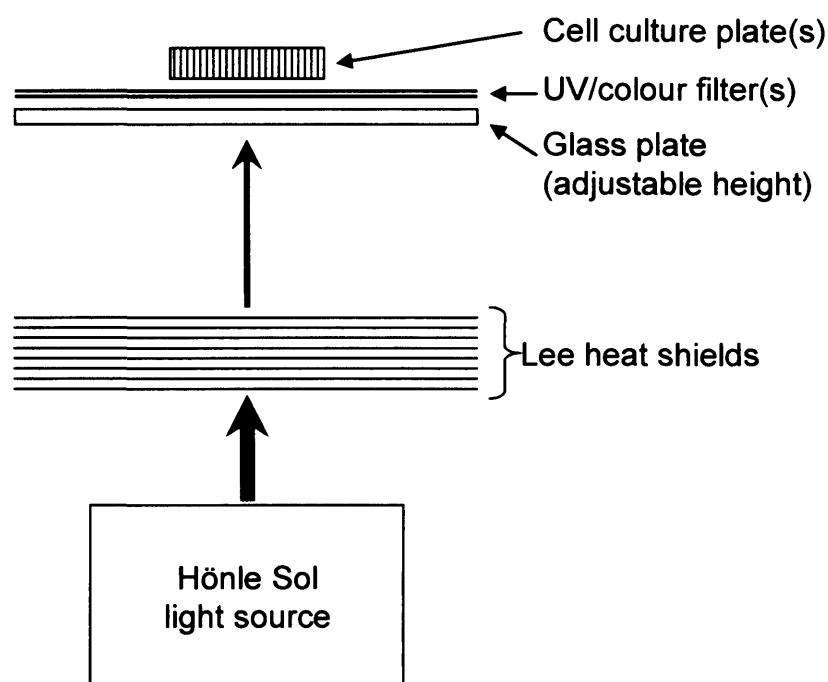
Figure 2.2 *Experimental setup for light exposure experiments, with cells illuminated from below. Irradiance and temperature measurements were taken at the position on the glass plate where the cell culture plates were subsequently put for each experiment.*

Plates or flasks were placed above the lamp for 1 hour. For dark experiments, plates were wrapped in black foil and placed above the lamp to mimic temperature and air conditions experienced by light-exposed cells. Silver foil was placed between the black foil and the glass plate to prevent excess heat absorption. Spectral irradiance of the light source between 380 and 780 nm was measured in each experiment using a handheld spectroradiometer (Specbos 1201 with JETI LiMeS software; Glen Spectra, UK) to ensure consistency. Temperature was also monitored. If required, the light intensity was altered initially crudely by adjusting the height of the glass plate relative to the lamp, then more subtly by adding individual UV filters to act as additional neutral density filters.

After 1 hour exposure, liposome or rose bengal solutions were aspirated, cells washed twice with D-PBS, then either used immediately for further experiments, or returned to the incubator with normal growth medium containing 2% FCS for a further incubation period prior to processing.
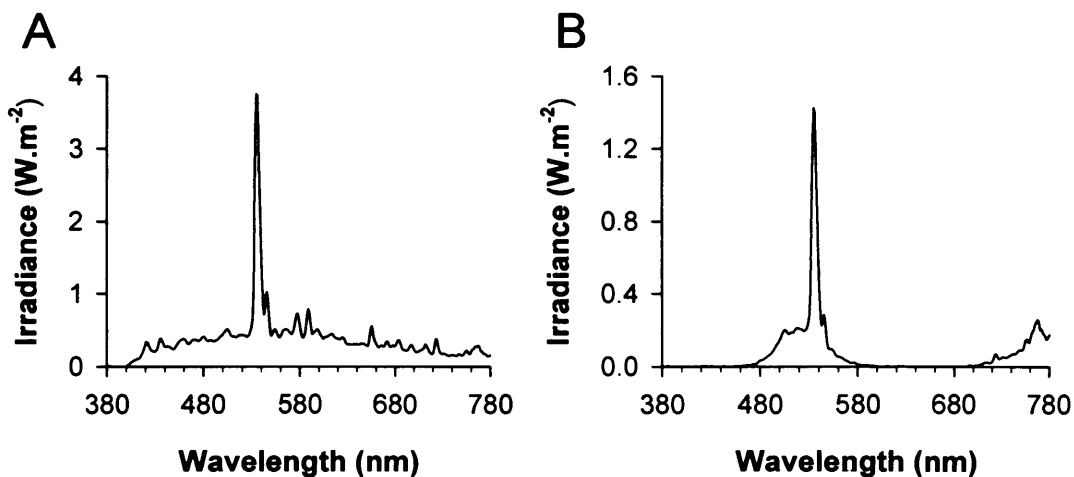
Figure 2.3 *Irradiance spectra of light to which cells were exposed. (A) White light with Lee UV and heat filters, adjusted to 15 mW.cm^{-2} for pDHA experiments. (B) Lee UV and heat filters with 090 "Dark Yellow Green" filter, to produce predominantly green light at 2.8 mW.cm^{-2} for rose bengal experiments.*

2.4 Cytotoxicity assays

2.4.1 Microscopy for cell morphology

Cells were visualized using an Olympus IX70 inverted microscope configured for phase contrast imaging, and images obtained using a Spot RT colour CCD camera and Spot Advanced software (Diagnostic Instruments Inc, UK).

2.4.2 MTT assay

3-(4,5-dimethylthiazol-2-yl)-2,5-diphenyl tetrazolium bromide (MTT) is reduced to formazan crystals by active mitochondria in living cells. Crystals can be dissolved and absorbance measured to provide a rapid assay of cell viability (Mosmann, 1983).

After exposure of cells to DHA or rose bengal in 24-well plates with or without post-incubation in fresh medium, cells were washed with PBS, and 250 µl MTT (Sigma; 0.5 mg.ml^{-1} in PBS) was added to each well. Plates were incubated at 37 °C for 1 hour. MTT solution was aspirated and formazan crystals dissolved by addition of 250 µl acidified isopropanol (isopropanol with 0.04 M HCl). Samples were transferred to 96-well plates and absorbance was measured at 590 nm in a microplate reader (Multiskan Ascent, Labsystems). Background measurements were carried out in cells exposed only to acidified isopropanol (i.e. no rose bengal/DHA, no MTT), or in later experiments, a reference filter at 690 nm was used, with absorbance values at this wavelength automatically subtracted off the absorbance at 590 nm.

For rose bengal experiments, which used multiple timepoints, mitochondrial viability after treatment was calculated as a percentage of control (i.e. 0 mM rose bengal from the same plate, and after identical incubation periods as the treated cells), after background subtraction. For pDHA experiments, mitochondrial

viability was calculated as a percentage of dark control (i.e. 0 mM pDHA in the dark-maintained plate of paired light/dark exposures).

2.4.3 Monitoring of membrane integrity

Propidium iodide (PI) can not normally cross the intact cell membrane of live cells, therefore, it is only taken up by cells showing loss of membrane integrity and is commonly used as a marker of necrotic cell death. Uptake could also indicate alteration in membrane structure or function due to direct interaction with peroxidized lipids. After entering the cell, PI binds to DNA thus labelling nuclei of cells with compromised membranes.

Following exposure to pDHA and light at 15 mW.cm^{-2}, cells were washed then labelled immediately, or put in fresh medium for 2 hours first then labelled. Cells were incubated for 15 minutes at 37 °C in 1 µg.ml^{-1} PI in PBS. Cells were co-labelled with 3 µg.ml^{-1} Hoechst 33342 to allow total cell numbers to be counted. Cells were washed and imaged immediately using the Olympus IX70 inverted microscope described above, using filter sets optimized for blue emission (for Hoechst; excitation: 330 – 385 nm; longpass emission filter: > 420 nm) and red emission (for PI; excitation: 510 – 550 nm; longpass emission filter: > 590 nm).

2.4.4 TUNEL assay for cleavage of DNA

One of the biochemical changes of apoptosis is the non-random cleavage of DNA into 180 base pair fragments. This cleavage results in exposure of free 3'-OH termini which can be enzymatically labelled with the TUNEL (Terminal dUTP Nick-End Labelling) assay (Gavrieli *et al.*, 1992).

TUNEL was carried out using the ApopTag® Plus Rhodamine *In Situ* Apoptosis Detection Kit (Chemicon International, USA), according to the instructions supplied with the kit. Cells were grown in 4-well chamber slides, and used after at least 1 week in 2% FCS medium. After exposure to pDHA +/- 15 mW.cm^{-2} light, cells were incubated in medium for 12 hours, then rinsed in PBS. Cells were then fixed in 1% paraformaldehyde for 10 minutes at room temperature,

then washed with PBS twice. Post-fixation was carried out with 2:1 ethanol:acetic acid for 5 minutes at -20 °C. After washing with PBS, equilibration buffer (supplied with kit) was applied for 10 seconds. This was removed and cells were incubated with working strength TdT enzyme (prepared according to kit instructions) for 1 hour at 37 °C. Working strength stop/wash buffer (from kit) was added and left to incubate for 10 minutes at room temperature after 15 seconds of agitation. Cells were washed with PBS, and working strength anti-digoxigenin-rhodamine conjugate (affinity purified sheep polyclonal antibody) was added and left for 30 minutes at room temperature, in the dark. Cells were again washed with PBS. Vectashield mounting medium containing Hoechst 33342 (to label all cell nuclei; 3 $\mu g.ml^{-1}$) was added and a coverslip applied. Cells were imaged using a Leica DMRA2 upright microscope and images obtained using a Leica DC500 CCD camera and Leica QFluoro software (Leica, UK).

2.5 Effects of PE on production of reactive oxygen species by pDHA

2.5.1 Singlet oxygen production

Photogeneration and decay of singlet oxygen was monitored by time-resolved detection of phosphorescence at 1270 nm by a nitrogen-cooled germanium detector (Applied Detector Co., Fresno, CA, USA) coupled to an Agilent digitizing scope (Infiniium 54830B DSO, Agilent, Santa Clara, USA) interfaced with a Risc computer (Acorn, Swadlincote, UK) (Rozanowska et al., 1998). Photoexcitation of the sample was induced by a 5 ns laser pulse at 420 nm from a Q-switched Nd:YAG laser (Continuum Surelite II; Santa Clara, USA) equipped with an optical parametric oscillator (Panther OPO; Continuum, Santa Clara, USA). Apparatus is shown in Figure 2.4. The laser intensity reaching the sample was reduced by insertion of neutral density filters into the light path. The transmission spectra of these filters were measured using a spectrophotometer to calculate the reduction in laser intensity caused by insertion of one or more filters into the light path.

Singlet oxygen decay was fitted to an exponential curve (excluding the initial contribution from laser scatter and fluorescence), extrapolated to time zero (corresponding to the laser pulse) to calculate initial emission intensity as a function of laser intensity (see Figure 2.5). The relative laser energy of each pulse was measured by a photodiode (positioned before the neutral density filters) and used to normalize the emission intensity values obtained. Normalized initial emission intensity values were then plotted as a linear function of laser intensity (i.e. intensity of the laser beam reaching the sample after passing through the neutral density filters). In concentration-matched samples, slopes of the fitted straight lines gave the relative singlet oxygen yield. Quantum yields of singlet oxygen generation (i.e. the number of singlet oxygen molecules generated per photon absorbed) were calculated using measurements obtained after matching sample absorbances to that of all-*trans*-retinal (ATR; quantum yield of 0.30 ± 0.04 (Rozanowska *et al.*, 1998)), using Equation 2.1 below.
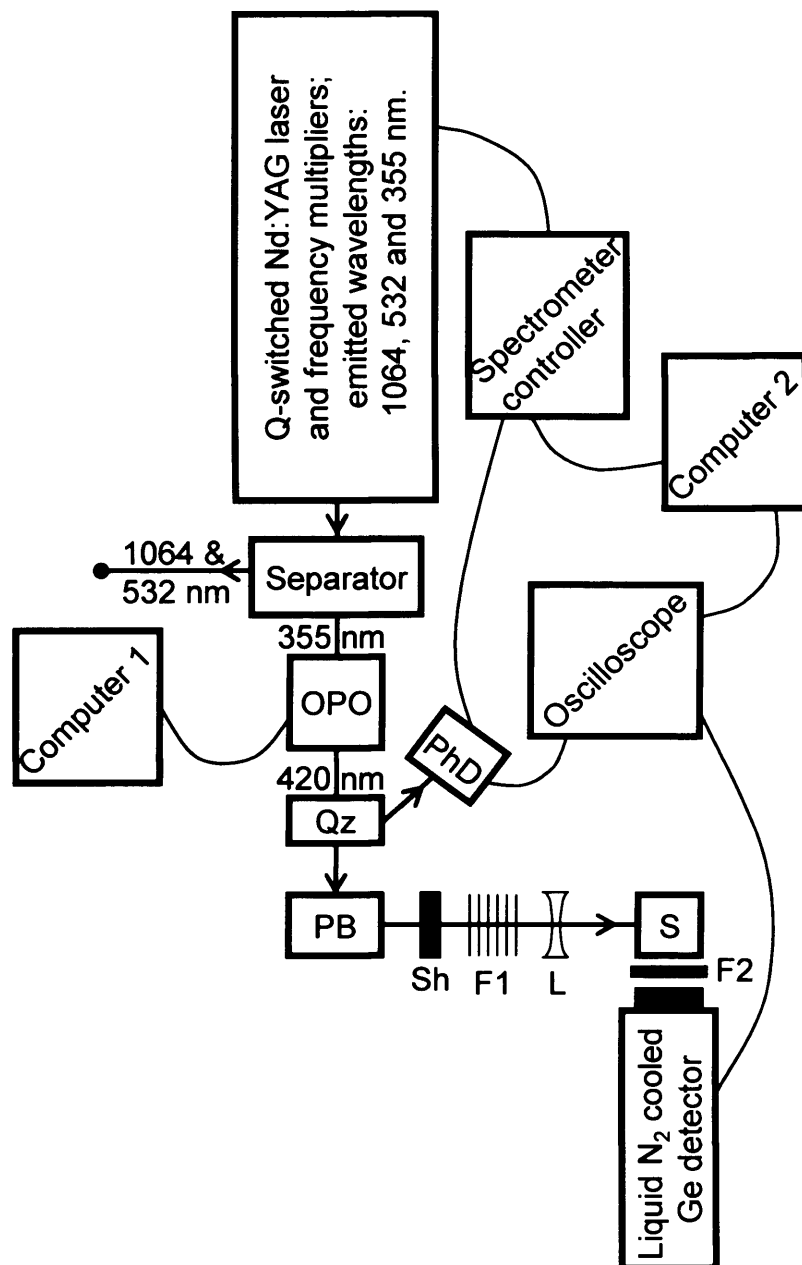
Figure 2.4 Schematic diagram of singlet oxygen detection apparatus. OPO: optical parametric oscillator; Qz: quartz plate, PhD: photodiode – for measuring relative laser pulse energy; PB: Pellin Broca prism; Sh: shutter; F1: neutral density filters (0-16) for regulation of laser intensity; L: diverging lens (optional); S: sample in a quartz cell; F2: Si filter cutting off stray light below 1100 nm and an interference filter with transmission maximum at 1260 nm; blue line = laser light path.
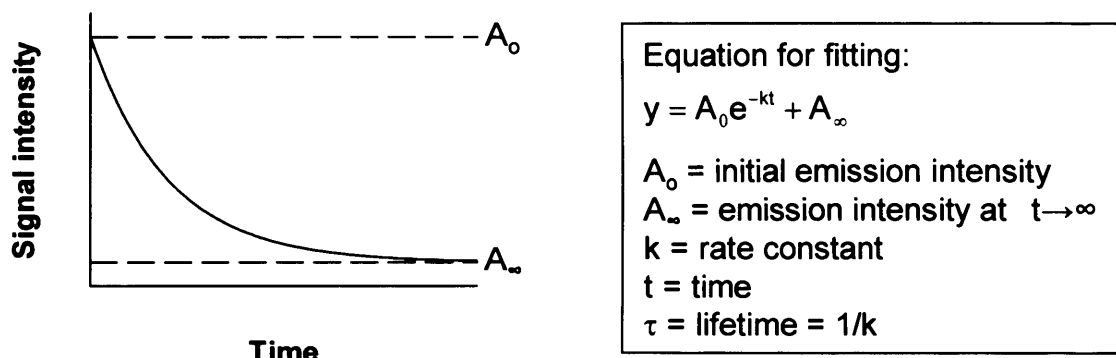
Figure 2.5 *Hypothetical curve fit by an exponential equation to model the decay of singlet oxygen (monitoring signal intensity at 1270 nm over time), showing the equation of the curve and values used in further analysis.*

$$\Phi_x = \frac{\Phi_{ATR} \cdot slope_x}{slope_{ATR}}$$

Φ = quantum yield
slope = slope of fitted initial emission intensity values
x = sample
ATR = all-*trans*-retinal

Equation 2.1 *Equation for calculation of quantum yield of singlet oxygen production, using ATR as a standard singlet oxygen producer.*

2.5.2 Laser flash photolysis to monitor transient formation

Laser flash photolysis experiments (Bensasson *et al.*, 1993a) were carried out with a Q-switched Nd:YAG laser (Continuum Surelite II; Santa Clara, USA) as the excitation source (Rozanowska *et al.*, 1998). Samples were exposed to a 5 ns laser pulse at 420 nm and absorbance of transient species was monitored between 300 and 660 nm (at 10 nm intervals) using a xenon lamp as a monitoring light source, two monochromators (Spectra Kinetics Monochromators, Applied Photophysics, UK), and a photomultiplier coupled to a digitizing scope (Infiniium 54830B DSO Agilent, Santa Clara, USA) interfaced with a Risc computer (Acorn, Swadlincote). See Figure 2.6 for a diagram of the apparatus. Transient difference spectra were produced by plotting averaged absorbance at

selected time points in the kinetic measurements at each wavelength (multiple adjacent data points surrounding each selected time point were averaged).

To determine the effect of oxygen on the rate of decay of the observed transient species and recovery to the ground state, measurements were repeated at key wavelengths (i.e. wavelengths corresponding to maxima and minima in the transient difference spectra), in both argon-saturated (oxygen-depleted) and air-equilibrated (oxygen present) conditions. The bimolecular rate constant of quenching of the transient by oxygen in air-equilibrated benzene was calculated using the rate constants obtained after fitting to an exponential equation, and Equation 2.2 below.

$$k_Q = \frac{k_{air} - k_{Ar}}{[O_2]_{benz}}$$

k_Q = rate of quenching by oxygen ($M^{-1}s^{-1}$)
k_{air} = rate constant in air-saturated sample
k_{Ar} = rate constant in argon-saturated sample
$[O_2]_{benz}$ = $[O_2]$ in air-saturated benzene
        = 1.91×10^{-3} M *

Equation 2.2: *Equation for calculation of the bimolecular rate constant of quenching of the transient(s) by oxygen in air-saturated benzene at room temperature.* *(Murov, 1973).*
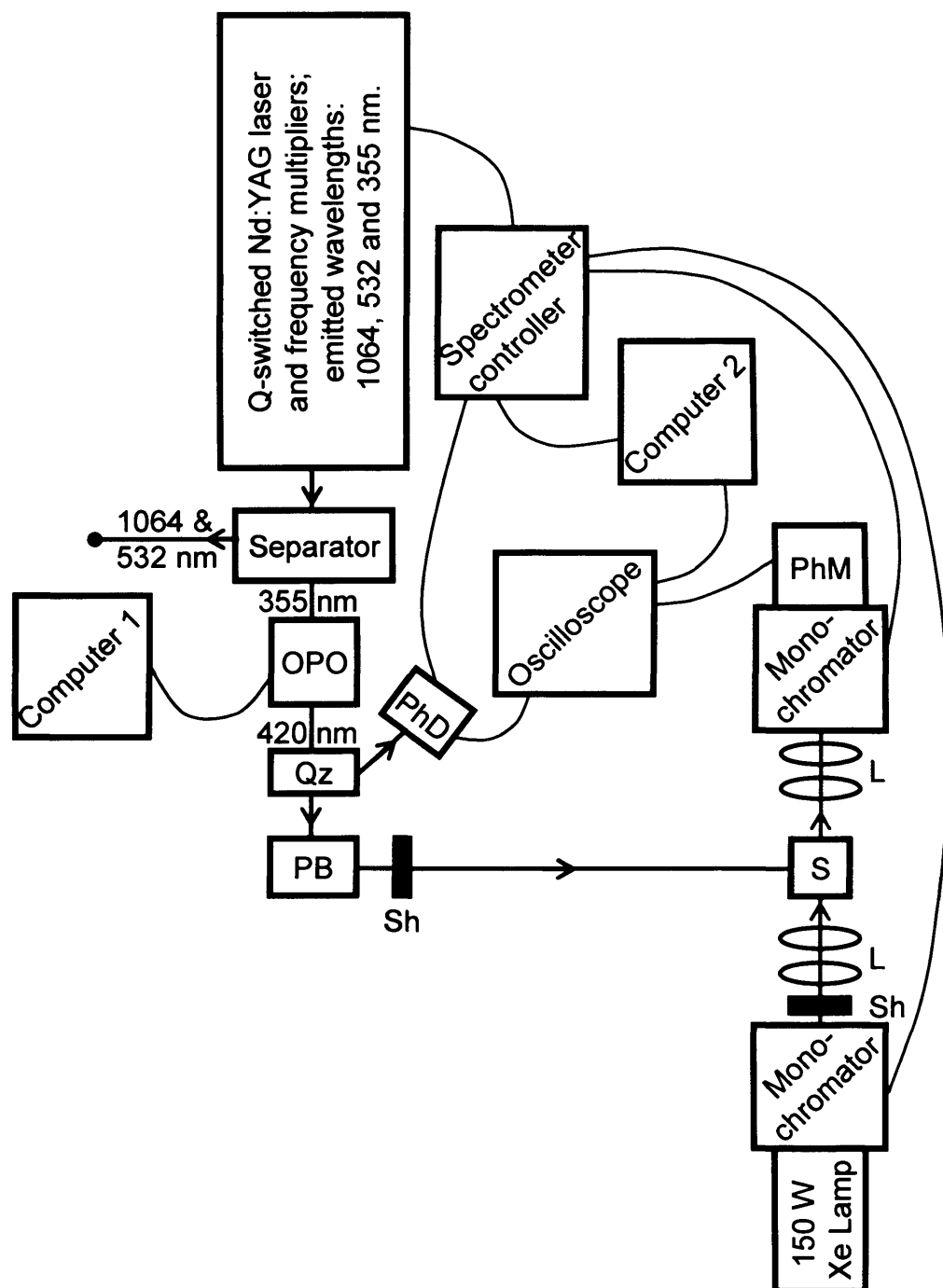
Figure 2.6 *Schematic diagram of flash photolysis apparatus. OPO: optical parametric oscillator; Qz: quartz plate, PhD: photodiode — for measuring relative laser energy; PB: Pellin Broca prism; Sh: shutters; S: sample in a quartz cell; PhM: photomultiplier; L: lenses forming analysing beam; blue line: laser light path; green line: analysing light path.*

2.5.3 Superoxide assay

Superoxide production was measured using a previously published assay which monitors superoxide-mediated reduction of cytochrome C (Boulton *et al.*, 1993). The assay medium consisted of Hank's balanced salt solution (HBSS pH 7.6; Sigma), 50 μM cytochrome C (Sigma) and 0.05% cetyltrimethylammonium bromide (CTAB; Sigma), with or without liposomes containing 0.1 mM pDHA in the presence of 40 mol% POPE or POPC. Selected samples also contained superoxide dismutase (SOD: 250 U.ml^{-1}; Sigma) or catalase (250 U.ml^{-1}; Sigma) Stock solutions of each reagent were made in HBSS.

Samples were prepared in cuvettes with an optical path length of 1 cm, and were stirred throughout. Initial measurements were taken at t = 0 minutes, immediately after the reagents were combined, then samples were exposed to light and spectral measurements were repeated every 10-15 minutes, as indicated. Controls consisted of: (a) assay buffer without liposomes, and (b) assay buffer with liposomes, dark-maintained throughout (except for the monitoring light during spectral measurements). Absorbance increases at 550 nm were used to calculate reduction of cytochrome C using the extinction coefficient of 21 mM^{-1}.cm^{-1} (Boulton *et al.*, 1993). These values indicate concentrations of superoxide responsible for the observed cytochrome C reduction. Where necessary, due to variations in background scattering, the absorbance at 680 nm was first subtracted off the spectra, and samples were normalized at the isosbestic points at 542 and 556 nm.

Results for samples with pDHA in the light, pDHA in the dark and pDHA + catalase in light were compared by nonlinear regression, fitting data to an exponential curve (Figure 2.7), followed by statistical comparisons of k and A_∞ values. This allowed comparison of pDHA + POPC and pDHA + POPE.

Equation for fitting:

$$y = y_0 + A_\infty(1 - e^{-kt})$$

y_0 = initial value at t=0
A_∞ = value at t→∞
k = rate of product formation
t = time
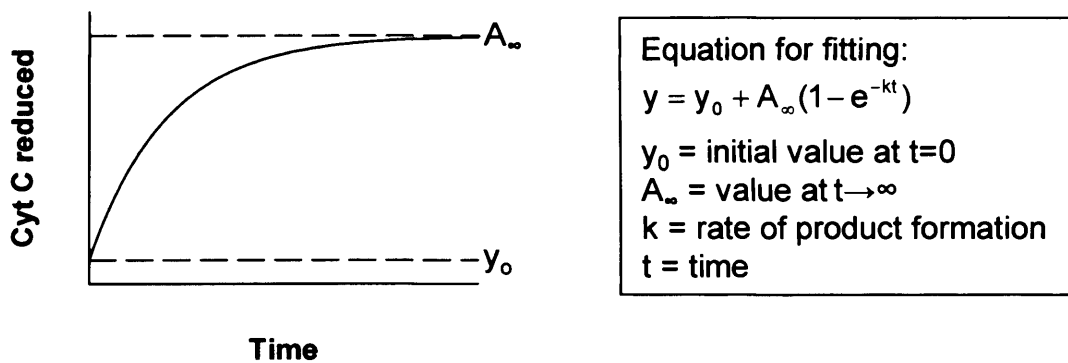
Figure 2.7 *Hypothetical curve fit by exponential equation to model increase in levels of reduced cytochrome C, showing the equation of the curve and values used in further analysis*

As other data sets (i.e. no pDHA, pDHA + SOD) did not fit to an exponential curve, further comparisons were carried out on levels of cytochrome C reduction at 60 minutes for all samples, within their respective groups i.e. pDHA + POPC or pDHA + POPE.

2.6 Lysosomal function studies

2.6.1 Isolation of bovine photoreceptor outer segments

Retinas were isolated from fresh bovine eyes. Muscle and fat were removed from the orbit, and eyes put into Betadine solution (AAH, UK). Eyes were transferred to a tissue culture hood for the remainder of the process. An incision was made in the orbit, posterior to the cornea, using a scalpel, and scissors were used to remove the anterior segment and vitreous. The retina was gently detached from the eye cup and cut at the optic nerve. Retinas were either refrigerated and used within 24 hours or frozen at -80 °C and thawed as required.

POS isolation was carried out following a modified version of the procedure published by Papermaster (Papermaster, 1982). Sterile conditions were maintained throughout. All solutions were filtered and pre-chilled and ice was used to ensure samples were maintained at a temperature of ~4 °C. Homogenization medium (see Table 2.1) was added to retinas (15 ml per 25

56

retinas) and a Teflon hand-held homogenizer was passed through the mixture three times. The homogenate was transferred to a cold centrifuge tube then back into the homogenizer tube, and homogenization repeated. The homogenate was centrifuged at 1500 × g for 4 minutes at 4 °C (U-32R; Hettich Zentrifugen, 1617 rotor; Boeco, Germany).

	Fresh retina (34% w/w)	Frozen retina (30% w/w)
42% sucrose	191 g	162 g
1 M NaCl	13 ml	13 ml
0.1 M MgCl$_2$	0.4 ml	0.4 ml
1 M Tris-acetate	1 ml	1 ml
Add ddH$_2$O to obtain:	230 g	226 g

Table 2.1 *Composition of homogenization media for POS isolation from fresh or frozen bovine retinas.*

The supernatant was decanted into centrifuge tubes, and the pellet was re-homogenized as above with a further 15 ml homogenization buffer, and re-centrifuged. The total volume of supernatant after the 2 centrifugations was determined before transferring to a cold 500 ml conical flask. Two equivalent volumes of 0.01 M tris-acetate buffer (ice cold, pH 7.4) were added gradually while stirring. The POS were then pelleted by centrifugation at 1500 × g for 4 minutes at 4 °C. The pellet was re-suspended in 1.10 g.ml^{-1} sucrose solution (see Table 2.2) and repeatedly passed through an 18- then 21-gauge needle, rapidly ejecting the solution against the wall of the plastic tube each time.

	Density (g.ml^{-1})		
	1.10	**1.11**	**1.15**
42% sugrose (g)	31.2	34.2	46.5
0.1 M MgCl$_2$ (µl)	50	50	50
1 M tris-acetate (µl)	50	50	50
Add ddH$_2$O to obtain:	55	55.5	57.5

Table 2.2 *Composition of sucrose solutions used for sucrose gradient during POS isolation from bovine retinas.*

Sucrose gradients were prepared using 1.15 and 1.11 g.ml^{-1} sucrose solutions carefully layered into centrifuge tubes to ensure negligible mixing at the interface. The crude POS suspension in 1.10 g.ml^{-1} sucrose was then carefully layered onto the gradient. After centrifugation at 50000 × g for 30 minutes at 4 °C in an ultracentrifuge (Sorvall Ultra-Pro 80, Sorvall Products, L.P., Newtown, Connecticut), POS were carefully removed from the 1.11/1.15 g.ml^{-1} interface using a sterile Pasteur pipette. POS were recovered by dilution in 0.01 M tris-acetate and centrifugation in the ultracentrifuge at 45000 × g for 20 minutes. The resultant POS pellet was then re-suspended in D-PBS and yield counted using a haemocytometer. After each isolation procedure a small amount of POS suspension was added to a cell culture flask with medium and monitored for at least 24 hours to ensure no bacterial contamination. Prior to experimental use, POS were diluted to the required concentration in normal cell culture medium.

2.6.2 Feeding cells with POS + pDHA

For feeding experiments, controls were fed with medium only (DMEM:F12 medium containing 2% FCS), and other treatments included POS, pDHA or POS with pDHA. POS were fed at 1x10^7 POS.ml^{-1} (Mukherjee *et al.*, 2007b) and multiple pDHA liposome concentrations were used, as indicated in the results section. After preparation of different combinations of medium/POS/pDHA, all

samples were sonicated for 15 minutes, with the aim of aiding insertion of pDHA lipids from liposomes into POS. The solutions were applied to cells and medium was changed every two days, with POS/pDHA included in each feed. Each treatment was carried out in duplicate or triplicate wells of a 24-well cell culture plate, with "n" indicating total number of separate plates.

2.6.3 Acridine orange labelling to monitor lysosomal integrity

After feeding with pDHA +/- POS for 2 weeks, cells were detached from 24-well plates as described in Section 2.2.1 and either kept in the dark or exposed to light (15 mW.cm^{-2}) for 1 hour. Cells were then incubated with 5 μg.ml^{-1} acridine orange for 15 minutes at 37 °C to allow uptake (Brunk *et al.*, 1997). After labelling, cells were centrifuged at 700 × *g* then re-suspended in PBS to remove excess acridine orange. Acridine orange uptake and distribution in the cell was then monitored by either flow cytometry or microscopy.

2.6.3.1 Microscopy of acridine orange loaded cells

To allow for quick localization of cells using the microscope, thus reducing the photosensitizing effects of acridine orange, cell nuclei were labelled using Hoechst 33342 (3 μg.ml^{-1}) simultaneously with acridine orange labelling. Cells were rinsed then put on a microscope slide and covered with a coverslip immediately prior to imaging using a fluorescence microscope (Leica DM 6000B with a Leica DFC 350 FX camera; Leica, UK).

2.6.3.2 Flow cytometry of acridine orange loaded cells

For flow cytometry, cells were transported to the flow cytometer (BD FACSCalibur with CellQuest software, BD Life Sciences, UK) on ice, in a dark container. Cells were taken up by the flow cytometer and passed through a laser beam at 488 nm and forward and side scatter (to determine size and granularity of the cells respectively) and fluorescence emission data were collected. Detectors and filters allowed separation of emitted fluorescent light into three channels with different peak wavelengths: FL1 = 530 nm emission, FL2 = 585 nm and FL3 = 650 nm. Sensitivity of the detectors was altered to ensure that the fluorescence signal of unlabelled cells was limited to the lowest decade of the

fluorescence intensity histogram, and that labelled cells did not exceed the limits of the 4 decade scale.

Prior to data collection, a gate was set on the forward scatter (FSC) vs. side scatter (SSC) plot to exclude cell debris in the bottom left hand corner. For each sample, data was collected until 10,000 "events", assumed to be cells, were counted within this gate. For acridine orange labelling experiments, FSC and SSC data was collected for each sample, as were FL1 (green emission) and FL3 (red emission). Data analysis and presentation was carried out using WinMDI 2.8 software (The Scripps Research Institute, USA).

2.6.4 Lysosomal enzyme assays

To determine whether pDHA affects RPE lysosomal enzyme function, phosphatase and glucosaminidase activities were assayed using p-nitrophenyl phosphate or p-nitrophenyl β-D-glucosaminide substrates (Sigma, UK) respectively, with active enzymes expected to release p-nitrophenol which can be measured spectrophotometrically (Shamsi and Boulton, 2001).

Cells were lysed in 0.2% Triton X-100 (Sigma) in dH_2O for 5 minutes at room temperature on a rocker. 25 µl of cell lysate was combined with 25 µl pDHA in D-PBS, or D-PBS alone, in 96-well plates. Alternatively, purified acid phosphatase enzyme (from wheat germ; Sigma, UK) was used instead of cell lysate. Light (or dark) exposure was then carried out, then plates were removed from the lamp and enzyme activity assays were carried out as described below.

For all assays, controls were carried out with no cell lysate/enzyme (but with all concentrations of pDHA) to monitor background absorbance, and also with no substrate. A standard curve was created using 100 µl p-nitrophenol (Sigma, UK) at a range of concentrations in 0.1 M acetate buffer (pH 4.5), plus 100 µl of 0.2 M NaOH. The Pierce BCA Protein Assay (Section 2.6.4.3) was carried out in parallel in each experiment to allow normalization of enzyme activity to protein levels.

2.6.4.1 Phosphatase enzyme activity

After light treatment, 50 μl of 10 mM p-nitrophenyl phosphate in acetate buffer (0.2 M, pH 4.5) was added to the pDHA + lysate/enzyme mixture. Samples were incubated for 30 minutes at 37 °C. The reaction was then stopped by addition of 100 μl NaOH (0.2 M). Absorbance at 405 nm was measured in a plate reader.

2.6.4.2 Glucosaminidase enzyme activity

After light treatment, 50 μl of 10 mM p-nitrophenyl β-D-glucosaminide in citrate buffer (0.2 M, pH 4.5) were added to the pDHA + lysate/enzyme mixture. Samples were incubated for 45 minutes at 37 °C. The reaction was stopped by addition of 100 μl of 0.8 M glycine-NaOH. Absorbance at 405 nm was read in a plate reader.

2.6.4.3 Measurement of protein concentration

Protein concentration in cell lysates was measured using the commercially available Pierce BCA Protein Assay kit (Thermo Scientific, UK). This colorimetric assay measures reduction of Cu^{2+} to Cu^{1+} by proteins using bicinchoninic acid (BCA). The microplate procedure was followed, according to the kit instruction booklet. Briefly, 25 μl of each standard or sample was put in a 96-well plate and combined with 200 μl of freshly made working reagent: a 50:1 combination of BCA reagent A (containing sodium carbonate, sodium bicarbonate, BCA and sodium tartrate in 0.1 M sodium hydroxide) : BCA reagent B (4% cupric sulphate). Incubation was carried out at 37 °C for 30 minutes. Plates were then cooled to room temperature and absorbance at 570 nm was measured using a plate reader. A standard curve was carried out simultaneously for each experiment using 0-2 mg.ml^{-1} bovine serum albumin (BSA). All samples were assayed in triplicate wells.

2.6.5 Intracellular deposit formation

2.6.5.1 Flow cytometry analysis of changes in fluorescence

After long-term feeding of ARPE-19 cells with POS and/or pDHA, cells were washed with PBS then detached with trypsin as described in Section 2.2.1. They were then transported on ice to the flow cytometer immediately and data collected as for acridine orange experiments described in Section 2.6.3.2 above, but with detectors optimized for unlabelled cells used in this experiment. Data was collected for FSC, SSC and FL1 channels.

2.6.5.2 Transmission electron microscopy for monitoring deposit formation

All reagents for preparation of transmission electron microscopy (TEM) specimens were purchased from Agar Scientific (UK) unless stated otherwise.

After long-term feeding, cells were detached by trypsinization then centrifuged to form pellets, as described in Section 2.2.1. Pellets were fixed for 1 hour at 4 °C in a mixture of glutaraldehyde and osmium tetroxide buffered with 0.05 M imidazole (Sigma, UK), pH 7.4 (1 part 2.5% glutaraldehyde + 2 parts of 1% osmium tetroxide, both in 0.05 M imidazole). The pellet was scraped from the side periodically to enable full penetration of the fixative. After fixation, the pellet was broken up and samples were centrifuged. Samples were then embedded in 3% (w/v) agar (Difco Laboratories, MI, USA) which was first dissolved by heating then allowed to cool prior to embedding of samples. Pellets were scraped from the side to ensure total immersion in the agar. After solidification of the agar, the samples were removed from the tubes and cut to remove excess agar from around the specimens, and to provide several small pieces of agar-embedded pellet for each treatment. These were then washed 4 times for 10 minutes each in dH$_2$O to remove excess fixatives, then stained with 0.5% aqueous uranyl acetate for 60 minutes in the dark at 4 °C.

Specimens were dehydrated in a graded series of ethanol concentrations (Fisher Scientific, UK) for 10 minutes each: 30%, 50%, 70%, 80%, 90% and 3 x 100%. They were then incubated in propylene oxide for 2 x 10 minutes. Samples were

infiltrated with resin overnight at room temperature in a fume hood – in a 1:1 mixture of propylene oxide and araldite mix (composed of 5g araldite CY 212: 5g DDSA : 0.15g BDMA). The following day samples were transferred into fresh resin (i.e. araldite mixture without propylene oxide) in plastic moulds and embedded at 60 °C for 48 hours, after which the resin had become polymerized and solid.

Blocks were sections using an Ultracut microtome (Reichert-Jung E, Austria) – with ultrathin sections (60 – 90 nm) collected on pioloform coated copper grids. Each block was sectioned at three different depths i.e. superficial, intermediate and deep; with each block derived from one POS-feeding-treatment. Sections were counterstained first in 2% uranyl acetate for 10 minutes, washed briefly twice in dH$_2$O, then in Reynold's lead citrate for 5 minutes, again followed by two brief washes in dH$_2$O. Sections were examined using a transmission electron microscope (Philips EM400T; Eindhoven, Netherlands) operated at 80 kV accelerating voltage. Intracellular granules were then counted in 10 whole cells for each treatment (with the 10 cells distributed over the three depths of the same block). These were counted on the microscope during imaging, allowing magnification as required to differentiate between mitochondria and other granules. Representative images were taken for each treatment. Two types of granules were encountered: granular and homogeneous (more lipofuscin-like). These were counted separately.

2.7 Statistical analysis

Normalization of data and calculation of means and SD/SEM were carried out using Microsoft Office Excel 2003. Linear and non-linear regression were carried out using GraphPad Prism 3.02 and SigmaPlot 9.0. All further statistical analyses were carried out using GraphPad Instat 3.06, GraphPad Prism 3.02 or SigmaStat 3.5. Tables of P-values for all post-tests carried out after significant ANOVA tests and for one-sample t-tests and selected other comparisons are included in Appendices 1-4.

Chapter 3:
Peroxidation of DHA

3.1 Introduction

Photoreceptors and RPE cells contain high levels of known photosensitizers, including all-*trans*-retinal in photoreceptors, and lipofuscin in the RPE. In conjunction with the regular high fluxes of light reaching the retina and high levels of oxygen due to the high metabolic requirements of visual transduction, these are able to photosensitize singlet oxygen and free radical production (Delmelle, 1978; Boulton *et al.*, 1993; Rozanowska *et al.*, 1995). Additionally, photoreceptors depend on several iron-containing enzymes for normal function of phototransduction, photoreceptor disc renewal and retinoid recycling (referenced in He *et al.*, 2007), therefore iron is readily available in the retina. In fact, levels of iron (including easily chelatable iron) have been shown to increase in retinas with AMD (Hahn *et al.*, 2003). In addition to the Fenton reaction which results in formation of the highly reactive hydroxyl radical, iron can induce decomposition of lipid hydroperoxides to form lipid alkoxyl radicals (Halliwell and Gutteridge, 1984). This is an important step, in conjunction with singlet oxygen and free radical production, in initiation and propagation of the lipid peroxidation cascade, as shown in Figure 1.6 (Buettner, 1993; Yin and Porter, 2005).

These factors are all conducive to DHA peroxidation, especially taking into account its polyunsaturated structure. Indeed, DHA peroxidation products have been found in photoreceptors and RPE cells, and also in drusen and inter/intra-laminar deposits on the basolateral surface of the RPE cell layer, particularly at the level of Bruch's membrane (Crabb *et al.*, 2002; Gu *et al.*, 2003a; Ng *et al.*, 2008). Additionally, it previously been demonstrated that DHA peroxidizes readily by exposure to air, resulting in formation of blue-light absorbing chromophores which are able to photosensitize production of singlet oxygen and superoxide (personal communication: M.B. Rozanowska).

The aim of this chapter is to compare two methods of DHA oxidation, and determine optimal conditions for accumulation of lipophilic blue-light absorbing chromophores. Due to the difficulties of identifying specific individual molecules or markers of lipid peroxidation, the time-course and final end-points of

peroxidation were monitored in different lipid preparations (dry film vs. aqueous liposome suspension) by observing degradation of native DHA and formation of key markers of peroxidation (conjugated dienes, conjugated trienes, and carbonyls), and absorbance of visible light. This was carried out in preparation for the study of potential effects of pDHA in cells of the retina, investigated in further chapters of this thesis.

3.2 Experimental design

3.2.1 Peroxidation of DHA

Two different sample types were used for producing peroxidized lipids: lipids in liposomes (two batches), and lipids as a dry film in a glass flask (one batch). Those peroxidized as liposomes would be physiologically similar to lipid peroxidation in membranes, with access to water which could result in hydrolysis reactions. DHA peroxidized as a film could follow other pathways of peroxidation, and be more similar to lipids inside lipophilic deposits such as lipofuscin and lipid-rich Bruch's membrane deposits.

3.2.2 Monitoring of peroxidation

Many natural lipids show an absorption peak in UV light close to 200 nm (Recknagel and Glende, 1984). In this thesis, the DHA absorption was monitored at 210 nm, to prevent any overlap with absorption by the solvents used. Peroxidation of DHA can result in formation of products with conjugated diene structures which absorb light at approximately 230 nm (Pryor and Castle, 1984; Recknagel and Glende, 1984; Corongiu et al., 1989), and also trienes and ketone dienes which can be observed as additional absorption shoulders/peaks at 260-280 nm (Recknagel and Glende, 1984; Kim and LaBella, 1987; Butovich, 2005; Butovich et al., 2006). For analysis here, wavelengths of 240 and 270 nm were selected for monitoring, with 240 nm expected to indicate conjugated diene formation, but offset slightly from 230 nm to reduce overlap with the DHA absorption peak at 210 nm. Therefore, reduction in the size of the peak at 210 nm

and increases at 240 and 270 nm may be used to monitor increases in the level of peroxidation.

When observed by UV-visible spectroscopy, however, these peaks can not be clearly separated – with the absorbance value for 210 nm likely to be partially overlapped by the 230/240 nm conjugated diene peak/shoulder. Furthermore, conjugated diene levels may in fact decrease with prolonged duration of peroxidation due to further degradation and formation of other products (Kim and LaBella, 1987), and the absorbance shoulder of conjugated trienes and other products at 270 nm may overlap with that of conjugated tetraenes, which show a broad characteristic absorbance peak at ~300 nm (Knight *et al.*, 1999; Kuklev and Smith, 2004). Thus, quantification of these changes is difficult but should still provide an indicator of changes that have occurred with time. Absorption at 210 nm can be assumed to indicate the upper limit of unperoxidized DHA present in samples, and may overestimate the value if contaminated by the absorbance of species exhibiting a peak/shoulder at 230 nm. In an attempt to overcome this problem, HPLC was used as this method allows separation of most peroxidation products from the unperoxidized DHA.

In addition to monitoring changes in absorption of UV light as an indicator of peroxidation, absorption spectroscopy was used to monitor absorption of visible light at wavelengths >400 nm in concentrated pDHA samples. As the anterior eye in the adult human blocks shorter wavelengths, observation of products able to absorb at >400 nm would be required to validate any theory that pDHA may act as a photosensitizer in the adult retina.

3.3 Results

3.3.1 General observations

Over time, both the lipid film and liposomes changed colour from light yellow to darker yellow/orange.

At the earlier time points of lipid peroxidation for the first batch of liposomes, absorption spectra were only measured for the chloroform-soluble fraction of the extracted liposomes. With time, however, a change in colour in the upper methanol-soluble phase was noticed, becoming yellow rather than colourless as observed earlier, so from the 132 day time point onwards absorption spectra were also measured for this phase.

In the same batch of liposomes, in addition to the colour change in the upper phase, increased duration of peroxidation resulted in the formation of an apparently insoluble brown interphase between the upper methanol/PBS phase and the lower chloroform phase (as indicated in Figure 2.1). This layer appeared to increase in quantity as peroxidation of the samples progressed. However, it was found to gradually disappear and dissolve into the upper methanol/PBS phase when repeat extractions were carried out. For the lipids allowed to peroxidize as a dry film, there was very little material observed between the two main extraction phases.

Following these observations in the first batch of liposomes, the second batch of liposomes, which was to be used in further experiments in this thesis, was allowed to peroxidize for a considerably shorter period (18 days vs. 175 days), to minimize the formation of polar products and loss of pDHA into the upper methanol/PBS phase, and therefore to maximize levels of blue-absorbing chromophores in the lower chloroform phase.

3.3.2 Analysis of chloroform-soluble phase

3.3.2.1 UV-visible spectroscopy

Figure 3.1A shows absorption spectra of the chloroform-soluble component of the lipid extraction from the first batch of liposomes, dissolved in acetonitrile + methanol (20:1 v/v). Changes in absorbance values over time of the peaks/shoulders at selected wavelengths are shown more clearly in Figure 3.1B. These results show that with time, absorbance at 210 nm decreases representing a loss of native DHA as it becomes peroxidized. Conversely, there is a slight initial increase in absorbance at 240 and 270 nm, and thus levels of peroxidation

products, but this reaches a plateau and does not increase further to account for the loss of unperoxidized DHA. This could be counteracted by the formation of polar products extracting in the methanol/PBS phase as discussed above. Even at the earliest time points there is absorption at longer wavelengths, indicating that the DHA is already (unintentionally) partially peroxidized, demonstrating how readily this process occurs.
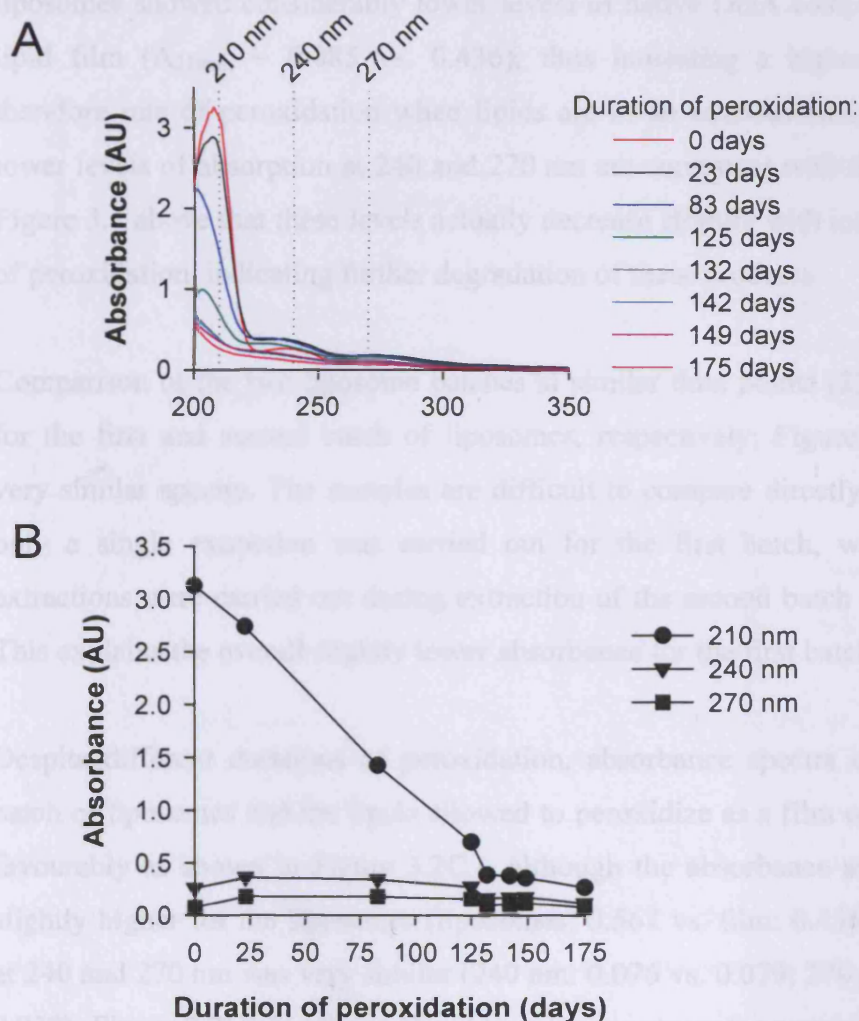
Figure 3.1 *Monitoring of DHA peroxidation with UV/visible absorption spectroscopy. (A) Absorption spectra for the chloroform soluble component of extracted pDHA liposomes, measured in acetonitrile + methanol (20:1 v/v). Measurements were taken at time points up to 175 days of peroxidation, and maximum extracted (p)DHA concentration was 0.12 mM. (B) Graph showing changes in absorbance at key wavelengths (210, 240 and 270 nm) over time, taken from the spectra in (A).*

Figure 3.2 shows different comparisons of absorption spectra of the three different batches of DHA at matched concentrations. The three samples were: two batches peroxidized as liposomes, and DHA peroxidized as a lipid film and later made into liposomes. All samples were freshly extracted and diluted as described above.

Figure 3.2A indicates that over the same length of time, DHA peroxidized in liposomes showed considerably lower levels of native DHA compared with the lipid film (A_{210nm} = 0.085 vs. 0.436), thus indicating a higher degree and therefore rate of peroxidation when lipids are in an aqueous environment. The lower levels of absorption at 240 and 270 nm are consistent with the findings in Figure 3.1 above that these levels actually decrease slightly with increased extent of peroxidation, indicating further degradation of these products.

Comparison of the two liposome batches at similar time points (23 and 18 days for the first and second batch of liposomes, respectively; Figure 3.2B) shows very similar spectra. The samples are difficult to compare directly, however, as only a single extraction was carried out for the first batch, whereas repeat extractions were carried out during extraction of the second batch of liposomes. This explains the overall slightly lower absorbance for the first batch.

Despite different durations of peroxidation, absorbance spectra of the second batch of liposomes and the lipids allowed to peroxidize as a film compared very favourably as shown in Figure 3.2C – although the absorbance at 210 nm was slightly higher for the liposomes (liposomes: 0.567 vs. film: 0.436), absorbance at 240 and 270 nm was very similar (240 nm: 0.076 vs. 0.079; 270 nm: 0.035 vs. 0.032). Figure 3.2C also shows the absorption spectrum for unperoxidized DHA indicating, as expected, greater absorbance at 210 nm (A = 0.769) compared with the peroxidized samples, and lower absorbances at 240 and 270 nm (0.040 and 0.021 respectively).
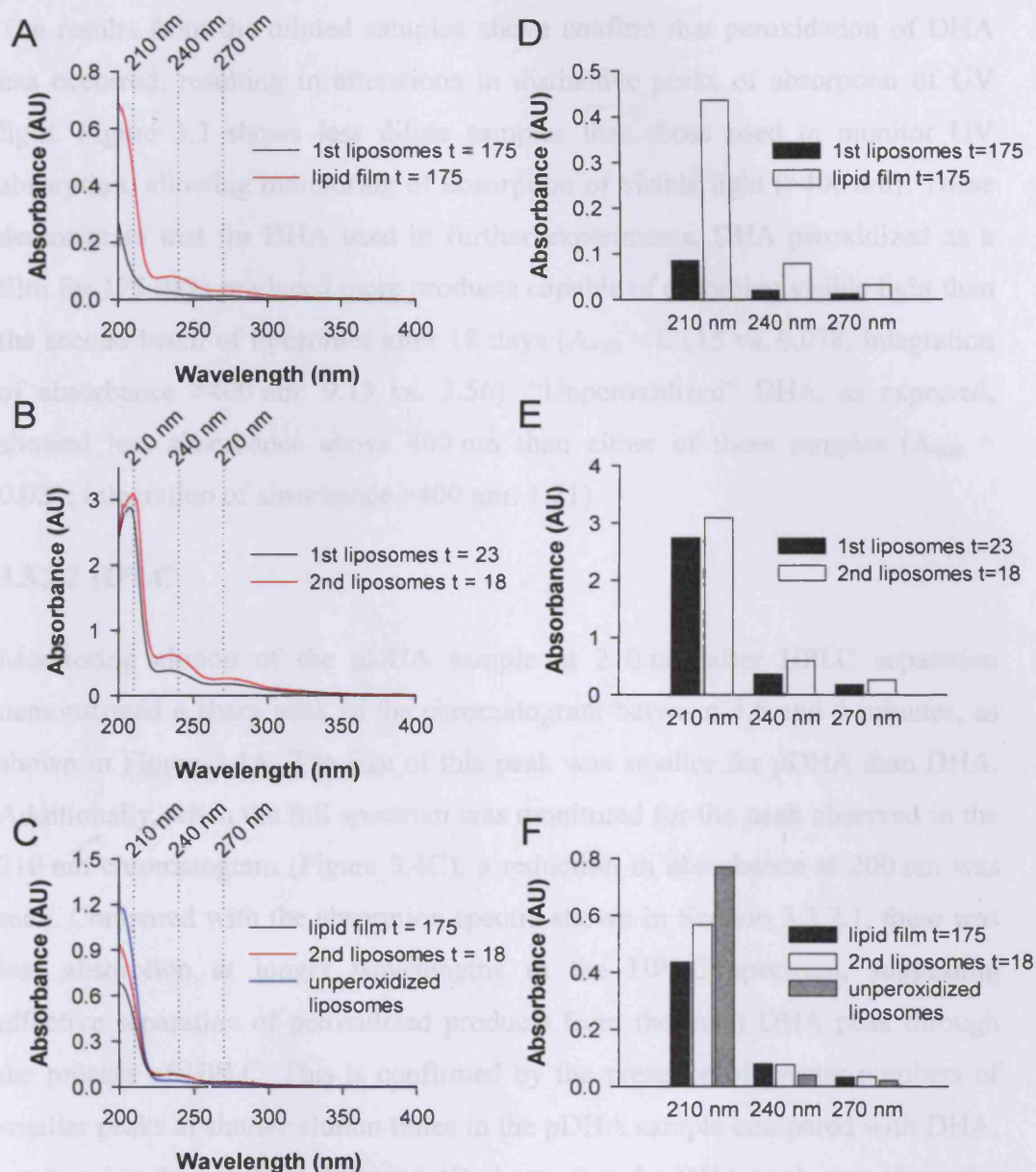
Figure 3.2 *Comparison of absorption spectra after DHA peroxidation in liposomes or as a dry lipid film. Spectra are shown for the chloroform soluble phase of extracted liposomes measured in acetonitrile + methanol (20:1 v/v), and graphs compare key wavelengths. (A) Comparison of the end-point of DHA peroxidation as liposomes (first batch) vs. a lipid film after 175 days (max. 0.012 mM DHA); (B) comparison of two sets of liposomes at similar times: after 23 days of peroxidation for the first liposomes, and the 18 day end-point for the second liposomes (max. 0.12 mM DHA); (C) comparison of peroxidation end-points of lipids used in further experiments: DHA peroxidized as either a lipid film or as liposomes (second batch), and unperoxidized DHA (max. 0.012 mM DHA).*

The results from the diluted samples above confirm that peroxidation of DHA has occurred, resulting in alterations in distinctive peaks of absorption of UV light. Figure 3.3 shows less dilute samples than those used to monitor UV absorption, allowing monitoring of absorption of visible light (>400 nm). These demonstrate that for DHA used in further experiments, DHA peroxidized as a film for 175 days produced more products capable of absorbing visible light than the second batch of liposomes after 18 days (A_{400} = 0.115 vs. 0.078; integration of absorbance >400 nm: 9.13 vs. 3.56). "Unperoxidized" DHA, as expected, showed less absorbance above 400 nm than either of these samples (A_{400} = 0.026; integration of absorbance >400 nm: 1.21).

3.3.2.2 HPLC

Monitoring elution of the pDHA sample at 210 nm after HPLC separation demonstrated a sharp peak in the chromatogram between 3.5 and 4 minutes, as shown in Figure 3.4A. The size of this peak was smaller for pDHA than DHA. Additionally, when the full spectrum was monitored for the peak observed in the 210 nm chromatogram (Figure 3.4C), a reduction in absorbance at 200 nm was seen. Compared with the absorption spectra shown in Section 3.3.2.1, there was less absorption at longer wavelengths in the HPLC spectrum, suggesting effective separation of peroxidized products from the main DHA peak through the process of HPLC. This is confirmed by the presence of greater numbers of smaller peaks at shorter elution times in the pDHA sample compared with DHA, as shown in Figure 3.4B. Figure 3.4D shows that the DHA peak area (from the 210 nm chromatogram) initially reduced between 0 and 2 days of peroxidation but did not reduce further with increased duration of peroxidation.
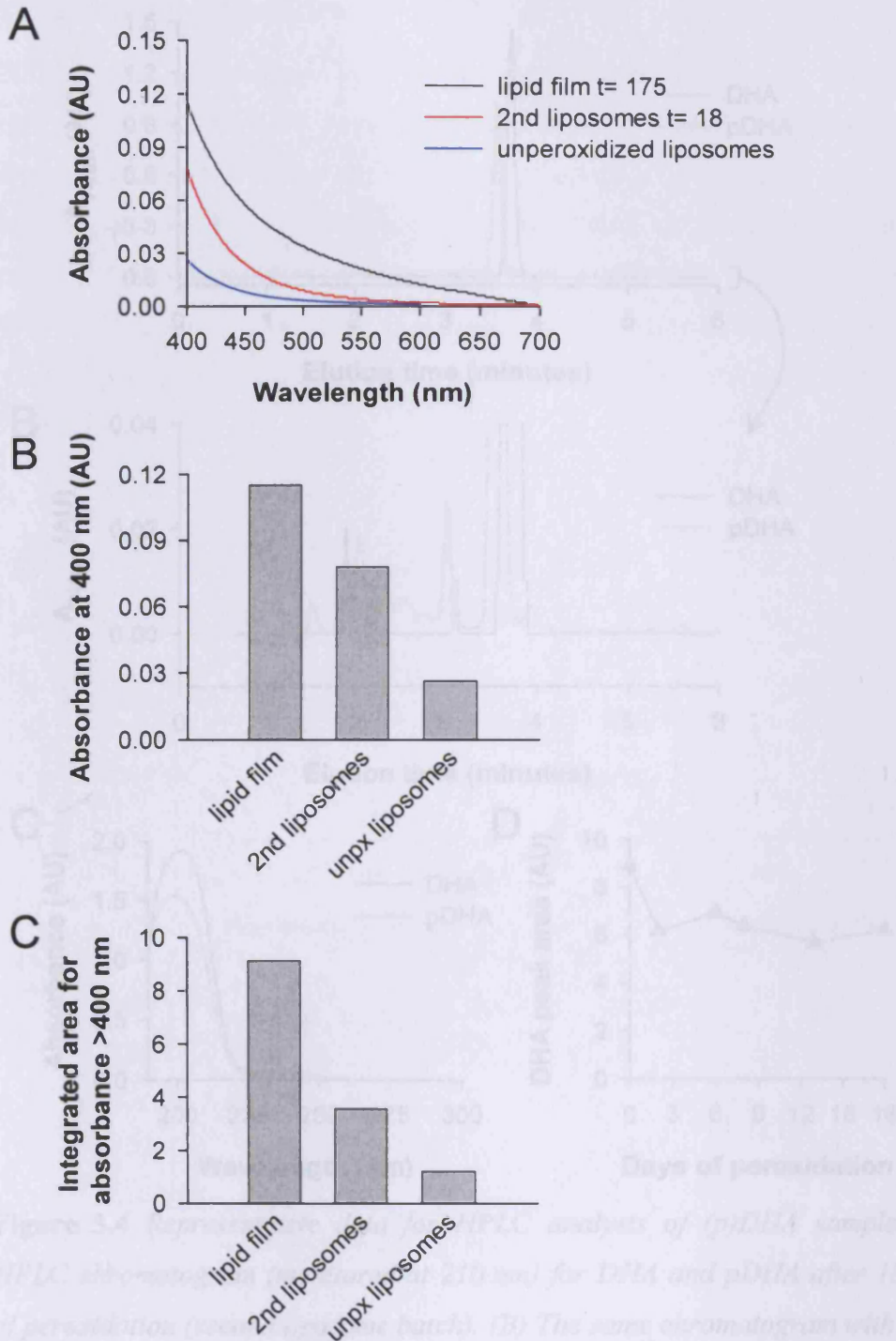
Figure 3.3 *Comparison of absorption of visible light by (p)DHA samples to be used in future experiments, at peroxidation end-points. (A) Absorption spectra of concentrated samples, corresponding to 1.2 mM intact DHA, with duration of peroxidation (days) indicated. (B) Comparison of absorbance at 400 nm. (C) Comparison of integrated total absorbance between 400 and 700 nm.*
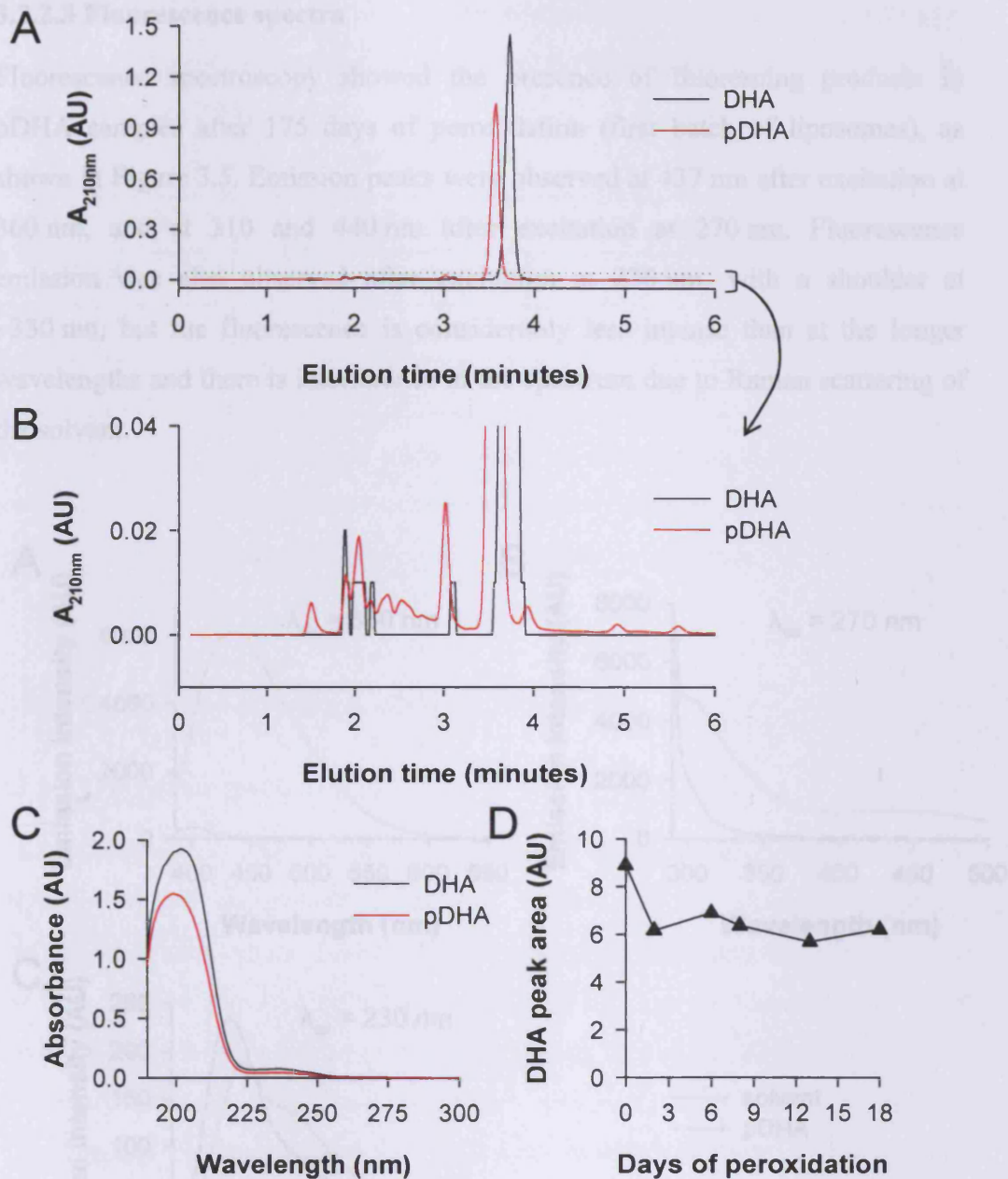
Figure 3.4 *Representative data for HPLC analysis of (p)DHA samples. (A) HPLC chromatogram (monitored at 210 nm) for DHA and pDHA after 18 days of peroxidation (second liposome batch). (B) The same chromatogram with the y-axis amplified to show smaller peaks. (C) Spectra at the elution time of the main DHA elution peaks. (D) Graph showing peak areas for the main DHA peak in HPLC chromatograms monitored at 210 nm. Each injection corresponded to 275 nmol (p)DHA.*

3.3.2.3 Fluorescence spectra

Fluorescence spectroscopy showed the presence of fluorescing products in pDHA samples after 175 days of peroxidation (first batch of liposomes), as shown in Figure 3.5. Emission peaks were observed at 437 nm after excitation at 360 nm, and at 310 and 440 nm after excitation at 270 nm. Fluorescence emission was also observed after excitation at 230 nm, with a shoulder at ~330 nm, but the fluorescence is considerably less intense than at the longer wavelengths and there is interference in the spectrum due to Raman scattering of the solvent.
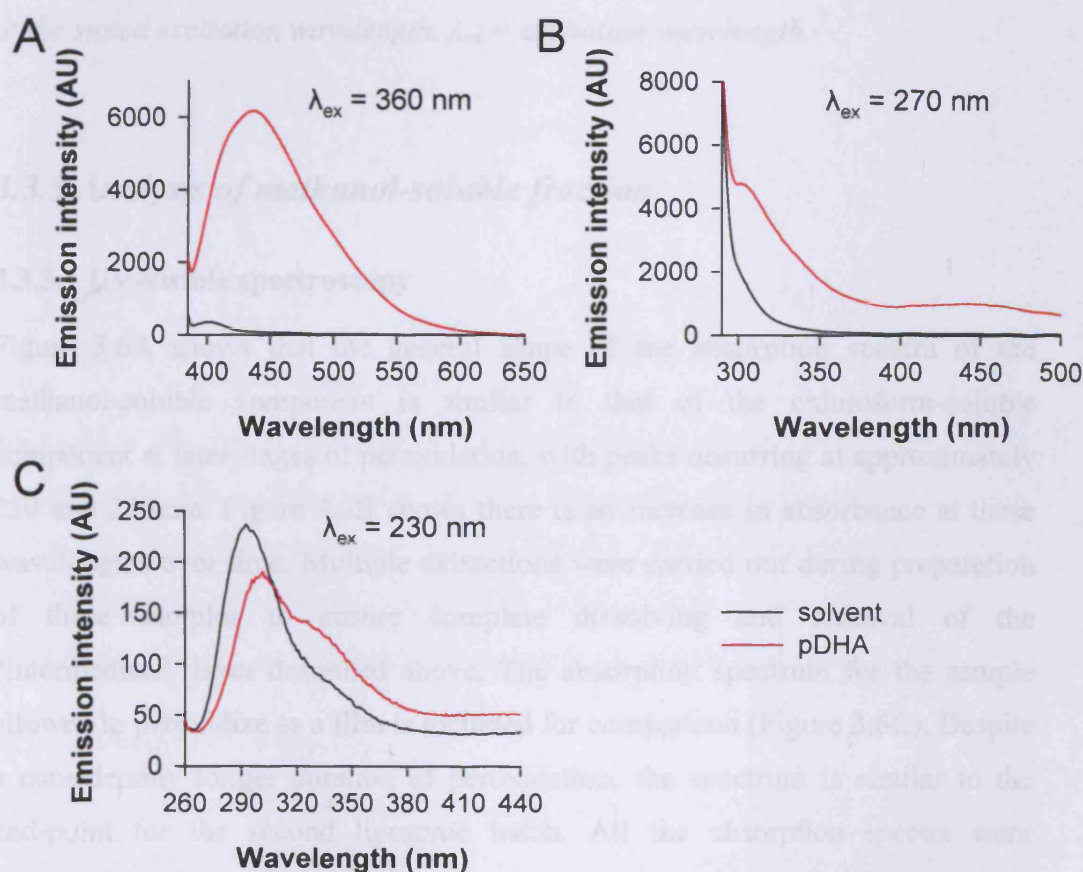
Figure 3.5 *Fluorescence emission spectra of DHA samples (first liposome batch, peroxidized for 175 days) extracted in the chloroform phase, dissolved in acetonitrile/methanol, after excitation at (A) 360 nm: peak at 437 nm; (B) 270 nm: peaks at 310 nm and 440 nm; (C) 230 nm: shoulder: ~330 nm. Note differences in scale between spectra.*

Variations in DHA concentrations for the samples, shown in Table 3.1, were due to the requirement of absorbance at the relevant excitation wavelength to be below 0.1 as described above.

λ_{ex} (nm)	concentration (mM)	absorbance at λ_{ex}
360	1.2	0.036
270	0.12	0.073
230	0.012	0.026

Table 3.1 *Concentrations and absorbances of samples used for fluorescence measurements. 1 in 10 dilutions were carried out to ensure absorbance below 0.1 at the stated excitation wavelength.* λ_{ex} = *excitation wavelength.*

3.3.3 Analysis of methanol-soluble fraction

3.3.3.1 UV-visible spectroscopy

Figure 3.6A shows that the general shape of the absorption spectra of the methanol-soluble component is similar to that of the chloroform-soluble component at later stages of peroxidation, with peaks occurring at approximately 230 and 270 nm. Figure 3.6B shows there is an increase in absorbance at these wavelengths over time. Multiple extractions were carried out during preparation of these samples to ensure complete dissolving and removal of the "intermediate" layer described above. The absorption spectrum for the sample allowed to peroxidize as a film is included for comparison (Figure 3.6C). Despite a considerably longer duration of peroxidation, the spectrum is similar to the end-point for the second liposome batch. All the absorption spectra were truncated at 220 nm due to interference from the solvents used. Although methanol and PBS do not absorb at these wavelengths, absorption was observed in the solvent indicating contamination by chloroform during the extraction process, as discussed in Section 2.1.3.1.
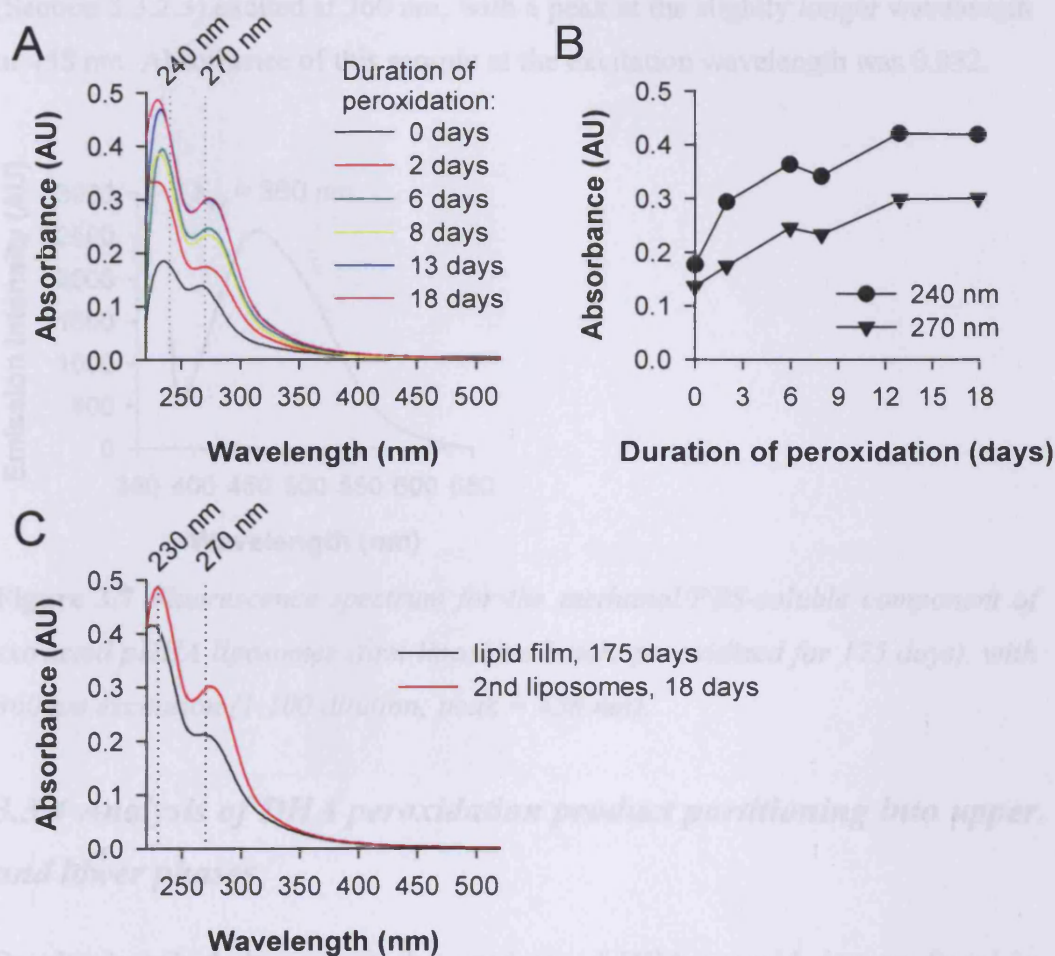
Figure 3.6 *Absorption spectra of the methanol/PBS phase of pDHA liposome extracts. (A) Absorption spectra and (B) graph showing changes at 240 and 270 nm for the second liposome batch, diluted 1:10 (after multiple extractions); (C) Comparison of absorption spectra at end-points for lipids peroxidized as a lipid film and in the second batch of liposomes (extracted and diluted 1:10).*

3.3.3.2 Fluorescence spectra

When running background samples (i.e. methanol + PBS, but no lipids), it was found that this solvent combination showed considerable levels of fluorescence at excitation wavelengths of 230 and 270 nm (possibly due to chloroform content retained in the upper phase during the extraction process, as for the absorption spectra Section 3.3.3.1 above). Therefore, for methanol/PBS phase extracts, only 360 nm was used for fluorescence excitation. Figure 3.7 shows a sample spectrum, demonstrating similar fluorescence to the chloroform-soluble sample

(Section 3.3.2.3) excited at 360 nm, with a peak at the slightly longer wavelength of 458 nm. Absorbance of this sample at the excitation wavelength was 0.032.
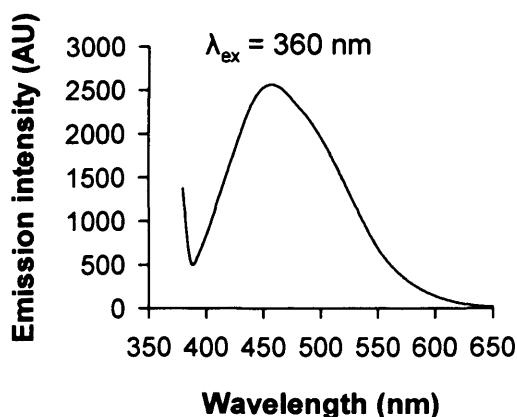
Figure 3.7 *Fluorescence spectrum for the methanol/PBS-soluble component of extracted pDHA liposomes (first liposome batch, peroxidized for 175 days), with 360 nm excitation (1:100 dilution; peak = 458 nm).*

3.3.4 Analysis of DHA peroxidation product partitioning into upper and lower phases

Results described above show that products of DHA peroxidation are found in both the chloroform and the methanol/PBS phases during extraction. To calculate the ratio of products in these two phases, absorption spectra were integrated to calculate total absorbance above either 300 or 400 nm, then normalized to equal volume (Figure 3.8A and B and Table 3.2). This analysis shows that approximately 10% of molecules which absorb light at >300 nm separate into the methanol/PBS phase, compared with 90% which extract in the chloroform phase. This ratio is approximately equal for both the samples. In contrast, when comparing absorbance >400 nm, i.e. visible light, which was used in later experiments in this thesis, the percentage of absorbing molecules in the lipid film preparation which extracts to the methanol/PBS phase is reduced to only 3% (compared with 11% for the liposome preparation).

A

B
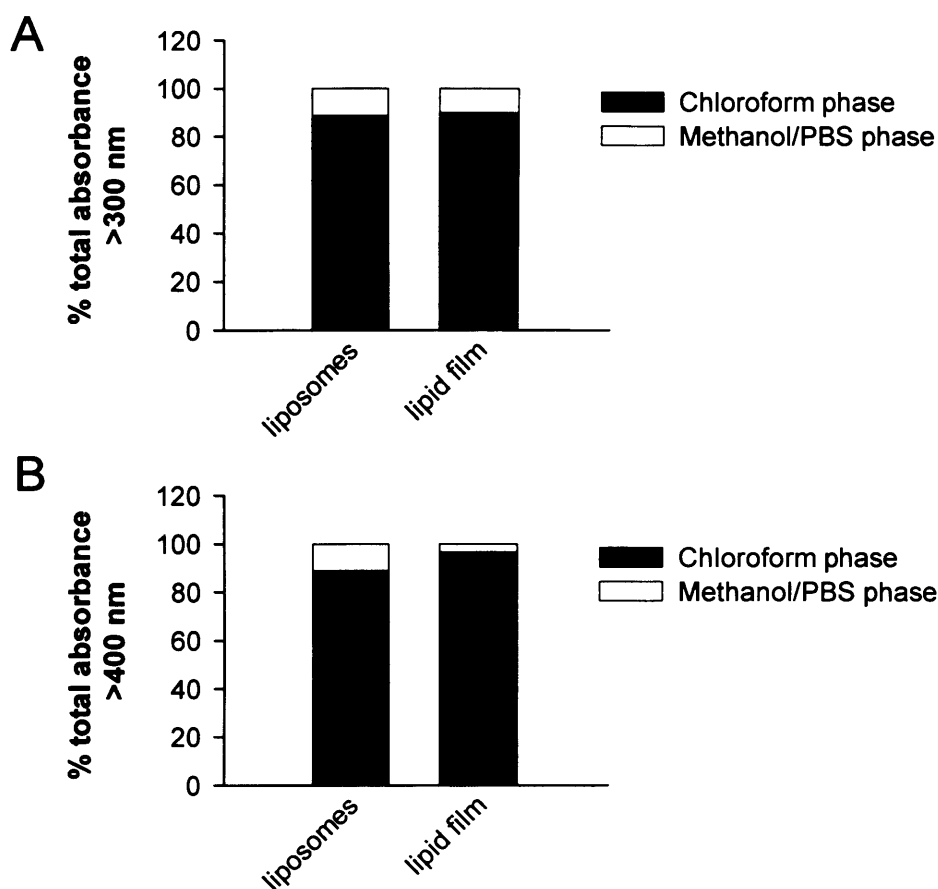
Figure 3.8 *Comparison of partitioning into chloroform and methanol/PBS phases after peroxidation as liposomes (second batch, 18 days) or lipid film (175 days). (A) Comparison of integrated absorbance between 300 and 600 nm; (B) comparison of integrated absorbance between 400 and 600 nm.*

integrated region	absorbance ratio	
	liposomes	lipid film
>300 nm	89%:11%	90:10
>400 nm	89:11	97:3

Table 3.2 *Comparison of ratios of chloroform phase to methanol/PBS phase absorption after correcting for extraction volume, for wavelengths longer than either 300 or 400 nm.*

3.4 Discussion

The observations in this chapter confirm that DHA autoxidation occurs readily *in vitro* and that the rate thereof varies depending on the microenvironment of the lipids.

Absorption spectroscopy showed that even "unperoxidized" DHA samples, which have been carefully prepared under argon throughout and stored under argon immediately after preparation of liposomes, exhibited absorbance at longer wavelengths. This is indicative of the presence of peroxidation products. Thus, the samples, although not allowed to peroxidize, were not 100% unperoxidized. This could be due to contamination of lipids, glassware or PBS with metal ions, for example iron, which would promote lipid peroxidation as described in Chapter 1. Similarly, it can not be assumed that all DHA in the "peroxidized DHA" samples was completely peroxidized, as shown by a clear absorbance peak still evident at ~210 nm.

An unexpected observation in monitoring peroxidation of DHA was the formation of the "interphase" during lipid extraction, which increased with duration of peroxidation. In the second liposomes, a gradual increase in absorbance in the methanol/PBS phase was observed (up to 18 days of peroxidation), indicating increased formation of polar products with time, with limited amount of material in the interphase. At later stages of peroxidation, as monitored in the first liposomes (up to 175 days), a thick, dark layer formed, apparently consisting of polar products, as they dissolved into the upper layer after repeat extractions. This indicated an excess of these products, saturating the methanol/PBS layer until "fresh" methanol/PBS mixture was added during subsequent repeat extractions.

In contrast, DHA allowed to peroxidize as a film for 175 days appeared more similar in appearance to the second liposomes, peroxidized for only 18 days, than the first liposomes which were peroxidized for the same length of time (i.e. 175 days). There was similar absorbance in the methanol/PBS phase, and very little interphase material. This indicates lower levels of peroxidation compared with

the first liposomes, a finding which correlates with absorbance measurements of the extracted chloroform phase. Here, the first liposome batch showed 80% lower absorbance at 210 nm compared with the lipid film samples peroxidized for the same length of time, indicating greater degradation of native DHA. Again, the lipid film sample was more similar to the second liposomes which were peroxidized for 10% of the duration of the first liposomes, as these showed similar absorption spectra for the chloroform phase.

As the lipid film and the first liposomes were allowed to peroxidize simultaneously, on the same heating block and in the same environment, the only difference was the microenvironment of the lipids: i.e. the presence of water and also possibly redox active metal ions in the liposome preparation. As the phase transition for DHA-PC is very low (approximately -70 °C; Kariel *et al.*, 1991), the lipids in the film should be mobile and able to interact freely with each other, with no added benefit with the addition of water. The hydration state could, however, be a crucial variable as it could facilitate hydrolysis of the lipids, and would aid with diffusion of metal ions between liposomes. Obviously the liposome model for lipid peroxidation appears more physiologically relevant to retinal lipid membranes, as cell membranes, like lipid bi-layers in liposomes, are in contact on both surfaces with aqueous solutions. However, peroxidation as a film is relevant to lipofuscin and lipid deposits in Bruch's membranes, as lipids contained within these may be isolated from water.

The formation of chloroform-insoluble degradation products has implications for further experiments in this thesis: in those experiments involving antioxidants (Chapters 5 and 6), peroxidized liposomes were extracted and only the chloroform phase was used for addition of antioxidants and re-forming of liposomes. It is possible that in this process a large number of DHA peroxidation products were removed, which could result in lower toxicity compared with the original starting pDHA prior to extraction. However, removal of those polar hydrophilic products found in the methanol/PBS phase may in fact make the samples more representative of any likely drusen or lipofuscin-like substances in the retina. In both of these lipid-rich components of the aged retina, hydrophilic degradation products of lipids are unlikely to be retained as they would more

likely diffuse away. Indeed, after Folch's extraction of human lipofuscin samples, no absorption of light above 200 nm is detectable in the upper methanol/PBS phase, suggesting they do not contain equivalent products (Pawlak *et al.*, 2002; Rozanowska *et al.*, 2004).

Loss of DHA products into the methanol/PBS phase rather than retention in the chloroform phase could explain the plateau in formation of conjugated dienes and trienes seen in the first liposome batch, as these products may have been formed then degraded further into polar products. This is similar to findings with free fatty acids (Kim and LaBella, 1987).

Fluorescence of peroxidized DHA was consistent with previous findings, that formation of fluorescent compounds increases with the extent of peroxidation (Gutteridge *et al.*, 1982; Kim and LaBella, 1987). The fluorescence emission peak of pDHA from the chloroform phase of extraction is measured here as 437 nm (i.e. blue) upon excitation at 360 nm. This is consistent with data for homogenized retina samples which have been allowed to oxidize *in vitro* (Eldred and Katz, 1989). In contrast, lipofuscin – both *in situ* and when isolated – shows yellow fluorescence with emission peaking at 570-605 nm, increasing in intensity with age (Eldred and Katz, 1989; Boulton *et al.*, 1990; Docchio *et al.*, 1991). The difference between peroxidized lipid and lipofuscin fluorescence has led to debate on the validity of the theory that lipofuscin formation is induced by lipid peroxidation (Eldred and Katz, 1989,1991; Sharma and James, 1991). Lipofuscin has however been shown to contain DHA (Bazan *et al.*, 1990). The observed change in fluorescence from blue to yellow may be caused by interaction and cross-linking of peroxidized lipids with other components of lipofuscin, or due to the actions of lysosomal enzymes (Eldred and Katz, 1989). Alternatively, it has been suggested that as yet unidentified blue-absorbing chromophores(s) may transfer energy to A2E, an important component of lipofuscin which in fact shows yellow emission properties similar to lipofuscin (Haralampus-Grynaviski *et al.*, 2003). From data shown here, pDHA could be proposed as a candidate for this absorbing chromophore.

Results here have clearly shown the potential for DHA peroxidation products to absorb light above 400 nm. This is vital to this project as the phototoxicity of pDHA is investigated in later chapters using visible light, above ~400 nm, and in the intact adult human eye, very little light below 400 nm reaches the retina as it is blocked by the lens and cornea. Only in the very young eye there is a small transmission band peaking at 320 nm (Boettner and Wolter, 1962).

Similarities between the lipids peroxidized as a film and the second liposomes justify the use of both of these preparations in further experiments described in the rest of this thesis. As there is still some variation between these two, their use has been kept to separate sets of experiments.

In summary, DHA autoxidation has led to formation of products which are capable of absorbing blue light, providing liposomes which are suitable for use in further experiments to monitor pDHA (photo-)toxicity.

Chapter 4:
Cytotoxicity studies

4.1 Introduction

As discussed in Chapters 1 and 3, DHA is present in high levels in the outer retina (i.e. photoreceptors and RPE), and is easily peroxidized, as demonstrated in Chapter 3, and DHA peroxidation products have been identified in and around the RPE cell layer – in photoreceptor outer segments, in the RPE including in lipofuscin granules, and in drusen deposits found beneath the RPE cell layer (Crabb *et al.*, 2002; Gu *et al.*, 2003a; Ng *et al.*, 2008). pDHA has also been shown to be photoexcitable *in vitro* (personal communication, M.B. Rozanowska) resulting in production of reactive oxygen species. Thus, considering the high light fluxes in the retina it is possible that pDHA could be phototoxic to RPE cells. The increase in pDHA levels observed with age and progression of AMD (Gu *et al.*, 2003a) could therefore play a role in the age-related RPE cell dysfunction observed.

Toxicity due to reactive oxygen species may culminate in either of two forms of cell death: apoptosis or necrosis. Key features of these two processes are shown in Figure 4.1. Apoptosis, also known as programmed cell death, can be induced by a multitude of internal or external triggers, leading to a tightly controlled cascade of events, shown in Figure 4.2, culminating in cell death. This process is often essential during normal development. *In vivo*, waste products of apoptotic cells are usually efficiently removed by phagocytic cells meaning neighbouring cells remain unaffected. In contrast, necrosis often occurs due to "accidental" insult, and due to its rapid culmination with permeabilized and effectively burst cells, and the nature of the toxic insult, it is prone to affect groups of cells. In certain situations, such as *in vitro* cell culture environments where phagocytic cells are not present to remove apoptotic residues, apoptosis does not resolve properly, and cells begin to show apparently necrotic attributes such as loss of membrane integrity – a process sometimes called secondary necrosis. This is not, however, a valid form of cell death when studying toxicity of an agent, as this would not occur in most tissues *in vivo*.
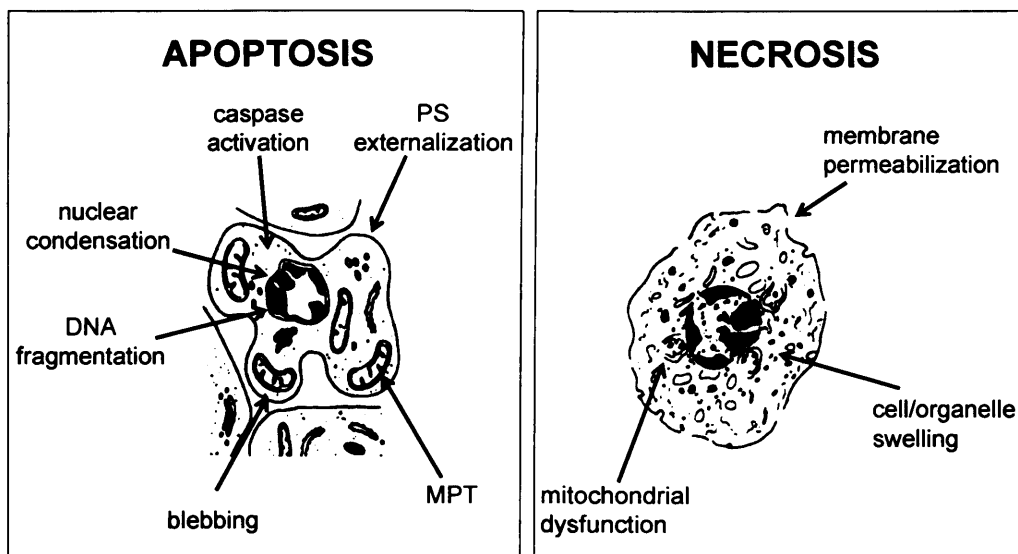
Figure 4.1 *Comparison of key features of apoptotic and necrotic forms of cell death. PS = phosphatidylserine; MPT = mitochondrial permeability transition. Cell images taken from:* www.imm.ki.se/sft/bilder/Image1.jpg
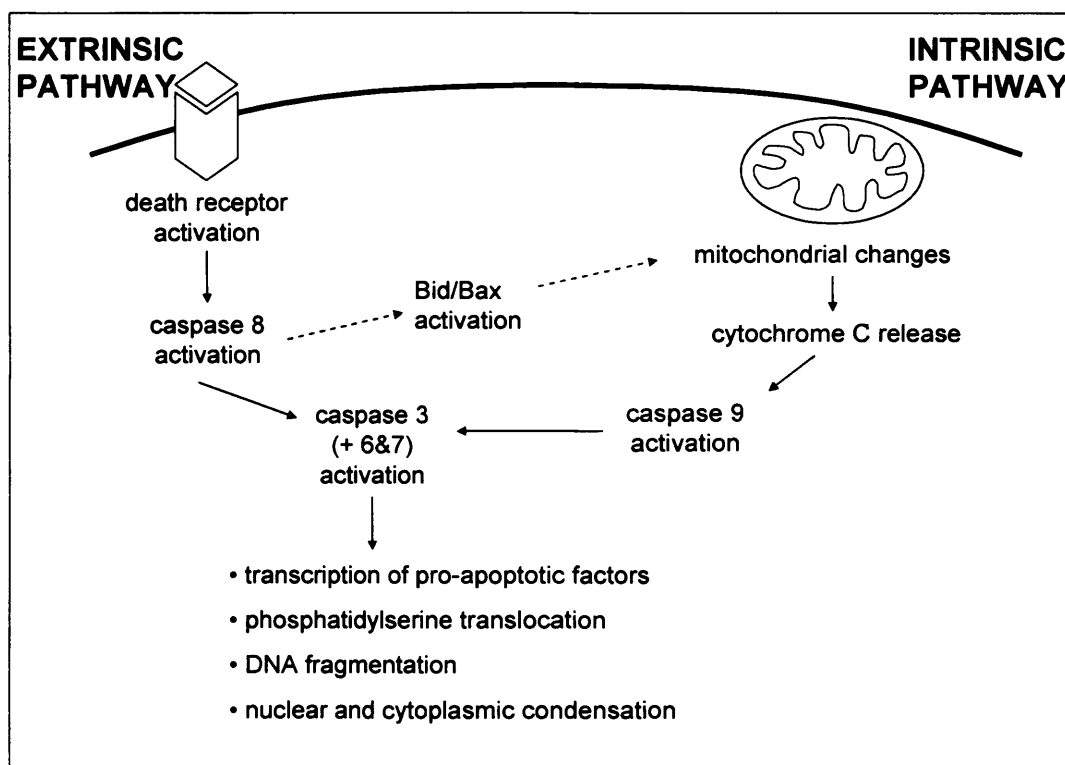
Figure 4.2 *Pathways of apoptotic cell death, principally divided into extrinsic and intrinsic routes, with possible crossover via Bid/Bax activation.*

In this thesis, multiple assays were used to monitor the pathways of cell death involved in pDHA (photo-)toxicity. Different time points were tested initially during optimization of the assays, as the rate of the apoptotic cascade can vary depending on the insult. Additionally, multiple assays were carried out to ensure signals were not missed and to try to monitor which pathway was involved.

It is believed that reactive oxygen species induced apoptosis occurs via the mitochondrial, or intrinsic, pathway (Dumont *et al.*, 1999). At high levels of insult, it is possible for some species, for example hydrogen peroxide, to cause necrosis rather than apoptosis due to oxidation of caspase enzymes (Hampton and Orrenius, 1997). Additionally, reactive oxygen species may simply cause extensive lethal damage to the cell membrane. The pathway of cell death induced by pDHA therefore warrants investigation.

The aim of this chapter was to quantify levels of (photo-)toxicity induced by pDHA in different conditions, and then to further understand the pathways by which the observed cell death occurred.

4.2 Experimental design

4.2.1 Exposure of cells to DHA

Cells were exposed to (p)DHA in the form of externally applied liposomes. The aim of this procedure was to mimic the situation *in vivo* where pDHA is found in close contact with RPE cells – either in photoreceptor membranes which normally lie adjacent to and in intimate contact with the apical surface of the RPE, or Bruch's membrane deposits which are in close contact with the basal surface of the RPE cell layer.

4.2.2 Light exposure and subsequent analysis of cell viability

Initially, the effects of a known photosensitizing agent, rose bengal, on ARPE-19 cells were monitored to observe the cellular response to phototoxic insult. Following peroxidation of DHA, its phototoxicity was also studied.

To monitor cell viability, the MTT assay of mitochondrial activity was used initially. This measures the reductive capacity of mitochondria. MTT assay was carried out either immediately or 24 hours later, allowing cells to either recover, or for the apoptotic cascade to continue resulting in cell death. Loss of activity therefore indicates overall levels of cell death. Cells were then imaged using phase contrast microscopy to monitor changes in gross morphology. Other indicators of apoptosis were then monitored: nuclear condensation (using Hoechst labelling) and DNA cleavage (using TUNEL). Additionally, propidium iodide was used to monitor membrane integrity. Loss of integrity at initial stages of cell death would indicate necrosis.

After exposure to rose bengal +/- light for 1 hour, cells were "post-incubated" in fresh medium with 2% FCS for different durations, as stated in the results. All MTT results were normalized to control for the same cell culture plate deemed to be 100% mitochondrial activity i.e. 0 mM RB with identical light exposure conditions and post-incubation period.

DHA exposure +/- light was carried out for 1 hour, then for the MTT assay, cells were washed and either tested immediately or put in fresh medium for 24 hours first. For other apoptosis assays following DHA exposure, duration of post-incubation was varied to ensure that crucial steps in the cascade of cell death events were not missed. Times are stated in the relevant results sections.

4.3 Results

4.3.1 Confirmation of ARPE-19 cell identity

As expected, positive labelling of cultured ARPE-19 cells with cytokeratin 18 was observed as shown in Figure 4.3, confirming a pure epithelial cell culture without contamination by other retinal cell types.
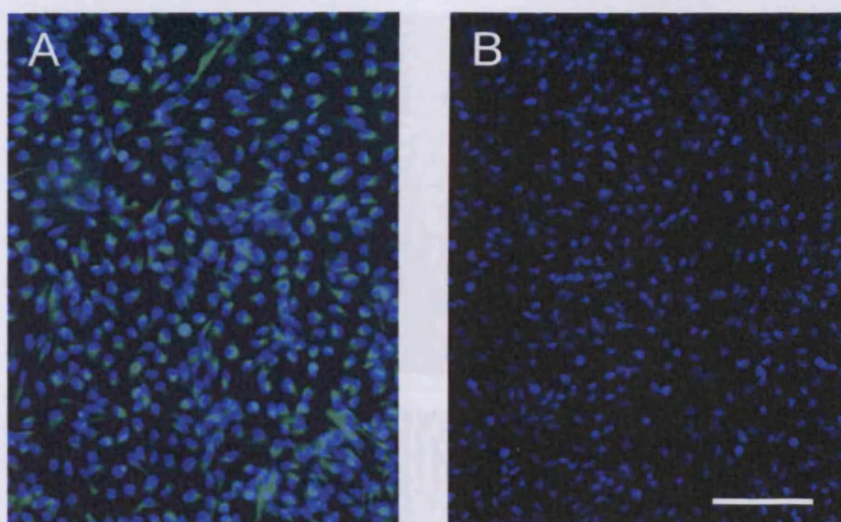
Figure 4.3 *Cytokeratin 18 labelling of ARPE-19 cells. (A) Cells labelled with both cytokeratin (green) and Hoechst 33342 (blue); (B) control slide showing labelling with only Hoechst. Bar = 100 µm.*

4.3.2 Rose Bengal cytotoxicity

4.3.2.1 Cell morphology

Cells exposed to the lower concentrations of rose bengal (≤ 0.1 µM) showed no major morphological changes when observed by phase contrast microscopy (see Figure 4.4). At increasing concentrations, considerable changes in morphology were evident, with cell shrinkage (causing bright areas in images due to increased thickness of samples and difficulties in focussing on the full depth) and some cell detachment observed. At the highest concentration of 1 µM, however, the cells appeared to remain attached, although they were completely different in appearance to unaffected cells – with cells becoming more spindly, and often with visible nuclei.

Figure 4.4 *Phase contrast images of ARPE-19 cells 17 hours after exposure to light and rose bengal at indicated concentrations. Bar represents 50 μm.*

4.3.2.2 MTT assay

Rose bengal had a concentration-dependent effect on cell viability in the presence of light, as measured by MTT assay (see Figure 4.5A), with all concentrations ≥ 0.2 μM at all time points showing statistically significant reduction in mitochondrial function compared with control (0 μM rose bengal with matched light exposure/post-incubation conditions; *P*-values for comparisons are shown in Appendix 1). The cytotoxic effect of rose bengal increased with increased time after exposure (in the presence of light). Cells

90

exposed to rose bengal in dark conditions showed no significant changes in mitochondrial activity compared with control. Figure 4.5B shows that light and post-incubation alone had no significant effect on MTT absorbance values in 0 μM rose bengal controls (one-way ANOVA P-value = 0.9652).
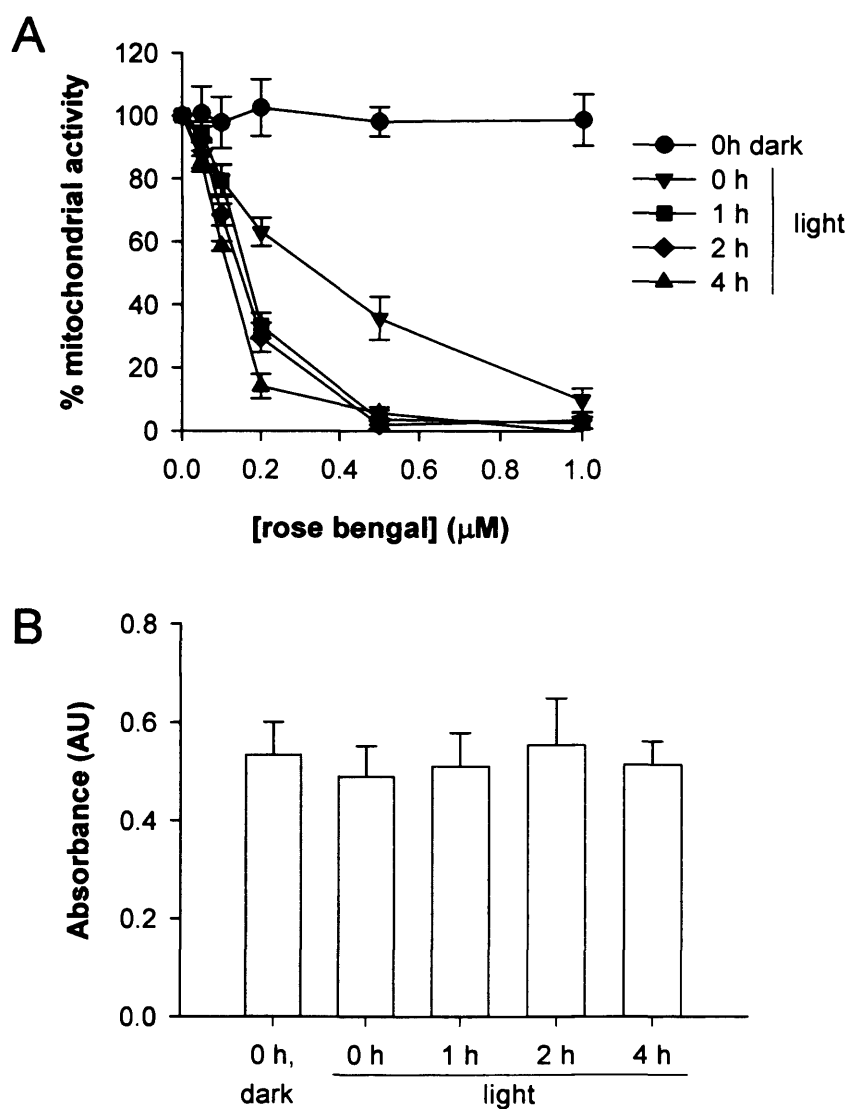
Figure 4.5 *Results of MTT assay after rose bengal exposure. (A) MTT assay was carried out at the indicated time after 1 hour rose bengal exposure, with 2.8 mW.cm^{-2} green light except where labelled as "dark". Mitochondrial activity was calculated as percentage of control (i.e. 0 μM rose bengal with same light conditions). (B) Raw MTT absorbance values at 590 nm for control cells (0 μM rose bengal) at different time points after exposure. Error bars indicate SEM; n = 3 or 4.*

4.3.3 pDHA cytotoxicity

4.3.3.1 Cell morphology

As shown in Figure 4.6, cell morphology did not appear to have altered greatly 24 hours after exposure to 1 mM pDHA in the dark, although 2 mM pDHA appeared to increase the occurrence of smaller cells on the surface. When cells were exposed to pDHA in light conditions, morphology was severely altered, with appearance of spindles extending from cells and eventually no clearly distinguishable cell outlines. Cell detachment did not appear to be as severe as after treatment with rose bengal.
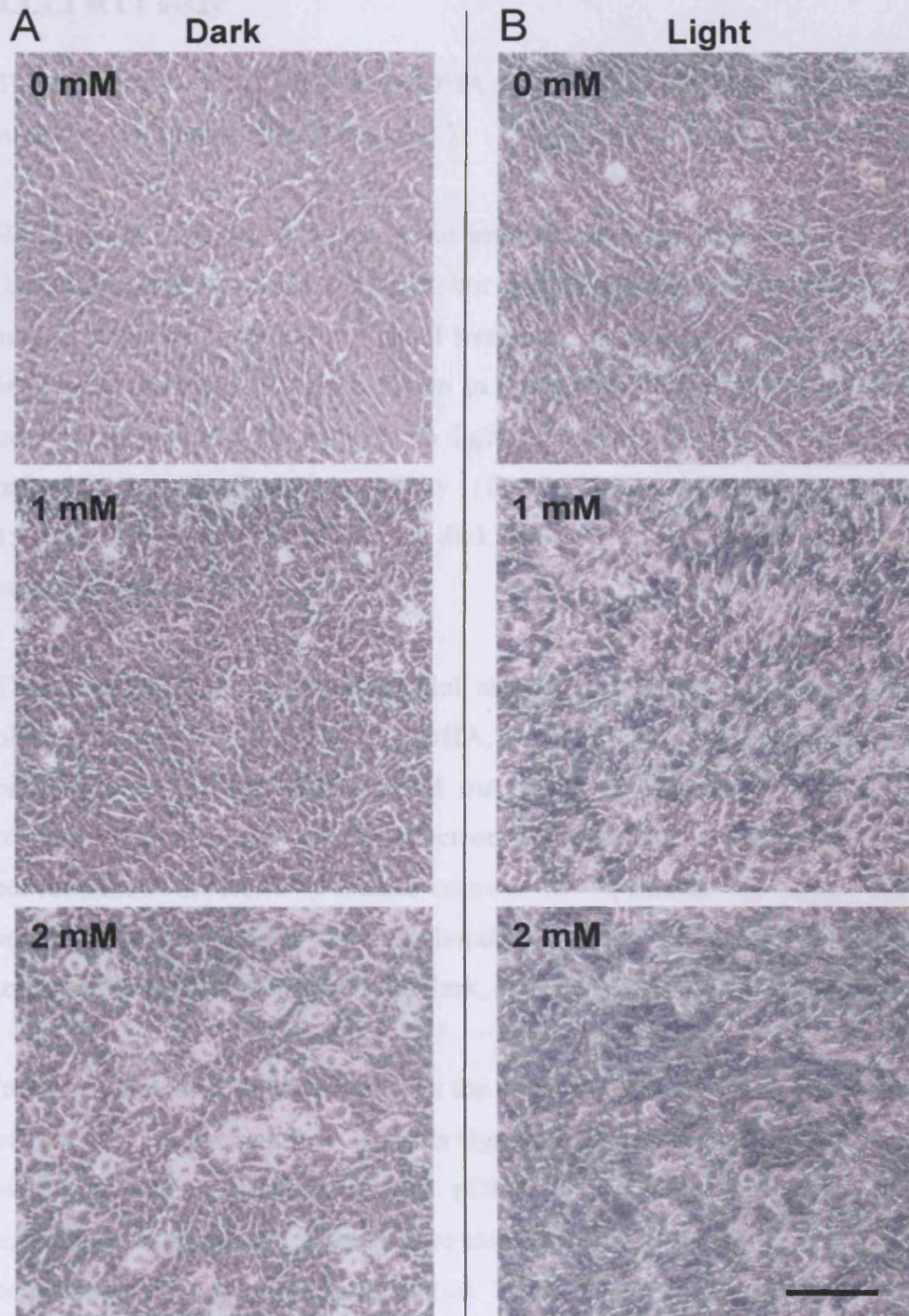
Figure 4.6 *Effects of pDHA on cell morphology. Phase contrast images taken 24 hours after exposure to pDHA at the indicated concentrations. (A) Cells exposed to pDHA in dark conditions; (B) cells exposed to pDHA with light. Bar = 100 μm.*

4.3.3.2 MTT assay

The effects of 1 hour DHA and pDHA exposure on mitochondrial activity of ARPE-19 cells are shown in Figure 4.7.

When the MTT assay was carried out immediately after exposure, 2 mM DHA (i.e. unperoxidized) caused a slight but significant decrease in mitochondrial activity compared with control in all treatment conditions i.e. light and dark at both light intensities (P-values shown in Appendix 1). 24 hours later, however, only DHA treated cells exposed to light at $9 \, mW.cm^{-2}$ showed a significant reduction in mitochondrial activity ($P = 0.0176$), while cells exposed to $15 \, mW.cm^{-2}$ or maintained in the dark showed no significant difference to control ($P > 0.05$ for all).

The effect of DHA on mitochondrial activity was smaller than the effect of pDHA. After exposure to 2 mM (p)DHA, in each of the four conditions (either 9 or $15 \, mW.cm^{-2}$, with MTT carried out either after 0 hs or 24 hs), pDHA produced a significantly greater effect on mitochondrial activity than the same concentration of DHA (P-values shown in Appendix 1). Light did not significantly alter effects on mitochondrial activity of either peroxidized or unperoxidized DHA compared with dark, at this maximal 2 mM concentration.

Increasing the length of time between the exposure of cells to DHA and carrying out the MTT assay from 0 to 24 hours significantly increased the observed effect on mitochondrial activity at 2 mM pDHA, in both light exposed and dark maintained experiments. Tukey's post-tests revealed P-values of <0.001 for all comparisons of equivalent samples (i.e. 2 mM pDHA, either 9 or $15 \, mW.cm^{-2}$ experiments, in light-exposed or dark-maintained samples) at 0 hs vs. 24 hs.
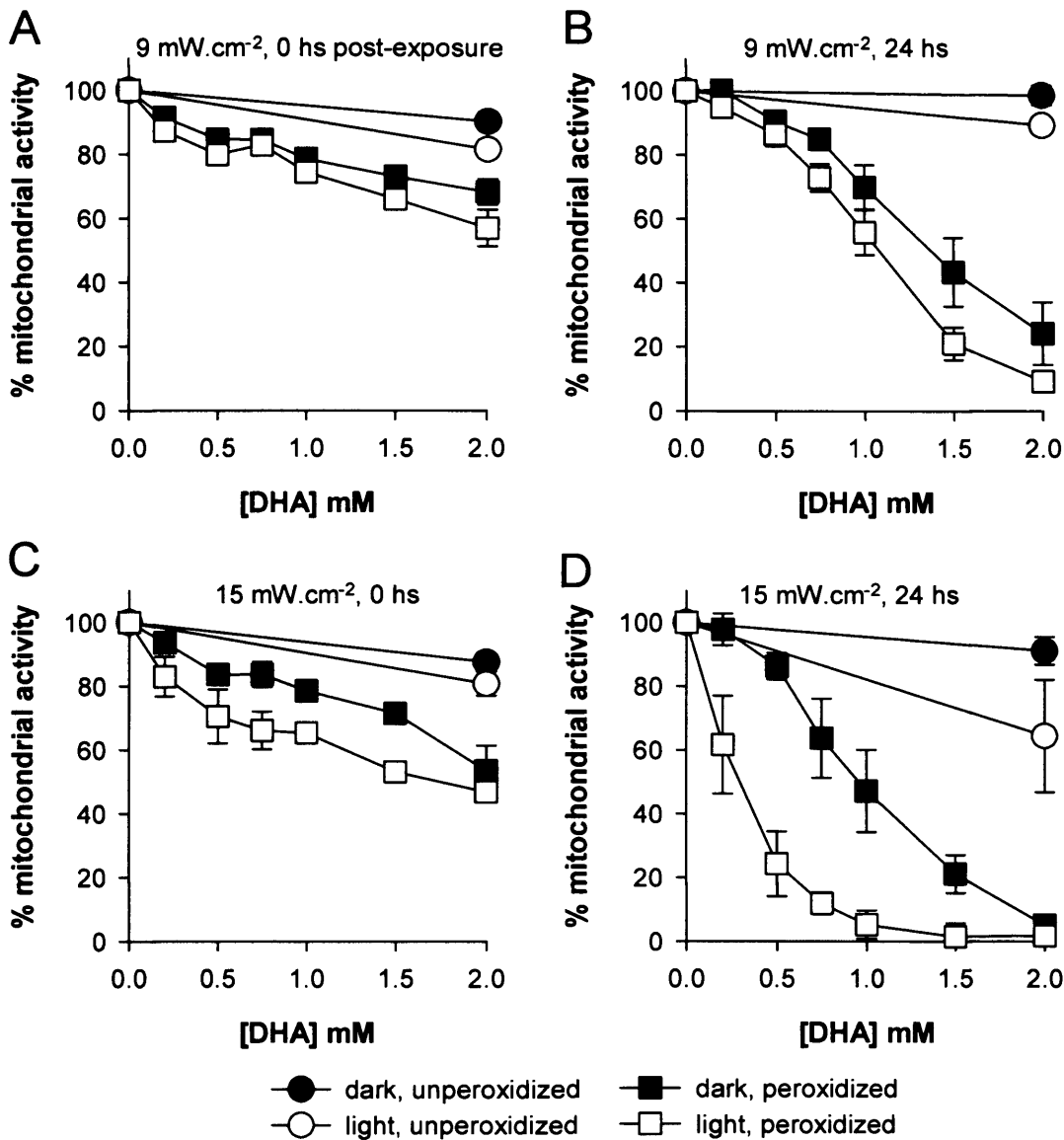
Figure 4.7 *Effects of pDHA and irradiance levels on mitochondrial activity, measured by MTT assay at different time points after exposure. Mitochondrial activity is expressed as a percentage of control (i.e. 0 mM DHA). Bars = SEM; n = 3-6.*

Further comparisons of data collected 24 hours after DHA exposure was enabled by fitting data to a sigmoidal curve. This allowed calculation of EC50 values, indicating the pDHA concentration which induced a 50% reduction in mitochondrial activity. Curve fits are shown in Figure 4.8. Comparisons of these values using F-tests showed that light did not significantly increase the effect of pDHA at 9 mW.cm^{-2} (EC50: 1.36 mM (dark) vs. 1.06 mM (light), $P = 0.506$). At

15 mW.cm^{-2}, however, light did significantly decrease the EC50 value, thus indicating an increase in toxicity of pDHA (EC50: 0.94 mM vs. 0.26 mM dk vs. lt; $P < 0.0001$). Data also showed that in light-exposed cells, increasing the light intensity from 9 mW.cm^{-2} (EC50: 1.06 mM) to 15 mW.cm^{-2} (EC50: 0.26 mM) significantly increased the effects of pDHA (P < 0.0001)
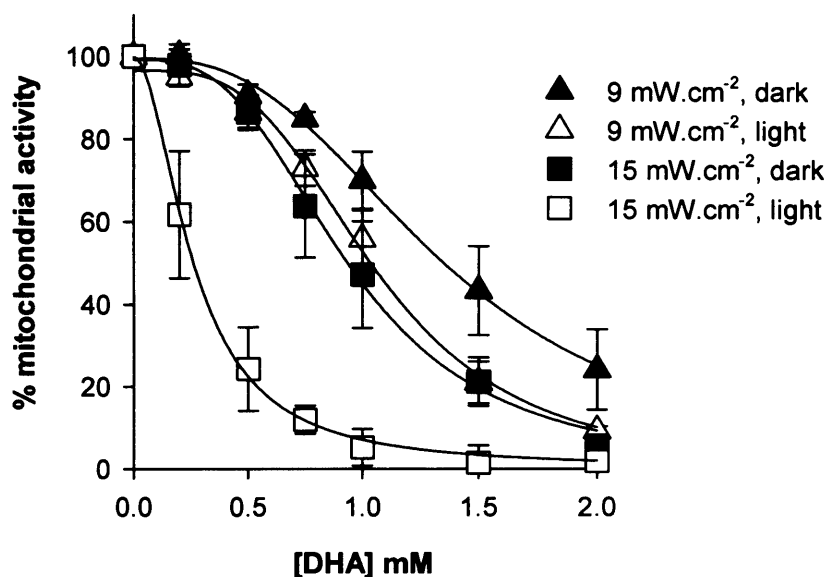
Figure 4.8 *Sigmoidal curve-fits of mitochondrial activity data for MTT assays carried out 24 hours after exposure of cells to pDHA in dark or light, at 9 or 15 mW.cm^{-2}.*

4.3.3.3 Propidium iodide labelling for membrane integrity

Minimal uptake and nuclear labelling of PI was observed in ARPE-19 cells treated with pDHA + light for 1 hour either immediately or 2 hours after exposure (Figures 4.9 and 4.10). This confirms that these cells do not undergo necrotic cell death within this time period, and that pDHA did not interfere with membrane integrity in a way that altered permeability to PI. This is confirmed by lack of significant difference between numbers of PI-labelled nuclei after different treatments (ANOVA: *P* = 0.291).
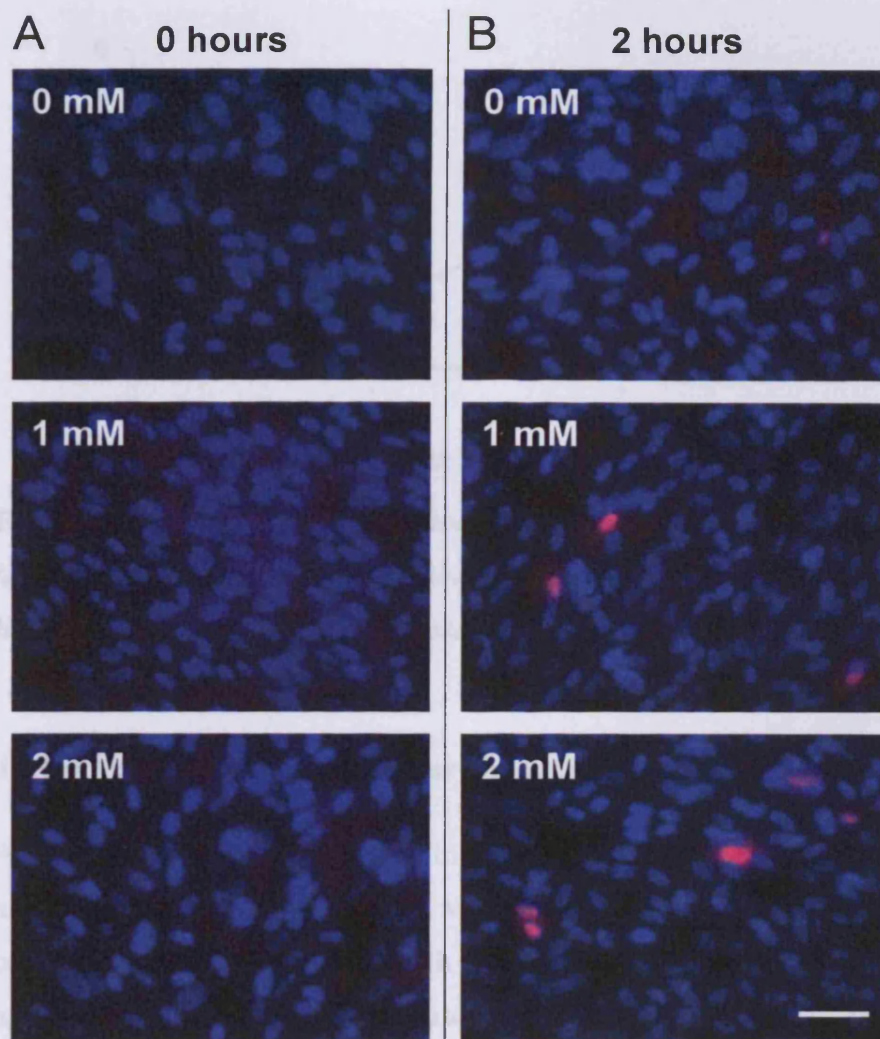
Figure 4.9 *Representative images of propidium iodide labelling of cells after exposure to indicated concentrations of pDHA + 15 mW.cm^{-2} light. (A) Labelled immediately after exposure; (B) labelled after 2 hours post-incubation in fresh medium. Blue = Hoechst; pink = dual labelling with Hoechst and PI. Bar = 50 μm.*

Figure 4.10 *Effects of pDHA treatment on membrane integrity as indicated by PI labelling of nuclei. Cells were labelled immediately after exposure or after 2 hours of post-incubation in fresh medium. Bars = SEM; n = 3.*

4.3.3.4 Apoptotic changes: nuclear condensation and DNA cleavage

After 12 hours of post-incubation in fresh medium following exposure to pDHA and light, changes in cell nuclei were observed, with increased incidence of condensed nuclei and labelling with the TUNEL assay. Additionally, cell density appeared to decrease with increased pDHA concentration (Figures 4.11 and 4.12). However, there was no statistically significant change in total cell number per slide, or prevalence of TUNEL stained nuclei (ANOVA: $P > 0.05$ for both). The number of cells with condensed nuclei did, however, increase significantly (ANOVA: $P = 0.0004$), from $< 1\%$ with 0 mM pDHA to ~25% with 1 mM pDHA ($P < 0.001$), and to 14.5% after treatment with 2 mM pDHA ($P < 0.05$). Additionally, the total number of cells showing no indicators of apoptosis (i.e. "normal nuclei" in 4.12A) did change significantly (ANOVA: $P = 0.021$), from approximately 150 cells in control slides to 103 after 1 mM pDHA (31% reduction; $P < 0.05$) and to 82 after 2 mM pDHA (45% reduction; $P < 0.05$).
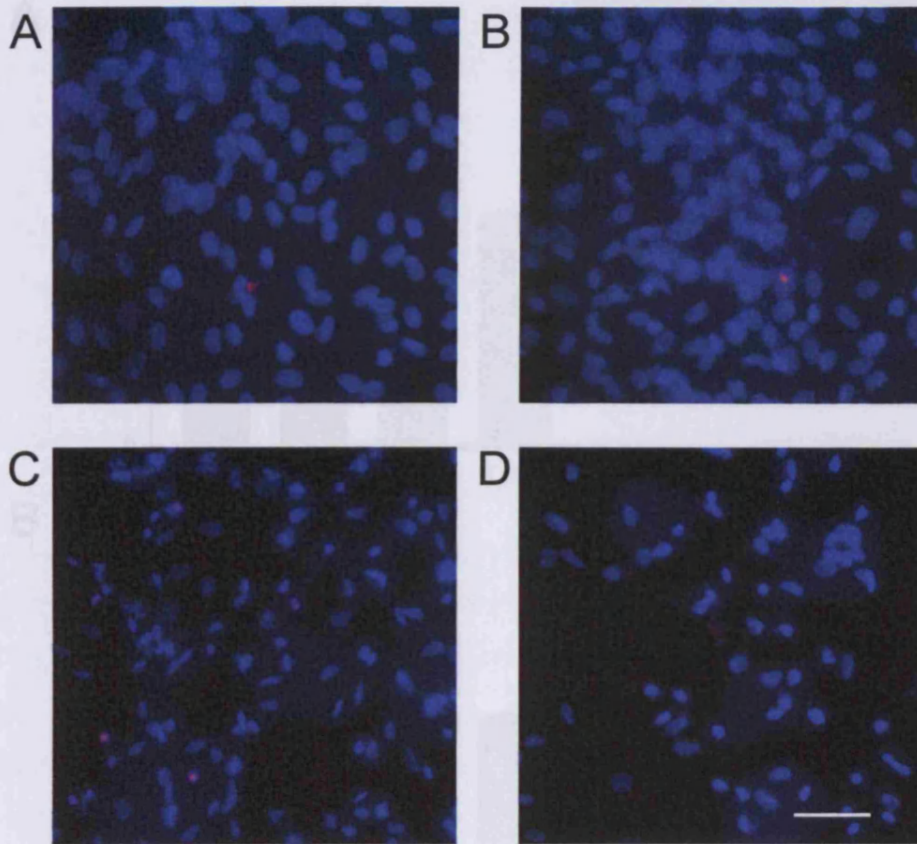
Figure 4.11 *Images showing the effects of pDHA on DNA cleavage and nuclear condensation. Cells were exposed to (A) 0 mM, (B) 0.5 mM, (C) 1 mM or (D) 2 mM pDHA in 15 mW.cm^{-2} light. All cells were fixed and processed 12 hours after exposure. Blue = Hoechst; red/pink = TUNEL. Bar = 50 μm.*

Figure 4.12 *Effects of pDHA on cell nuclei and cell attachment 12 hours after exposure to pDHA. (A) Effects of pDHA on nuclear condensation and (B) DNA cleavage. Total height of stacked bars indicates the average number of adherent cells in each image. As data from the two graphs is from the same images, the cell totals for each concentration are identical in both. Bars = SEM; n = 3-4.*

4.4 Discussion

Cytokeratin 18 labelling confirmed the identity of RPE cells as epithelial cells. Although the antibody used was not specific for RPE cells, the lack of other epithelial cells in the retina allowed the use of this antibody to ensure there was no contamination by other retinal cells. Contamination would be unlikely as ARPE-19 is a well established cell-line, and it was purchased after identification by the supplier using more specific markers (RPE65 and CRALBP).

The use of the ARPE-19 cell line instead of primary cell cultures has certain implications. ARPE-19 is a spontaneously arisen cell-line derived from primary cultures of a human 19-year-old donor. Cells are structurally and functionally similar to RPE cells *in vivo*. They grow as an adherent polarized monolayer, and form tight junctions with similar barrier properties to native RPE cells. They also accumulate pigment with increased time in culture (Dunn *et al.*, 1996). Several studies have been carried out, however, which indicate important differences in the RNA and protein expression profiles between primary RPE cells and ARPE-19 cells, and the effects of culture conditions on these profiles. The most notable differences include down-regulation in ARPE-19 of proteins involved in retinoid metabolism (resulting in inability of the cells to regenerate 11-*cis*-retinal from all-*trans*-retinol) and changes in expression of cytoskeleton-related elements (Alge *et al.*, 2003; Tian *et al.*, 2005; Alge *et al.*, 2006).

Despite the differences compared with primary RPE cells, the use of ARPE-19 cells provides an overall advantage: they are readily available and divide rapidly to provide uniform and stable cultures with which to carry out experiments. Thus, there are no requirements to obtain fresh donor eyes and carry out isolation and purification on a regular basis in order to maintain a supply of high numbers of cells. Variation in ages and pathology in donor human eyes would cause further issues, particularly in light of the fact that most experiments in this thesis involved investigation of the effects of light on cells – variation in levels of intrinsic light-absorbing and potentially photosensitizing agents, such as lipofuscin, would increase baseline variability between cell cultures. Thus, the use of the ARPE-19 cell line was chosen instead.

The main purpose of this chapter was to further understand the response of ARPE-19 cells to photosensitizer-induced toxicity. As expected, rose bengal proved to be a potent inducer of ARPE-19 cell death causing gross changes in cell morphology and reduction in mitochondrial activity measured by the MTT assay. There was no effect of rose bengal in the dark, showing its specific light-induced effects. In contrast, pDHA caused cell death in light and dark conditions. The toxicity of pDHA was, however, greater after light treatment suggesting that pDHA does have photosensitizing properties.

Normal light levels to which the retina is exposed in indirect outdoor daylight range from approximately 0.01 to 0.1 mW.cm^{-2}, which is similar to the irradiance of indoor light sources on the retina (Sliney, 1983). Light doses used in DHA experiments here were 1 hour at 9 or 15 mW.cm^{-2}, which are therefore equivalent to 90 or 150 hours of exposure at the maximum likely retinal irradiance in normal daylight This shows one of the limitations of the model used here, in which the response to an acute light exposure is monitored rather than the long-term exposure to normal daylight levels more likely to be encountered by the average adult human being. However, it should be noted that the light intensities used here were significantly lower than those of direct sunlight focused on the retina, or optometric equipment such as ophthalmoscopes (~70 mW.cm^{-2} for indirect, 30 mW.cm^{-2} for direct) and slit lamps (>200 mW.cm^{-2}), or surgical lamps used in operating theatres (25 mW.cm^{-2}) (Calkins et al., 1980; Sliney, 1983). Cytotoxicity of pDHA is already observed after 1 hour exposure to the lower irradiance of 9 mW.cm^{-2}, which is equivalent to only 2.7 minutes of exposure to a slit lamp.

Using variables measured for rod outer segments (Lamb and Pugh, 2004): i.e. dimensions of photoreceptors (length: 25 μm, diameter 2 μm) and spacing of discs (1 disc (i.e. 2 membranes) per 0.03 μm), rhodopsin density in disc membranes (25,000 μm^{-2}), and numbers of outer segments in contact with each RPE cell (~25), in addition to relative levels of lipids to proteins (480 nmol per mg total protein in young and 716 in old retinas; Bazan et al., 1990), the molecular weight of rhodopsin (~38800) and rhodopsin levels as a percentage of total protein in outer segments (~80%; Fliesler and Anderson, 1983), the amount of DHA to which RPE cells are exposed in vivo can be estimated. Calculations give values from 1.3×10^{-13} to 1.9×10^{-13} moles of DHA per RPE cell (from young to old retinas), if total DHA from each whole photoreceptor is taken into account. This does not take into account any DHA contained within RPE cells or at the basolateral surface in Bruch's membrane. By comparison, ARPE-19 cells grown in culture were exposed to a DHA range of 2.3×10^{-13} to 2.3×10^{-12} mol DHA per cell (based on the concentration range used in MTT experiments of 0.2 mM to 2 mM and an average count of cells contained within a cell culture well). Although the maximal in vitro levels and the in vivo values differ by more

than 10 times, the *in vivo* value is close to the lowest concentration used. Obviously the conditions and environment of the DHA *in vivo* vs. *in vitro* differ greatly, particularly in that in intact retinas, RPE processes extend into the POS layer, increasing the surface area of contact and possible interactions. However, this comparison of exposure levels shows the concentrations used in experiments are meaningful.

MTT results show clear increases in death of ARPE-19 cells with increased pDHA concentration, particularly when MTT assay was carried out 24 hours after exposure. This delay (indicating initial maintenance of active mitochondria), in addition to the lack of PI labelling at short time points, strongly suggests a role for apoptotic cell death in the loss of cell viability observed. Significant increases in cell numbers showing condensed nuclei support this finding. Quantification of DNA cleavage by TUNEL assay showed no significant change. This finding could, however, be compromised by the large numbers of cells detached in the processing of these samples, as further analysis did show a significant decline in non-apoptotic cells.

Although pDHA causes cell dysfunction in the dark, the finding that light exacerbates pDHA toxicity is extremely important for a tissue such as the retina. The level of toxicity observed in the dark would be unlikely to fluctuate greatly or suddenly over short time periods if darkness is maintained, thus allowing the retina to adapt to the conditions e.g. by providing and replenishing intrinsic antioxidants. Exposure to light, however, produces rapid temporal variations in conditions to which the retina would need to respond at onset of the "insult". The finding that light exacerbates pDHA toxicity is, therefore, extremely important for a tissue such as the retina.

In summary, pDHA causes delayed cell death in ARPE-19 cells, probably *via* the apoptotic pathway of cell death, with a greater toxicity observed with higher light intensities.

Chapter 5:
Effects of antioxidants on
pDHA toxicity

5.1 Introduction

As described in Chapter 3, DHA peroxidation may occur readily in the retina, due to the structure and abundance of DHA itself, and the presence of photosensitizers, iron and high levels of oxygen. To end the propagation of the peroxidation chain of events, a termination step is required. Antioxidants play an important chain-breaking role to terminate lipid peroxidation and prevent further damage that may occur through the species produced. Thus, they may limit direct damage by lipid peroxidation products to other cellular components or formation of conjugates with other cellular molecules such as proteins, potentially leading to undegradable material such as lipofuscin – a matter which is investigated further in later chapters of this thesis.

As discussed in Chapter 1, there is an important role for antioxidants in maintenance of cellular homeostasis in the retina and various antioxidants have been used clinically in attempts to reduce or delay the onset of AMD, with varying levels of success. In addition to providing a basis for potential therapeutic pathways, the *in vitro* use of different antioxidants with known mechanisms of action may aid in further identification of pathways of toxicity of different agents, as in this chapter, in which pDHA phototoxicity to ARPE-19 cells is studied. The antioxidants used in this thesis and their known mechanisms of action are discussed in greater detail here.

5.1.1 Zeaxanthin and α-tocopherol

α-Tocopherol is a lipid-soluble free radical scavenger. Hydrogen donation from the phenol group in α-tocopherol to a lipid peroxyl radical results in formation of an α-tocopherol phenoxy radical which is relatively unreactive with other lipids and oxygen (Burton and Ingold, 1984).

$$LOO^{\bullet} + TOH \rightarrow LOOH + TO^{\bullet}$$
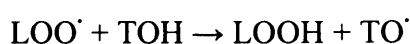
The reaction can act as a chain breaking termination step in the cycle of lipid peroxidation, as the rate constant for this reaction, $\sim 8 \times 10^4 \ M^{-1}.s^{-1}$, is almost 4

105

orders of magnitude faster than the interaction between the lipid peroxyl radical and lipids: $\sim 10 \text{ M}^{-1}.\text{s}^{-1}$, with both constants estimated for biological membranes (Burton and Ingold, 1981; Buettner, 1993; Mukai *et al.*, 1993a; Mukai *et al.*, 1993b). It is also possible for α-tocopherol radicals to adduct to lipid peroxyl radicals:

$$LOO^{\cdot} + TO^{\cdot} \rightarrow TO\text{-}OOL$$
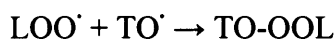
In addition to these antioxidant actions, α-tocopherol radicals are thought to play a pro-oxidant role if they accumulate to high concentrations, by interacting with lipids, resulting in lipid radical formation (Mukai *et al.*, 1993a; Mukai *et al.*, 1993b).

$$TO^{\cdot} + LH \rightarrow TOH + L^{\cdot}$$
$$TO^{\cdot} + LOOH \rightarrow TOH + LOO^{\cdot}$$
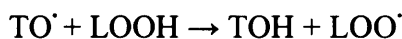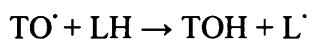
Use of additional antioxidants which can repair the tocopherol radical reduces this problem. Previous *in vitro* studies using α-tocopherol in conjunction with carotenoids and ascorbic acid showed a synergistic protective effect against photosensitizer-induced lipid peroxidation and cell death (Böhm *et al.*, 1998; Wrona *et al.*, 2003; Wrona *et al.*, 2004).

Zeaxanthin is a member of the carotenoid family. Carotenoids, in addition to their ability to repair α-tocopherol as described above and interact with other radicals, are able to quench singlet oxygen by energy transfer (Burton and Ingold, 1984; Liebler and McClure, 1996; Edge *et al.*, 1997; Young and Lowe, 2001). This is an efficient process due to the lower triplet state energy of carotenoids compared with singlet oxygen. Following the transfer of energy, singlet oxygen returns to its triplet state, and zeaxanthin dissipates the transferred energy to its surroundings and returns to its ground state (Britton, 1995; Foote and Clennan, 1995). An additional property of zeaxanthin is its ability to alter membrane structure and function. It aligns perpendicularly within the membrane, and may affect water and oxygen movement through the membrane and thus slow down propagation of lipid peroxidation (Snodderly, 1995; Young and

Lowe, 2001). As with α-tocopherol, it has been suggested that carotenoids may be pro-oxidant in certain situations, particularly in high oxygen conditions and in the presence of high carotenoid concentrations. Carotenoid pro-oxidant actions have been attributed to formation of carotenoid radicals and autoxidation resulting in formation of aldehyde and ketone products (Handelman *et al.*, 1991; Young and Lowe, 2001; Hurst *et al.*, 2005).

5.1.2 Phosphatidylethanolamine

The phosphatidylethanolamine (PE) polar head group has a free primary amine (Figure 5.1). Various studies have demonstrated that lipid peroxidation products, namely lipid aldehydes, may interact with the free amine, leading to formation of Schiff base and Michael adducts (Jain, 1984; Guichardant *et al.*, 1998; Guichardant *et al.*, 2002; Bacot *et al.*, 2003; Bacot *et al.*, 2007), and that PE-aldehyde adducts form in low density lipoproteins (Heller *et al.*, 2000; Zieseniss *et al.*, 2001). Considering the large number of different products potentially formed during peroxidation of DHA, PE may provide a pathway for deactivation or stabilization of these products, or at least a number of them.
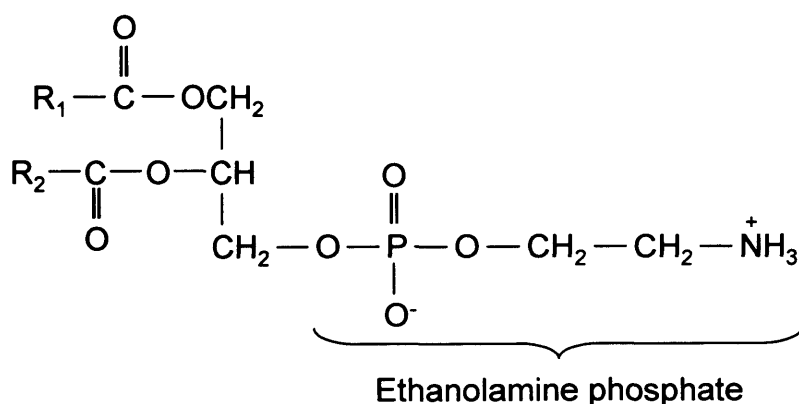
Figure 5.1 *Phosphatidylethanolamine structure, indicating the polar ethanolamine phosphate headgroup containing a free primary amine. R_1 and R_2 indicate fatty acid side chains (Halliwell and Gutteridge, 2007b).*

5.1.3 Glutathione, glutathione S-transferase and N-acetylcysteine

Glutathione (GSH) is able to conjugate with certain lipid peroxidation products, resulting in less toxic adducts. Specifically, lipid-derived aldehydes such as 4-hydroxynonenal (4-HNE, derived from arachidonic acid) and 4-HHE (derived from DHA), the breakdown products of lipid hydroperoxides, are electrophilic and therefore readily react with thiol groups, including that in GSH (Esterbauer, 1993; Choudhary *et al.*, 2003; Guichardant *et al.*, 2004; Choudhary *et al.*, 2005). The aldehyde may then be further metabolised for example by reduction. This process may be enhanced in the presence of glutathione-S-transferase (GST), which catalyzes the conjugation of aldehydes with GSH (Esterbauer, 1993; Choudhary *et al.*, 2003). It has also been shown that other DHA peroxidation products such as the family of neuroprostanes are able to form conjugates with GSH (Fam *et al.*, 2002). GSH can also react with and deactivate free radicals and singlet oxygen (Halliwell and Gutteridge, 2007c). It is also a specific co-factor for glutathione peroxidase which is able to reduce peroxides (e.g. hydrogen peroxide and lipid peroxides which have been freed from membranes) by producing water and oxidizing reduced GSH (Halliwell and Gutteridge, 2007c):

$$H_2O_2 + 2GSH \rightarrow GSSG + 2H_2O$$

$$LOOH + 2GSH \rightarrow GSSG + H_2O + LOH$$
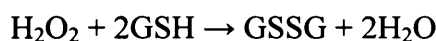
Aldehydes may also react directly with another low molecular weight thiol compound, *N*-acetylcysteine (NAC), also by forming a thio-ether linkage (Esterbauer *et al.*, 1991). Thus, excesses of thiols such as NAC and GSH can overcome binding of lipid aldehydes to thiols on cellular proteins in addition to binding free lipid aldehydes (Esterbauer *et al.*, 1991). Additionally, NAC is taken up by cells more readily than GSH. In the cytoplasm, NAC can be metabolized to the GSH precursor, cysteine. Thus, in addition to its direct actions as a thiol antioxidant, NAC may be used to replenish cellular GSH levels (Tanito *et al.*, 2002; Franco *et al.*, 2007).

The aim of this chapter is to determine the effects of various antioxidant agents on the effects of pDHA, in order to further understand the pathways by which pDHA is toxic.

5.2 Experimental design

For all experiments in this chapter, MTT assay was carried out 24 hours after 1 hour of exposure to DHA +/- antioxidants, +/- light (15 mW.cm^{-2}).

5.2.1 Zeaxanthin and α-tocopherol

Initial experiments were carried out with separate pDHA liposomes with either zeaxanthin or α-tocopherol incorporated. Later experiments used zeaxanthin dissolved in DMSO to avoid zeaxanthin degradation during liposomal preparation. To monitor potential degradation of zeaxanthin, liposome samples were removed from the individual wells after cell + light exposure and extracted in chloroform/methanol by the modified Folch's method described in Section 2.1.2.1 above. Absorbance spectra were then measured, and compared to spectra of freshly prepared zeaxanthin in PBS (i.e. not exposed to cells or light) which was also extracted *via* the same procedure.

Zeaxanthin was used at concentrations of 1, 2 and 4 μM, and α-tocopherol at 10, 20 and 40 μM. These concentrations are equivalent to or higher than those previously shown to be protective in combination to ARPE-19 cells exposed to photodynamic damage (Wrona *et al.*, 2004). The zeaxanthin concentrations used are considerably higher than measured plasma concentrations of 0.09 μM (SD 0.04) (Curran-Celentano *et al.*, 2001), yet the presence of a regulated uptake mechanism results in accumulation of zeaxanthin and lutein in the retina to levels which are higher than xanthophyll levels in any other tissue (Bhosale *et al.*, 2004; Whitehead *et al.*, 2006). DHA was used at either 0.5 or 1.5 mM depending on observed toxicity in each set of experiments. The reduction in toxicity of pDHA observed in the second set of experiments, and therefore the need for a higher concentration, could be due to the presence of DMSO which has been shown to have antioxidant effects (Santos *et al.*, 2003).

5.2.2 Phosphatidylethanolamine

To study the effects of PE on pDHA toxicity, liposomes were made using pDHA and POPE at a concentration of 40 mol%. This is based on published PE levels in the retina: 34.5 mol% of total rod outer segment (ROS) phospholipids in young and 35.9% in old samples (Bazan *et al.*, 1990), and 43.2% of total retinal phospholipids (Fliesler and Anderson, 1983). In an attempt to control for any dilution or other effect of adding 40 mol% phospholipids, liposomes were also made using 40 mol% POPC with pDHA. As addition of these phospholipids would alter liposome properties, initial experiments were carried out to check pDHA toxicity in these new liposomes, with 3 mM chosen to ensure sufficient levels of toxicity to be able to monitor any changes induced by POPE.

5.2.3 Glutathione, glutathione S-transferase and N-acetylcysteine

To study the effects of GST and related antioxidants, pDHA was used at a concentration of 2 mM. GSH and NAC were both used at 0.5 mM and GST at $4\ U.ml^{-1}$ (all Sigma, UK). These concentrations were based on the expected activity of GST: assuming maximal lipid peroxidation and aldehyde formation i.e. 2 aldehydes per DHA-PC, with 1 U of GST able to conjugate 1 μmol to reduced glutathione per minute, $4\ U.ml^{-1}$ should theoretically be able to catalyze reactions to bind and inactivate all the aldehyde groups within one minute. GSH and/or NAC were not used at concentrations high enough to fully facilitate this inactivation as these concentrations affected pH of the medium used, therefore a lower concentration was used.

5.3 Results

5.3.1 Zeaxanthin and α-tocopherol

Figure 5.2 below shows results for MTT assay carried out with either zeaxanthin or α-tocopherol incorporated into pDHA liposomes. pDHA caused a reduction in mitochondrial activity to 80% and 61% in dark and light exposed cells respectively. Zeaxanthin showed no protective effect against pDHA (photo-)

110

toxicity, and in fact showed a significant reduction in mitochondrial activity at the highest concentration, with mitochondrial activity reduced to 66% and 41%, in dark and light, respectively (4 μM zeaxanthin; P <0.05). In contrast, α-tocopherol was able to reduce pDHA toxicity in a dose-dependent manner, with 20 and 40 μM able to significantly improve mitochondrial activity compared with pDHA alone (P <0.01 and <0.001 respectively) to greater than 90%, such that they were no longer significantly different to control levels (P >0.05). Full tables of P-values are contained in Appendix 2.
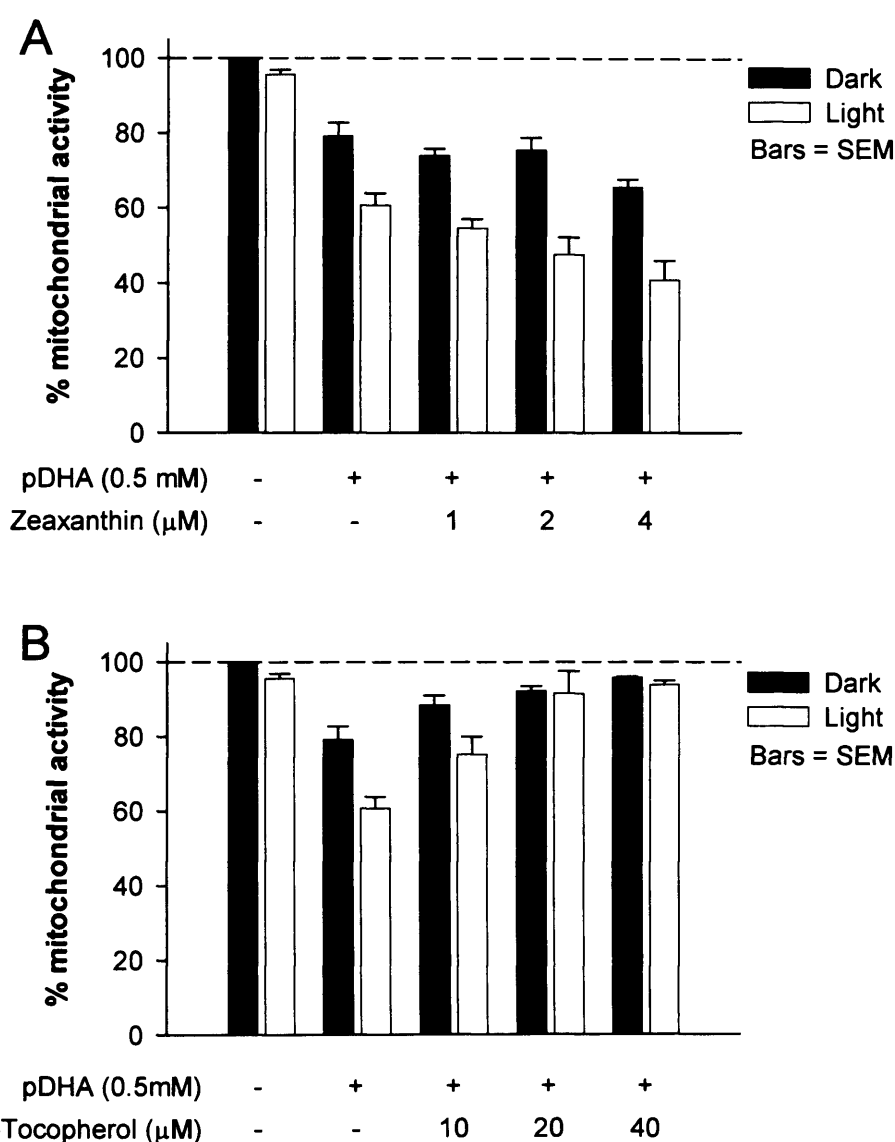
Figure 5.2 *MTT results for ARPE-19 cells exposed to pDHA liposomes with (A) zeaxanthin or (B) α-tocopherol, and either light-exposed or dark-maintained. All data were normalized to dark control. n=3.*

As previous studies have shown that the presence of multiple antioxidants is important, further experiments were carried out using both zeaxanthin and α-tocopherol in combination, with zeaxanthin added after dissolving in DMSO rather than incorporated into liposomes, to minimize its degradation prior to exposure to cells. Figure 5.3 shows a significant reduction in mitochondrial activity due to pDHA in light treatment only (P <0.001), with no significant positive effect of either antioxidant, either alone or in combination.

pDHA (1.5 mM)	-	+	+	+	+	+	+	+
α-Tocopherol (µM)	-	-	20	20	40	40	-	-
Zeaxanthin (µM)	-	-	-	4	-	4	1	4
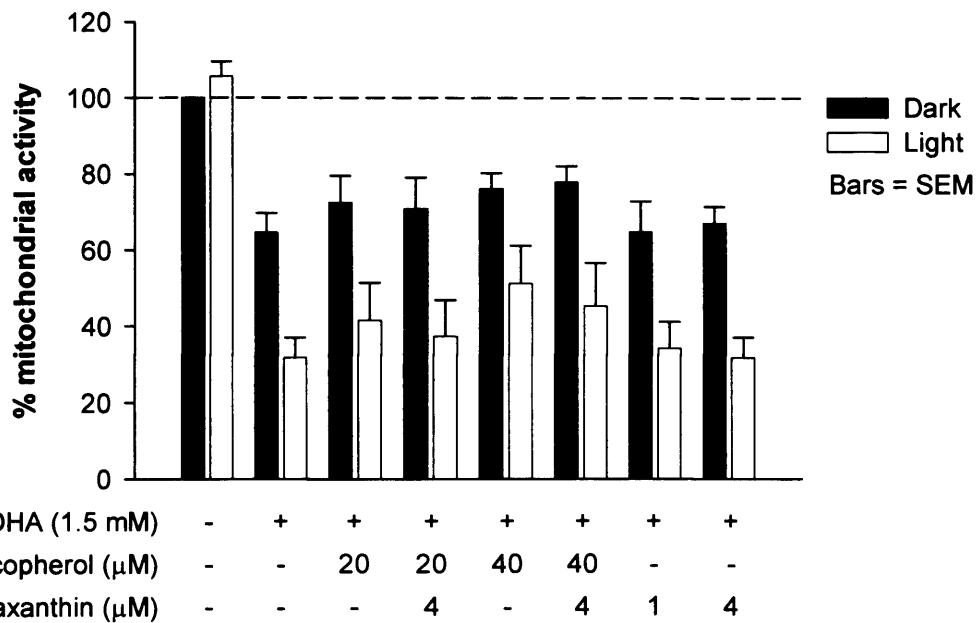
Figure 5.3 *MTT results for ARPE-19 cells exposed to pDHA liposomes with α-tocopherol and/or zeaxanthin. All treatments included 0.2% DMSO as carrier or carrier control. All data were normalized to dark control. n = 3 for dark, n = 4 for light exposed.*

Figure 5.4 shows absorption spectra measured to monitor potential changes in zeaxanthin after exposure to cells and light. These results show that the distinctive absorption peaks of zeaxanthin (at ~450 and 480 nm) in the presence of α-tocopherol closely matched that of untreated zeaxanthin even after exposure to light for 1 hour. In contrast, absorption decreased for zeaxanthin alone (i.e. without α-tocopherol) in the dark, and decreased further after light treatment. This indicates degradation of zeaxanthin and could explain lack of positive effects when zeaxanthin was added alone without α-tocopherol in the experiments described above.
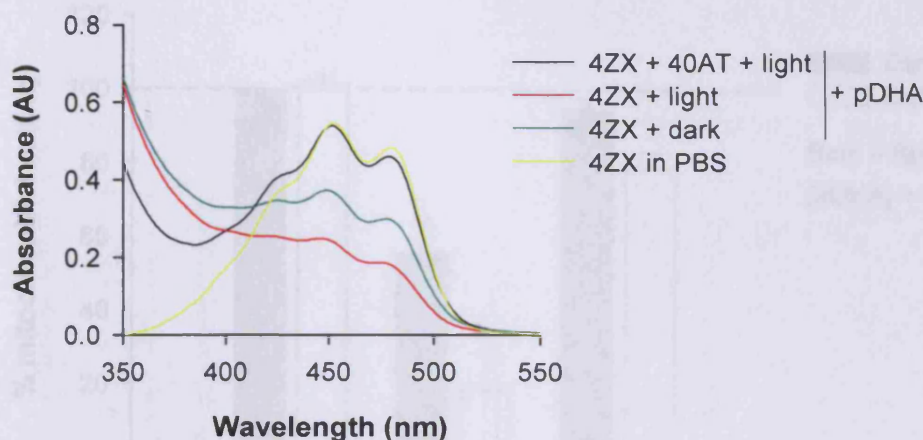
Figure 5.4 *Absorption spectra of extracted liposomes after cell exposure, compared with freshly prepared zeaxanthin diluted in PBS prior to extraction. AT = α-tocopherol; ZX = zeaxanthin.*

5.3.2 Phosphatidylethanolamine

Figure 5.5 compares the effects of pDHA with and without POPE on mitochondrial activity. An overall ANOVA *P*-value of <0.0001 indicates significant difference between these values. Post-tests indicate that pDHA (in liposomes with 40 mol% POPC) decreased mitochondrial activity significantly compared with controls (P <0.001 for light and dark): by 46% in dark-maintained (P <0.001 vs. control) and 83% in light-exposed cells (P <0.001 vs. control) and with a significantly greater effect in light vs. dark (P <0.01). The pDHA induced toxicity was significantly reversed in the presence of 40 mol% POPE instead of POPC (pDHA-POPC vs. pDHA-POPE: P <0.01 in dark, P <0.001 in light), and caused mitochondrial activity to return to levels which were no longer significantly different to their respective light/dark controls. There was no significant difference between dark- and light-maintained control cells (i.e. no pDHA).
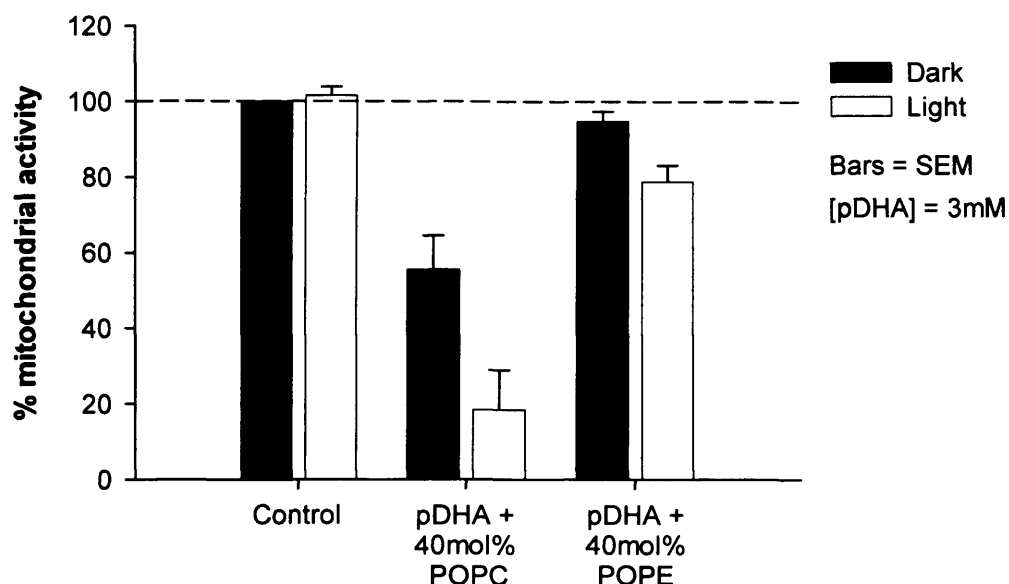
Figure 5.5 *MTT results for ARPE-19 cells exposed to pDHA liposomes with 40 mol% POPE or POPC. All data were normalized to dark control. n = 4.*

5.3.3 Glutathione, glutathione S-transferase and N-acetylcysteine

Figure 5.6 shows, in agreement with previous experiments, that 2 mM pDHA had a significant effect on mitochondrial activity, with reductions to 56% in dark (P <0.001) and 20% in light (P <0.001). For light-exposed cells, addition of GSH or NAC separately to pDHA significantly increased mitochondrial activity compared with cells treated with pDHA alone (P <0.001 and <0.05 respectively), with activity in the presence of GSH no longer significantly different to control (i.e. no pDHA). GST, however, had no protective effect, either singularly or when added to either GSH or NAC. Adding all 3 reagents – GSH, NAC and GST – to pDHA had no further protective effect than adding either GSH or NAC in combination with GST.

pDHA (2mM)	-	+	+	+	+	+	+	+
GSH (0.5 mM)	-	-	+	-	-	+	-	+
NAC (0.5 mM)	-	-	-	+	-	-	+	+
GST (4 U.ml⁻¹)	-	-	-	-	+	+	+	+
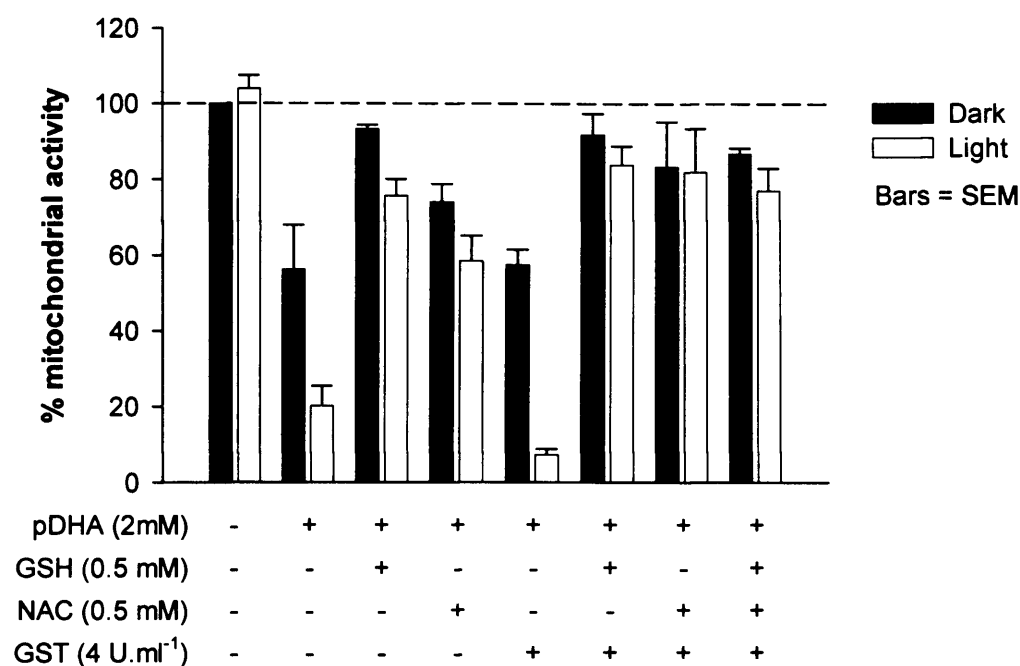
Figure 5.6 *MTT results for ARPE-19 cells exposed to pDHA with or without GSH/GST/NAC. All treatments were normalized to dark control. $n \geq 3$.*

5.4 Discussion

This chapter has demonstrated that several agents are effective in protecting cells from (photo-)oxidative damage induced by pDHA.

The free radical scavenger α-tocopherol had a positive effect in one set of experiments with 0.5 mM pDHA, however it had no effect at the higher concentration of 1.5 mM pDHA. It should be noted that these experiments used different liposomes, with the latter having undergone additional intermediate steps in preparation during addition of antioxidants (as liposomes from the first experiments were "recycled" and used to make further liposomes). Also, in the second set of experiments, pDHA exposure was carried out in the presence of DMSO, either as a solvent for zeaxanthin or as a carrier control in all other wells. DMSO may act as an antioxidant (Santos *et al.*, 2003), and could therefore decrease overall toxicity of pDHA, and additionally, could alter the pathways of oxidative reactions induced by pDHA, thus altering the efficacy of different antioxidants, as was observed here. Nevertheless, results suggest that in the

presence of more lipid peroxides α-tocopherol appears less effective – possibly due to the balance of its antioxidant vs. pro-oxidant effects altering, or perhaps due to different modes of action of products found in more heavily peroxidized DHA samples, or increased probability of radicals reacting with other pDHA molecules instead of α-tocopherol, due to higher pDHA levels.

Surprisingly, considering that pDHA is known to produce singlet oxygen (MB Rozanowska personal communication; see also Chapter 6), zeaxanthin was not able to reduce toxicity, and appeared unable to salvage α-tocopherol and amplify its antioxidant effects. Evidence from UV-visible spectroscopy showed that zeaxanthin degraded during these experiments. This explains the lack of antioxidant activity. It has previously been shown for β-carotene that aldehyde degradation products absorb at shorter wavelengths than the unoxidized form, and that these products are toxic to cells (Hurst et al., 2005), thus it could be postulated that this is also possible for zeaxanthin, and indeed occurred in these experiments. As described in Chapter 4, retinal light irradiance would be lower than the acute model used here – with cells here exposed to a dose of light (1 hour at 15 mW.cm^{-2}) equivalent to 150 hours of continuous retinal exposure to maximal normal daylight. In more physiological light exposures, zeaxanthin would be less prone to photodegradation, and could be protected by further antioxidants, such as water-soluble ascorbate, which would normally be present but are not included in the in vitro situation studied here. It is also more likely that zeaxanthin and other antioxidants could be replenished from the circulation over this time period.

Experiments with GSH showed that this thiol antioxidant was able to almost completely prevent the cell death caused by pDHA, as could NAC, a precursor to GSH which also contains a thiol group. As discussed above, these molecules could act as free radical scavengers, as a co-factor for GSH peroxidase (GSH) or by adducting with lipid aldehydes and other degradation products. The latter would prevent subsequent adduction of these products to other cellular components, which would otherwise have a detrimental effect on cell function, potentially leading to cell dysfunction and death observed in these results. Surprisingly, GST had no effect on cell viability. In these experiments,

antioxidants were combined with pDHA prior to applying to cells. Perhaps in the several minutes between these two steps the GSH and NAC are able to bind to aldehydes or other derivatives within the lipid mixture, thus, no further change would occur in the presence of GST – if GSH and NAC have fully interacted with lipids, the enzyme can have no further effect. It is not surprising that GST alone had no effect as the liposomes are applied to the cells externally where there would not be GSH for the GST to catalyze the reaction of. It is of course possible that some pDHA is internalized – either by phagocytosis or incorporation into the cell membrane. For the former, GST could enter too but as these components will then be contained within a phagosome there is still likely to be an issue of access to GSH. If DHA incorporates into the cell plasma membrane, this would not necessarily allow access of GST into the cytoplasm.

Phosphatidylethanolamine also successfully reduced the toxic effects of pDHA. As it is known the amine group of PE can interact with lipid aldehydes, these results suggest a crucial role for lipid aldehydes in the toxicity of pDHA. However, as PE is not a well defined traditional antioxidant, further work has been carried out in Chapter 6 to further elucidate the mechanisms by which it acts as an antioxidant in protecting cells from pDHA-induced damage.

Chapter 6:
Pathways of pDHA (photo-)reactivity

6.1 Introduction

Although it has been shown in Chapter 4 that pDHA is phototoxic to ARPE-19 cells, the precise pathways by which this toxicity occurred were not discussed. In Chapter 5, however, various antioxidants and detoxifying agents were shown to have protective effects on cell viability in the presence of pDHA (measured by MTT assay). Although several of these antioxidants have known mechanisms of action, POPE does not. The large protective effect seen in experiments in Chapter 5 therefore warrants further investigation.

It has previously been demonstrated that photoexcitation of pDHA as 16:0;22:6PC or as a free fatty acid results in an increase in O_2 uptake, and formation of superoxide (measured by spin-trapping) and singlet oxygen (personal communication: MB Rozanowska). To further understand the potential relevance of these pathways to this project, and to better understand the mechanism by which POPE was protective to cells, experiments were carried out to monitor singlet oxygen production and transient formation, and also superoxide production *via* an alternative assay in which reduction of cytochrome C by superoxide was monitored. These experiments were carried out using pDHA phospholipid, with 40 mol% of either POPE or POPC.

6.2 Experimental design

6.2.1 Singlet oxygen production

Singlet oxygen production was measured in two separate sets of experiments:

(1) Relative yield of singlet oxygen measured in samples containing equal concentrations of pDHA in the presence of 40 mol% POPE or POPC

(2) Quantum yield of singlet oxygen measured in samples with matched absorbances at the excitation wavelength (420 nm) to ensure equal numbers of absorbed photons, with ATR as a standard of known quantum yield

Liposomes containing 60 mol% pDHA and 40 mol% of either POPC or POPE were extracted in chloroform/methanol as described in Section 2.1.3.1 above. Chloroform-enriched phases were then dried under argon and dissolved in benzene prior to measurement of absorption spectra.

The same initial samples were used for both sets of experiments, but diluted as required. To ensure that the incident laser energy was uniform across the irradiated surface area and to reduce the irradiance of the samples a diverging lens was put in the path of the laser beam for the second (quantum yield) set of experiments (see Figure 2.4)

Transmission spectra of the neutral density filters (used to reduce laser intensity in singlet oxygen measurements) were measured to calculate the average reduction in light intensity caused by the filters (Figure 6.1A). The mean reduction in transmission at 420 nm, the laser excitation wavelength in these experiments, was 8.92% (SD 0.26%) per filter. Figure 6.1B shows expected relative laser intensity over the range of filter numbers used in these experiments.
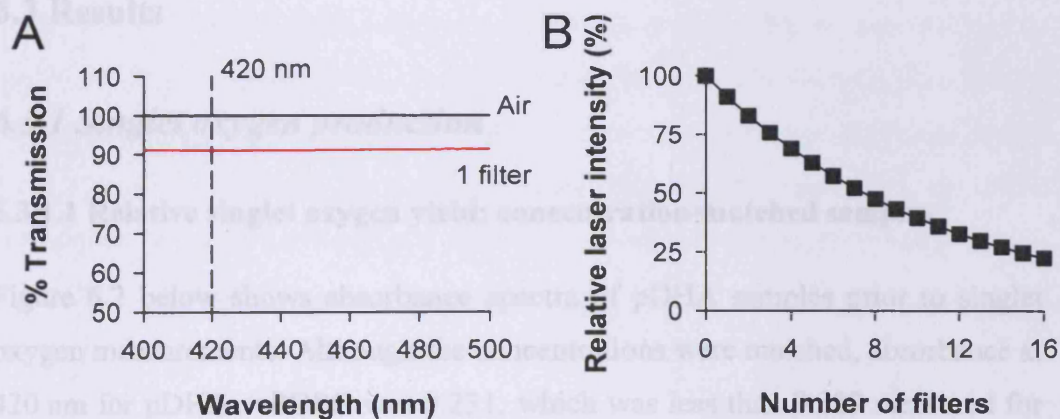
Figure 6.1 *Effects of neutral density filters on light transmission. (A) Transmission spectra with either air only or with 1 filter; (B) calculated relative laser energy at 420 nm with 0 to 16 filters in the light path.*

6.2.2 Laser flash photolysis

Liposomes containing pDHA, with POPE or POPC, were extracted and prepared as for singlet oxygen measurement. Absorption spectra in benzene were then

120

measured to ensure optical densities at 420 nm were matched, at approximately 0.2. Samples were depleted of oxygen by bubbling for 20 minutes with argon prior to measurement, then passing argon over the samples throughout measurement. Where required, samples were bubbled with air to obtain air-saturated (oxygen present samples), containing 1.91 mM oxygen (Murov, 1973).

6.2.3. Superoxide production

Initial experiments were carried out to find an optimal concentration of pDHA at which to carry out monitoring of superoxide production – ensuring that saturation levels of cytochrome C reduction were not reached, and that background absorbance levels due to light scattering caused by pDHA liposomes was not too high to allow accurate measurement of changes in absorbance at 550 nm. Based on these results, subsequent experiments were carried out with liposomes containing 0.1 mM pDHA in liposomes, with 40 mol% POPC or POPE.

6.3 Results

6.3.1 Singlet oxygen production

6.3.1.1 Relative singlet oxygen yield: concentration-matched samples

Figure 6.2 below shows absorbance spectra of pDHA samples prior to singlet oxygen measurements. Although the concentrations were matched, absorbance at 420 nm for pDHA + POPC was 0.231, which was less than 0.389 measured for pDHA + POPE.
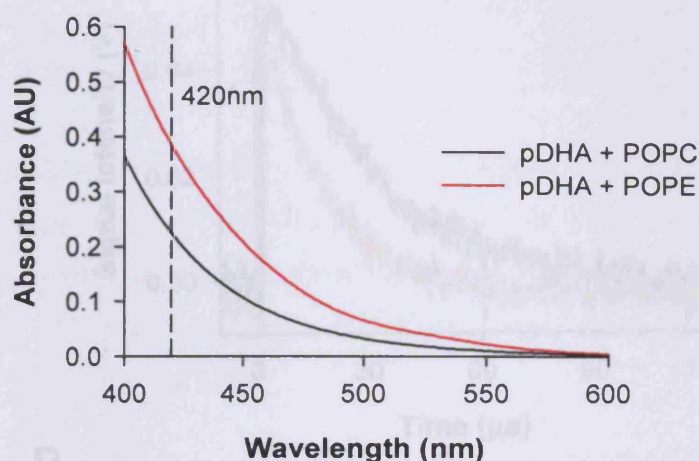
Figure 6.2 *Absorbance spectra for matched concentrations of pDHA + POPE and pDHA + POPC in benzene, prior to singlet oxygen measurement.*

Singlet oxygen kinetic traces are shown in Figure 6.3A with linear regression of the initial intensity values (normalized to laser pulse energy) shown in Figure 6.3B. A comparison of signal lifetime values and slopes (indicating yields of singlet oxygen production) of pDHA + POPE and pDHA + POPC is shown in Table 6.1. This shows a large difference in lifetime of singlet oxygen: 31.2 μs in the POPC sample, compared with only 17.4 μs in the POPE sample. The results of the linear regression indicate a slightly shallower slope and therefore lower yield of singlet oxygen in samples containing POPE. However, the 95% confidence intervals for the slopes of the two samples overlap, suggesting a non-significant difference.
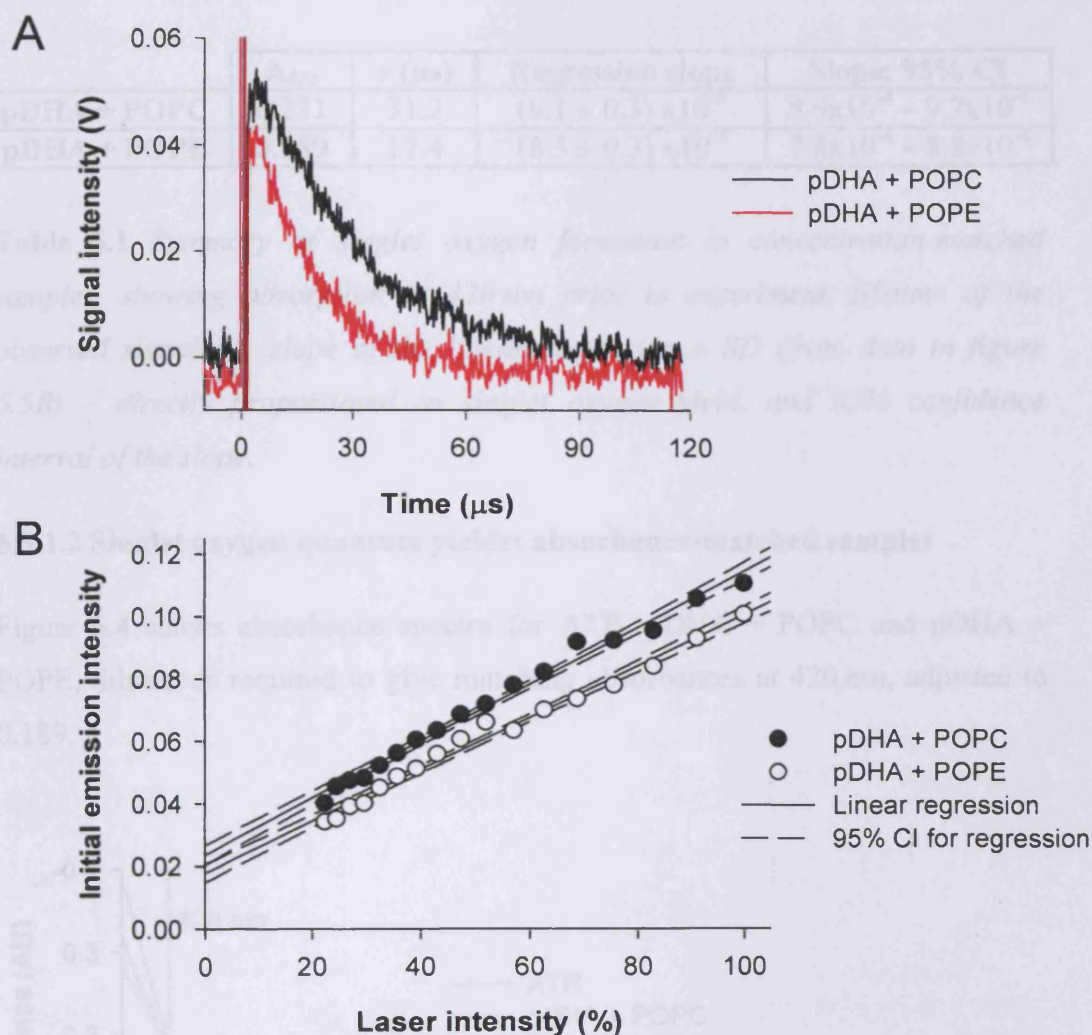
Figure 6.3 *Singlet oxygen production in samples of matched concentration of pDHA in the presence of POPC or POPE. (A) Singlet oxygen phosphorescence kinetics for pDHA + POPC and pDHA + POPE at 39% laser intensity (with similar laser pulse energy). (B) Linear regression of initial signal intensity values, based on single measurements over a range of laser intensities. 95% confidence intervals of the linear regression are indicated by dashed lines.*

	A_{420}	τ (µs)	Regression slope	Slope: 95% CI
pDHA + POPC	0.231	31.2	$(9.1 \pm 0.3) \times 10^{-4}$	$8.6 \times 10^{-4} - 9.7 \times 10^{-4}$
pDHA + POPE	0.389	17.4	$(8.3 \pm 0.3) \times 10^{-4}$	$7.8 \times 10^{-4} - 8.8 \times 10^{-4}$

Table 6.1 *Summary of singlet oxygen formation in concentration-matched samples, showing absorption at 420 nm prior to experiment, lifetime of the observed signal (τ), slope of the linear regression ± SD (from data in figure 6.5B) – directly proportional to singlet oxygen yield, and 95% confidence interval of the slope.*

6.3.1.2 Singlet oxygen quantum yields: absorbance-matched samples

Figure 6.4 shows absorbance spectra for ATR, pDHA + POPC and pDHA + POPE, diluted as required to give matching absorbances at 420 nm, adjusted to 0.189.
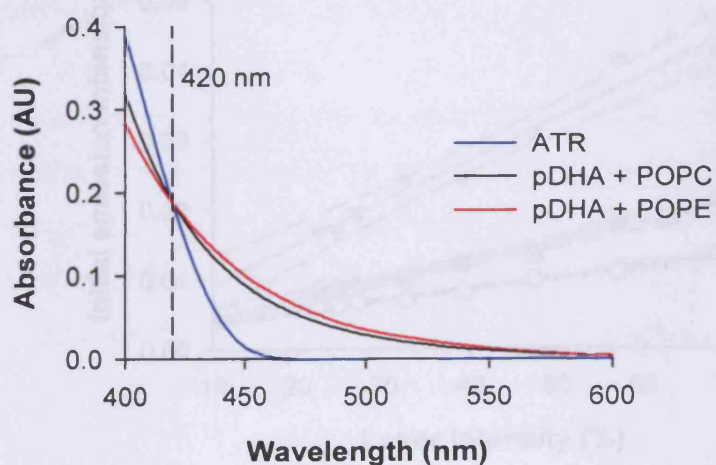
Figure 6.4 *Absorbance spectra for ATR, pDHA + POPC and pDHA + POPE samples, with absorbances matched to the arbitrary value of 0.189 at 420 nm.*

When absorbances at 420 nm were matched, the yield of singlet oxygen production in pDHA + POPC was greater than for pDHA + POPE as indicated by the initial phosphorescence intensities in Figure 6.5A and the steeper slope of the fitted data in Figure 6.5B. When compared to the slope of ATR it was possible to calculate quantum yields for singlet oxygen production, summarized in Table 6.2. Results show a higher quantum yield of singlet oxygen production

124

by pDHA + POPC (0.14 ± 0.02) compared with pDHA + POPE (0.08 ± 0.01). Measured intensities of singlet oxygen phosphorescence were lower in this experiment compared with those presented in Figure 6.3 above due to the insertion of the diverging lens into the laser pathway.
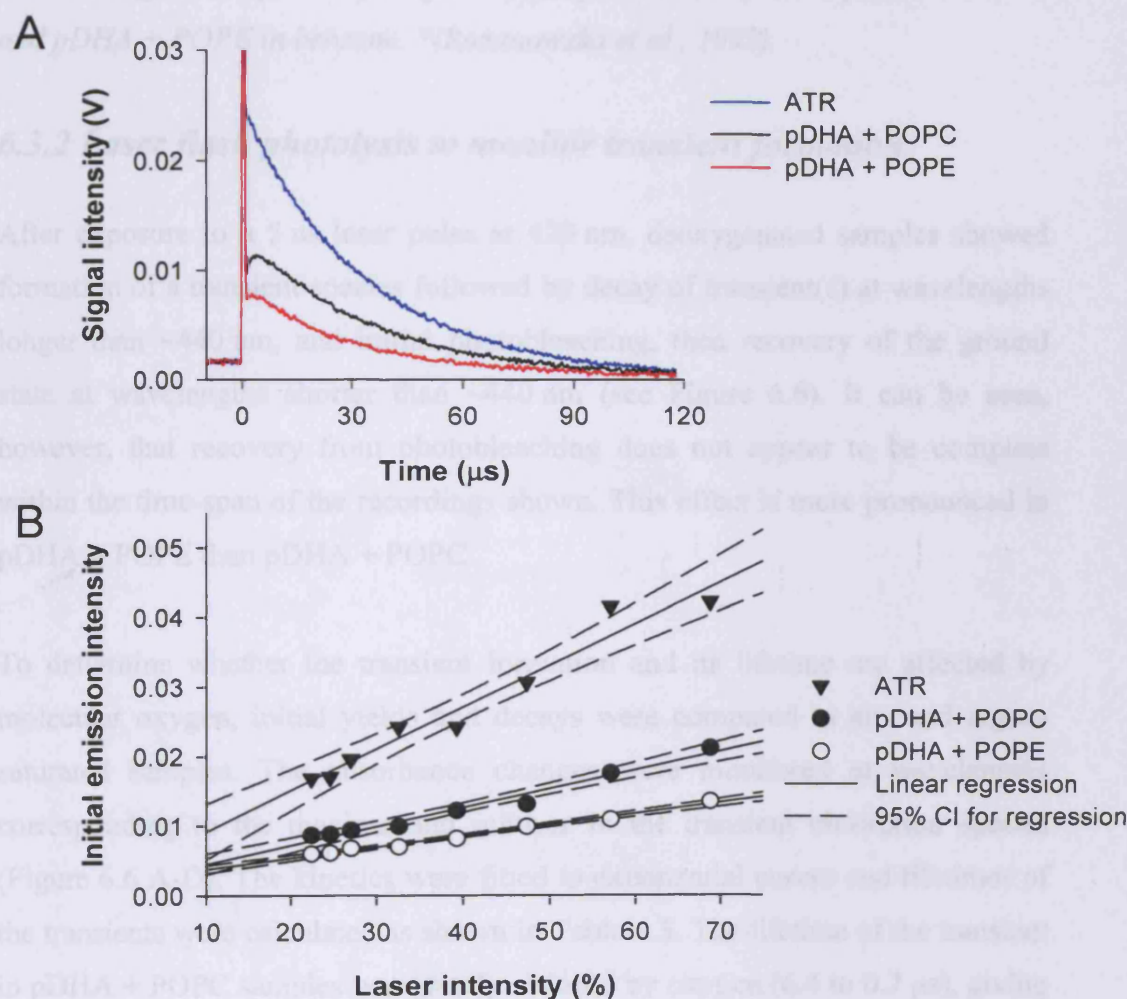
Figure 6.5 *Singlet oxygen production in samples of matched absorbance. (A) Singlet oxygen phosphorescence kinetics for ATR, pDHA + POPC and pDHA + POPE, at 39% laser intensity (with similar laser pulse energy). (B) Linear regression of initial signal intensity values, based on single measurements over a range of laser intensities. 95% confidence intervals of the linear regression are indicated by dashed lines.*

	Quantum yield
ATR	0.30 ± 0.04 *
pDHA + POPC	0.14 ± 0.02
pDHA + POPE	0.08 ± 0.01

Table 6.2 *Quantum yields of singlet oxygen production by ATR, pDHA + POPC and pDHA + POPE in benzene. *(Rozanowska et al., 1998).*

6.3.2 Laser flash photolysis to monitor transient formation

After exposure to a 5 ns laser pulse at 420 nm, deoxygenated samples showed formation of a transient species followed by decay of transient(s) at wavelengths longer than ~440 nm, and initial photobleaching, then recovery of the ground state at wavelengths shorter than ~440 nm (see Figure 6.6). It can be seen, however, that recovery from photobleaching does not appear to be complete within the time-span of the recordings shown. This effect is more pronounced in pDHA + POPE than pDHA + POPC.

To determine whether the transient formation and its lifetime are affected by molecular oxygen, initial yields and decays were compared in air- and argon-saturated samples. The absorbance changes were monitored at wavelengths corresponding to the maxima and minima in the transient absorption spectra (Figure 6.6 A-D). The kinetics were fitted to exponential curves and lifetimes of the transients were calculated as shown in Table 6.3. The lifetime of the transient in pDHA + POPC samples was greatly reduced by oxygen (6.4 to 0.7 μs), giving a bimolecular rate constant for quenching of the transient by oxygen (indicating rates of interaction of the formed transient(s) with oxygen) of 6.8 x $10^8 M^{-1}.s^{-1}$. For pDHA + POPE, the transient lifetime reduce from 16.7 to 0.9 μs with a rate constant for interaction with oxygen of 5.8 x $10^8 M^{-1}.s^{-1}$. Comparing the two samples, the transient lifetime in argon-saturated samples was 2.6-fold longer in the presence of POPE (16.7 μs) compared with POPC (6.4 μs), but oxygen-saturated samples showed similar lifetimes. The rate constant for quenching by oxygen was, however, 17% greater for the pDHA + POPC samples compared with pDHA + POPE.
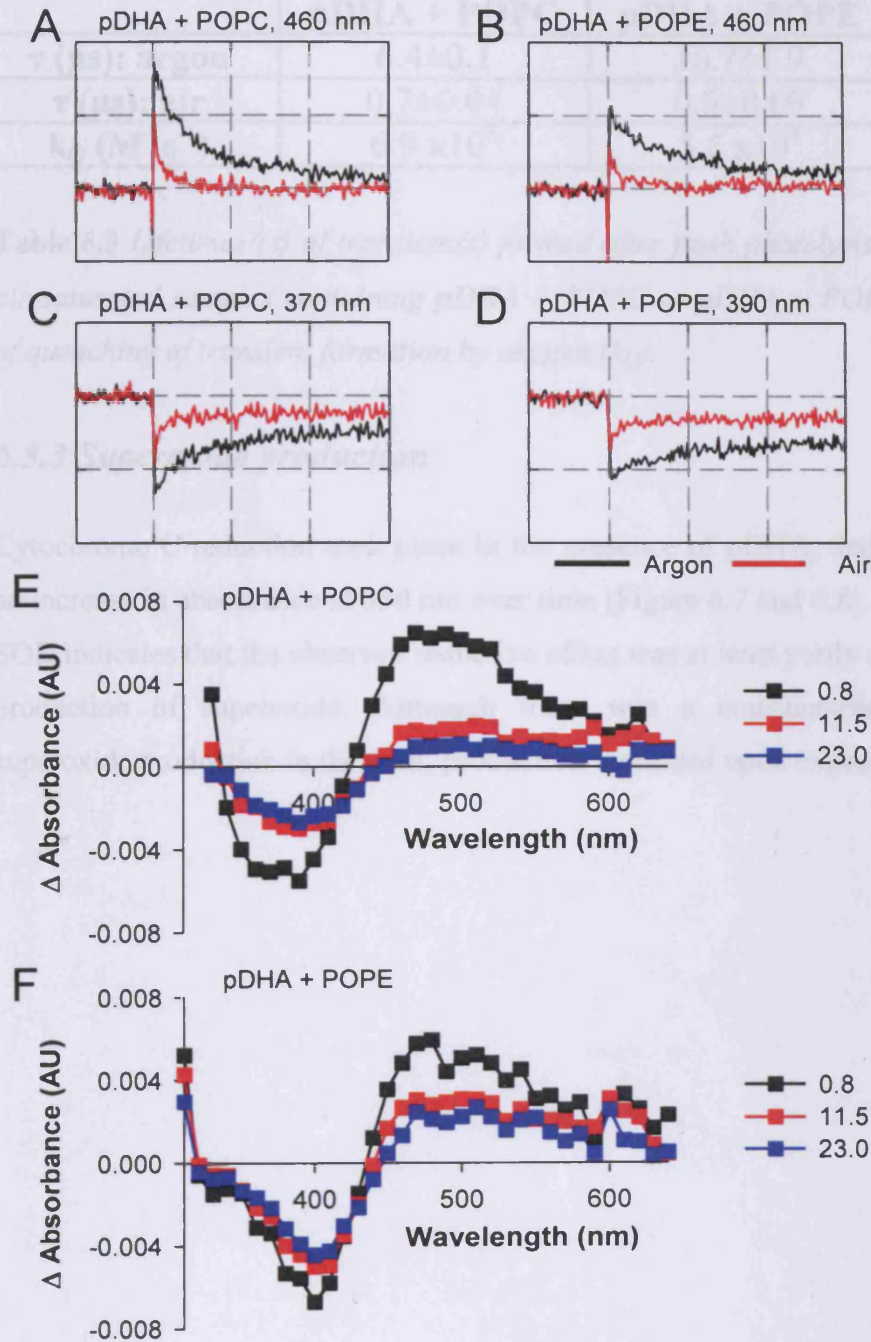
Figure 6.6 *Laser flash photolysis of pDHA. (A-D): Kinetics of absorbance change for pDHA + POPC (A+C) and pDHA + POPE (B+D), showing initial formation then decay (A+B) and photobleaching (C+D) of the transient(s), in argon and air saturated samples. Kinetics are shown for indicated wavelengths, representing maximal absorbance/photobleaching for each sample. Vertical interval = 0.005 absorbance change (AU); horizontal interval = 15 μs. (E) Transient difference spectra for pDHA + POPC and (F) for pDHA + POPE for data averaged around three selected time points.*

127

	pDHA + POPC	pDHA + POPE
τ (μs): argon	6.4±0.1	16.7±1.9
τ (μs): air	0.7±0.04	0.9±0.09
k_Q (M^{-1}s^{-1})	6.9 x10^8	5.5 x10^8

Table 6.3 *Lifetimes (τ) of transient(s) formed after flash photolysis of argon- or air-saturated samples containing pDHA + POPC or pDHA + POPE, and rates of quenching of transient formation by oxygen (k_Q).*

6.3.3 Superoxide production

Cytochrome C reduction took place in the presence of pDHA, demonstrated by an increase in absorbance at 550 nm over time (Figure 6.7 and 6.8). Inhibition by SOD indicates that the observed reductive effect was at least partly attributable to production of superoxide. Although there was a considerable amount of superoxide production in the dark, production increased upon exposure to light.
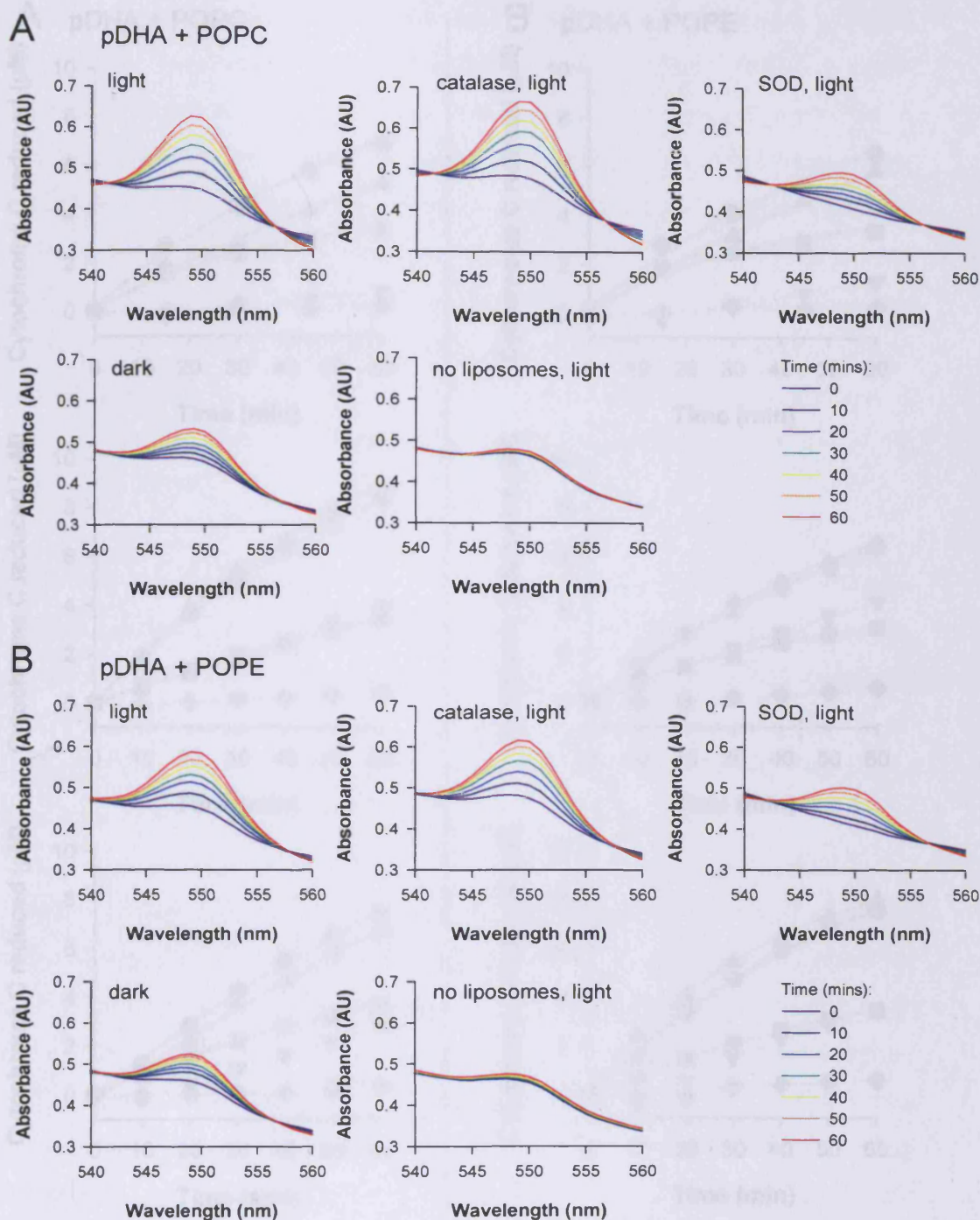
Figure 6.7 *Spectral changes in absorbance over time. Increase in absorbance at 550 nm indicates cytochrome C reduction by superoxide. (A) Samples containing liposomes with pDHA + POPC and (B) pDHA + POPE, with or without 250 U.mL^{-1} catalase or SOD, and irradiated with light or incubated in dark, as indicated. Representative data shown were obtained in a single experiment.*
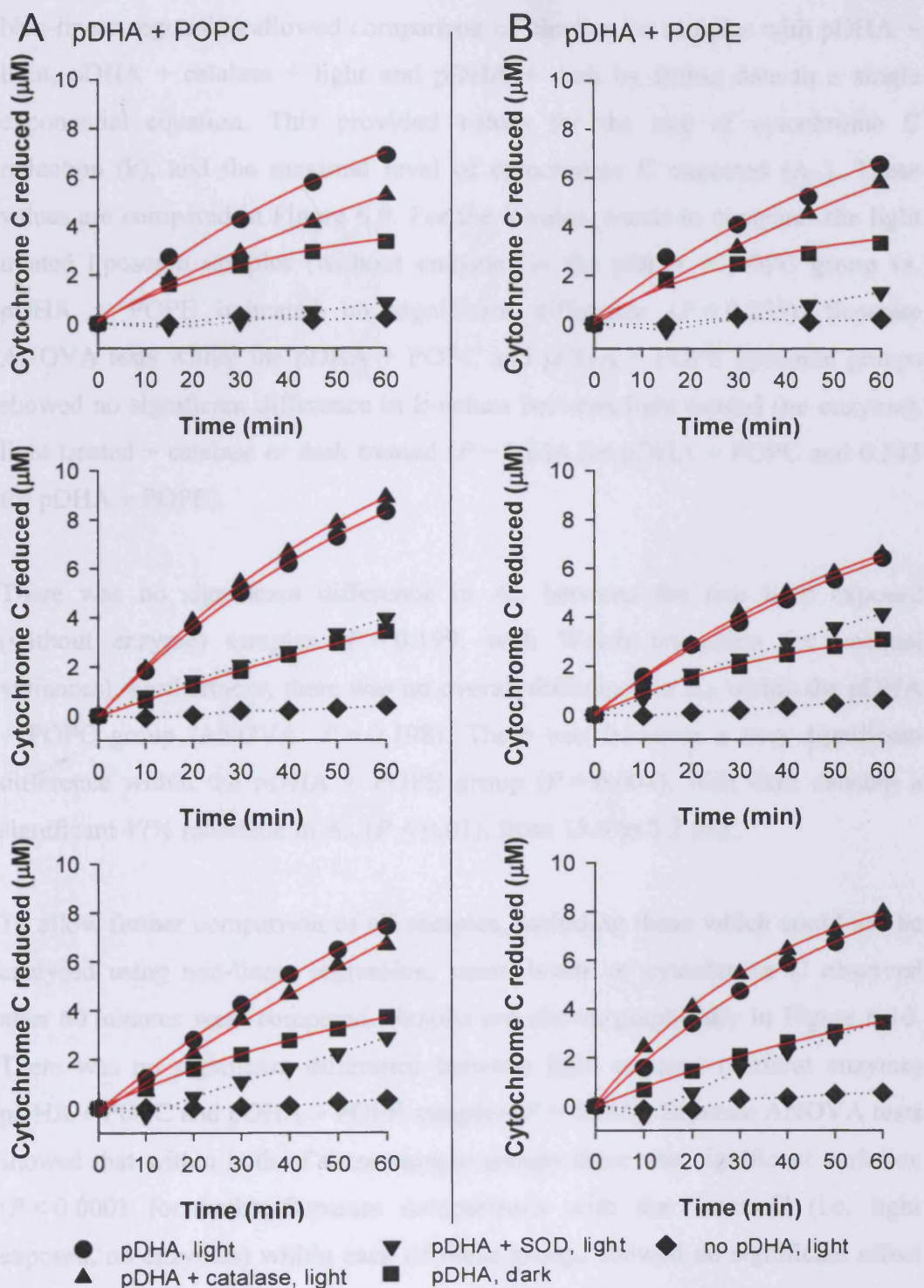
Figure 6.8 *Graphs showing changes in reduced cytochrome C levels in 3 independent experiments for samples containing (A) pDHA + POPC liposomes and (B) pDHA + POPE liposomes, with or without 250 U.mL⁻¹ catalase or SOD, and irradiated with light or incubated in dark, as indicated. Red lines indicate nonlinear regression curve fits. Other data sets which did not fit the equation are joined by dotted lines.*

130

Non-linear regression allowed comparison of kinetics for samples with pDHA + light, pDHA + catalase + light and pDHA + dark by fitting data to a single exponential equation. This provided values for the rate of cytochrome C reduction (k), and the maximal level of cytochrome C expected (A_∞). These values are compared in Figure 6.9. For the k-value, t-tests to compare the light treated liposome samples (without enzyme) in the pDHA + POPC group vs. pDHA + POPE indicated no significant difference ($P = 0.255$). Separate ANOVA tests within the pDHA + POPC and pDHA + POPE liposome groups showed no significant difference in k-values between light treated (no enzyme), light treated + catalase or dark treated ($P = 0.614$ for pDHA + POPC and 0.543 for pDHA + POPE).

There was no significant difference in A_∞ between the two light exposed (without enzyme) samples ($P = 0.199$, with Welch correction for unequal variances). Furthermore, there was no overall difference in A_∞ within the pDHA + POPC group (ANOVA: $P = 0.198$). There was however a very significant difference within the pDHA + POPE group ($P = 0.004$), with dark causing a significant 47% reduction in A_∞ ($P < 0.01$), from 15.4 to 8.2 μM.

To allow further comparison of all samples, including those which could not be analysed using non-linear regression, mean levels of cytochrome C observed after 60 minutes were compared. Results are shown graphically in Figure 6.10. There was no significant difference between light exposed (without enzyme) pDHA + POPC and pDHA + POPE samples ($P = 0.245$). Separate ANOVA tests showed that within both of these sample groups there was significant variation ($P < 0.0001$ for both). Separate comparisons with the "control" (i.e. light exposed, no enzymes) within each of these groups showed no significant effect of catalase, but extremely significant reduction in final cytochrome C levels in the presence of SOD, in the absence of pDHA, and in dark maintained samples ($P < 0.01$ for all).

131
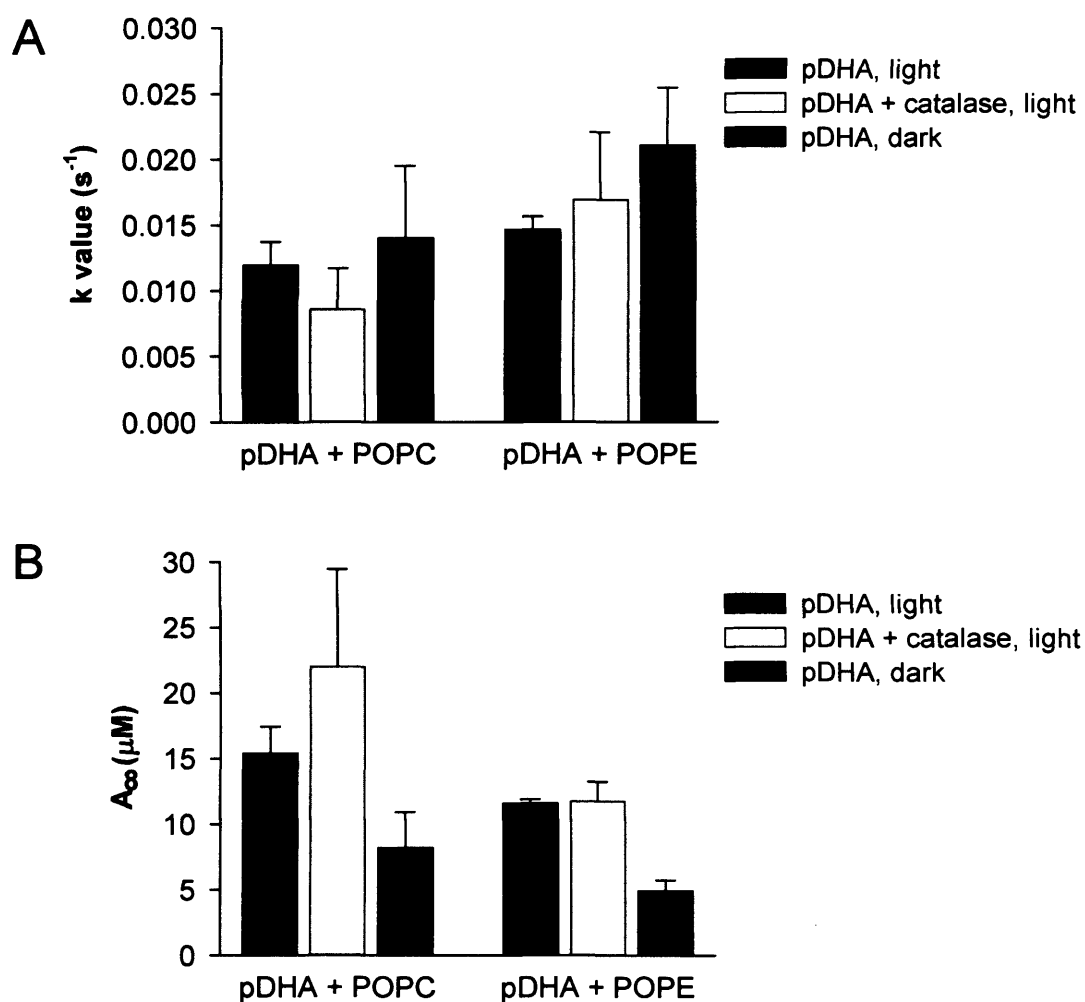
Figure 6.9 *Comparison of non-linear regression values for cytochrome C reduction assay showing: (A) rate of formation of reduced cytochrome C (k); (B) maximum levels of reduced cytochrome C as time approaches ∞ (A_∞). Bars indicate mean of 3 experiments. Error bars = SEM.*
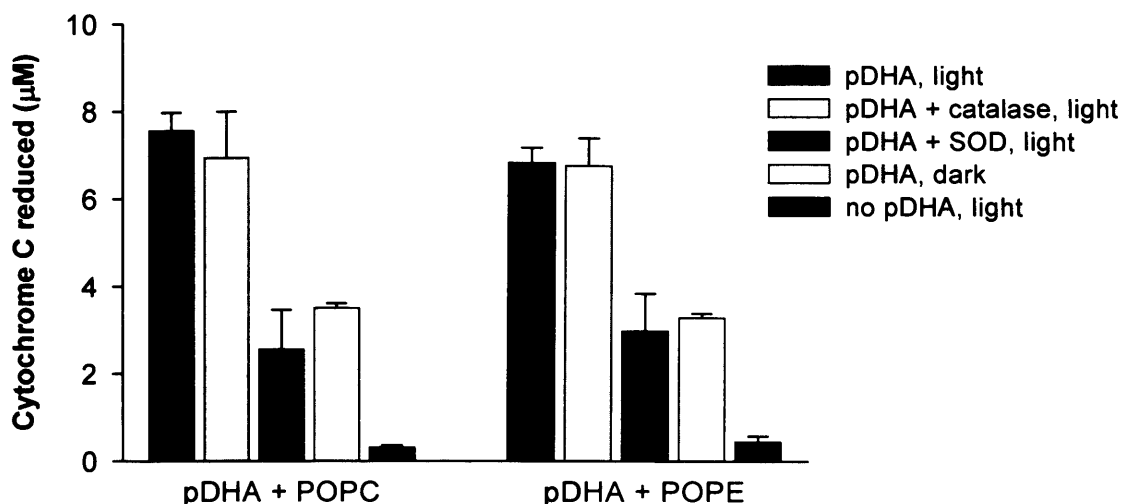
Figure 6.10 *Levels of reduced cytochrome C after 60 minutes incubation, for samples containing pDHA + POPC or pDHA + POPE, with or without 250 U.mL^{-1} catalase or SOD, and irradiated with light or incubated in dark, as indicated. Bars indicate mean of 3 experiments. Error bars = SEM.*

6.4 Discussion

This chapter has attempted to investigate the mechanism responsible for reduction of phototoxicity of pDHA in the presence of POPE, as observed in cell culture experiments in Chapter 5.

Photoexcitation of pDHA, in the presence of either POPC or POPE, resulted in formation of singlet oxygen. Although the quantum yield of singlet oxygen production is greater in the presence of POPC, this could be counteracted by an increased absorption of samples with POPE, thereby still giving equal yields. The expected ratio of singlet oxygen yields of concentration-matched samples (excited at 420 nm) may be calculated, based on their respective quantum yields (measured in Section 6.3.1.2) and absorbance values (Section 6.3.1.1) which allow estimation of the ratio of absorbed photons by each sample, as shown in Figure 6.11. This gives a calculated ratio of 1.22, which compares well with the measured ratio, 1.10, calculated using relative yields measured in Section 6.3.1.1.

$$A = \log\left(\frac{I_0}{I_0 - I_A}\right) \quad \text{(1a)}$$

$$I_A/I_0 = 1 - 10^{-A} \quad \text{(1b)}$$

$$\Psi \propto \Phi \cdot I_A \quad \text{(2)}$$

Calculated ratio of pDHA + POPC yield: pDHA + POPE yield

$$\frac{\Psi_{PC}}{\Psi_{PE}} = \frac{\Phi_{PC} \cdot (I_A)_{PC}}{\Phi_{PC} \cdot (I_A)_{PE}} \quad \text{(3a)}$$

$$= \frac{\Phi_{PC} \cdot (1 - 10^{-A_{PC}})}{\Phi_{PC} \cdot (1 - 10^{-A_{PE}})} \quad \text{(3b)}$$

$$= 1.22$$

Measured ratio

$$\frac{\Psi_{PC}}{\Psi_{PE}} = 1.10$$

A = absorbance
I_0 = incident light (equal for all samples)
I_A = absorbed light
Ψ = yield
Φ = quantum yield
PC = pDHA + POPC samples
PE = pDHA + POPE samples

Figure 6.11 *Equations and calculations to compare calculated yield ratios, using quantum yield and absorbance values, and measured yield ratios. Equation 1b is derived as a rearrangement of 1a. 3a is derived from 2, and 3b is derived from incorporation of 1b into 3a.*

These experiments, therefore, do not show a role for POPE in reducing the yield of singlet oxygen produced by pDHA. There does, however, seem to be a difference in lifetime of the singlet oxygen produced. Without POPE, singlet oxygen lifetime was comparable with the published expected lifetime of singlet oxygen in benzene: 30 μs (Bensasson *et al.*, 1993b; Foote and Clennan, 1995). In the presence of POPE the singlet oxygen lifetime decreased, indicating efficient quenching of singlet oxygen by POPE and/or POPE-pDHA adducts. To confirm whether POPE is able to quench singlet oxygen, further experiments could be carried out in which singlet oxygen production by another photosensitizer such as rose bengal is monitored, and increasing concentrations of POPE or a mixture of pDHA and POPE are added to monitor any quenching ability.

To investigate the possible mechanisms by which singlet oxygen was formed, laser flash photolysis was carried out to monitor formation of transient excited states in pDHA samples, in the presence of either POPE or POPC. Photoexcitation of the samples resulted in formation of transient(s), and also photobleaching, followed by decay and recovery respectively. Recovery from photobleaching was not complete within the time-span of the recordings, particularly in the presence of POPE. In argon-saturated (oxygen depleted) samples, the presence of POPE resulted in a longer transient lifetime. In air-saturated (oxygen present) samples, however, POPE did not affect the lifetime of the transient. The precise identity of the transient formed in these experiments has not been elucidated. However, singlet oxygen formation occurs via energy transfer from an excited triplet state molecule (e.g. excited photosensitizer), therefore, the observed quenching of the transient by oxygen, and formation of singlet oxygen already described above imply that the transient observed here is likely to be a triplet state species. To confirm this, further experiments could be carried out using a triplet energy acceptor, for example β-carotene or related carotenoids. These compounds have a low triplet energy level (e.g. <95 kJ.mol^{-1} for β-carotene) and can therefore be excited to a triplet state by most other triplet states. This results in a shift in the absorption maximum of the carotenoid to a longer wavelength (compared with the singlet state), with a high absorption coefficient, thus allowing straightforward detection of its formation (Bensasson et al., 1993a).

Light exposure of pDHA liposomes containing either POPC or POPE resulted in increased levels of reduced cytochrome C. There was, however, no difference between pDHA + POPC and pDHA + POPE liposome samples. The formation of reduced cytochrome C did not occur linearly with time, but instead appeared to reach a plateau. This indicates either a limiting factor in the formation of superoxide or the reduction of cytochrome C, or loss of reduced cytochrome C through re-oxidation. Potential pathways are summarized in Figure 6.12.
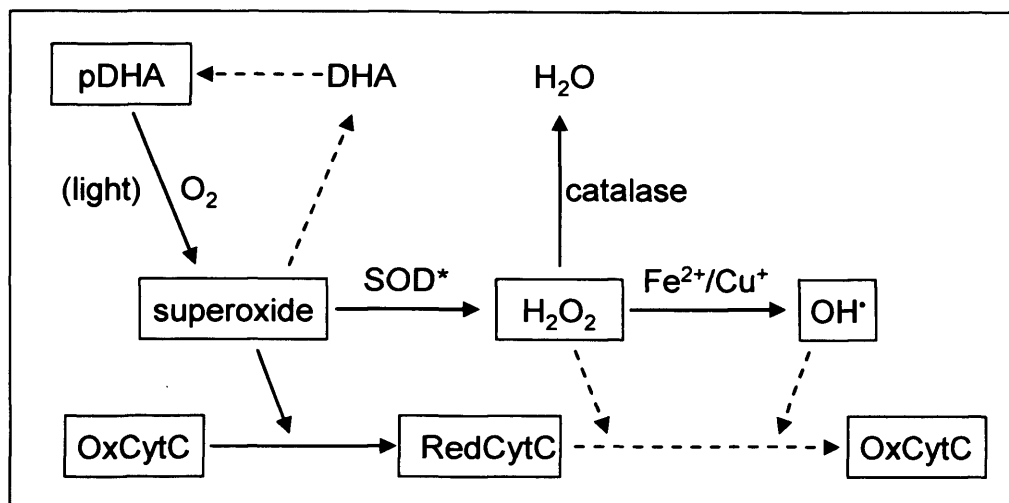
Figure 6.12 *Schematic diagram of actual and speculated pathways involved in the cytochrome C reduction assay used in this chapter. Dotted arrows = speculated pathways; OxCytC = oxidized cytochrome C; RedCytC = reduced cytochrome C; H_2O_2 = hydrogen peroxide; $OH^{\cdot}$ = hydroxyl radical. * dismutation of superoxide may also occur spontaneously.*

It is difficult to confirm the role of any of these factors: oxygen supply is plentiful due to stirring of samples throughout the experiments; the substrate, cytochrome C, is available in excess (starting concentration was 50 μM compared with maximal reduced cytochrome C levels observed after 60 minutes of approximately 9 μM). Other alternatives include depletion of the photosensitizer, pDHA, over the time-span of the experiment, or alternative routes of degradation of superoxide which could occur more quickly than the rate at which it interacts with and reduces cytochrome C. These could include dismutation to hydrogen peroxide (spontaneous or via SOD where included) or interaction with pDHA. An additional factor not controlled for in these experiments is metal ion levels: if superoxide is formed and dismutates to hydrogen peroxide, this could cause re-oxidation of cytochrome C. However, catalase, an enzyme which degrades hydrogen peroxide, showed no effect on cytochrome C reduction in these experiments so hydrogen peroxide is unlikely to play a direct role here. In the presence of metal ions however, Fenton reactions may result in rapid formation of hydroxyl radicals which could instead re-oxidize cytochrome C. These pathways are summarized in Figure 6.12 (Halliwell and Gutteridge, 2007a).

Addition of SOD resulted in lower levels of reduced cytochrome C at 60 minutes. To confirm that this was due to direct enzyme actions in dismutating superoxide rather than the protein acting as an alternative substrate for pDHA or (photo-)generated reductive species, results can be compared with catalase experiments: catalase was present in a similar absolute concentration (0.85 mg.ml^{-1} catalase vs. 0.96 mg.ml^{-1} SOD), thus providing similar levels of amino acid residues as potential targets. Yet catalase caused no alterations in reduced cytochrome C levels. Therefore, the positive effect of SOD confirms that superoxide is responsible for the observed reduction of cytochrome C. Kinetics of cytochrome C reduction in the presence of SOD is, however, very different to the samples without SOD. Graphs suggest that SOD initially protects cytochrome C, causing a lag period before cytochrome C reduction commences, between 10 and 20 minutes after the start of light exposure. This could be due to inactivation of SOD – potentially by the light exposure – or by interaction with pDHA, neither of which was investigated here.

In summary, although pDHA samples appear to produce both singlet oxygen and superoxide, POPE does not reduce the production of these compounds to a level which could explain its protective effect observed in MTT cell culture experiments in Chapter 5. POPE does, however, shorten the lifetime of singlet oxygen, but because the yield of production is the same as without POPE, the effects of this shortening would depend on the rate of interaction of singlet oxygen with other targets in the cell experiments and their concentrations relative to PE. The presence of PE reduced singlet oxygen lifetime to ~17 μs, almost half the lifetime of singlet oxygen produced by pDHA without PE. These measurements were carried out in benzene, where the expected lifetime of singlet oxygen is 30 μs (Bensasson *et al.*, 1993b; Foote and Clennan, 1995). In lipid suspensions in water (using pure phosphatidylcholine), and cell membranes, singlet oxygen lifetime is decreased by two thirds (compared with benzene) to ~10 μs (Baier *et al.*, 2005). The lifetime in water is even shorter: 3.5-4 μs (Bensasson *et al.*, 1993b; Baier *et al.*, 2005). If the quenching ability of PE is similar in these other situations and can halve the singlet oxygen lifetime, this

could have a large impact on the likelihood of singlet oxygen produced by pDHA interacting with other molecules to cause toxicity.

Another potential pathway of POPE-mediated protection is via the interaction of PE with lipid aldehydes. Peroxidation of LC-PUFA leads to the production of a large number of products and includes the formation of lipid aldehydes which have previously been shown to form Schiff base adducts with amines (Boutaud *et al.*, 1999; Bernoud-Hubac *et al.*, 2001; Gu *et al.*, 2003b), and are able to form Michael adducts with ethanolamine phospholipids (Bacot *et al.*, 2007). Therefore, PE may act as a substrate for this reaction when combined with pDHA, thereby potentially deactivating pDHA, or at least a large number of the peroxidation products present in the mixture. This could prevent further phototoxic reactions, or prevent interaction of pDHA aldehydes with proteins during cell exposure experiments. Changes in absorbance observed in samples containing pDHA + POPE compared with pDHA + POPC suggest that formation of adducts between pDHA and POPE do, in fact, occur. To further investigate this matter, pDHA-PE adducts and adducts with cellular proteins could be identified using tandem mass spectroscopy, and the protective effects of POPE could be compared with other known (natural and synthetic) lipid aldehyde scavengers. This could at least provide an indication of whether or not this mechanism is important in the observed toxicity of pDHA, and may better explain the protective role of POPE.

Chapter 7:
Effects of pDHA on RPE degradative functions

7.1 Introduction

As discussed in Chapter 1, RPE cells play a vital support role to photoreceptor cells. One of the important processes carried out by RPE cells is the phagocytosis of spent photoreceptor outer segments, to remove peroxidized lipids and other waste materials. Lipid peroxidation may in fact result in increased phagocytosis by providing tags for CD36 mediated phagocytosis (Sun *et al.*, 2006). To aid with this process, RPE are in very close contact with POS (Gu *et al.*, 2003a). After internalization, material needs to be degraded prior to complete removal from the RPE, either through Bruch's membrane and removal via the blood supply, or via a recycling process to be re-incorporated into newly formed POS discs. It has previously been shown that normal components of the (aged) retina, e.g. lipofuscin and A2E, as well as oxidized POS fed to cells, are able to reduce the degradative capacity of lysosomes via various pathways (Wihlmark *et al.*, 1996; Bermann *et al.*, 2001; Shamsi and Boulton, 2001; Finnemann *et al.*, 2002; Bergmann *et al.*, 2004; Kaemmerer *et al.*, 2007).

The aims of this chapter are to monitor whether pDHA is able to alter the structure and function of lysosomes in a way that reduces their capacity to degrade phagocytosed material, and to monitor changes in cellular fluorescence and accumulation of undegraded material.

7.2 Experimental design

7.2.1 Cell viability after feeding with POS +/- pDHA

Initial observations after long-term feeding of cells with pDHA included changes in the colour of the culture medium— becoming rather more pink than normal (usually correlated with cell death – personal observation), particularly at the highest pDHA concentrations and longest time points. Additionally, it took longer to collect equivalent cell numbers by flow cytometry, implying lower cell concentrations and therefore initial cell numbers. Therefore, MTT assays were carried out after pDHA/POS feeding to monitor this problem.

Phototoxicity of internalized pDHA to ARPE-19 cells after long-term feeding was also investigated. After feeding as described above, cells were washed then put in fresh medium for 24 hours to allow for internalization of any attached photoreceptors and/or liposomes prior to light exposure.

7.2.2 Lysosomal integrity after feeding with POS +/- pDHA

Acridine orange is a hydrophobic molecule with green fluorescence at low concentrations at neutral pH, e.g. in the cytoplasm (Brunk *et al.*, 1995; Öllinger and Brunk, 1995). Its hydrophobicity allows it to transfer across cell and organelle membranes. At acidic pH, acridine orange becomes protonated and can no longer cross membranes. Instead, it aggregates, allowing accumulation against the concentration gradient in acidic compartments of the cell e.g. lysosomes, resulting in red fluorescence (de Duve *et al.*, 1974; Öllinger and Brunk, 1995). This allows clear fluorescent labelling of lysosomes, with simultaneous excitation of the red and green emitting forms possible by illumination with blue light (488 nm) during either fluorescence microscopy or flow cytometry. On exposure to bright blue light, acridine orange acts as a photosensitizer and is able to damage lysosomal membranes, thus resulting in a loss of the pH gradient, de-protonation of the acridine orange and a loss of red fluorescence, and increased cytoplasmic green fluorescence (Brunk *et al.*, 1997). Therefore it is important to image the cells as quickly as possible and maintain cells in darkness after loading.

Acridine orange may also label RNA (red), however this requires higher concentrations than those used in these experiments (5 µg.ml^{-1}), so is unlikely to have any effect on monitoring of lysosomal labelling (Antunes *et al.*, 2001).

Acridine orange labelling was monitored using two methods: fluorescence microscopy and flow cytometry. Microscopy allowed an overall check that acridine orange labelling was consistent with lysosomal labelling i.e. visible as granular red fluorescence, rather than for example, cytoplasmic red fluorescence which could possibly occur if cytoplasmic pH were to be drastically alter by bursting lysosomes. This technique has severe limitations, however, as imaging

is relatively slow, and due to issues with phototoxicity of acridine orange itself, it is absolutely essential that all samples are treated identically. Therefore, after initial observations by fluorescence microscopy, flow cytometry was used for rapid analysis of large numbers of cells.

7.2.3 Intracellular deposit formation after feeding with POS +/- pDHA

Two methods were used to monitor formation of intracellular deposits in ARPE-19 cells fed with POS and/or pDHA. Initially, flow cytometry was used as a rapid way to monitor changes in fluorescence. However, to correlate these findings with levels of lipofuscin-like granule formation, it was necessary to carry out imaging of the cells using TEM. This provides high resolution imaging of individual cells, and allows clear identification of electron-dense granules.

7.3 Results

7.3.1 MTT assay after feeding with POS/pDHA

7.3.1.1 Effects of long-term feeding on cell viability

When cells were fed with POS +/- pDHA for up to 3 weeks, mitochondrial activity showed significant differences between feeding treatments (two-way ANOVA $P < 0.001$; Figure 7.1). For cells fed for two weeks, Tukey's post-tests showed a significant 20% increase in activity after feeding with POS + 10 μM pDHA ($P < 0.001$) and a significant 14% decrease after feeding with POS + 20 μM pDHA ($P = 0.001$), compared with control. There was no significant overall difference between the two time points investigated (2-way ANOVA $P = 0.314$), however after 3 weeks of feeding, supplemented cells varied to a greater extent from the control cells, with all showing a significant difference, with increases to 115%, 121% and 128% for POS + 0, 5, and 10 μM pDHA respectively, and a decrease to 62% for POS + 20 μM ($P = 0.004$ for all comparisons with cells fed POS only, and $P < 0.001$ for all cells fed POS + pDHA).
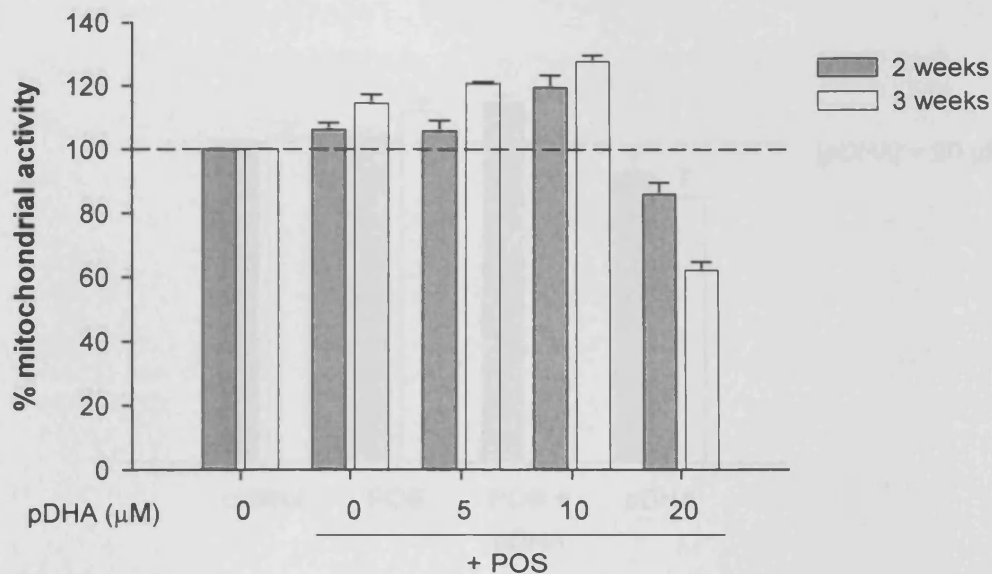
Figure 7.1 *MTT assay carried out after feeding cells for 2 or 3 weeks with POS +/- pDHA at the indicated concentrations. All treatments were normalized to control cells at the same time point. Bars = SEM; n = 3-6.*

7.3.1.2 Phototoxicity of pDHA after long-term feeding

In separate experiments, cells were fed with POS and/or 20 μM pDHA in liposomes for 2 weeks, then washed and left for 24 hours to allow internalization of any bound POS/liposomes. Cells were then exposed to light (15 mW.cm^{-2}) or maintained in the dark for one hour, and the MTT assay was carried out 24 hours later (Figure 7.2). Two-way ANOVA showed no significant difference between light and dark treated cells (P = 0.674). However, the different feeding conditions did significantly alter mitochondrial activity between groups (P < 0.001). In dark conditions, pDHA alone caused a significant decrease compared with POS + pDHA (P = 0.01), and in light conditions, pDHA alone caused a significant reduction in mitochondrial activity, to 83%, compared with all other treatments (P = 0.023 vs. control, P = 0.002 vs. POS, P < 0.001 vs. POS + pDHA).
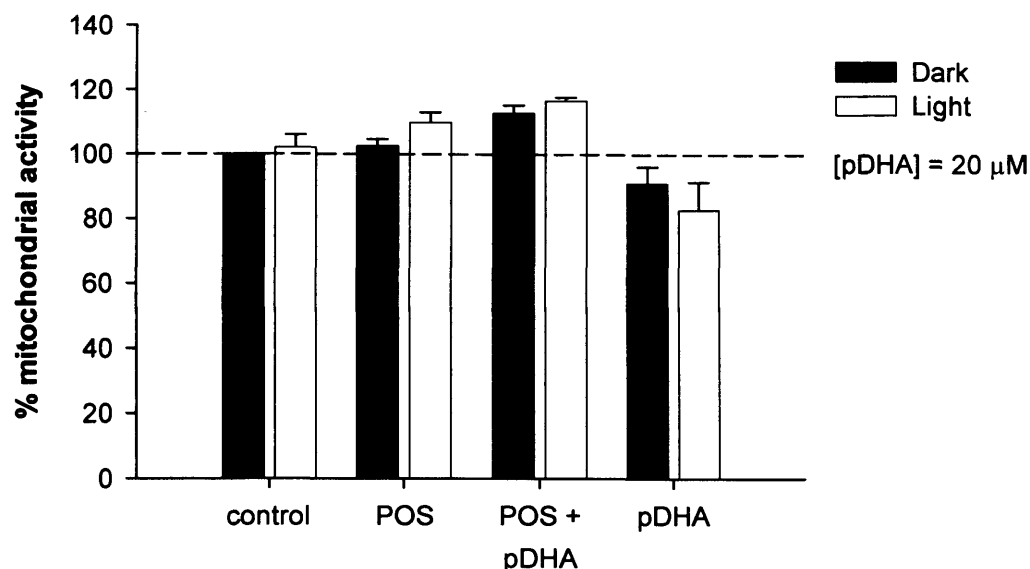
Figure 7.2 *MTT assay carried out after 2 weeks of feeding cells with POS and/or pDHA, followed by 1 hour light exposure (15 mW.cm^{-2}), then 24 hours post-incubation in fresh medium. All treatments were normalized to the dark control. Bars = SEM; n=3.*

7.3.2 Lysosomal integrity

7.3.2.1 Fluorescence microscopy of acridine orange labelled cells

Cells labelled with acridine orange showed granular red fluorescence indicative of lysosomal uptake of this fluorophore (Figure 7.3). The images indicate that intact lysosomes were present after all treatments, and that there was rather variable staining, even in different cells within the same treatment. As detached cells were used and they were rather dispersed on the slides, no further analysis of these images was carried out. Instead, flow cytometry was used to allow more rapid collection of fluorescence data of far greater numbers of cells with reduced risk of acridine orange induced phototoxicity.
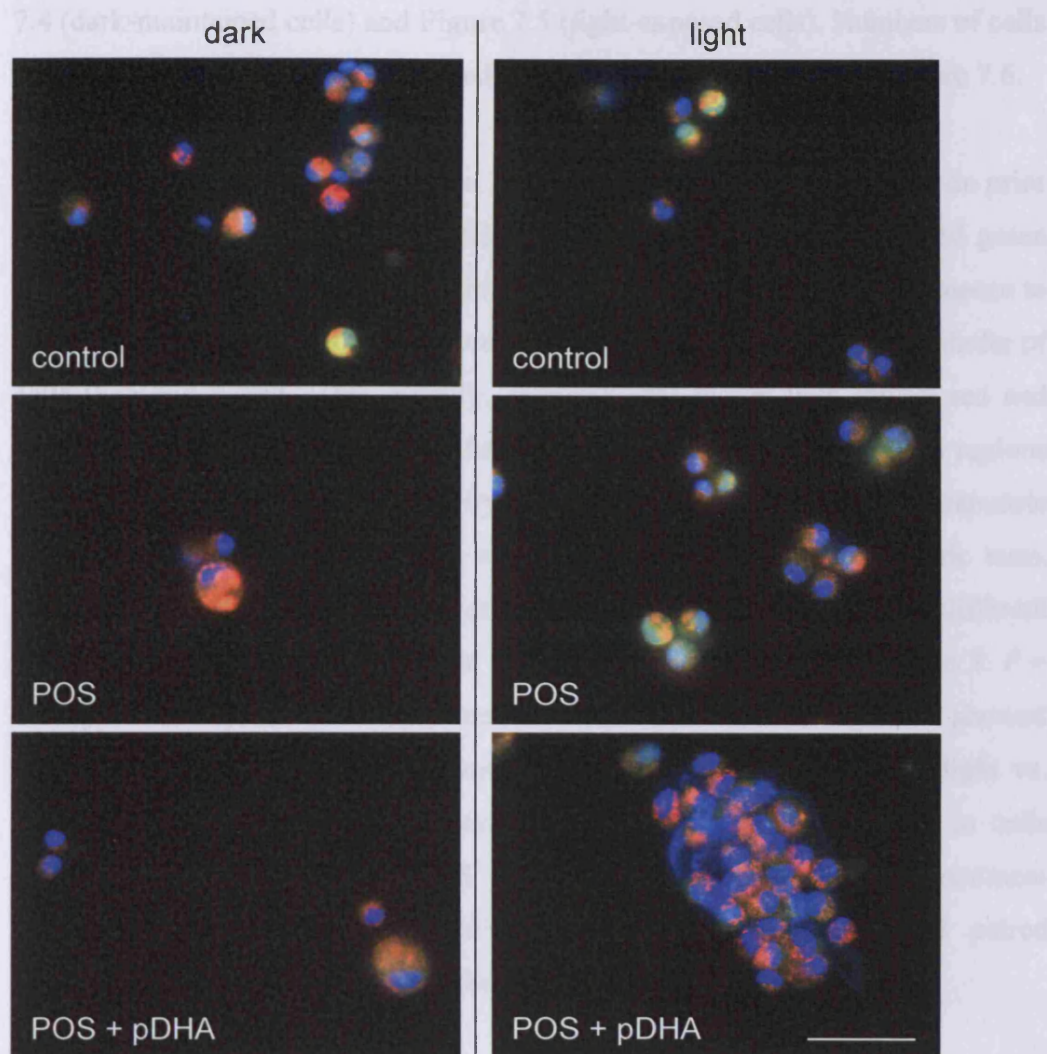
Figure 7.3 *Cells labelled with acridine orange after 2 weeks of feeding as indicated, then either dark-maintained or exposed to light (15 mW.cm⁻²) for 1 hour prior to labelling. Blue = Hoechst labelling of nuclei; green = cytoplasmic acridine orange; red = lysosomal acridine orange. Bar = 50 μM.*

7.3.2.2 Flow cytometry of acridine orange labelled cells

Flow cytometry was used to monitor levels of red and green fluorescence (FL3 and FL1 respectively) in cells labelled with acridine orange. Results show partitioning of "events" (assumed to be individual cells) into 3 regions with different ratios of red to green fluorescence, as marked on scatter plots in Figure

7.4 (dark-maintained cells) and Figure 7.5 (light-exposed cells). Numbers of cells in each of these regions were counted. Mean values are compared in Figure 7.6.

The majority of cells fell into region 2 (between 73 and 94%, depending on prior treatment). This region includes cells with the greatest levels of red and green fluorescence of all the regions. Region 3, which has similar green fluorescence to region 2 but reduced red fluorescence, contained the majority of the remainder of cells (between 4 and 21%). Finally, region 4, the region with lowest red and green fluorescence, contained very few cells (between 0.3 and 3.9%). For regions 2 and 3, data failed tests for normality and equal variances, so the non-parametric Kruskal-Wallis ANOVA on ranks was carried out instead of parametric tests. This test showed no significant difference in cell counts between different feeding treatments in either of these regions (region 2: $P = 0.099$; region 3: $P = 0.100$). Two-way ANOVA (parametric) for cell counts in region 4 showed significant variation between treatments ($P < 0.001$) but no effect of light vs. dark (P = 0.342). Tukey's post-tests indicated a significant increase in cells counted after feeding with 20 µM pDHA compared with all other treatment groups, from an average of ~0.5% to ~3.9% ($P < 0.001$ for all paired comparisons), but no significant differences between other treatments.
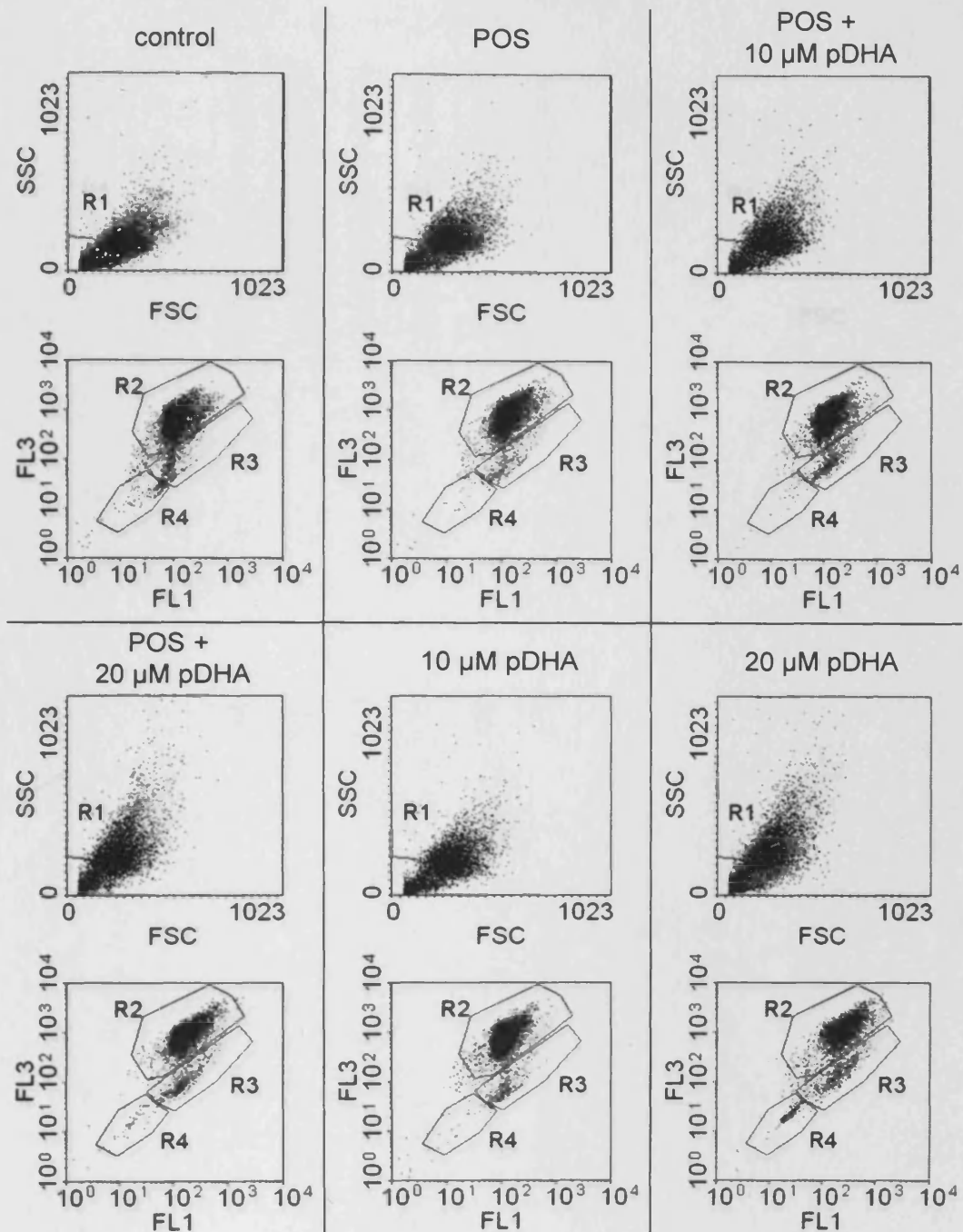
Figure 7.4 *Representative flow cytometry scatter plots from a single experiment for cells fed for 2 weeks with POS and/or pDHA, then maintained in the dark for 1 hour and labelled with acridine orange. Region 1 (R1) on the upper FSC/SSC plot was used to gate "events" for counts and other plots. The lower FL1/FL3 plots show gated events (i.e. those within R1 only), and are labelled for regions 2, 3 and 4 (R2, R3 and R4), which were used for further analysis and cell counting. FL1 = green fluorescence emission; FL3 = red fluorescence emission (arbitrary units).*
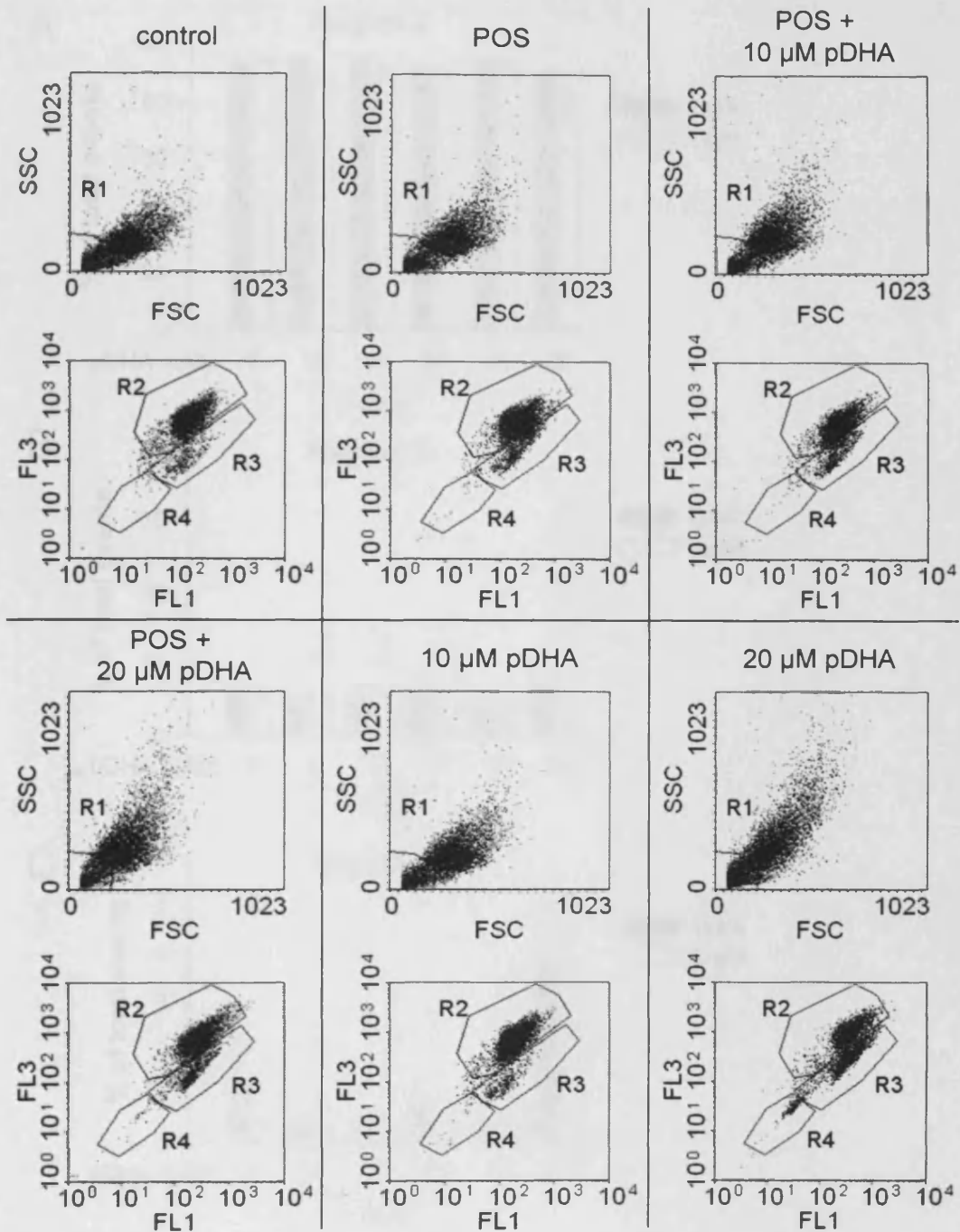
Figure 7.5 *Representative flow cytometry scatter plots from a single experiment for cells fed for 2 weeks with POS and/or pDHA, then exposed to light (15 mW.cm⁻²) for 1 hour and labelled with acridine orange. Region 1 (R1) on the FSC/SSC plot was used to gate "events" for counts and other plots. The lower FL1/FL3 plots show gated, and are labelled for regions 2, 3 and 4 (R2, R3 and R4), which were used for further analysis and cell counting. FL1 = green fluorescence emission; FL3 = red fluorescence emission (arbitrary units).*
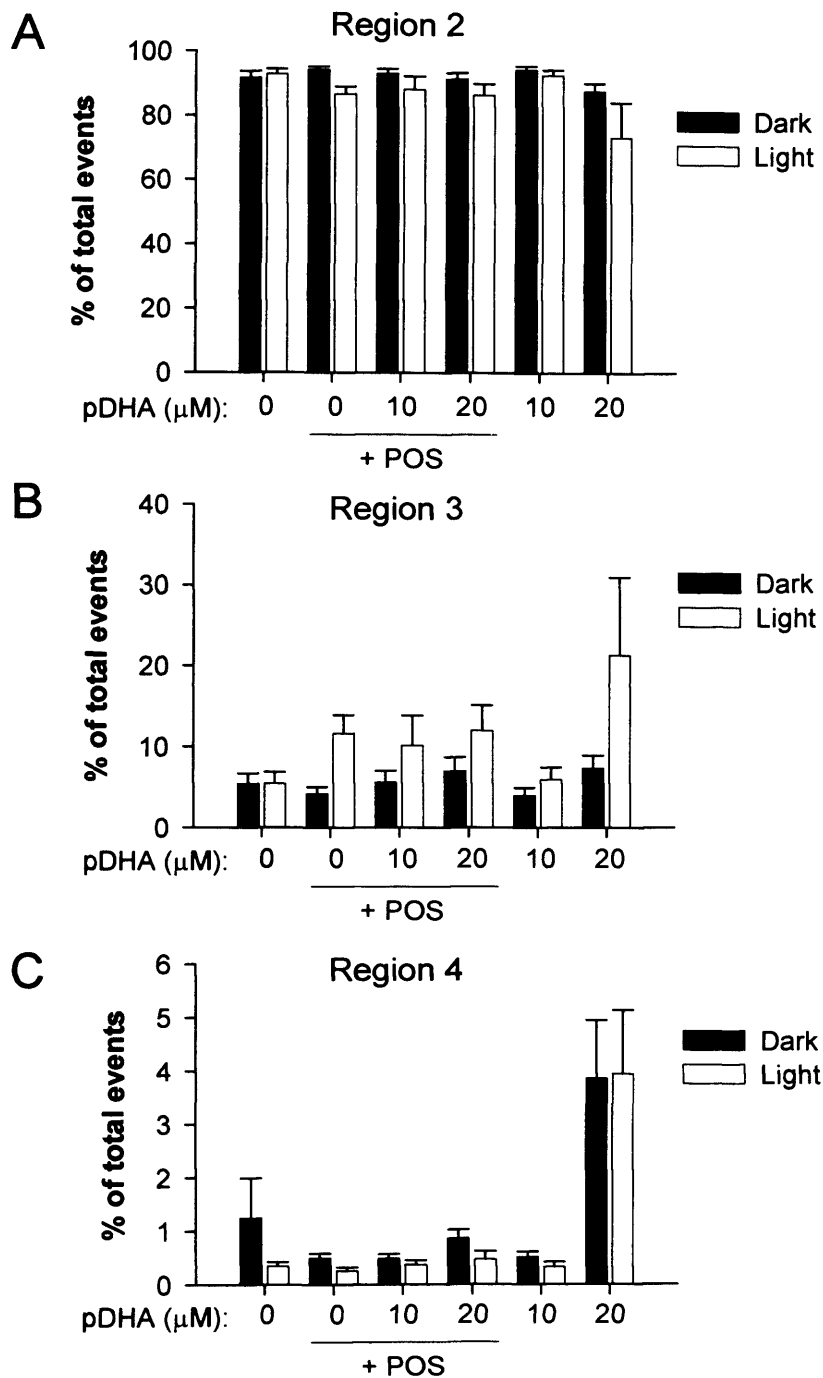
Figure 7.6 *Counts of "events" within each region as marked on the FL1 vs. FL3 plots. Graphs correspond to counts within (A) region 2; (B) region 3; (C) region 4. Bars = SEM; n = 3.*

To further elucidate the differences between cells in the different regions of the fluorescence scatter plot described above, Figure 7.7 shows FSC/SSC plots to monitor cell size (forward scatter, FSC) and granularity (side scatter, SSC) of the cells in each region. All plots in Figure 7.7 were gated to include only those cells

149

in region 1 (from the FSC/SSC plot, to remove the majority of non-cellular debris). These were then further gated to show only data points for cells within each region. The plots show that cells from regions 2 and 3 are distributed evenly throughout the total population of cells, whereas cells from region 4 showed lower forward and side scatter, indicated smaller size and reduced granularity.
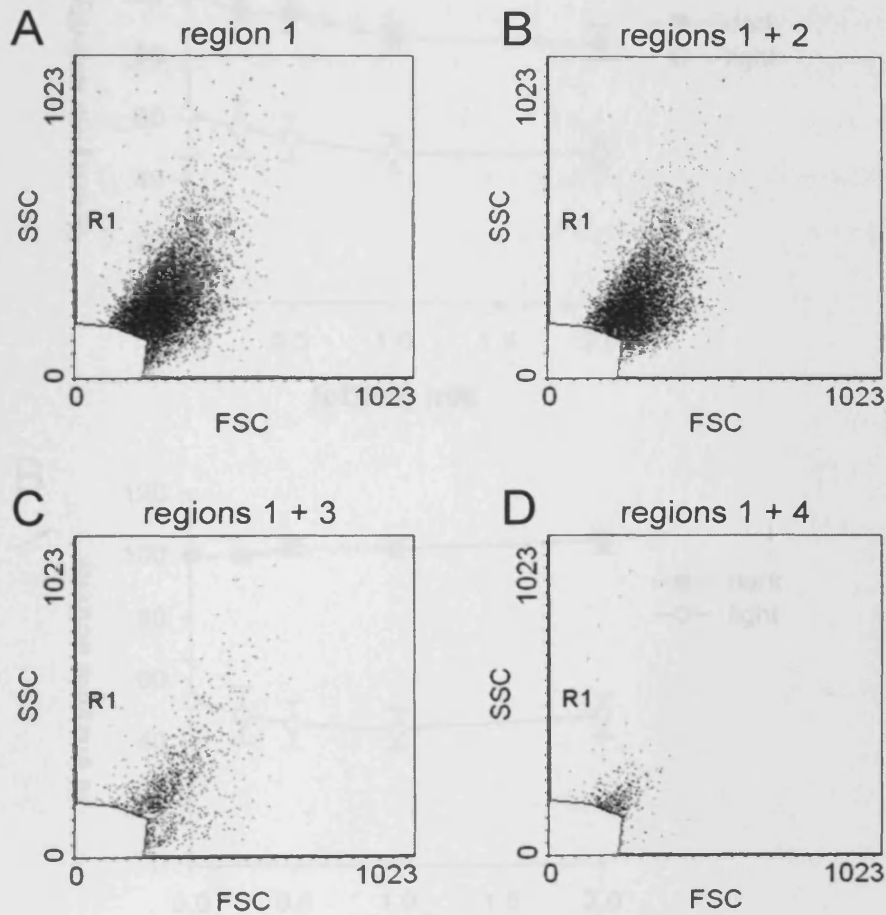
Figure 7.7 *Flow cytometry FSC/SSC plots of cells from each of the regions established in fluorescence scatter plots above. (A) Scatter plot of all cells which were used for further analysis and counting, (B) cells contained within region 1 (in FSC/SSC plot) and region 2 (from fluorescence plots); (C) cells from region 1 and region 3; (D) cells from region 1 and region 4.*

7.3.3 Lysosomal enzyme activity

Cell lysates were initially exposed to pDHA in the presence of intense light (48 mW.cm^{-2}) for 1 hour, but it was found that in controls (i.e. no pDHA), phosphatase activity was reduced by ~40% and glucosaminidase by ~45%

(Figure 7.8) compared with dark-maintained. Within each treatment – i.e. light or dark – there was no further significant effect of pDHA on activity of either enzyme compared with control.
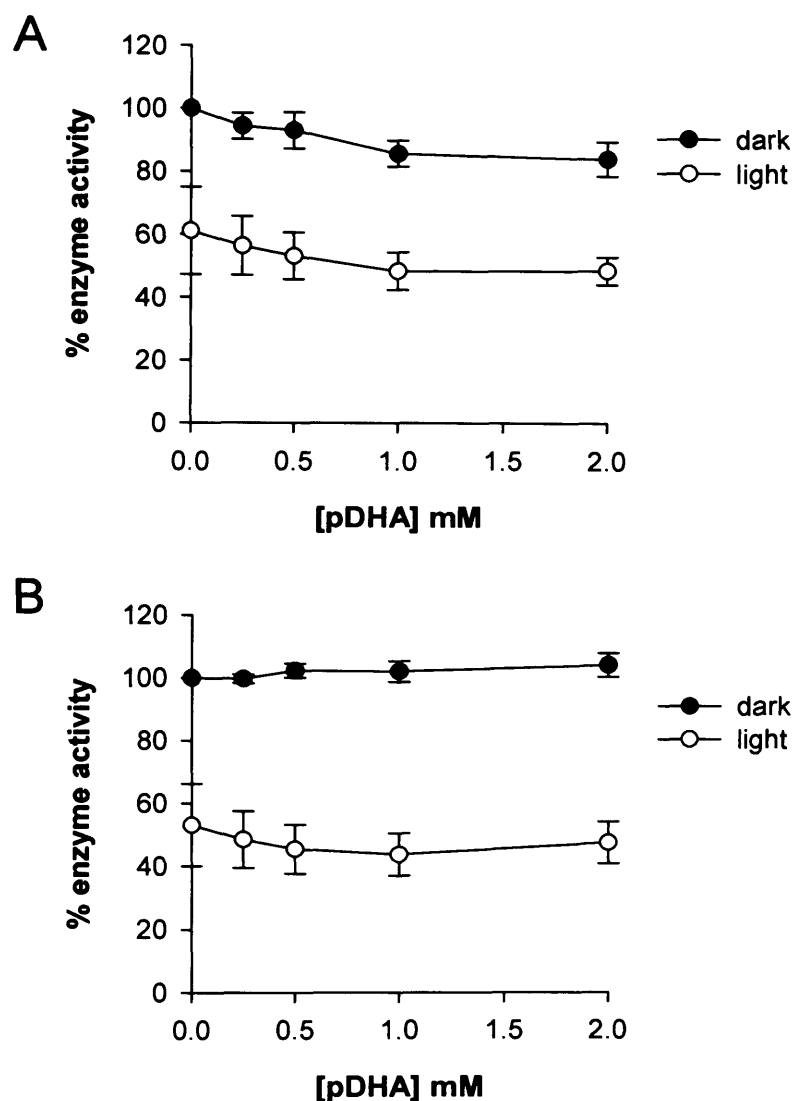
Figure 7.8 *Assays of enzyme activity in cell lysates, after 1 hour exposure to 48 mW.cm^{-2} light, normalized to activity in the dark control. (A) Phosphatase activity; (B) glucosaminidase activity. Bars = SEM; n = 3.*

To overcome the large reduction in enzyme activity observed in light-treated cell lysates compared with dark-maintained, the light intensity was reduced for subsequent experiments and lysates were exposed for a longer period of time: 2.8 mW.cm^{-2} for 24 hours. In these experiments, there was no significant

difference between dark and light controls (Figure 7.9). Phosphatase activity in cell lysates was not significantly affected by DHA compared with controls (ANOVA P = 0.680), but there was a difference in light treated vs. dark maintained (ANOVA P < 0.001) in the presence of pDHA – at 1 mM pDHA, activity decreased significantly from 121% (dark) to 69% (light; P = 0.002) and on exposure to 2 mM pDHA, from 117% to 59% (P = 0.001). There was no significant difference in phosphatase activity of pure acid phosphatase enzyme in light vs. dark (P = 0.248) or due to the presence of pDHA (P = 0.086). Glucosaminidase activity of cell lysates was not affected by light vs. dark (P = 0.994), however pDHA did significantly affect activity (P = 0.017), with 2 mM causing a significant increase in activity in dark conditions, from 100% in control to 205% in the presence of 2 mM pDHA (P = 0.024).
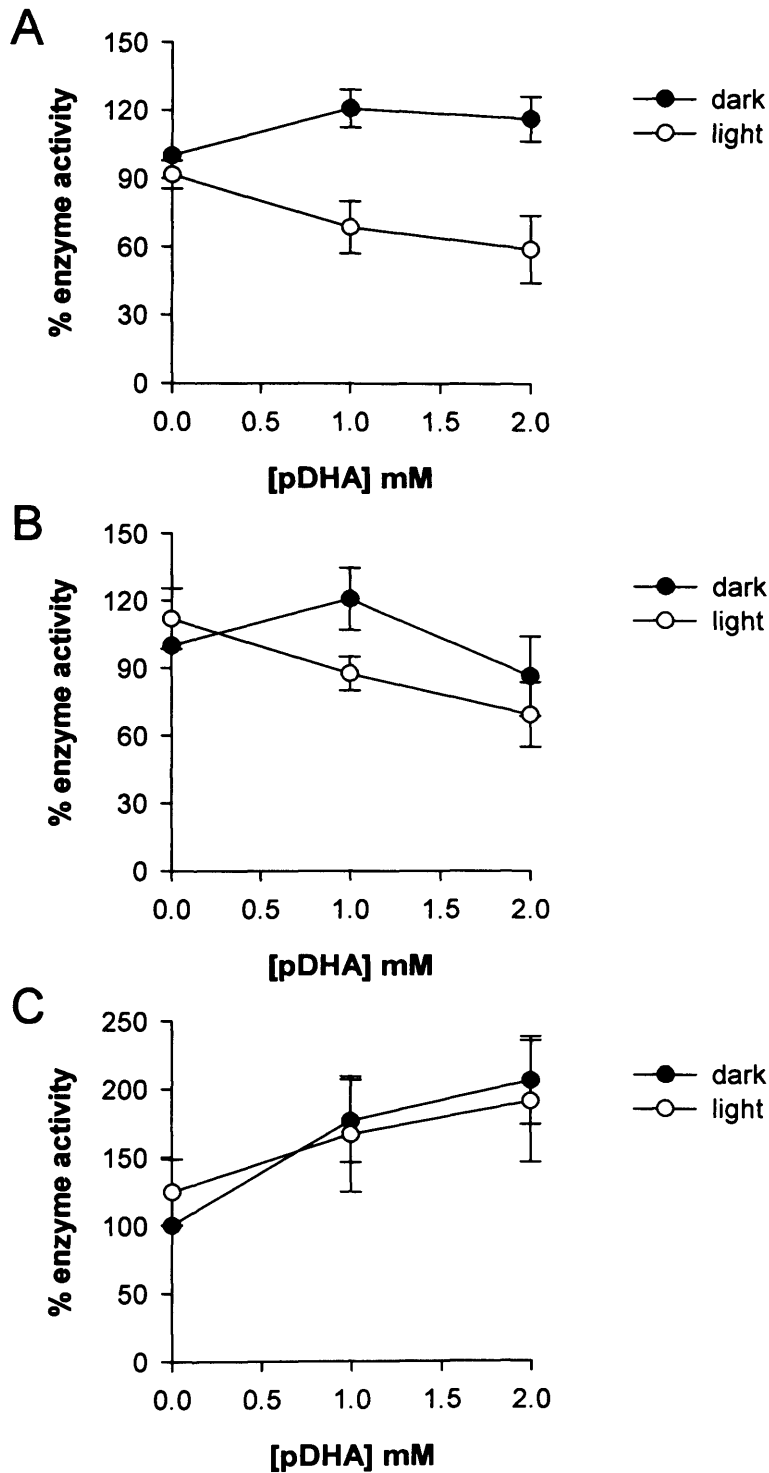
Figure 7.9 *Assays of enzyme activity after exposure to pDHA with 2.8 mW.cm^{-2} light, or dark, for 24 hours, normalized to activity in the dark control. (A) Phosphatase activity in cell lysates; (B) phosphatase activity of pure acid phosphatase; (C) glucosaminidase activity in cell lysates. Bars = SEM; n = 3-4.*

7.3.4 Intracellular deposit formation

7.3.4.1 Monitoring changes in fluorescence by flow cytometry

Feeding cells with POS with or without pDHA liposomes caused significant variation in cellular fluorescence at all of the time points investigated i.e. 1, 2, 3 and 4 weeks ($P < 0.001$ for all; Figures 7.10 and 7.11). In all cases, feeding cells with POS significantly increased fluorescence in comparison with control approximately 6-fold (P-values are shown in Appendix 4), with no further increase caused by addition of 5 μM pDHA to the liposomes. At 1, 2 and 3 weeks however, a further significant increase in fluorescence – approximately 10-fold (compared with control) after 1 and 2 weeks, and 18-fold after 3 weeks of feeding – was observed after addition of 20 μM pDHA to the POS. This concentration could not be used for the 4 week feeding trial as it resulted in cell detachment, indicating cell death. Instead, 10 μM pDHA was used at this time point only, but this resulted in no significant increase in fluorescence above that observed after feeding POS alone. Feeding cells with 20 μM pDHA alone (no POS) for 2 weeks resulted in a significant ~5-fold increase in fluorescence compared with control ($P = 0.033$), but this fluorescence still remained significantly lower (approximately 50%) than POS + 20 μM pDHA ($P = 0.007$). Feeding cells for 4 weeks with either 5 or 10 μM pDHA (without POS) resulted in no significant change in fluorescence emission compared with control cells ($P = 0.928$ and 0.102 respectively).

It should also be noted that the peak width (indicating variation within the samples) varied with treatment. Of note, the cells fed POS, POS + 5 μM pDHA or POS + 10 μM pDHA showed a broader peak than control cells. In contrast, those fed POS + 20 μM pDHA, or pDHA alone (all concentrations) showed a narrower peak, similar to the control cells.

Further comparisons were also carried out between the different time points after feeding cells with control medium, POS, POS + 5 μM pDHA and POS + 20 μM pDHA (see Figure 7.12) for 1 to 4 weeks. Two-way ANOVA confirmed significant effects of both duration of feeding and the actual treatments cells were

exposed to ($P < 0.001$ for both). Feeding for 4 weeks did not give any significant change in fluorescence compared with the other time points, however there was variation between 1 week and 2 weeks ($P = 0.004$) and 1 week and 3 weeks of feeding ($P < 0.001$). The main difference between all of these time points compared with 4 weeks, is that they included cells which were fed with POS + 20 µM pDHA, which the 4 week time point did not. Overall, all treatments differed significantly from each other (all $P < 0.001$) except for POS vs. POS + 5 µM pDHA which showed no significant difference ($P = 0.861$), correlating with the findings at each individual time point described above.
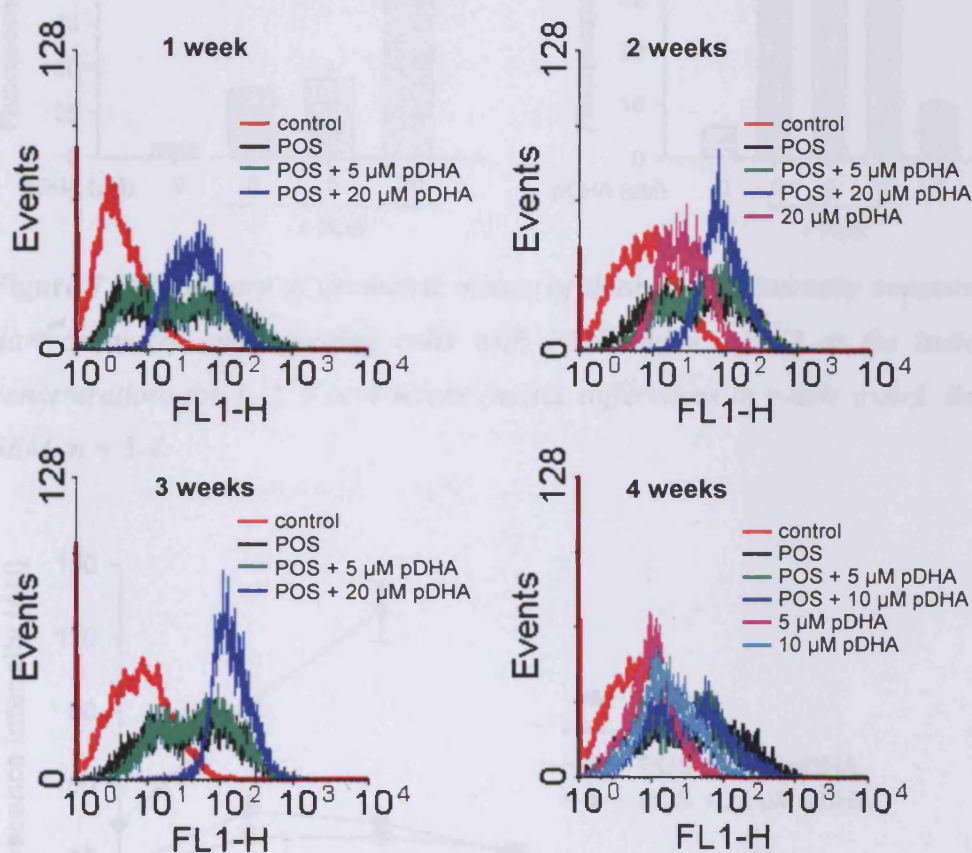
Figure 7.10 *Representative flow cytometry data from individual wells in a single experiment showing histograms for green fluorescence emission in cells fed with POS and/or pDHA, for between 1 and 4 weeks. A total of 10,000 cells was counted for each condition and time point. FL-1H indicates green fluorescence intensity (arbitrary units).*
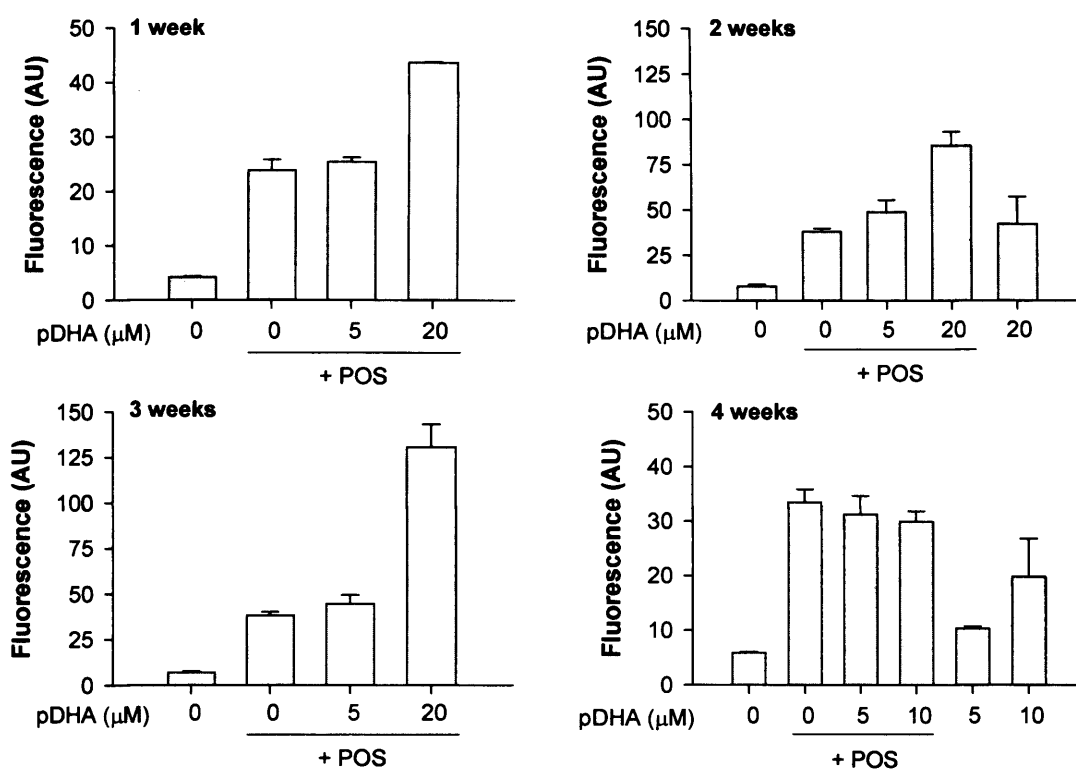
Figure 7.11 *Summary of geometric means of fluorescence intensity measured by flow cytometry, after feeding cells with POS and/or pDHA at the indicated concentrations for 1, 2, 3 or 4 weeks (notice differences in y-axis scale). Bars = SEM; n = 3-4.*
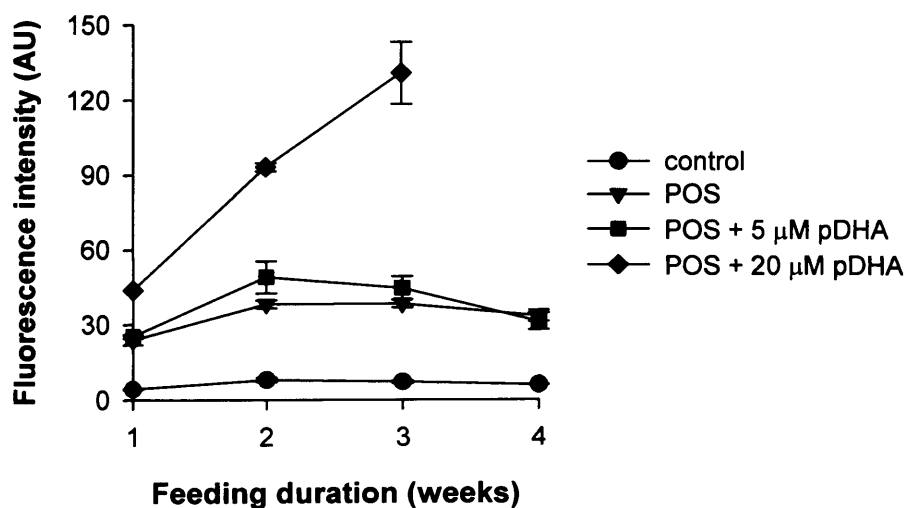
Figure 7.12 *Changes in fluorescence after feeding cells with POS +/- pDHA, for between 1 and 4 weeks. Bars = SEM; n = 3-4.*

7.3.4.2 Monitoring of granule formation using TEM

TEM images of cells fed for two or four weeks with medium alone (control), bovine POS or POS + pDHA liposomes (20 μM pDHA for two weeks, and 10 μM for 4 weeks, corresponding to the highest concentrations used in flow cytometry fluorescence measurements), are shown in Figure 7.13. Graphs in Figure 7.14 show the average number of granules counted per ARPE-19 cell cross-section. Counts were divided into two types of granules: "granular" – possibly early stage phagolysosomes – and "homogeneous" – lipofuscin-like granules. Although the number of granules per cell appears to double in control cells after 4 weeks of feeding compared with 2 weeks, this difference was not significant. There were, however, overall differences in total granules, homogeneous granules and granular granules over all treatments (one-way ANOVA P-values: <0.001, <0.001 and 0.034 respectively). Post-tests revealed significant increase in total and homogeneous granule numbers in cells fed for 2 weeks with POS + DHA compared with control (total granules increased from 20 to 35 granules; $P = 0.001$; homogeneous increased from 2.2 to 11.5, $P = 0.01$). A significant increase in homogeneous granules was also observed after 4 weeks of feeding with POS + DHA compared with control (increased from 2.7 to 12.5, $P = 0.006$). No further statistically significant changes were observed.
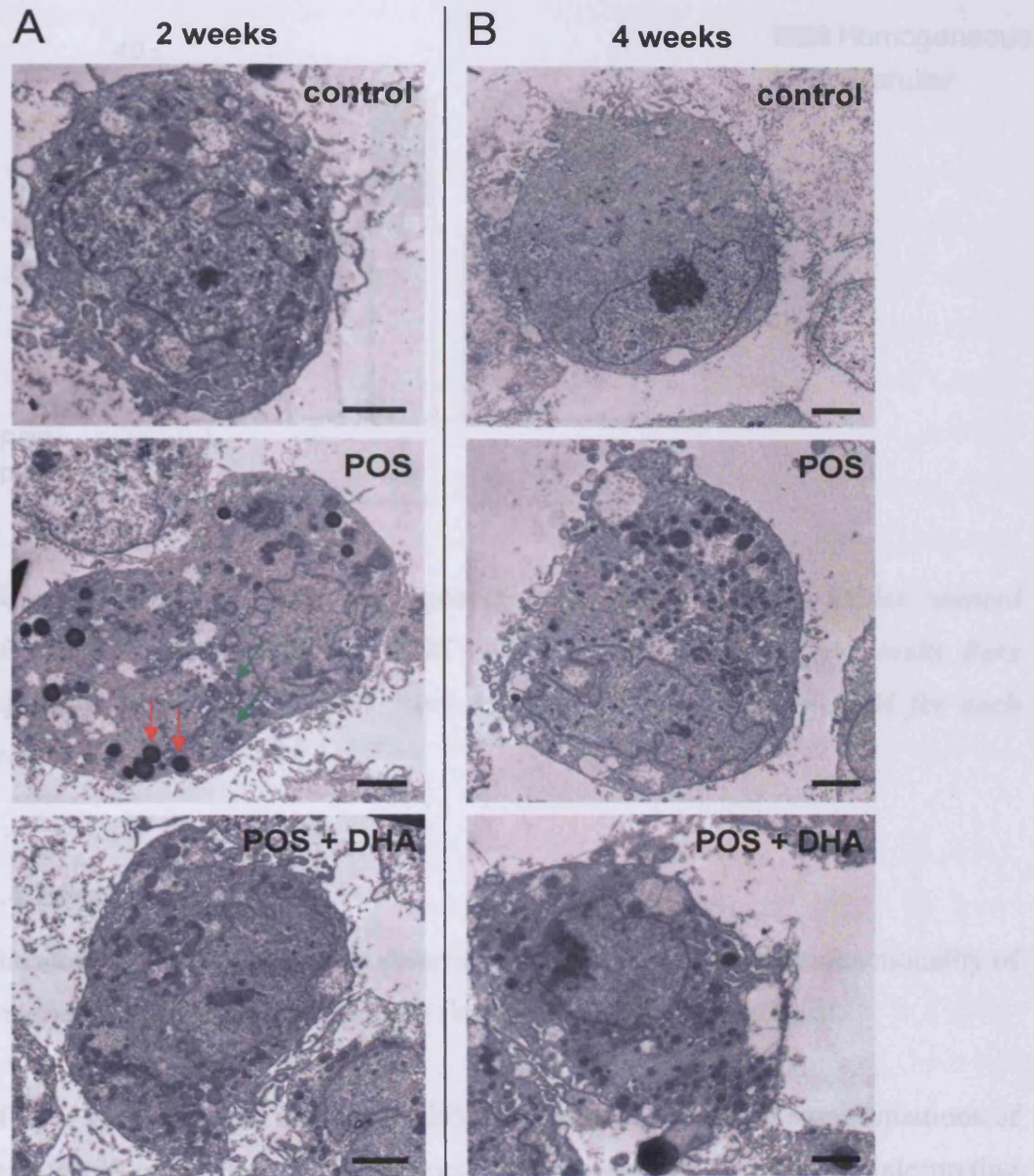
Figure 7.13 *TEM images of cells fed with POS +/- pDHA liposomes for (A) 2 weeks or (B) 4 weeks. Green arrows = examples of "granular" granules; red arrows = "homogeneous" granules; scale bars = 2 μm.*
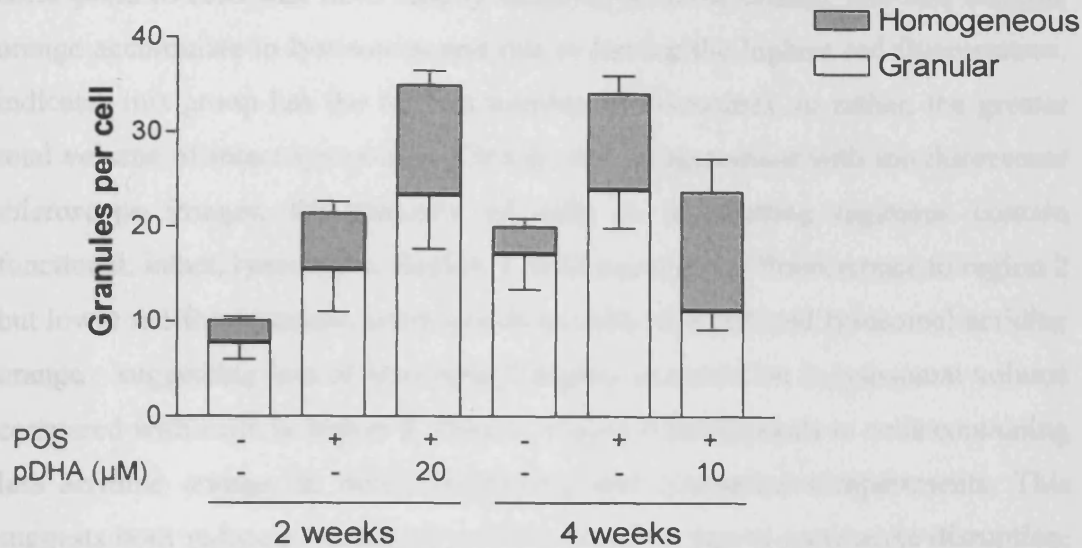
Figure 7.14 *Average number of granular and homogeneous granules counted per cell after feeding cells with POS +/- pDHA liposomes for 2 or 4 weeks. Bars represent the mean of counts from 10 different cells. Bars = SEM for each granule type.*

7.4 Discussion

The aim of this chapter was to determine the effects of pDHA on functionality of lysosomes, and their ability to fully degrade phagocytosed material.

MTT assays indicated that cell viability is reduced slightly in some situations of cells fed 20 µM pDHA. This suggests that caution should be taken in interpreting results with these concentrations, as it is possible that cells may have died and detached, thus potentially leading to underestimation of the observed effects if these cells are the "most" loaded with pDHA/POS. The MTT results justify the use of lower concentrations for the 4-week feeding programme, to reduce the risk of even further cell death.

Acridine orange labelled cells separated into three regions on fluorescence scatter plots obtained using flow cytometry (Figures 7.4 and 7.5). It is likely that these three regions correspond to 3 distinct populations of cells. Region 2 (with maximal green and red fluorescence compared with the other regions) should

correspond to cells that have readily taken up acridine orange, and had acridine orange accumulate in lysosomes and due to having the highest red fluorescence, indicates this group has the highest number of lysosomes, or rather, the greater total volume of intact lysosomes. Clearly, and in agreement with the fluorescent microscope images, the majority of cells in all feeding regimens contain functional, intact, lysosomes. Region 3, with equal green fluorescence to region 2 but lower red fluorescence, corresponds to cells with reduced lysosomal acridine orange – suggesting loss of lysosomal integrity or reduction in lysosomal volume compared with cells in region 2. Finally, region 4 corresponds to cells containing less acridine orange, in both cytoplasmic and lysosomal compartments. This suggests both reduced lysosomal volume, possibly due to membrane disruption, and also reduction in cytoplasmic volume, otherwise equivalent green fluorescence to that observed in regions 2 and 3 would be expected. This correlates with the reduced cell volume shown in Figure 7.7, and indicates these cells could be undergoing apoptotic cell shrinkage.

As only very small changes in acridine orange fluorescence were detected, another approach to these experiments would be to induce changes in green fluorescence, to take advantage of increased sensitivity of detection of this wavelength by the flow cytometer, to detect smaller changes. In the current protocol, because cells are loaded with acridine orange after any potential lysosomal damage has occurred, all cells should contain the same cytoplasmic concentration as it is taken up (and released) passively. Cells with intact lysosomes would contain more aggregated acridine orange, but this would not affect cytoplasmic levels if cells are imaged or analysed by flow cytometry quickly, with minimal light exposure. As an alternative, cells could be prepared as for the current protocol and loaded with acridine orange, then if all cells were to be exposed to intense light, all those with intact lysosomes would undergo photosensitized loss of lysosomal membrane integrity due to the acridine orange (Brunk et al., 1997), resulting in release of aggregated acridine orange, and an increase in cytoplasmic (green) fluorescence. Thus, those cells which had previously had greater numbers of intact lysosomes would now show greater green fluorescence compared with those that had fewer intact lysosomes. Obviously this would require strict control of light exposure between

experiments, and prompt measurement of samples by flow cytometry after exposure to prevent leakage of non-aggregated acridine orange from the cells.

As one of the important functions of RPE cells is to phagocytose and digest spent POS, loss of lysosomal function would limit this process and this could result in build-up of material in RPE. Considering the nature of the phagocytosed material, this is likely to lead to build-up of phototoxic material, which could lead to production of reactive oxygen species, thus resulting in damage to various cellular components. Additionally, it is widely thought that lysosomal rupture can result in cell death via the apoptotic pathway, and that this may occur in response to oxidative stress. This process is thought to involve lysosomal iron, and to result in release of lytic enzymes such as cathepsin D, normally involved in degradation of phagocytosed material, which can act upon other targets in the cytoplasm, such as mitochondria or pro-caspase enzymes. This can result in activation of the apoptotic pathway, or necrosis at higher levels of insult (Brunk *et al.*, 1995; Brunk *et al.*, 1997; Antunes *et al.*, 2001).

Light exposure of cells fed with either lipofuscin or *in vitro* peroxidized POS has previously been shown to cause loss of lysosomal integrity, measured using acridine orange (Wihlmark *et al.*, 1997; Davies *et al.*, 2001). Considering the presence of pDHA in lipofuscin granules and peroxidized POS, and the ability of lysosomal leakage to cause cell death as described above, these previous results suggest that this pathway could play a role in pDHA-induced RPE cell death. Although the findings here show limited lysosomal disruption, further study is essential to confirm this. There are indications of differences in lysosomal integrity between dark and light treated cells but due to the limited data, no significant differences can be confirmed.

Phosphatase and glucosaminidase activities of RPE cell extracts were shown here to be significantly altered in the presence of pDHA. Light caused a significant reduction in phosphatase activity in the presence of pDHA, in agreement with published data showing that lipofuscin causes a reduction in lysosomal enzyme activity (Wassell *et al.*, 1999; Shamsi and Boulton, 2001). In contrast, glucosaminidase activity was increased in the presence of pDHA, with no effect

of light. In this thesis, only two types of enzymatic activity were investigated – phosphatase and glucosaminidase. Obviously there is a great deal of scope for expanding these experiments to include other enzymes – in particular cathepsin D, a major proteolytic enzyme which has been shown to play an important role in degradation of phagocytosed POS (Rakoczy *et al.*, 1997).

Feeding cells with pDHA was shown to cause an increase in cellular fluorescence and presence of intracellular lipofuscin-like granules. Increases in cellular fluorescence do not necessarily indicate accumulation of undegraded material, as it is possible for lipids from liposomes to incorporate directly into the cell membrane, rather than entering the cells via phagocytosis. It is therefore essential to complement fluorescence data with TEM images. Results for feeding for 2 weeks correlate strongly – with POS increasing both fluorescence and granule numbers, and addition of 20 μM pDHA causing a further increase in both. At 4 weeks, the higher 20 μM pDHA concentration could not be used, so direct comparisons between the two time points are not possible. However, fluorescence and TEM data do correlate at the longer time point, showing an increase in fluorescence and granule formation in the presence of POS, but no further increase caused by the addition of 10 μM pDHA. These observations could be explained by the findings, described above, that pDHA was able to alter lysosomal integrity and enzyme function. It should also be considered that lipid peroxidation may result in an increase in rates of phagocytosis (Finnemann and Silverstein, 2001; Sun *et al.*, 2006), thereby potentially overwhelming degradative capacity of the cell, and potentially also leading to an increase in undegraded material.

In summary, this chapter has shown that pDHA is able to alter the degradative capacity of RPE cells, by causing changes in lysosomal enzyme activity and loss of lysosomal integrity. These changes could cause RPE cell dysfunction directly – by inducing apoptosis after lysosomal leakage – or indirectly by causing accumulation of phototoxic material within cells.

Chapter 8:
Discussion and conclusions

8.1 General discussion

The overall aim of this thesis was to determine whether pDHA is (photo-)toxic to RPE cells, and thus, through this or other pathways, it may play a role in the pathogenesis of AMD. Results shown here have demonstrated that pDHA is highly toxic to RPE cells *in vitro*, and can lead to lysosomal dysfunction and formation of fluorescent and undegraded material within RPE cells. The physiological relevance of these *in vitro* findings is discussed below.

The *in vitro* peroxidation of DHA occurred readily by autoxidation. The rate of peroxidation was greater when lipids were prepared as liposomes compared with a dry film. Thus, the hydration state appears to play an important role in peroxidation. POS disc membranes where DHA would be found in the retina are surrounded by aqueous cytoplasm, thus making the peroxidation of DHA in the form of liposomes more physiologically relevant than DHA peroxidized as a lipid film.

Other sources of pDHA within the retina, such as lipofuscin and lipid deposits in Bruch's membrane, are in fact lipophilic granules that only have contact with water at their surface. Thus, DHA within these deposits would have limited access to water. The rate of peroxidation could therefore be different to membrane lipids, and would be more similar to that of the lipid film studied. However, the starting concentrations of pDHA within these granules are likely to be higher than in POS, as unperoxidized DHA would be recycled to POS rather than accumulating in lipofuscin etc. Also, the known ability of DHA peroxides to induce photosensitized production of reactive oxygen species, as shown in this thesis, and the exclusion of water-soluble antioxidants, would further enhance the process of autoxidation in these deposits.

The easily peroxidizable nature of DHA combined with continual light exposure and the presence of photosensitizers in POS (e.g. ATR and A2E (Pawlak *et al.*, 2003)) suggest that levels of pDHA would increase with age of photoreceptor discs, with the oldest and most peroxidized discs/lipids found at the distal end of POS. This is consistent with findings that lipid peroxidation may provide signals for increased phagocytosis (Finnemann and Silverstein, 2001; Sun *et al.*, 2006), and thus the theory that phagocytosis is a necessary process, acting as a surrogate antioxidant – by

physically removing peroxidized POS tips (Winkler, 2008). Findings in this thesis confirm the need to remove or detoxify these peroxidized lipids, as extracellular pDHA is clearly able to directly induce (photo-)toxicity in RPE cells. The protective effects of antioxidants are important here, as these could firstly prevent or reduce the peroxidation of pDHA, and may also subsequently reduce toxicity, as occurred in experiments carried out in this thesis.

The presence of pDHA in extracellular Bruch's membrane deposits *in vivo* provides another pathway of direct cytotoxicity of extracellular pDHA. The action of antioxidants within these granules could be limited, as their lipophilic interior would prevent penetration of water-soluble antioxidants. As discussed in Chapters 1 and 5, a combination of antioxidants is often required to provide protection from oxidative stress (Böhm *et al.*, 1998; AREDS Research Group, 2001; Wrona *et al.*, 2003; Moeller *et al.*, 2006) – with lipophilic antioxidants potentially providing initial deactivation of lipid radicals or other species, and resultant antioxidant radicals in turn being mopped up by water soluble antioxidants which may then be removed *via* the circulation. In these lipophilic deposits it is therefore possible for semioxidized antioxidants to accumulate and act in a pro-oxidant manner, as described in Chapter 5. Water soluble antioxidants could, however, act on any reactive oxygen species released from the granules, either into the extracellular space or into nearby cells, where greater levels of enzymatic antioxidants would also be present compared with outside the cell (Halliwell and Gutteridge, 2007c).

Reductions in the levels of diet-derived antioxidants occur with age, possibly due to decreased ingestion and/or absorption (Newsome *et al.*, 1994). This could explain the increased levels in both lipid peroxidation products and other downstream products such as lipofuscin and Bruch's membrane deposits. Reduced antioxidant activity could lead to increased severity of lipid peroxidation, and lack of detoxification of reactive oxygen species produced by the various sources of pDHA, thus exacerbating not only the direct effects of pDHA, but also the pathway of formation of lipofuscin and sub-RPE deposits, resulting in an ever worsening cycle of peroxidation and subsequent damage.

Experimental findings of the protective effects of PE have proven to be interesting. PE showed protection against pDHA-induced toxicity in cell experiments, yet showed no decrease in yields of superoxide or singlet oxygen production by pDHA. The presence of PE did, however, decrease the lifetime of singlet oxygen, suggesting a quenching role. As the expected lifetime of singlet oxygen is considerably shorter in lipid-only environments and in membranes compared with benzene, this further reduction by PE could have implications for the ability of singlet oxygen produced by pDHA to interact with other molecules, thus potentially affecting its toxicity.

Toxicity of pDHA was observed not only upon light exposure, but also to a lesser extent in dark conditions. As singlet oxygen is caused by photo-activation of pDHA, toxicity in the dark suggests that other mechanisms must also be involved. Production of superoxide apparently does not contribute significantly, as PE is able to protect cells and maintain viability at control levels, whereas it had no effects on superoxide production by pDHA liposomes. *In vivo,* it is possible that RPE cells could be protected from pDHA-induced superoxide production by extracellular SOD – the main, and possibly only, extracellular antioxidant enzyme (Halliwell and Gutteridge, 2007c). It is unlikely this enzyme would play a role *in vitro,* however, as pDHA exposures were short (1 hour) and medium was changed immediately before the exposure. Therefore, as discussed in Chapters 5 and 6, the role of PE in protecting cells may be via the ability of PE to form adducts with lipid peroxides, particularly lipid aldehydes. The change in absorption spectrum of pDHA + POPE compared with pDHA + POPC does suggest the formation of such adducts. However, further biochemical studies would need to be carried out to confirm this.

Although not studied here, the formation of PE-pDHA adducts could also have implications on lysosomal function. Lysosomal enzyme function was altered by pDHA in this study, but the exact mechanisms were not investigated. As it is known that lipid peroxidation products can interact with proteins, including enzymes such as lysosomal degradative enzymes, it could be speculated that increased levels of PE could inhibit this effect, and possibly preserve lysosomal enzyme activity.

Although superoxide does not appear to have a major impact on extracellular pDHA toxicity, it could play a role in the ability of pDHA to disrupt lysosomal function. pDHA which is internalized in the process of POS phagocytosis could produce superoxide, as demonstrated in Chapter 6. Because of the low pH in lysosomes, it is likely that superoxide would become protonated to form the considerably more reactive hydroperoxyl radical ($HO_2^\bullet$). This radical, along with singlet oxygen, could react with unsaturated lipids of the lysosomal membrane to cause lysosomal rupture. $HO_2^\bullet$ can also travel through the membrane more easily than superoxide, potentially leading to more widespread damage (Halliwell and Gutteridge, 2007a). Both lysosomal rupture, and release of $HO_2^\bullet$ without rupture, could lead to cell dysfunction.

Lipofuscin has previously been shown to be phototoxic to RPE cells (Wassell *et al.*, 1999; Davies *et al.*, 2001) and to photosensitize the production of superoxide and singlet oxygen (Boulton *et al.*, 1993; Rozanowska *et al.*, 1995; Rozanowska *et al.*, 1998). Additionally, lipofuscin can photo-induce lipid peroxidation (Wassell *et al.*, 1999). However, the actual identity of the photosensitizing agent(s) within lipofuscin is not yet known. pDHA has been shown in this work to be capable of all of these actions – production of singlet oxygen and superoxide have been demonstrated here (Chapter 6), and both of these could contribute to lipid peroxidation. Additionally, pDHA shows stronger absorption at shorter visible wavelengths, consistent with the wavelength dependence of lipofuscin actions (Rozanowska *et al.*, 1995; Rozanowska *et al.*, 1998). Thus, due to the known presence of pDHA in lipofuscin granules (Gu *et al.*, 2003a; Ng *et al.*, 2008), it may be postulated that pDHA is in fact responsible for the phototoxicity of lipofuscin. In addition to direct toxicity, pDHA may play a role in photo-activation of A2E. It has been suggested that this component of lipofuscin can not act solely as the main contributor of lipofuscin phototoxicity, but may require transfer of energy from a blue-absorbing chromophores (Haralampus-Grynaviski *et al.*, 2003). Again, it could be proposed that pDHA could carry out this function, thus playing a second role in inducing toxicity of lipofuscin.

The effects of pDHA on cultured cells were studied extensively in this project. A summary is shown in Figure 8.1, extrapolated to the context of the intact retina to demonstrate the potential implications of the *in vitro* findings in this thesis on the RPE and photoreceptors *in vivo*. This extrapolation is based on the known presence of

pDHA in POS, lipofuscin in RPE cells, and in Bruch's membrane deposits (Crabb *et al.*, 2002; Gu *et al.*, 2003a; Ng *et al.*, 2008), and the known photosensitizing abilities of lipofuscin (Boulton *et al.*, 1993; Rozanowska *et al.*, 1995; Rozanowska *et al.*, 1998).

This figure shows: (A) increased peroxidation of DHA in aged discs of the POS, resulting in extracellular phototoxic insult to RPE cells. (B) Phagocytosis of distal POS tips (B) leads to further peroxidation of DHA in phagolysosomes and photosensitized production of reactive oxygen species, leading to direct effects on lysosomal enzyme activity, loss of lysosomal integrity, and increased accumulation of lipofuscin. (C) The presence of pDHA in lipofuscin, drusen and Bruch's membrane deposits leads to intra- and extracellular phototoxic insults on RPE cells. (D) Overall, the combined effects of pDHA result in RPE dysfunction, with subsequent POS dysfunction and impairment of the visual transduction cascade. Contributing factors to these effects are the presence of high levels of light and oxygen. Antioxidants are expected to be able to play a protective role against pDHA toxic insult.
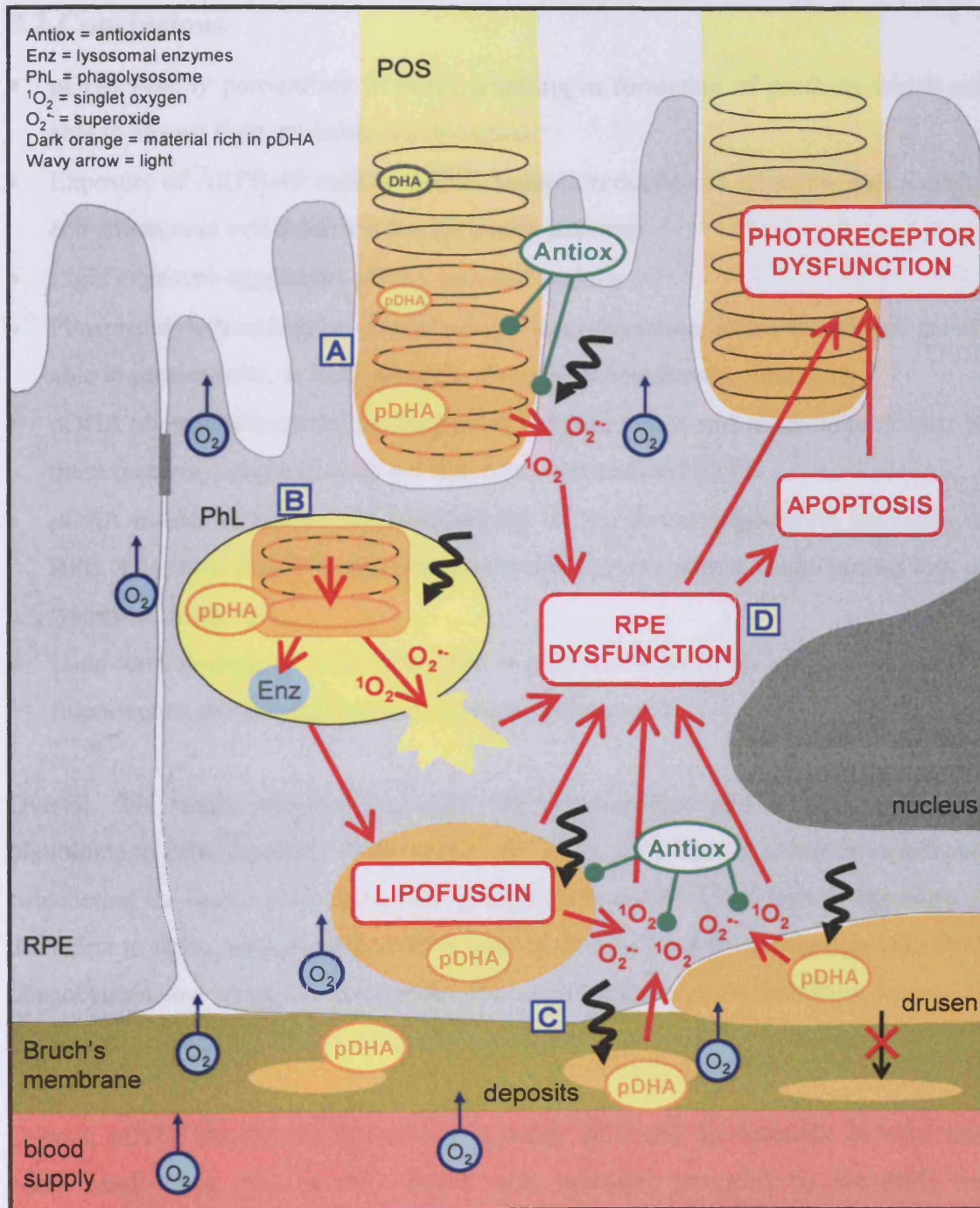
Figure 8.1 *Summary of the findings of this thesis, extrapolated to the context of the intact retina. (A)DHA peroxidation and phototoxicity in POS; (B) DHA peroxidation and phototoxicity in phagolysosomes; (C) DHA as a photosensitizing constituent of lipofuscin, drusen and Bruch's membrane deposits; (D) final outcome of RPE dysfunction as a result of the multiple sources and pathways of pDHA toxicity.*

8.2 Conclusions

- pDHA readily peroxidizes *in vitro*, resulting in formation of products which are able to absorb light at visible wavelengths

- Exposure of ARPE-19 cells to pDHA induces reduction in mitochondrial activity and subsequent cell death via the apoptosis pathway

- Light exposure aggravates pDHA-induced toxicity

- Phosphatidylethanolamine, glutathione, N-acetylcysteine, and α-tocopherol are all able to protect cells, at least partially, from pDHA-induced cytotoxicity

- pDHA photosensitizes the production of singlet oxygen and superoxide. Yields of these reactive oxygen species are not, however, reduced by PE

- pDHA is able to reduce the functionality of lysosomal degradation pathways in RPE cells, specifically by altering lysosomal enzyme activity and causing loss of lysosomal integrity

- Long-term feeding of cells with POS + pDHA results in an increase of cellular fluorescence and accumulation of undegraded material

Overall, this thesis provides evidence that extracellular pDHA can be directly phototoxic to cells, resulting in apoptotic cell death. This finding is highly significant considering the levels of DHA in close proximity to the RPE, and regular exposure of the retina to light. Additionally, pDHA may be internalized in conjunction with POS phagocytosis, and result in dysfunction of lysosomal degradation pathways, leading to accumulation of undegraded fluorescent – potentially phototoxic – material.

Overall, pDHA clearly has the ability to cause RPE cell dysfunction. *In vivo*, this could result in a loss of the support role normally provided by the RPE for photoreceptors, potentially resulting in dysfunction or death of these cells too, and eventual disruption to the visual pathway. The similarities between the observed effects of pDHA and published work on lipofuscin suggest that pDHA plays a prominent role in age-related changes in the retina, and the pathogenesis of AMD.

8.3 Future work

Precise identification of the products formed during DHA peroxidation could lead to identification of a marker of oxidative damage in the retina. This could potentially be detected *in vivo* using non-invasive Raman or fluorescence techniques, and could provide a target for future therapeutic intervention. It would be of interest to identify products which separate into the polar and non-polar phases during lipid extraction, and to investigate the phototoxicity of the lipids in these two phases separately.

As discussed in Chapters 1 and 5, lipid aldehydes have previously been shown to interact with proteins. Samples could be extracted from long-term feeding experiments and analysed for formation of such adducts, to further understand the mechanisms by which pDHA affects POS degradation.

Many components of Chapter 7 warrant further investigation. Longer feeding durations could make results more relevant to *in vivo* accumulation of undegraded material. Further studies of acridine orange labelling and lysosomal integrity could be carried out, including investigating whether light exposure of fed cells can lead to delayed apoptosis, possibly as a result of lysosomal rupture. Many other lysosomal enzymes, particularly cathepsin D, could be investigated for inhibition by pDHA.

The use of freshly isolated primary RPE cells is important to show the relevance of the findings in ARPE-19 cells, and also to investigate whether cells of different ages have adapted to a certain extent to greater levels of oxidative stress due to the presence of pDHA/lipofuscin etc.

Broader experiments could also be carried out using animal models – mimicking the experiments of subretinal linoleic acid injection (Tamai *et al.*, 2002), but using pDHA, to investigate whether the wider context of the retina alters the effect of pDHA observed *in vitro*. Alternatively, formation of pDHA in retinas subjected to oxidative stress *in vivo* could be monitored. Using an intact animal would also allow investigations of broader responses to pDHA such as that of the immune system, and also whether pDHA deposits could play a role in inducing neovascularization.

Appendices

Appendix 1 – Statistical results for Chapter 4

All *P*-values marked with grey are considered to be "not significant" (i.e. ≥ 0.05).

Post-incubation	Rose bengal concentration				
	0.05µM	0.1µM	0.2µM	0.5µM	1µM
0h, dk	0.9352	0.808	0.8095	0.7186	0.8895
0h, lt	0.054	0.0234	0.0037	0.0025	0.0002
1h, lt	0.1077	0.0562	0.0037	0.0009	0.0004
2h, lt	0.3086	0.0118	0.0043	0.0002	0.0007
4h, lt	0.0214	0.0001	0.0002	<0.0001	<0.0001
24h, lt	0.2948	0.3532	0.0199	0.0133	0.0126

Table A1.1 *P-values for one-sample t-tests to compare mitochondrial activity results of treated cells with control 100% value (corresponding to data in Figure 4.5A).*

9mW.cm^{-2} 0hs   *P* = 0.001

	DHA lt	pDHA dk	pDHA lt
DHA dk	0.581	0.017	0.001
DHA lt		0.178	0.011
pDHA dk			0.224

9mW.cm^{-2} 24hs   *P* < 0.001

	DHA lt	pDHA dk	pDHA lt
DHA dk	0.706	<0.001	<0.001
DHA lt		<0.001	<0.001
pDHA dk			0.264

15mW.cm^{-2} 0hs   *P* < 0.001

	DHA lt	pDHA dk	pDHA lt
DHA dk	0.707	0.002	<0.001
DHA lt		0.008	0.001
pDHA dk			0.683

15mW.cm^{-2} 24hs   *P* < 0.001

	DHA lt	pDHA dk	pDHA lt
DHA dk	0.360	0.002	0.001
DHA lt		0.015	0.006
pDHA dk			0.996

Table A1.2 *P-values for one-way ANOVA (indicated above each table) and Tukey's post-tests to compare the effects of 2 mM (p)DHA on mitochondrial activity at either 9 or 15 mW.cm^{-2} light (corresponding to data in Figure 4.7). dk = dark; lt = light.*

	Ohs	24 hs
9mW.cm^{-2} dk	0.0404	0.6488
9mW.cm^{-2} lt	0.0007	0.0176
15mW.cm^{-2} dk	0.0348	0.1802
15mW.cm^{-2} lt	0.0355	0.1369

Table A1.3 *P-values for one-sample t-tests to compare mitochondrial activity of cells treated with 2 mM DHA (unperoxidized; either 9 or 15 mW.cm^{-2} light intensity) with control 100% value (corresponding to data in Figure 4.7). dk = dark; lt = light.*

9 mW.cm^{-2} $P < 0.001$

	Ohs lt	24 hs dk	24 hs lt
Ohs dk	0.592	<0.001	<0.001
Ohs lt		0.01	<0.001
24 hs dk			0.323

15 mW.cm^{-2} $P < 0.001$

	Ohs lt	24 hs dk	24 hs lt
Ohs dk	0.723	<0.001	<0.001
Ohs lt		<0.001	<0.001
24 hs dk			0.950

Table A1.4 *P-values for one-way ANOVA and Tukey's post-tests to compare the effects of 2 mM pDHA on mitochondrial activity when MTT assay was carried out at Ohs vs. 24 hs post-exposure, at either 9 or 15 mW.cm^{-2} light (corresponding to data in Figure 4.7). dk = dark; lt = light.*

	9 mW.cm^{-2}, dark	9 mW.cm^{-2}, light	15 mW.cm^{-2}, dark	15 mW.cm^{-2}, light
EC50	1.36	1.06	0.94	0.26
SE	0.44	0.10	0.15	0.05
df	35	31	17	24

Table A1.5 *Non-linear regression parameters obtained from sigmoidal curve-fit of MTT assay data for cells exposed to pDHA and assay carried out 24 hours after exposure (corresponding to data in Figure 4.8). SE = standard error; df = degrees of freedom. These values were used to calculate the student t ratio and P-value.*

$$t = \frac{EC50_1 - EC50_2}{\sqrt{SE_1^2 + SE_2^2}}$$

Equation A1.1 *Equation used to calculated the t-ratio, subsequently used to calculate the P-value using the student t-test distribution, using Microsoft Excel, for comparison of EC50 values (corresponding to data in Figure 4.8).*

	0.5 mM	1 mM	2 mM
0 mM	>0.05	<0.001	<0.05
0.5 mM		<0.05	>0.05
1 mM			>0.05

Table A1.6 *P-values for one-way Tukey's post-tests (following one-way ANOVA, P = 0.0004) to compare the effects of pDHA on nuclear condensation (corresponding to data in Figure 4.12A).*

Appendix 2 – Statistical results for Chapter 5

All *P*-values marked with grey are considered to be "not significant" (i.e. ≥ 0.05).

Treatment	ANOVA *P*-value
Zeaxanthin, light	<0.0001
Zeaxanthin, dark	<0.0001
α-Tocopherol, light	0.0002
α-Tocopherol, dark	0.0003

Table A2.1 *One-way ANOVA P-values to compare mitochondrial activity in light or dark maintained cells with pDHA, supplemented with either zeaxanthin or α-tocopherol (corresponding to data in Figure 5.2A (zeaxanthin) and 5.2B (α-tocopherol)).*

LIGHT	pDHA	pDHA+ZX1	pDHA+ZX2	pDHA+ZX4
Control	<0.001	<0.001	<0.001	<0.001
pDHA		>0.05	>0.05	<0.05
pDHA+ZX1			>0.05	>0.05
pDHA+ZX2				>0.05

DARK	pDHA	pDHA+ZX1	pDHA+ZX2	pDHA+ZX4
Control	<0.01	<0.001	<0.001	<0.001
pDHA		>0.05	>0.05	<0.05
pDHA+ZX1			>0.05	>0.05
pDHA+ZX2				>0.05

LIGHT	pDHA	pDHA+AT10	pDHA+AT20	pDHA+AT40
Control	<0.001	<0.05	>0.05	>0.05
pDHA		>0.05	<0.01	<0.001
pDHA+AT10			>0.05	<0.05
pDHA+AT20				>0.05

DARK	pDHA	pDHA+AT10	pDHA+AT20	pDHA+AT40
Control	<0.001	<0.05	>0.05	>0.05
pDHA		>0.05	<0.01	<0.01
pDHA+AT10			>0.05	>0.05
pDHA+AT20				>0.05

Table A2.2 *P-values for Tukey-Kramer post-tests, corresponding to one-way ANOVA tests in Table A2.1, to compare mitochondrial activity in light or dark maintained cells exposed to pDHA, supplemented with either zeaxanthin or α-tocopherol (corresponding to data in Figure 5.2A (zeaxanthin) and 5.2B (α-tocopherol)). ZX = zeaxanthin; AT = α-tocopherol; numbers indicate antioxidant concentration (μM).*

Table A2.3 *P-values for Tukey-Kramer post-tests, (one-way ANOVA P-value <0.0001) to compare mitochondrial activity in light or dark maintained cells exposed to pDHA, supplemented with zeaxanthin and/or α-tocopherol (corresponding to data in Figure 5.3. ZX = zeaxanthin; AT = α-tocopherol; numbers indicate antioxidant concentration (μM); dk = dark-maintained (all others are light-exposed).*

	control dk	pDHA dk	20AT dk	20AT+4ZX dk	40AT dk	40AT+4ZX dk	1ZX dk	4ZX dk	control	pDHA	20AT	20AT+4ZX	40AT	40AT+4ZX	1ZX
4ZX	<0.001	>0.05	<0.05	<0.05	<0.05	<0.01	>0.05	>0.05	>0.05	<0.05	>0.05	>0.05	>0.05	>0.05	>0.05
1ZX	<0.001	>0.05	>0.05	<0.05	<0.05	>0.05	>0.05	>0.05	<0.05	>0.05	>0.05	>0.05	>0.05	>0.05	
40AT+4ZX	<0.001	>0.05	>0.05	<0.05	>0.05	>0.05	>0.05	>0.05	<0.05	>0.05	>0.05	>0.05	>0.05		
40AT	<0.01	>0.05	>0.05	<0.05	>0.05	>0.05	>0.05	>0.05	<0.05	>0.05	>0.05	>0.05			
20AT+4ZX	<0.001	>0.05	>0.05	<0.05	<0.05	>0.05	>0.05	>0.05	>0.05	<0.05	>0.05				
20AT	<0.001	>0.05	>0.05	<0.05	>0.05	>0.05	>0.05	>0.05	<0.001	>0.05					
pDHA	<0.001	>0.05	<0.05	<0.05	<0.05	<0.01	>0.05	>0.05	<0.001						
control	>0.05	<0.05	>0.05	>0.05	>0.05	>0.05	<0.05	<0.05							
4ZX dk	>0.05	>0.05	>0.05	>0.05	>0.05	>0.05	>0.05								
1ZX dk	>0.05	>0.05	>0.05	>0.05	>0.05	>0.05									
40AT+4ZX dk	>0.05	>0.05	>0.05	>0.05	>0.05										
40AT dk	>0.05	>0.05	>0.05	>0.05											
20AT+4ZX dk	>0.05	>0.05	>0.05												
20AT dk	>0.05	>0.05													
pDHA dk	>0.05														

	POPC dk	POPE dk	control lt	POPC lt	POPE lt
control dk	<0.001	>0.05	>0.05	<0.001	>0.05
POPC dk		<0.01	<0.001	<0.01	>0.05
POPE dk			>0.05	<0.001	>0.05
control lt				<0.001	>0.05
POPC lt					<0.001

Table A2.3 *P-values for one-way Tukey Kramer post-tests (following one-way ANOVA, P < 0.0001) to compare the effects of pDHA + POPE or pDHA + POPC (as indicated) on mitochondrial activity (corresponding to data in Figure 5.5). dk = dark; lt = light; POPC = cells exposed to pDHA + POPC liposomes; POPE = cells exposed to pDHA + POPE liposomes.*

Table A2.4 *P-values for Tukey-Kramer post-tests, (one-way ANOVA P-value <0.0001) to compare mitochondrial activity in light or dark maintained cells exposed to pDHA, supplemented with GST, GSH and/or NAC (corresponding to data in Figure 5.6). ZX = zeaxanthin; AT = α-tocopherol; numbers indicate antioxidant concentration (μM); dk = dark-maintained (all others are light-exposed).*

	pDHA dk	pDHA + GSH dk	pDHA + NAC dk	pDHA + GST dk	pDHA + GST + GSH dk	pDHA + GST + NAC dk	pDHA + GSH + NAC dk	pDHA + GSH + NAC + GST dk	control	pDHA	pDHA + GSH	pDHA + NAC	pDHA + GST	pDHA + GST + GSH	pDHA + GST + NAC	pDHA + GSH + NAC	pDHA + NAC + GST
control dk	<0.001	>0.05	>0.05	>0.05	>0.05	>0.05	>0.05	>0.05	>0.05	<0.001	>0.05	<0.05	>0.05	>0.05	>0.05	>0.05	>0.05
pDHA dk		<0.05	>0.05	<0.02	>0.05	>0.05	>0.05	>0.05	<0.001	<0.01	>0.05	>0.05	>0.05	>0.05	>0.05	>0.05	>0.05
pDHA + GSH dk			>0.05	>0.05	>0.05	>0.05	>0.05	>0.05	>0.05	<0.001	>0.05	>0.05	>0.05	>0.05	>0.05	>0.05	>0.05
pDHA + NAC dk				>0.05	>0.05	>0.05	>0.05	>0.05	>0.05	<0.01	>0.05	>0.05	>0.05	>0.05	>0.05	>0.05	>0.05
pDHA + GST dk					>0.05	>0.05	>0.05	>0.05	>0.05	<0.05	>0.05	>0.05	>0.05	>0.05	>0.05	>0.05	>0.05
pDHA + GST + GSH dk						>0.05	>0.05	>0.05	<0.01	<0.05	>0.05	>0.05	>0.05	>0.05	>0.05	>0.05	>0.05
pDHA + GST + NAC dk							>0.05	>0.05	>0.05	<0.001	>0.05	>0.05	>0.05	>0.05	>0.05	>0.05	>0.05
pDHA + GSH + NAC dk								>0.05	>0.05	<0.001	>0.05	>0.05	>0.05	>0.05	>0.05	>0.05	>0.05
pDHA + GSH + NAC + GST dk									>0.05	<0.001	>0.05	>0.05	>0.05	>0.05	>0.05	>0.05	>0.05
control										<0.001	>0.05	<0.05	<0.001	<0.001	<0.001	<0.001	<0.001
pDHA											<0.001	>0.05	<0.001	<0.001	<0.001	>0.05	>0.05
pDHA + GSH												>0.05	<0.001	>0.05	>0.05	>0.05	>0.05
pDHA + NAC													<0.001	<0.01	<0.001	>0.05	<0.05
pDHA + GST														>0.05	>0.05	>0.05	>0.05
pDHA + GST + GSH															>0.05	<0.001	>0.05
pDHA + GST + NAC																>0.05	>0.05

Appendix 3 – Statistical results for Chapter 6

All P-values marked with grey are considered to be "not significant" (i.e. ≥ 0.05).

liposomes:	k	A_∞
pDHA + POPC	0.614	0.198
pDHA + POPE	0.543	0.004

Table A3.1 *P-values for one-way ANOVA to investigate differences in A_∞ and k values for pDHA + POPC and pDHA + POPE groups (corresponding to Figure 6.9).*

pDHA, light vs:	P-value
pDHA + catalase, light	>0.05
pDHA, dark	<0.01

Table A3.2 *P-values for one-way ANOVA Dunnett's post-test to investigate difference in A_∞ values between pDHA + POPE samples (corresponding to Figure 6.9B).*

pDHA, light vs:	P-value
pDHA + catalase, light	>0.05
pDHA + SOD, light	<0.01
pDHA, dark	<0.01
no pDHA, light	<0.01

Table A3.3 *P-values for one-way ANOVA Dunnett's post-test (comparison with control i.e. pDHA, light) to investigate differences in reduced cytochrome C levels at t = 60 minutes within pDHA + POPC group (corresponding to Figure 6.10). Initial ANOVA value: P < 0.0001.*

pDHA, light vs:	P-value
pDHA + catalase, light	>0.05
pDHA + SOD, light	<0.01
pDHA, dark	<0.01
no pDHA, light	<0.01

Table A3.4 *P-values for one-way ANOVA Dunnett's post-test to investigate differences in reduced cytochrome C levels at t = 60 minutes within pDHA + POPE group (corresponding to Figure 6.10). Initial ANOVA value: P < 0.0001.*

Appendix 4 – Statistical results for Chapter 7

All *P*-values marked with grey are considered to be "not significant" (i.e. ≥ 0.05).

2 WEEKS	POS	POS + 5 µM pDHA	POS + 10 µM pDHA	POS + 20 µM pDHA
Cont	0.145	0.366	<0.001	0.001
POS		1	0.002	<0.001
POS + 5 µM pDHA			0.006	<0.001
POS + 10 µM pDHA				<0.001

3 WEEKS	POS	POS + 5 µM pDHA	POS + 10 µM pDHA	POS + 20 µM pDHA
Cont	0.004	<0.001	<0.001	<0.001
POS		0.439	0.008	<0.001
POS + 5 µM pDHA			0.303	<0.001
POS + 10 µM pDHA				<0.001

Table A4.1 *P-values for two-way ANOVA to investigate the effects on mitochondrial activity of feeding cells with POS +/- pDHA for 2 or 3 weeks (corresponding to Figure 7.1). Initial ANOVA P-values were: P = 0.314 for comparison of 2 weeks vs. 3 weeks, and P < 0.001 for comparison of the feeding treatments.*

DARK	POS	POS + pDHA	pDHA
control	0.974	0.178	0.453
POS		0.339	0.253
POS + pDHA			0.01

LIGHT	POS	POS + pDHA	pDHA
control	0.567	0.105	0.023
POS		0.667	0.002
POS + pDHA			<0.001

Table A4.2 *P-values for two-way ANOVA to investigate the effects on mitochondrial activity of feeding cells with POS +/- pDHA for 2 weeks, followed by exposure to light or maintenance in the dark (corresponding to Figure 7.2). Initial ANOVA P-values were: P = 0.674 for comparison of light vs. dark, and P < 0.001 for comparison of the feeding treatments.*

	POS	POS + 10 μM pDHA	POS + 20 μM pDHA	10 μM pDHA	20 μM pDHA
control	0.964	0.981	1.000	0.977	<0.001
POS		1.000	0.993	1.000	<0.001
POS + 10 μM pDHA			0.997	1.000	<0.001
POS + 20 μM pDHA				0.997	<0.001
10 μM pDHA					<0.001

Table A4.3 *P-values for two-way ANOVA to investigate the effects on cell numbers in region 4 of FL1/FL3 scatter plots of feeding cells with POS +/- pDHA for 2 weeks, followed by exposure to light or maintenance in the dark and loading with acridine orange (corresponding to Figure 7.6C). Initial ANOVA P-values were: P = 0.674 for comparison of light vs. dark, and P < 0.001 for comparison of the feeding treatments.*

	Phosphatase	Glucosaminidase
Dark	0.148	0.706
Light	0.825	0.955

Table A4.4 *P-values for one-way ANOVA to investigate effects of pDHA on enzyme activities in cell lysates (corresponding to Figure 7.8)*

A

comparison	phosphatase (lysate)	phosphatase (enzyme)	glucosaminidase
light vs. dark	<0.001	0.248	0.994
concentration	0.680	0.086	0.017

B

[pDHA]	light vs dark
0 mM	0.552
1 mM	0.002
2 mM	0.001

C

comparison	dark group	light group
0 vs. 1 mM	0.113	0.570
0 vs. 2 mM	0.024	0.270
1 vs. 2 mM	0.756	0.831

Table A4.5 *(A) P-values for two-way ANOVA to investigate effects of pDHA concentration and light vs. dark on enzyme activities in cell lysates or pure acid phosphatase enzyme (corresponding to Figure 7.9). Tukey's post-tests were subsequently carried out only for data sets with significant ANOVA P-values (i.e. P < 0.05); (B) P-values for Tukey's post-tests for phosphatase activity in cell lysates, comparing effects of light vs. dark at each pDHA concentration; (C) P-values for Tukey's post-tests for glucosaminidase activity in cell lysates, comparing effects of different pDHA concentrations in both light and dark experiments.*

1 WEEK	POS	POS + 5 µM pDHA	POS + 20 µM pDHA
control	<0.001	<0.001	<0.001
POS		0.705	<0.001
POS + 5 µM pDHA			<0.001

2 WEEKS	POS	POS + 5 µM pDHA	POS + 20 µM pDHA	20 µM pDHA
control	0.045	0.005	<0.001	0.033
POS		0.786	0.002	0.994
POS + 5 µM pDHA			0.013	0.965
POS + 20 µM pDHA				0.007

3 WEEKS	POS	POS + 5 µM pDHA	POS + 20 µM pDHA
control	0.042	0.017	<0.001
POS		0.911	<0.001
POS + 5 µM pDHA			<0.001

4 WEEKS	POS	POS + 5 µM pDHA	POS + 10 µM pDHA	5 µM pDHA	10 µM pDHA
control	0.001	0.002	0.003	0.928	0.102
POS		0.996	0.970	0.004	0.111
POS + 5 µM pDHA			1.000	0.009	0.230
POS + 10 µM pDHA				0.014	0.340
5 µM pDHA					0.403

Table A4.6 *P-values for one-way ANOVA Tukey's post-test, for comparing effects of feeding cells with POS +/- pDHA on cellular fluorescence intensity, at 4 different durations of feeding (corresponding to Figure 7.11). Initial ANOVA P-values were < 0.001 for all.*

A

	2 weeks	3 weeks	4 weeks
1 week	0.004	<0.001	0.170
2 weeks		0.309	0.708
3 weeks			0.074

B

	POS	POS + 5 µM pDHA	POS + 20 µM pDHA
control	<0.001	<0.001	<0.001
POS		0.861	<0.001
POS + 5 µM pDHA			<0.001

Table A4.7 *P-values for post-tests following two-way ANOVA to investigate the effects of duration of feeding and different feeding regimes on cellular fluorescence (corresponding to Figure 7.12. Initial ANOVA P-values were < 0.001 for both of these effects.*

TOTAL COUNT	2wks POS	2wks POS+DHA	4wks control	4wks POS	4wks POS+DHA
2wks control	0.393	0.001	0.541	0.002	0.194
2wks POS		0.201	1.000	0.259	0.998
2wks POS+DHA			0.123	1.000	0.403
4wks control				0.164	0.986
4wks POS					0.486

HOMOGENEOUS	2wks POS	2wks POS+DHA	4wks control	4wks POS	4wks POS+DHA
2wks control	0.740	0.010	1.000	0.042	0.003
2wks POS		0.264	0.842	0.573	0.125
2wks POS+DHA			0.017	0.994	0.999
4wks control				0.068	0.006
4wks POS					0.940

GRANULAR	2wks POS	2wks POS+DHA	4wks control	4wks POS	4wks POS+DHA
2wks control	0.748	0.079	0.560	0.062	0.990
2wks POS		0.727	1.000	0.662	0.973
2wks POS+DHA			0.880	1.000	0.273
4wks control				0.833	0.894
4wks POS					0.225

Table A4.8 *Tukey's post-test P-values for comparison of total, homogeneous and granular granule numbers in cells fed for either 2 weeks or 4 weeks with either control medium, POS, or POS + pDHA, corresponding to data shown in Figure 7.14. Initial one-way ANOVA P-values for the groups were: < 0.001 (for both total granules and homogeneous granules) and 0.034 for granular granules. Grey-coloured cells indicate non-significant P-values (i.e. P > 0.05).*

Appendix 5 – Conference presentations of this work

L. Bakker, M. Boulton, M. Różanowska: *Phototoxicity of peroxidized docosahexaenoic acid in retinal pigment epithelial cells.* 1st Meeting of the International Society for Ocular Cell Biology (ISOCB), September 2006, Cambridge, UK (poster).

L. Bakker, A. Pawlak, B. Różanowski, M. Boulton, M. Różanowska: *Phototoxicity of peroxidized docosahexaenoate.* Society for Free Radical Biology and Medicine 13th Annual Meeting, November 2006, Denver, USA, (poster).

L. Bakker, M.E. Boulton, M. Różanowska: *Mechanisms of phototoxicity of peroxidized docosahexaenoate and protection by antioxidants.* Society for Free Radical Biology and Medicine 14th Annual Meeting, November 2007, Washington DC, USA, (poster).

M. Różanowska, L. Bakker, M.E. Boulton, A. Pawlak, B. Różanowski: *Protective effects of phosphatidylethanolamine (PE) against (photo)toxicity to the retinal pigment epithelium (RPE) of peroxidized docosahexaenoate (DHE).* 2nd Meeting of the International Society for Ocular Cell Biology (ISOCB), September 2008, San Diego, USA.

References

Abdelsalam A, Del Priore L, Zarbin MA (1999) Drusen in age-related macular degeneration: pathogenesis, natural course, and laser photocoagulation-induced regression. *Survey of Ophthalmology.* 44:1-29.

Abe T, Yoshida M, Yoshioka Y, Wakusawa R, Tokita-Ishikawa Y, Seto H, Tamai M, Nishida K (2007) Iris pigment epithelial cell transplantation for degenerative retinal diseases. *Progress in Retinal and Eye Research.* 26:302-321.

Alge CS, Suppmann S, Priglinger SG, Neubauer AS, May CA, Hauck S, Welge-Lussen U, Ueffing M, Kampik A (2003) Comparative proteome analysis of native differentiated and cultured dedifferentiated human RPE cells. *Investigative Ophthalmology & Visual Science.* 44:3629-3641.

Alge CS, Hauck SM, Priglinger SG, Kampik A, Ueffing M (2006) Differential protein profiling of primary versus immortalized human RPE cells identifies expression patterns associated with cytoskeletal remodeling and cell survival. *Journal of Proteome Research.* 5:862-878.

Allikmets R, Shroyer NF, Singh N, Seddon JM, Lewis RA, Bernstein PS, Peiffer A, Zabriskie NA, Li Y, Hutchinson A, Dean M, Lupski JR, Leppert M (1997) Mutation of the Stargardt disease gene (ABCR) in age-related macular degeneration. *Science.* 277:1805-1807.

Ambati J, Ambati BK, Yoo SH, Ianchulev S, Adamis AP (2003a) Age-related macular degeneration: Etiology, pathogenesis, and therapeutic strategies. *Survey of Ophthalmology.* 48:257-293.

Ambati J, Anand A, Fernandez S, Sakurai E, Lynn BC, Kuziel WA, Rollins BJ, Ambati BK (2003b) An animal model of age-related macular degeneration in senescent Ccl-2- or Ccr-2-deficient mice. *Nature Medicine.* 9:1390-1397.

Antunes F, Cadenas E, Brunk UT (2001) Apoptosis induced by exposure to a low steady-state concentration of H_2O_2 is a consequence of lysosomal rupture. *Biochemical Journal.* 356:549-555.

AREDS Research Group (2001) A randomized, placebo-controlled, clinical trial of high-dose supplementation with vitamins C and E, beta carotene, and zinc for age-related macular degeneration and vision loss: AREDS report no. 8. *Archives of Ophthalmology.* 119:1417-1436.

AREDS Research Group (2005) Risk factors for the incidence of advanced age-related macular degeneration in the Age-Related Eye Disease Study (AREDS): AREDS report no. 19. *Ophthalmology.* 112:533-539.e531.

Augustin AJ, Puls S, Offermann I (2007) Triple therapy for choroidal neovascularization due to age-related macular degeneration: verteporfin PDT, bevacizumab, and dexamethasone. *Retina.* 27:133-140.

Bacot S, Bernoud-Hubac N, Baddas N, Chantegrel B, Deshayes C, Doutheau A, Lagarde M, Guichardant M (2003) Covalent binding of hydroxy-alkenals 4-HDDE, 4-HHE, and 4-HNE to ethanolamine phospholipid subclasses. *Journal of Lipid Research.* 44:917-926.

Bacot S, Bernoud-Hubac N, Chantegrel B, Deshayes C, Doutheau A, Ponsin G, Lagarde M, Guichardant M (2007) Evidence for in situ ethanolamine phospholipid adducts with hydroxy-alkenals. *Journal of Lipid Research.* 48:816-825.

Baier J, Maier M, Engl R, Landthaler M, Baumler W (2005) Time-resolved investigations of singlet oxygen luminescence in water, in phosphatidylcholine, and in aqueous suspensions of phosphatidylcholine or HT29 cells. *Journal of Physical Chemistry B.* 109:3041-3046.

Baker BN, Moriya M, Maude MB, Anderson RE, Williams TP (1986) Oil droplets of the retinal epithelium of the rat. *Experimental Eye Research.* 42:547-557.

Bartlett H, Eperjesi F (2003) Age-related macular degeneration and nutritional supplementation: a review of randomised controlled trials. *Ophthalmic and Physiological Optics.* 23:383-399.

Bashshur ZF, Bazarbachi A, Schakal A, Haddad ZA, El Haibi CP, Noureddin BN (2006) Intravitreal bevacizumab for the management of choroidal neovascularization in age-related macular degeneration. *American Journal of Ophthalmology.* 142:1-9.

Bazan HEP, Bazan NG, Feeney-Burns L, Berman ER (1990) Lipids in human lipofuscin-enriched subcellular fractions of two age populations: comparison with rod outer segments and neural retina. *Investigative Ophthalmology & Visual Science.* 31:1433-1443.

Bazan NG, Rodriguez de Turco EB, Gordon WC (1993) Pathways for the uptake and conservation of docosahexaenoic acid in photoreceptors and synapses - biochemical and autoradiographic studies. *Canadian Journal of Physiology and Pharmacology.* 71:690-698.

Ben-Shabat S, Parish CA, Vollmer HR, Itagaki Y, Fishkin N, Nakanishi K, Sparrow JR (2002) Biosynthetic studies of A2E, a major fluorophore of retinal pigment epithelial lipofuscin. *Journal of Biological Chemistry.* 277:7183-7190.

Bensasson RV, Land EJ, Truscott TG (1993a) Pulse radiation techniques: flash photolysis and pulse radiolysis. In: *Excited States and Free Radicals in Biology in Medicine. Contributions from Flash Photolysis and Pulse Radiolysis*, pp 65-100: Oxford University Press, Oxford.

Bensasson RV, Land EJ, Truscott TG (1993b) Activated forms of oxygen. In: *Excited States and Free Radicals in Biology in Medicine. Contributions from Flash Photolysis and Pulse Radiolysis*, pp 101-141: Oxford University Press, Oxford.

Berger JW, Fine SL (1999) Laser treatment for choroidal neovascularization. In: *Age-Related Macular Degeneration* (Berger JW, Fine SL, Maguire MG, eds), pp 279-296. St Louis, Missouri: Mosby, Inc.

Bergmann M, Schutt F, Holz FG, Kopitz J (2004) Inhibition of the ATP-driven proton pump in RPE lysosomes by the major lipofuscin fluorophore A2-E may contribute to the pathogenesis of age-related macular degeneration. *FASEB Journal*. 18:562-564.

Bermann M, Schutt F, Holz FG, Kopitz J (2001) Does A2E, a retinoid component of lipofuscin and inhibitor of lysosomal degradative functions, directly affect the activity of lysosomal hydrolases? *Experimental Eye Research*. 72:191-195.

Bernoud-Hubac N, Davies SS, Boutaud O, Montine TJ, Roberts LJ (2001) Formation of highly reactive gamma-ketoaldehydes (neuroketals) as products of the neuroprostane pathway. *Journal of Biological Chemistry*. 276:30964-30970.

Bernoud-Hubac N, Roberts LJ (2002) Identification of oxidized derivatives of neuroketals. *Biochemistry*. 41:11466-11471.

Besharse JC, Hollyfield JG, Rayborn ME (1977) Turnover of rod photoreceptor outer segments. II. Membrane addition and loss in relationship to light. *Journal of Cell Biology*. 75:507-527.

Besharse JC, Defoe DM (1998) Role of the retinal pigment epithelium in photoreceptor membrane turnover. In: *The Retinal Pigment Epithelium* (Marmor MF, Wolfensberger TJ, eds), pp 152-172. Oxford: Oxford University Press.

Bhosale P, Larson AJ, Frederick JM, Southwick K, Thulin CD, Bernstein PS (2004) Identification and characterization of a Pi isoform of glutathione S-transferase (GSTP1) as a zeaxanthin-binding protein in the macula of the human eye. *Journal of Biological Chemistry*. 279:49447-49454.

Bhutto IA, McLeod DS, Hasegawa T, Kim SY, Merges C, Tong P, Lutty GA (2006) Pigment epithelium-derived factor (PEDF) and vascular endothelial growth factor (VEGF) in aged human choroid and eyes with age-related macular degeneration. *Experimental Eye Research*. 82:99-110.

Bockelbrink A, Roll S, Ruether K, Rasch A, Greiner W, Willich SN (2008) Cataract surgery and the development or progression of age-related macular degeneration: a systematic review. *Survey of Ophthalmology*. 53:359-367.

Boettner EA, Wolter JR (1962) Transmission of the ocular media. *Investigative Ophthalmology & Visual Science*. 1:776-783.

Böhm F, Edge R, McGarvey DJ, Truscott TG (1998) β-Carotene with vitamins E and C offers synergistic cell protection against NOx. *FEBS Letters*. 436:387-389.

Bok D (1985) Retinal photoreceptor-pigment epithelium interactions - Friedenwald lecture. *Investigative Ophthalmology & Visual Science*. 26:1659-1694.

Boulton M, Docchio F, Dayhaw-Barker P, Ramponi R, Cubeddu R (1990) Age-related changes in the morphology, absorption and fluorescence of melanosomes and lipofuscin granules of the retinal pigment epithelium. *Vision Research.* 30:1291-1303.

Boulton M, Dontsov A, Jarvis-Evans J, Ostrovsky M, Svistunenko D (1993) Lipofuscin is a photoinducible free radical generator. *Journal of Photochemistry and Photobiology B: Biology.* 19:201-204.

Boulton M (1998) Melanin and the retinal pigment epithelium. In: *The Retinal Pigment Epithelium* (Marmor MF, Wolfensberger TJ, eds), pp 68-85. Oxford: Oxford University Press.

Boulton M, Rozanowska M, Wess T (2004) Ageing of the retinal pigment epithelium: implications for transplantation. *Graefes Archive for Clinical and Experimental Ophthalmology.* 242:76-84.

Boutaud O, Brame CJ, Salomon RG, Roberts LJ, Oates JA (1999) Characterization of the lysyl adducts formed from prostaglandin H_2 via the levuglandin pathway. *Biochemistry.* 38:9389-9396.

Brame CJ, Boutaud O, Davies SS, Yang T, Oates JA, Roden D, Roberts LJ (2004) Modification of proteins by isoketal-containing oxidized phospholipids. *Journal of Biological Chemistry.* 279:13447-13451.

Bresler NM, TAP Study Group (2001) Photodynamic therapy of subfoveal choroidal neovascularization in age-related macular degeneration with verteporfin: two-year results of 2 randomized clinical trials - TAP report 2. *Archives of Ophthalmology.* 119:198-207.

Britton G (1995) Structure and properties of carotenoids in relation to function. *FASEB Journal.* 9:1551-1558.

Brown DM, Kaiser PK, Michels M, Soubrane G, Heier JS, Kim RY, Sy JP, Schneider S (2006) Ranibizumab versus verteporfin for neovascular age-related macular degeneration. *New England Journal of Medicine.* 355:1432-1444.

Brunk UT, Zhang H, Dalen H, Ollinger K (1995) Exposure of cells to nonlethal concentrations of hydrogen peroxide induces degeneration-repair mechanisms involving lysosomal destabilization. *Free Radical Biology and Medicine.* 19:813-822.

Brunk UT, Dalen H, Roberg K, Hellquist HB (1997) Photo-oxidative disruption of lysosomal membranes causes apoptosis of cultured human fibroblasts. *Free Radical Biology and Medicine.* 23:616-626.

Buettner GR (1993) The pecking order of free radicals and antioxidants: lipid peroxidation, α-tocopherol, and ascorbate. *Archives of Biochemistry and Biophysics.* 300:535-543.

Burton GW, Ingold KU (1981) Autoxidation of biological molecules. 1. Antioxidant activity of vitamin E and related chain-breaking phenolic antioxidants in vitro. *Journal of the American Chemical Society.* 103:6472-6477.

Burton GW, Ingold KU (1984) β-Carotene: an unusual type of lipid antioxidant. *Science.* 224:569-573.

Butovich IA (2005) On the structure and synthesis of neuroprotectin D1, a novel anti-inflammatory compound of the docosahexaenoic acid family. *Journal of Lipid Research.* 46:2311-2314.

Butovich IA, Lukyanova SM, Bachmann C (2006) Dihydroxydocosahexaenoic acids of the neuroprotectin D family: synthesis, structure, and inhibition of human 5-lipoxygenase. *Journal of Lipid Research.* 47:2462-2474.

Cabral L, Unger W, Boulton M, Lightfoot R, McKechnie N, Grierson I, Marshall J (1990) Regional distribution of lysosomal enzymes in the canine retinal pigment epithelium. *Investigative Ophthalmology & Visual Science.* 31:670-676.

Calkins JL, Hochheimer BF, D'Anna SA (1980) Potential hazards from specific ophthalmic devices. *Vision Research.* 20:1039-1053.

Caygill CPJ, Hill MJ (1995) Fish, n-3 fatty acids and human colorectal and breast cancer mortality. *European Journal of Cancer Prevention.* 4:329-332.

Chader GJ, Pepperberg DR, Crouch R, Wiggert B (1998) Retinoids and the retinal pigment epithelium. In: *The Retinal Pigment Epithelium* (Marmor MF, Wolfensberger TJ, eds), pp 135-151. Oxford: Oxford University Press.

Chen HM, Anderson RE (1993a) Differential incorporation of docosahexaenoic and arachidonic acids in frog retinal pigment epithelium. *Journal of Lipid Research.* 34:1943-1955.

Chen HM, Anderson RE (1993b) Metabolism in frog retinal pigment epithelium of docosahexaenoic and arachidonic acids derived from rod outer segment membranes. *Experimental Eye Research.* 57:369-377.

Chen Y, Saari JC, Noy N (1993) Interactions of all-trans-retinol and long-chain fatty acids with interphotoreceptor retinoid-binding protein. *Biochemistry.* 32:11311-11318.

Chen Y, Houghton LA, Brenna JT, Noy N (1996) Docosahexaenoic acid modulates the interactions of the interphotoreceptor retinoid-binding protein with 11-cis-retinal. *Journal of Biological Chemistry.* 271:20507-20515.

Choudhary S, Srivastava S, Xiao T, Andley UP, Srivastava SK, Ansari NH (2003) Metabolism of lipid derived aldehyde, 4-hydroxynonenal in human lens epithelial cells and rat lens. *Investigative Ophthalmology & Visual Science.* 44:2675-2682.

Choudhary S, Xiao T, Srivastava S, Zhang W, Chan LL, Vergara LA, van Kuijk FJGM, Ansari NH (2005) Toxicity and detoxification of lipid-derived aldehydes in cultured retinal pigmented epithelial cells. *Toxicology and Applied Pharmacology.* 204:122-134.

Chua B, Flood V, Rochtchina E, Wang JJ, Smith W, Mitchell P (2006) Dietary fatty acids and the 5-year incidence of age-related maculopathy. *Archives of Ophthalmology.* 124:981-986.

Coffey PJ, Gias C, McDermott CJ, Lundh P, Pickering MC, Sethi C, Bird A, Fitzke FW, Maass A, Chen LL, Holder GE, Luthert PJ, Salt TE, Moss SE, Greenwood J (2007) Complement factor H deficiency in aged mice causes retinal abnormalities and visual dysfunction. *Proceedings of the National Academy of Sciences, USA.* 104:16651-16656.

Corongiu FP, Banni S, Dess MA (1989) Conjugated dienes detected in tissue lipid extracts by second derivative spectrophotometry. *Free Radical Biology and Medicine.* 7:183-186.

Crabb JW, Miyagi M, Gu X, Shadrach K, West KA, Sakaguchi H, Kamei M, Hasan A, Yan L, Rayborn ME, Salomon RG, Hollyfield JG (2002) Drusen proteome analysis: an approach to the etiology of age-related macular degeneration. *Proceedings of the National Academy of Sciences, USA.* 99:14682-14687.

Cruickshanks KJ, Klein R, Klein BEK (1993) Sunlight and age-related macular degeneration - the Beaver Dam Eye Study. *Archives of Ophthalmology.* 111:514-518.

Cunha-Vaz JG (2004) The blood-retinal barriers system. Basic concepts and clinical evaluation. *Experimental Eye Research.* 78:715-721.

Curran-Celentano J, Hammond BR, Jr., Ciulla TA, Cooper DA, Pratt LM, Danis RB (2001) Relation between dietary intake, serum concentrations, and retinal concentrations of lutein and zeaxanthin in adults in a Midwest population. *American Journal of Clinical Nutrition.* 74:796-802.

Das UN (2006) Essential fatty acids: biochemistry, physiology and pathology. *Biotechnology Journal.* 1:420-439.

Davies S, Elliott MH, Floor E, Truscot TG, Zareba M, Sarna T, Shamsi FA, Boulton ME (2001) Photocytotoxicity of lipofuscin in human retinal pigment epithelial cells. *Free Radical Biology and Medicine.* 31:256-265.

Davies SS, Amarnath V, Montine KS, Bernoud-Hubac N, Boutaud O, Montine TJ, Roberts LJ (2002) Effects of reactive gamma-ketoaldehydes formed by the isoprostane pathway (isoketals) and cyclooxygenase pathway (levuglandins) on proteasome function. *FASEB Journal.* 16:U266-U288.

de Duve C, de Barsy T, Poole B, Trouet A, Tulkens P, Van Hoof F (1974) Lysosomotropic agents. *Biochemical Pharmacology.* 23:2495-2531.

Delmelle M (1978) Retinal sensitized photodynamic damage to liposomes. *Photochemistry and Photobiology.* 28:357-360.

DeMar JC, Jr., Wensel TG, Anderson RE (1996) Biosynthesis of the unsaturated 14-carbon fatty acids found on the N termini of photoreceptor-specific proteins. *Journal of Biological Chemistry.* 271:5007-5016.

Docchio F, Boulton M, Cubeddu R, Ramponi R, Barker PD (1991) Age-related changes in the fluorescence of melanin and lipofuscin granules of the retinal pigment epithelium: a time-resolved fluorescence spectroscopy study. *Photochemistry and Photobiology.* 54:247-253.

Dontsov AE, Glickman RD, Ostrovsky MA (1999) Retinal pigment epithelium pigment granules stimulate the photo-oxidation of unsaturated fatty acids. *Free Radical Biology and Medicine.* 26:1436-1446.

Dumont A, Hehner SP, Hofmann TG, Ueffing M, Droge W, Schmitz ML (1999) Hydrogen peroxide-induced apoptosis is CD95-independent, requires the release of mitochondria-derived reactive oxygen species and the activation of NF-kappaB. *Oncogene.* 18:747-757.

Dunn KC, Aotaki-Keen AE, Putkey FR, Hjelmeland LM (1996) ARPE-19, a human retinal pigment epithelial cell line with differentiated properties. *Experimental Eye Research.* 62:155-169.

Ebrahem Q, Renganathan K, Sears J, Vasanji A, Gu X, Lu L, Salomon RG, Crabb JW, Anand-Apte B (2006) Carboxyethylpyrrole oxidative protein modifications stimulate neovascularization: Implications for age-related macular degeneration. *Proceedings of the National Academy of Sciences, USA.* 103:13480-13484.

Edge R, McGarvey DJ, Truscott TG (1997) The carotenoids as anti-oxidants - a review. *Journal of Photochemistry and Photobiology B: Biology.* 41:189-200.

El-Agamey A, Cantrell A, Land EJ, McGarvey DJ, Truscott TG (2004) Are dietary carotenoids beneficial? Reactions of carotenoids with oxy-radicals and singlet oxygen. *Photochemical and Photobiological Sciences.* 3:802-811.

Eldho NV, Feller SE, Tristram-Nagle S, Polozov IV, Gawrisch K (2003) Polyunsaturated docosahexaenoic vs docosapentaenoic acid - Differences in lipid matrix properties from the loss of one double bond. *Journal of the American Chemical Society.* 125:6409-6421.

Eldred GE, Katz ML (1989) The autofluorescent products of lipid peroxidation may not be lipofuscin-like. *Free Radical Biology and Medicine.* 7:157-163.

Eldred GE, Katz ML (1991) The lipid peroxidation theory of lipofuscinogenesis cannot yet be confirmed. *Free Radical Biology and Medicine.* 10:445-447.

Esterbauer H, Schaur RJ, Zollner H (1991) Chemistry and biochemistry of 4-hydroxynonenal, malonaldehyde and related aldehydes. *Free Radical Biology and Medicine.* 11:81-128.

Esterbauer H (1993) Cytotoxicity and genotoxicity of lipid-oxidation products. *American Journal of Clinical Nutrition.* 57:779S-785.

Evans JR, Fletcher AE, Wormald RP (2004) Age-related macular degeneration causing visual impairment in people 75 years or older in Britain: an add-on study to the Medical Research Council Trial of Assessment and Management of Older People in the Community. *Ophthalmology.* 111:513-517.

Fam SS, Murphey LJ, Terry ES, Zackert WE, Chen Y, Gao L, Pandalai S, Milne GL, Roberts LJ, Porter NA, Montine TJ, Morrow JD (2002) Formation of highly reactive A-ring and J-ring isoprostane-like compounds (A(4)/J(4)-neuroprostanes) in vivo from docosahexaenoic acid. *Journal of Biological Chemistry.* 277:36076-36084.

Feeney-Burns L, Hilderbrand ES, Eldridge S (1984) Aging human RPE: morphometric analysis of macular, equatorial, and peripheral cells. *Investigative Ophthalmology & Visual Science.* 25:195-200.

Finnemann SC, Bonilha VL, Marmorstein AD, Rodriguez-Boulan E (1997) Phagocytosis of rod outer segments by retinal pigment epithelial cells requires $\alpha v\beta 5$ integrin for binding but not for internalization. *Proceedings of the National Academy of Sciences, USA.* 94:12932-12937.

Finnemann SC, Silverstein RL (2001) Differential roles of CD36 and $\alpha v\beta 5$ Integrin in Photoreceptor Phagocytosis by the Retinal Pigment Epithelium. *Journal of Experimental Medicine.* 194:1289-1298.

Finnemann SC, Leung LW, Rodriguez-Boulan E (2002) The lipofuscin component A2E selectively inhibits phagolysosomal degradation of photoreceptor phospholipid by the retinal pigment epithelium. *Proceedings of the National Academy of Sciences, USA.* 99:3842-3847.

Fishkin NE, Sparrow JR, Allikmets R, Nakanishi K (2005) Isolation and characterization of a retinal pigment epithelial cell fluorophore: An all-trans-retinal dimer conjugate. *Proceedings of the National Academy of Sciences, USA.* 102:7091-7096.

Fliesler SJ, Anderson RE (1983) Chemistry and metabolism of lipids in the vertebrate retina. *Progress in Lipid Research.* 22:79-131.

Folch J, Lees M, Sloane Stanley GH (1957) A simple method for the isolation and purification of total lipids from animal tissues. *Journal of Biological Chemistry.* 226:497-509.

Foote CS, Clennan EL (1995) Properties and reactions of singlet dioxygen. In: *Active Oxygen in Chemistry* (Foote CS, Selverstone Valentine J, Greenberg A, Liebman JF, eds). Glasgow: Blackie Academic & Professional.

Forrester JV, Dick AD, McMenamin PG, Lee WR (2002) The eye: basic sciences in practice. Edinburgh London: W. B. Saunders.

Franco R, Panayiotidis MI, Cidlowski JA (2007) Glutathione depletion is necessary for apoptosis in lymphoid cells independent of reactive oxygen species formation. *Journal of Biological Chemistry.* 282:30452-30465.

Fung AE, Lalwani GA, Rosenfeld PJ, Dubovy SR, Michels S, Feuer WJ, Puliafito CA, Davis JL, Flynn JHW, Esquiabro M (2007) An optical coherence tomography-guided, variable dosing regimen with intravitreal ranibizumab (Lucentis) for neovascular age-related macular degeneration. *American Journal of Ophthalmology.* 143:566-583.e562.

Gavrieli Y, Sherman Y, Ben-Sasson SA (1992) Identification of programmed cell death in situ via specific labeling of nuclear DNA fragmentation. *Journal of Cell Biology.* 119:493-501.

German OL, Buzzi E, Rotstein NP, Rodríguez-Boulan E, Politi LE (2008) Retinal pigment epithelial cells promote spatial reorganization and differentiation of retina photoreceptors. *Journal of Neuroscience Research.* EPub ahead of print.

Gordon WC, Bazan NG (1990) Docosahexaenoic acid utilization during rod photoreceptor cell renewal. *Journal of Neuroscience.* 10:2190-2202.

Gordon WC, Rodriguez de Turco EB, Bazan NG (1992) Retinal pigment epithelial cells play a central role in the conservation of docosahexaenoic acid by photoreceptor cells after shedding and phagocytosis. *Current Eye Research.* 11:73-83.

Gordon WC, Bazan NG (1993) Visualization of H-3 docosahexaenoic acid trafficking through photoreceptors and retinal-pigment epithelium by electron microscopic autoradiography. *Investigative Ophthalmology & Visual Science.* 34:2402-2411.

Gouras P, Kong J, Tsang SH (2002) Retinal degeneration and RPE transplantation in Rpe65-/- mice. *Investigative Ophthalmology & Visual Science.* 43:3307-3311.

Grossfield A, Feller SE, Pitman MC (2006) A role for direct interactions in the modulation of rhodopsin by ω-3 polyunsaturated lipids. *Proceedings of the National Academy of Sciences, USA.* 103:4888-4893.

Gu XR, Meer SG, Miyagi M, Rayborn ME, Hollyfield JG, Crabb JW, Salomon RG (2003a) Carboxyethylpyrrole protein adducts and autoantibodies, biomarkers for age-related macular degeneration. *Journal of Biological Chemistry.* 278:42027-42035.

Gu XR, Sun MJ, Gugiu B, Hazen S, Crabb JW, Salomon RG (2003b) Oxidatively truncated docosahexaenoate phospholipids: Total synthesis, generation, and peptide adduction chemistry. *Journal of Organic Chemistry.* 68:3749-3761.

Guichardant M, Taibi-Tronche P, Fay LB, Lagarde M (1998) Covalent modifications of aminophospholipids by 4-hydroxynonenal. *Free Radical Biology and Medicine.* 25:1049-1056.

Guichardant M, Bernoud-Hubac N, Chantegrel B, Deshayes C, Lagarde M (2002) Aldehydes from n-6 fatty acid peroxidation. Effects on aminophospholipids. *Prostaglandins Leukotrienes and Essential Fatty Acids.* 67:147-149.

Guichardant M, Chantegrel B, Deshayes C, Doutheau A, Moliere P, Lagarde M (2004) Specific markers of lipid peroxidation issued from n-3 and n-6 fatty acids. *Biochemical Society Transactions.* 32:139-140.

Gutteridge JMC, Kerry PJ, Armstrong D (1982) Autoxidized and lipoxidase-treated polyunsaturated fatty acids : Autofluorescence associated with the decomposition of lipid peroxides. *Biochimica et Biophysica Acta - Lipids and Lipid Metabolism.* 711:460-465.

Hageman GS, Luthert PJ, Victor Chong NH, Johnson LV, Anderson DH, Mullins RF (2001) An integrated hypothesis that considers drusen as biomarkers of immune-mediated processes at the RPE-Bruch's membrane interface in aging and age-related macular degeneration. *Progress in Retinal and Eye Research.* 20:705-732.

Hageman GS, Anderson DH, Johnson LV, Hancox LS, Taiber AJ, Hardisty LI, Hageman JL, Stockman HA, Borchardt JD, Gehrs KM, Smith RJH, Silvestri G, Russell SR, Klaver CCW, Barbazetto I, Chang S, Yannuzzi LA, Barile GR, Merriam JC, Smith RT, Olsh AK, Bergeron J, Zernant J, Merriam JE, Gold B, Dean M, Allikmets R (2005) A common haplotype in the complement regulatory gene factor H (HF1/CFH) predisposes individuals to age-related macular degeneration. *Proceedings of the National Academy of Sciences, USA.* 102:7227-7232.

Hahn P, Milam AH, Dunaief JL (2003) Maculas affected by age-related macular degeneration contain increased chelatable iron in the retinal pigment epithelium and Bruch's membrane. *Archives of Ophthalmology.* 121:1099-1105.

Haines JL, Spencer KM, Pericak-Vance MA (2007) Bringing the genetics of macular degeneration into focus. *Proceedings of the National Academy of Sciences, USA.* 104:16725-16726.

Halliwell B, Gutteridge JM (1984) Oxygen toxicity, oxygen radicals, transition metals and disease. *Biochemical Journal.* 219:1-14.

Halliwell B, Gutteridge JMC (2007a) Chemistry of free radicals and related 'reactive species'. In: *Free Radicals in Biology and Medicine.* New York: Oxford University Press Inc.

Halliwell B, Gutteridge JMC (2007b) Cellular responses to oxidative stress. In: *Free Radicals in Biology and Medicine.* New York: Oxford University Press Inc.

Halliwell B, Gutteridge JMC (2007c) Antioxidant defences: endogenous and diet derived. In: *Free Radicals in Biology and Medicine.* New York: Oxford University Press Inc.

Hampton MB, Orrenius S (1997) Dual regulation of caspase activity by hydrogen peroxide: Implications for apoptosis. *FEBS Letters.* 414:552-556.

Handelman GJ, van Kuijk FJGM, Chatterjee A, Krinsky NI (1991) Characterization of products formed during the autoxidation of β-carotene. *Free Radical Biology and Medicine.* 10:427-437.

Haralampus-Grynaviski NM, Lamb LE, Clancy CMR, Skumatz C, Burke JM, Sarna T, Simon JD (2003) Spectroscopic and morphological studies of human retinal lipofuscin granules. *Proceedings of the National Academy of Sciences, USA.* 100:3179-3184.

Hawse P (2006) Blocking the blue. *British Journal of Ophthalmology.* 90:939-940.

He X, Hahn P, Iacovelli J, Wong R, King C, Bhisitkul R, Massaro-Giordano M, Dunaief JL (2007) Iron homeostasis and toxicity in retinal degeneration. *Progress in Retinal and Eye Research.* 26:649-673.

Heier JS, Boyer DS, Ciulla TA, Ferrone PJ, Jumper JM, Gentile RC, Kotlovker D, Chung CY, Kim RY, for the Focus Study Group (2006) Ranibizumab combined with verteporfin photodynamic therapy in neovascular age-related macular degeneration: year 1 results of the FOCUS Study. *Archives of Ophthalmology.* 124:1532-1542.

Heller JI, Crowley JR, Hazen SL, Salvay DM, Wagner P, Pennathur S, Heinecke JW (2000) p-Hydroxyphenylacetaldehyde, an aldehyde generated by myeloperoxidase, modifies phospholipid amino groups of low density lipoprotein in human atherosclerotic intima. *Journal of Biological Chemistry.* 275:9957-9962.

Hogan MJ, Wood I, Steinberg RH (1974) Phagocytosis by pigment epithelium of human retinal cones. *Nature.* 252:305-307.

Hollyfield JG, Besharse JC, Rayborn ME (1976) The effect of light on the quantity of phagosomes in the pigment epithelium. *Experimental Eye Research.* 23:623-635.

Hooper L, Thompson RL, Harrison RA, Summerbell CD, Ness AR, Moore HJ, Worthington HV, Durrington PN, Higgins JPT, Capps NE, Riemersma RA, Ebrahim SBJ, Smith GD (2006) Risks and benefits of omega 3 fats for mortality, cardiovascular disease, and cancer: systematic review. *British Medical Journal.* 332:752-760.

Hoppe G, O'Neil J, Hoff HF, Sears J (2004a) Products of lipid peroxidation induce missorting of the principal lysosomal protease in retinal pigment epithelium. *Biochimica et Biophysica Acta.* 1689:33-41.

Hoppe G, O'Neil J, Hoff HF, Sears J (2004b) Accumulation of oxidized lipid-protein complexes alters phagosome maturation in retinal pigment epithelium. *Cellular and Molecular Life Sciences.* 61:1664-1674.

Huang LL, Coleman HR, Kim J, de Monasterio F, Wong WT, Schleicher RL, Ferris FL, III, Chew EY (2008) Oral supplementation of lutein/zeaxanthin and omega-3 long chain polyunsaturated fatty acids in persons aged 60 years or older, with or without AMD. *Investigative Ophthalmology & Visual Science.* 49:3864-3869.

Hunt RC, Davis AA (1990) Altered expression of keratin and vimentin in human retinal pigment epithelial cells in vivo and in vitro. *Journal of Cellular Physiology.* 145:187-199.

Hurst JS, Saini MK, Jin G-F, Awasthi YC, van Kuijk FJGM (2005) Toxicity of oxidized β-carotene to cultured human cells. *Experimental Eye Research.* 81:239-243.

Jain SK (1984) The accumulation of malonyldialdehyde, a product of fatty-acid peroxidation, can disturb aminophospholipid organization in the membrane bilayer of human erythrocytes. *Journal of Biological Chemistry.* 259:3391-3394.

Jarrett SG, Boulton ME (2005) Antioxidant up-regulation and increased nuclear DNA protection play key roles in adaptation to oxidative stress in epithelial cells. *Free Radical Biology and Medicine.* 38:1382-1391.

Jiang LQ, Hamasaki D (1994) Corneal electroretinographic function rescued by normal retinal pigment epithelial grafts in retinal degenerative Royal College of Surgeons rats. *Investigative Ophthalmology & Visual Science.* 35:4300-4309.

Kaemmerer E, Schutt F, Krohne TU, Holz FG, Kopitz J (2007) Effects of lipid peroxidation-related protein modifications on RPE lysosomal functions and POS phagocytosis. *Investigative Ophthalmology & Visual Science.* 48:1342-1347.

Kanda A, Chen W, Othman M, Branham KEH, Brooks M, Khanna R, He S, Lyons R, Abecasis GaR, Swaroop A (2007) A variant of mitochondrial protein LOC387715/ARMS2, not HTRA1, is strongly associated with age-related macular degeneration. *Proceedings of the National Academy of Sciences, USA.* 104:16227-16232.

Kariel N, Davidson E, Keough KMW (1991) Cholesterol does not remove the gel-liquid crystalline phase transition of phosphatidylcholines containing two polyenoic acyl chains. *Biochimica et Biophysica Acta - Biomembranes.* 1062:70-76.

Kawai Y, Fujii H, Okada M, Tsuchie Y, Uchida K, Osawa T (2006) Formation of N^{ϵ}-(succinyl)lysine in vivo: a novel marker for docosahexaenoic acid-derived protein modification. *Journal of Lipid Research.* 47:1386-1398.

Kennedy CJ, Rakoczy PE, Constable IJ (1995) Lipofuscin of the retinal pigment epithelium: A review. *Eye.* 9:763-771.

Kim RS, LaBella FS (1987) Comparison of analytical methods for monitoring autoxidation profiles of authentic lipids. *Journal of Lipid Research.* 28:1110-1117.

Klein R (1999) Epidemiology. In: *Age-Related Macular Degeneration* (Berger JW, Fine SL, Maguire MG, eds), pp 31-55. St Louis, Missouri: Mosby, Inc.

Klein R, Klein BEK, Tomany SC, Meuer SM, Huang GH (2002a) Ten-year incidence and progression of age-related maculopathy: The Beaver Dam eye study. *Ophthalmology.* 109:1767-1779.

Klein R, Klein BEK, Tomany SC, Moss SE (2002b) Ten-year incidence of age-related maculopathy and smoking and drinking: the Beaver Dam Eye Study. *American Journal of Epidemiology.* 156:589-598.

Knight J, Taylor GW, Wright P, Clare AS, Rowley AF (1999) Eicosanoid biosynthesis in an advanced deuterostomate invertebrate, the sea squirt (Ciona intestinalis). *Biochimica et Biophysica Acta - Molecular and Cell Biology of Lipids.* 1436:467-478.

Kuklev DV, Smith WL (2004) Synthesis of long chain n-3 and n-6 fatty acids having a photoactive conjugated tetraene group. *Chemistry and Physics of Lipids.* 130:145-158.

Kuroki M, Voest EE, Amano S, Beerepoot LV, Takashima S, Tolentino M, Kim RY, Rohan RM, Colby KA, Yeo KT, Adamis AP (1996) Reactive oxygen intermediates increase vascular endothelial growth factor expression in vitro and in vivo. *Journal of Clinical Investigation.* 98:1667-1675.

Lamb LE, Simon JD (2004) A2E: A component of ocular lipofuscin. *Photochemistry and Photobiology.* 79:127-136.

Lamb TD, Pugh EN (2004) Dark adaptation and the retinoid cycle of vision. *Progress in Retinal and Eye Research.* 23:307-380.

Lavail MM, Li L, Turner JE, Yasumura D (1992) Retinal pigment epithelial cell transplantation in RCS rats: Normal metabolism in rescued photoreceptors. *Experimental Eye Research.* 55:555-562.

Liebler DC, McClure TD (1996) Antioxidant reactions of beta-carotene: Identification of carotenoid-radical adducts. *Chemical Research in Toxicology.* 9:8-11.

Liou GI, Bridges CDB, Fong SL, Alvarez RA, Gonzalez-Fernandez F (1982) Vitamin A transport between retina and pigment epithelium - an interstitial protein carrying endogenous retinol (interstitial retinol-binding protein). *Vision Research.* 22:1457-1467.

Litman B, Niu S-L, Polozova A, Mitchell D (2001) The role of docosahexaenoic acid containing phospholipids in modulating G protein-coupled signaling pathways. *Journal of Molecular Neuroscience.* 16:237-242.

Lopez PF, Sippy BD, Lambert HM, Thach AB, Hinton DR (1996) Transdifferentiated retinal pigment epithelial cells are immunoreactive for vascular endothelial growth factor in surgically excised age- related macular degeneration-related choroidal neovascular membranes. *Investigative Ophthalmology & Visual Science.* 37:855-868.

Macular Photocoagulation Study Group (1982) Argon laser photocoagulation for senile macular degeneration. Results of a randomized clinical trial. *Archives of Ophthalmology.* 100:912-918.

Macular Photocoagulation Study Group (1994) Visual outcome after laser photocoagulation for subfoveal choroidal neovascularization secondary to age-related macular degeneration. The influence of initial lesion size and initial visual acuity. . *Arch Ophthalmol.* 112:480-488.

Marin-Castano ME, Striker GE, Alcazar O, Catanuto P, Espinosa-Heidmann DG, Cousins SW (2006) Repetitive nonlethal oxidant injury to retinal pigment epithelium decreased extracellular matrix turnover in vitro and induced sub-RPE deposits in vivo. *Investigative Ophthalmology & Visual Science.* 47:4098-4112.

Marmor MF (1998) Structure, function, and disease of the retinal pigment epithelium. In: *The Retinal Pigment Epithelium* (Marmor MF, Wolfensberger TJ, eds), pp 3-9. Oxford: Oxford University Press.

Marshall J, Hussain AA, Starita C, Moore DJ, Patmore AL (1998) Aging and Bruch's membrane. In: *The Retinal Pigment Epithelium* (Marmor MF, Wolfensberger TJ, eds), pp 669-692. Oxford: Oxford University Press.

Matsumoto B, Defoe DM, Besharse JC (1987) Membrane turnover in rod photoreceptors - ensheathment and phagocytosis of outer segment distal tips by pseudopodia of the retinal pigment epithelium. *Proceedings of the Royal Society of London: Biological Sciences.* 230:339-354.

McCarty CA, Mukesh BN, Fu CL, Mitchell P, Wang JJ, Taylor HR (2001) Risk factors for age-related maculopathy: the Visual Impairment Project. *Archives of Ophthalmology.* 119:1455-1462.

McKechnie NM, Boulton M, Robey HL, Savage FJ, Grierson I (1988) The cytoskeletal elements of human retinal pigment epithelium: in vitro and in vivo. *Journal of Cell Science.* 91:303-312.

Moeller SM, Parekh N, Tinker L, Ritenbaugh C, Blodi B, Wallace RB, Mares JA, Group CRS (2006) Associations between intermediate age-related macular degeneration and lutein and zeaxanthin in the Carotenoids in Age-Related Eye Disease Study (CAREDS): ancillary study of the Women's Health Initiative. *Archives of Ophthalmology.* 124:1151-1162.

Morrow JD, Roberts LJ (1997) The isoprostanes: Unique bioactive products of lipid peroxidation. *Progress in Lipid Research.* 36:1-21.

Mosmann T (1983) Rapid colorimetric assay for cellular growth and survival - application to proliferation and cytotoxicity assays. *Journal of Immunological Methods.* 65:55-63.

Mukai K, Morimoto H, Okauchi Y, Nagaoka S-i (1993a) Kinetic study of reactions between tocopheroxyl radicals and fatty acids. *Lipids.* 28:753-756.

Mukai K, Sawada K, Kohno Y, Terao J (1993b) Kinetic study of the prooxidant effect of tocopherol. Hydrogen abstraction from lipid hydroperoxides by tocopheroxyls in solution. *Lipids.* 28:747-752.

Mukherjee PK, Marcheselli VL, Serhan CN, Bazan NG (2004) Neuroprotectin D1: A docosahexaenoic acid-derived docosatriene protects human retinal pigment epithelial cells from oxidative stress. *Proceedings of the National Academy of Sciences, USA.* 101:8491-8496.

Mukherjee PK, Marcheselli VL, Barreiro S, Hu J, Bok D, Bazan NG (2007a) Neurotrophins enhance retinal pigment epithelial cell survival through neuroprotectin D1 signaling. *Proceedings of the National Academy of Sciences, USA.* 104:13152-13157.

Mukherjee PK, Marcheselli VL, de Rivero Vaccari JC, Gordon WC, Jackson FE, Bazan NG (2007b) Photoreceptor outer segment phagocytosis attenuates oxidative stress-induced apoptosis with concomitant neuroprotectin D1 synthesis. *Proceedings of the National Academy of Sciences, USA.* 104:13158-13163.

Murov SL (1973) Handbook of Photochemistry. p 89. New York: Marcel Dekker, Inc.

Musiek ES, Cha JK, Yin HY, Zackert WE, Terry ES, Porter NA, Montine TJ, Morrow JD (2004) Quantification of F-ring isoprostane-like compounds (F-4-neuroprostanes) derived from docosahexaenoic acid in vivo in humans by a stable isotope dilution mass spectrometric assay. *Journal of Chromatography B-Analytical Technologies in the Biomedical and Life Sciences.* 799:95-102.

Nakamura MT, Nara TY (2003) Essential fatty acid synthesis and its regulation in mammals. *Prostaglandins Leukotrienes and Essential Fatty Acids.* 68:145-150.

Newsome DA, Miceli MV, Liles MR, Tate DJ, Oliver PD (1994) Antioxidants in the retinal pigment epithelium. *Progress in Retinal and Eye Research.* 13:101-123.

Ng EW, Adamis AP (2005) Targeting angiogenesis, the underlying disorder in neovascular age-related macular degeneration. *Canadian Journal of Ophthalmology.* 40:352-368.

Ng K-P, Gugiu B, Renganathan K, Davies MW, Gu X, Crabb JS, Kim SR, Rozanowska MB, Bonilha VL, Rayborn ME, Salomon RG, Sparrow JR, Boulton ME, Hollyfield JG, Crabb JW (2008) Retinal pigment epithelium lipofuscin proteomics. *Molecular & Cellular Proteomics.* 7:1397-1405.

Niu SL, Mitchell DC, Lim SY, Wen ZM, Kim HY, Salem N, Litman BJ (2004) Reduced G protein-coupled signaling efficiency in retinal rod outer segments in response to n-3 fatty acid deficiency. *Journal of Biological Chemistry.* 279:31098-31104.

Öllinger K, Brunk UT (1995) Cellular injury induced by oxidative stress is mediated through lysosomal damage. *Free Radical Biology and Medicine.* 19:565-574.

Omenn GS, Goodman GE, Thornquist MD, Balmes J, Cullen MR, Glass A, Keogh JP, Meyskens FL, Valanis B, Williams JH, Barnhart S, Hammar S (1996) Effects of a combination of beta carotene and vitamin A on lung cancer and cardiovascular disease. *New England Journal of Medicine.* 334:1150-1155.

Owen CG, Fletcher AE, Donoghue M, Rudnicka AR (2003) How big is the burden of visual loss caused by age related macular degeneration in the United Kingdom? *British Journal of Ophthalmology.* 87:312-317.

Papermaster DS (1982) Preparation of retinal rod outer segments. *Methods in Enzymology.* 81:48-52.

Pawlak A, Rozanowska M, Zareba M, Lamb LE, Simon JD, Sarna T (2002) Action spectra for the photoconsumption of oxygen by human ocular lipofuscin and lipofuscin extracts. *Archives of Biochemistry and Biophysics.* 403:59-62.

Pawlak A, Wrona M, Rozanowska M, Zareba M, Lamb LE, Roberts JE, Simon JD, Sarna T (2003) Comparison of the aerobic photoreactivity of A2E with its precursor retinal. *Photochemistry and Photobiology.* 77:253-258.

Porter NA, Caldwell SE, Mills KA (1995) Mechanisms of free radical oxidation of unsaturated lipids. *Lipids.* 30:277-290.

Pryor WA, Castle L (1984) Chemical methods for the detection of lipid hydroperoxides. *Methods in Enzymology.* 105:293-299.

Pulido JS (2002) Retina, choroid, and vitreous. St. Louis: Mosby, Inc.

Rakoczy PE, Lai CM, Baines M, Di Grandi S, Fitton JH, Constable IJ (1997) Modulation of cathepsin D activity in retinal pigment epithelial cells. *Biochemical Journal.* 324:935-940.

Recknagel RO, Glende EA (1984) Spectrophotometric detection of lipid conjugated dienes. *Methods in Enzymology.* 105:331-337.

Reich EE, Zackert WE, Brame CJ, Chen Y, Roberts LJ, Hachey DL, Montine TJ, Morrow JD (2000) Formation of novel D-ring and E-ring isoprostane-like compounds (D-4/E-4-neuroprostanes) in vivo from docosahexaenoic acid. *Biochemistry.* 39:2376-2383.

Resnikoff S, Pascolini D, Etya'ale D, Kocur I, Pararajasegaram R, Pokharel GP, Mariotti SP (2004) Global data on visual impairment in the year 2002. *Bulletin of the World Health Organization.* 82:844-851.

Rodriguez de Turco EB, Deretic D, Bazan NG, Papermaster DS (1997) Post-Golgi vesicles cotransport docosahexaenoyl-phospholipids and rhodopsin during frog photoreceptor membrane biogenesis. *Journal of Biological Chemistry.* 272:10491-10497.

Rodriguez de Turco EB, Parkins N, Ershov AV, Bazan NG (1999) Selective retinal pigment epithelial cell lipid metabolism and remodeling conserves photoreceptor docosahexaenoic acid following phagocytosis. *Journal of Neuroscience Research.* 57:479-486.

Rosenfeld PJ, Brown DM, Heier JS, Boyer DS, Kaiser PK, Chung CY, Kim RY (2006) Ranibizumab for neovascular age-related macular degeneration. *New England Journal of Medicine.* 355:1419-1431.

Roth F, Bindewald A, Holz FG (2004) Keypathophysiologic pathways in age-related macular disease. *Graefes Archive for Clinical and Experimental Ophthalmology.* 242:710-716.

Rotstein NP, Politi LE, Aveldano MI (1998) Docosahexaenoic acid promotes differentiation of developing photoreceptors in culture. *Investigative Ophthalmology & Visual Science.* 39:2750-2758.

Rotstein NP, Politi LE, German OL, Girotti R (2003) Protective effect of docosahexaenoic acid on oxidative stress- induced apoptosis of retina photoreceptors. *Investigative Ophthalmology & Visual Science.* 44:2252-2259.

Rozanowska M, Jarvis-Evans J, Korytowski W, Boulton ME, Burke JM, Sarna T (1995) Blue light-induced reactivity of retinal age pigment - in vitro generation of oxygen-reactive species. *Journal of Biological Chemistry.* 270:18825-18830.

Rozanowska M, Wessels J, Boulton M, Burke JM, Rodgers MAJ, Truscott TG, Sarna T (1998) Blue light-induced singlet oxygen generation by retinal lipofuscin in non-polar media. *Free Radical Biology and Medicine.* 24:1107-1112.

Rozanowska M, Korytowski W, Rozanowski B, Skumatz C, Boulton ME, Burke JM, Sarna T (2002a) Photoreactivity of aged human RPE melanosomes: A comparison with lipofuscin. *Investigative Ophthalmology & Visual Science.* 43:2088-2096.

Rozanowska M, Pawlak A, Rozanowski B, Skumatz C, Zareba M, Boulton ME, Burke JM, Sarna T, Simon JD (2004) Age-related changes in the photoreactivity of retinal lipofuscin granules: Role of chloroform-insoluble components. *Investigative Ophthalmology & Visual Science.* 45:1052-1060.

Rozanowska M, Sarna T (2005) Light-induced damage to the retina: role of rhodopsin chromophore revisited. *Photochemistry and Photobiology.* 81:1305-1330.

Rozanowska MB, Rozanowski B, Pawlak A, Sarna T, Simon JD (2002b) Photoreactivity of peroxidized docosahexaenoyl fatty acid. *Free Radical Biology and Medicine.* 33:358.

Ruckman J, Green LS, Beeson J, Waugh S, Gillette WL, Henninger DD, Claesson-Welsh L, Janjic N (1998) 2'-Fluoropyrimidine RNA-based aptamers to the 165-amino acid form of vascular endothelial growth factor ($VEGF_{165}$). *Journal of Biological Chemistry.* 273:20556-20567.

Salem N, Litman B, Kim HY, Gawrisch K (2001) Mechanisms of action of docosahexaenoic acid in the nervous system. *Lipids.* 36:945-959.

Santos NC, Figueira-Coelho J, Martins-Silva J, Saldanha C (2003) Multidisciplinary utilization of dimethyl sulfoxide: pharmacological, cellular, and molecular aspects. *Biochemical Pharmacology.* 65:1035-1041.

Sarks S, Cherepanoff S, Killingsworth M, Sarks J (2007) Relationship of basal laminar deposit and membranous debris to the clinical presentation of early age-related macular degeneration. *Investigative Ophthalmology & Visual Science.* 48:968-977.

Schaumberg DA, Hankinson SE, Guo Q, Rimm E, Hunter DJ (2007) A prospective study of 2 major age-related macular degeneration susceptibility alleles and interactions with modifiable risk factors. *Archives of Ophthalmology.* 125:55-62.

Schutt F, Davies S, Kopitz J, Holz FG, Boulton ME (2000) Photodamage to human RPE cells by A2-E, a retinoid component of lipofuscin. *Investigative Ophthalmology & Visual Science.* 41:2303-2308.

Schutt F, Holz FG (2001) Age-related macular degeneration: current concepts of pathogenesis and risk factors. In: *Age-related macular degeneration: current treatment concepts* (Alberti WE, Richard G, Sagerman RH, eds), pp 3-10. Berlin Heidelberg New York: Springer-Verlag.

Scott BL, Bazan NG (1989) Membrane docosahexaenoate is supplied to the developing brain and retina by the liver. *Proceedings of the National Academy of Sciences, USA.* 86:2903-2907.

Seagle B-LL, Gasyna EM, Mieler WF, Norris JR, Jr. (2006) Photoprotection of human retinal pigment epithelium cells against blue light-induced apoptosis by melanin free radicals from Sepia officinalis. *Proceedings of the National Academy of Sciences, USA.* 103:16644-16648.

Seddon JM, George S, Rosner B (2006) Cigarette smoking, fish consumption, omega-3 fatty acid intake, and associations with age-related macular degeneration: The US Twin Study of Age-Related Macular Degeneration. *Archives of Ophthalmology.* 124:995-1001.

Shamsi FA, Boulton M (2001) Inhibition of RPE lysosomal and antioxidant activity by the age pigment lipofuscin. *Investigative Ophthalmology & Visual Science.* 42:3041-3046.

Sharma SP, James TJ (1991) Existence of bluish-white fluorescing age-pigment - "pre- lipofuscin". *Free Radical Biology and Medicine.* 10:443-444.

Sliney DH (1983) Eye protective techniques for bright light. *Ophthalmology.* 90:937-944.

Snodderly DM (1995) Evidence for protection against age-related macular degeneration by carotenoids and antioxidant vitamins. *American Journal of Clinical Nutrition.* 62:1448S-1461.

Spaide RF, Ho-Spaide WC, Browne RW, Armstrong D (1999) Characterization of peroxidized lipids in Bruch's membrane. *Retina.* 19:141-147.

Sparrow JR, Parish CA, Hashimoto M, Nakanishi K (1999) A2E, a lipofuscin fluorophore, in human retinal pigmented epithelial cells in culture. *Investigative Ophthalmology & Visual Science.* 40:2988-2995.

Sparrow JR, Nakanishi K, Parish CA (2000) The lipofuscin fluorophore A2E mediates blue light-induced damage to retinal pigmented epithelial cells. *Investigative Ophthalmology & Visual Science.* 41:1981-1989.

Sparrow JR, Cai BL (2001) Blue light-induced apoptosis of A2E-containing RPE: Involvement of caspase-3 and protection by Bcl-2. *Investigative Ophthalmology & Visual Science.* 42:1356-1362.

Stillwell W, Wassall SR (2003) Docosahexaenoic acid: membrane properties of a unique fatty acid. *Chemistry and Physics of Lipids.* 126:1-27.

Strauss O (2005) The retinal pigment epithelium in visual function. *Physiological Reviews.* 85:845-881.

Sun MJ, Finnemann SC, Febbraio M, Shan L, Annangudi SP, Podrez EA, Hoppe G, Darrow R, Organisciak DT, Salomon RG, Silverstein RL, Hazen SL (2006) Light-induced oxidation of photoreceptor outer segment phospholipids generates ligands for CD36-mediated phagocytosis by retinal pigment epithelium - A potential mechanism for modulating outer segment phagocytosis under oxidant stress conditons. *Journal of Biological Chemistry.* 281:4222-4230.

Tamai K, Spaide RF, Ellis EA, Iwabuchi S, Ogura Y, Armstrong D (2002) Lipid hydroperoxide stimulates subretinal choroidal neovascularization in the rabbit. *Experimental Eye Research.* 74:301-308.

Tan JS, Mitchell P, Kifley A, Flood V, Smith W, Wang JJ (2007) Smoking and the long-term incidence of age-related macular degeneration: the Blue Mountains Eye Study. *Archives of Ophthalmology.* 125:1089-1095.

Tanito M, Nishiyama A, Tanaka T, Masutani H, Nakamura H, Yodoi J, Ohira A (2002) Change of redox status and modulation by thiol replenishment in retinal photooxidative damage. *Investigative Ophthalmology & Visual Science.* 43:2392-2400.

TAP Study Group (1999) Photodynamic therapy of subfoveal choroidal neovascularization in age-related macular degeneration with verteporfin: one-

year results of 2 randomized clinical trials--TAP report 1. *Archives of Ophthalmology.* 117:1329-1345.

Terrasa AM, Guajardo MH, Catala A (2003) Peroxidation stimulated by lipid hydroperoxides on bovine retinal pigment epithelium mitochondria - Effect of cellular retinol-binding protein. *International Journal of Biochemistry & Cell Biology.* 35:1071-1084.

The Eye Disease Case-Control Study Group (1992) Risk factors for neovascular age-related macular degeneration. . *Archives of Ophthalmology.* 110:1701-1708.

Tian J, Ishibashi K, Honda S, Boylan SA, Hjelmeland LM, Handa JT (2005) The expression of native and cultured human retinal pigment epithelial cells grown in different culture conditions. *British Journal of Ophthalmology.* 89:1510-1517.

Tinoco J (1983) Dietary requirements and functions of alpha-linolenic acid in animals. *Progress in Lipid Research.* 21:1-45.

Tomany SC, Cruickshanks KJ, Klein R, Klein BEK, Knudtson MD (2004) Sunlight and the 10-year incidence of age-related maculopathy - The Beaver Dam eye study. *Archives of Ophthalmology.* 122:750-757.

Trieschmann M, Beatty S, Nolan JM, Hense HW, Heimes B, Austermann U, Fobker M, Pauleikhoff D (2007) Changes in macular pigment optical density and serum concentrations of its constituent carotenoids following supplemental lutein and zeaxanthin: The LUNA study. *Experimental Eye Research.* 84:718-728.

Wagner BA, Buettner GR, Burns CP (1994) Free radical-mediated lipid peroxidation in cells: oxidizability is a function of cell lipid bis-allylic hydrogen content. *Biochemistry.* 33:4449-4453.

Walling C (1995) Autoxidation. In: *Active Oxygen in Chemistry* (Foote CS, Selverstone Valentine J, Greenberg A, Liebman JF, eds). London: Blackie Academic & Professional.

Wang N, Anderson RE (1992) Enrichment of polyunsaturated fatty acids from rat retinal pigment epithelium to rod outer segments. *Current Eye Research.* 11:783-791.

Wang N, Wiegand RD, Anderson RE (1992) Uptake of 22-carbon fatty acids into rat retina and brain. *Experimental Eye Research.* 54:933-939.

Wassell J, Davies S, Bardsley W, Boulton M (1999) The photoreactivity of the retinal age pigment lipofuscin. *Journal of Biological Chemistry.* 274:23828-23832.

Whitehead AJ, Mares JA, Danis RP (2006) Macular pigment: a review of current knowledge. *Archives of Ophthalmology.* 124:1038-1045.

Wihlmark U, Wrigstad A, Roberg K, Brunk UT, Nilsson SEG (1996) Formation of lipofuscin in cultured retinal pigment epithelial cells exposed to pre-oxidized

photoreceptor outer segments. *Acta Pathologica, Microbiologica, et Immunologica Scandinavica.* 104:272-279.

Wihlmark U, Wrigstad A, Roberg K, Nilsson SEG, Brunk UT (1997) Lipofuscin accumulation in cultured retinal pigment epithelial cells causes enhanced sensitivity to blue light irradiation. *Free Radical Biology and Medicine.* 22:1229-1234.

Williams C, Birch EE, Emmett PM, Northstone K (2001) Stereoacuity at age 3.5 y in children born full-term is associated with prenatal and postnatal dietary factors: a report from a population-based cohort study. *American Journal of Clinical Nutrition.* 73:316-322.

Wimmers S, Karl MO, Strauss O (2007) Ion channels in the RPE. *Progress in Retinal and Eye Research.* 26:263-301.

Winkler BS (2008) An hypothesis to account for the renewal of outer segments in rod and cone photoreceptor cells: renewal as a surrogate antioxidant. *Investigative Ophthalmology & Visual Science.* 49:3259-3261.

Wrona M, Korytowski W, Rozanowska M, Sarna T, Truscott TG (2003) Cooperation of antioxidants in protection against photosensitized oxidation. *Free Radical Biology and Medicine.* 35:1319-1329.

Wrona M, Rozanowska M, Sarna T (2004) Zeaxanthin in combination with ascorbic acid or alpha-tocopherol protects ARPE-19 cells against photosensitized peroxidation of lipids. *Free Radical Biology and Medicine.* 36:1094-1101.

Yamanaka WK, Clemans GW, Hutchinson ML (1980) Essential fatty acids deficiency in humans. *Progress in Lipid Research.* 19:187-215.

Yin H, Musiek ES, Gao L, Porter NA, Morrow JD (2005) Regiochemistry of neuroprostanes generated from the peroxidation of docosahexaenoic acid in vitro and in vivo. *Journal of Biological Chemistry.* 280:26600-26611.

Yin HY, Porter NA (2005) New insights regarding the autoxidation of polyunsaturated fatty acids. *Antioxidants & Redox Signaling.* 7:170-184.

Young AJ, Lowe GM (2001) Antioxidant and prooxidant properties of carotenoids. *Archives of Biochemistry and Biophysics.* 385:20-27.

Young RW (1967) The renewal of photoreceptor cell outer segments. *Journal of Cell Biology.* 33:61-72.

Young RW, Droz B (1968) The renewal of protein in retinal rods and cones. *Journal of Cell Biology.* 39:169-184.

Young RW, Bok D (1969) Participation of the retinal pigment epithelium in the rod outer segment renewal process. *Journal of Cell Biology.* 42:392-403.

Zareba M, Raciti MW, Henry MM, Sarna T, Burke JM (2006) Oxidative stress in ARPE-19 cultures: Do melanosomes confer cytoprotection? *Free Radical Biology and Medicine.* 40:87-100.

Zhou J, Jang YP, Kim SR, Sparrow JR (2006) Complement activation by photooxidation products of A2E, a lipofuscin constituent of the retinal pigment epithelium. *Proceedings of the National Academy of Sciences, USA.* 103:16182-16187.

Zieseniss S, Zahler S, Muller I, Hermetter A, Engelmann B (2001) Modified phosphatidylethanolamine as the active component of oxidized low density lipoprotein promoting platelet prothrombinase activity. *Journal of Biological Chemistry.* 276:19828-19835.